

Magnetic Adsorbents Displaying Switchable Ion-Exchange Behaviour

By

Thomas Clifford Willett

A thesis submitted to the University of Birmingham
for the degree of
DOCTOR OF PHILOSOPHY

School of Chemical Engineering
College of Engineering and Physical Sciences
May 2009

Thesis Abstract

Magnetic bioseparations based on non-porous adsorbents offer a low-fouling alternative to the porous materials required by conventional adsorbent separation techniques. Interest in magnetic bioseparations has been limited by the high cost of suitable magnetic adsorbents.

In this study a variety of techniques - including Ce(IV) initiation, surface ATRP and sulfonyl activation – were used to graft ion-exchanging polyelectrolyte surfaces on low cost non-porous polyvinyl alcohol-magnetite supports. Grafting of poly(2-vinyl pyridine) and poly(methacrylic acid) was fully characterised using solid and liquid state FTIR. Dense polyelectrolyte layers were seen, with Ce(IV) grafted layers accounting for up to 49% of grafted support mass. Values for ATRP and sulfonyl activations were 41% and 25% of support mass respectively. These included layers which correspond to the brush regime ($2R_g/D > 8$), as determined by Flory Radius calculations.

The above matrices were subsequently analysed with bind and elute studies using a model mixture of acidic and basic proteins. Switchable ion-exchange behaviour was demonstrated, with anion binding capacity >25 mg/g support at pH 5 and cation binding >25 mg/g seen for Ce(IV) grafted supports. Improved elution by pH was also seen, with up to 73% of bound lysozyme removed during a single elution at pH 5.

Dedication

To Su, for all the love, support and encouragement.

To my parents, for all the money.

Acknowledgements

I would like to thank:

Professor Owen Thomas and Dr Eirini Theodossiou for their guidance and support throughout my project.

Hazel Jennings, for being patient with me each time I have asked her for the same phonenumber three times in one day.

Elaine and Christine, for showing me where all the goodies are in the supply rooms; and Dave, for lending me tools for screwing, unscrewing and bashing things.

Poppy, Reza, Alison, Isaac, Kritsadanchalee, Evan, Haiyang, Peggy, Xue Jing, Sarika, Irene, Andrew, Geoff, Ken, Fideline and everybody else who has helped me in some way during my project work.

And finally a special shout out to my groupmate Yao Yu, whose charisma, humour and ability to believe that there really is a ghost in our lab has kept me going throughout Birmingham's 11 month long winters. Get well soon Yao!

List of acronyms

(as used throughout thesis)

2VP – 2-vinyl pyridine

ACN – Ammonium cerium(IV) nitrate

AEX – Anion exchange

AFM – Atomic Force Microscopy

ATR – Attenuated Total Reflectance

ATRP – Atom Transfer Radical polymerisation

BSA – Bovine serum albumin

CEX – Cation exchange

D – Intergraft Spacing

DMSO – Dimethyl sulfoxide

DNA – Deoxyribonucleic acid

EBA – Expanded Bed Adsorption chromatography

FTIR – Fourier-Transform Infrared spectroscopy

HGMF – High Gradient Magnetic Fishing

HGMS – High Gradient Magnetic Separations

IEC – Ion exchange chromatography

IEX – Ion exchange

IR – Infrared spectroscopy

LPO – Lactoperoxidase

MAA – Methacrylic acid

M-PVA – Magnetic poly(vinyl alcohol) beads, a product of Chemagen

MRI – Magnetic Resonance Imaging

P2VP – Poly(2-vinyl pyridine)

PAA – Poly(acrylic acid)

pI – Isoelectric point

PMAA – Poly(methacrylic acid)

PS – Polystyrene

PTBAA – Poly(tert-butyl acrylate)

PTBMA – Poly(tert-butyl methacrylate)

PVA – Poly(vinyl alcohol)

R_f – Flory Radius

RAFT – Reversible Addition Fragmentation Transfer polymerisation

ROMP – Ring Opening Metathesis polymerisation

RT – Room temperature

SDS – Sodium dodecyl sulphate

SDS-PAGE – Sodium dodecyl sulphate polyacrylamide gel electrophoresis

SEM – Scanning Electron Microscopy

STM – Scanning Tunneling Microscopy

TBMA – Tert-butyl methacrylate

TFA – Trifluoroacetic acid

TNBS – Picrylsulfonic acid (2,4,6-trinitrobenzenesulfonic acid)

Contents

1	Introduction	6
1.1	Project overview	6
1.2	Magnetic separations	7
1.2.1	History of magnetic research	7
1.2.2	Magnetic support separations.....	9
1.2.3	Magnetic separation theory	13
1.3	Adapting magnetic supports for bioseparations	18
1.3.1	Polymer brush chemistry	18
1.3.2	Switchable behavior in polymer brushes	20
1.3.3	Ion exchange	25
1.3.4	Switchable polymer brushes as ion exchange surfaces	28
1.3.5	Synthesis of polymer brushes on magnetic supports.....	30
1.3.6	Characterisation of polymer brushes	32
1.4	Choice of support	37
1.5	Outline of thesis	41
2	Polymer grafting by Ce(IV) initiated 'graft from'	43
2.1	Introduction	43
2.2	Materials and methods	50
2.2.1	Materials used	50
2.2.2	Base matrix preparation.....	50
2.2.3	Quenched Ce(IV) polymer grafting	51
2.2.4	Unquenched Ce(IV) polymer grafting	52
2.2.5	Ce(IV) mixed polymer grafting without second initiation	52
2.2.6	Hydrolysis of PTBMA grafted products	52
2.2.7	FTIR solid analysis	52
2.3	Results	53
2.3.1	FTIR peak assignments for grafted polymers	53
2.3.2	Ce(IV) initiated homopolymer brush grafting	55
2.3.3	Ce(IV) initiated mixed polymer brush grafting.....	62
2.4	Conclusions.....	68
3.	Polymer grafting sulfonyl chloride activated 'graft to'	72
3.1	Introduction	72
3.2	Materials and methods	76

3.2.1	Materials used	76
3.2.2	Solvent testing	76
3.2.3	Base matrix preparation	77
3.2.4	Tresyl chloride activation	77
3.2.5	Tosyl chloride activation	78
3.2.6	Amination of tresylated particles	78
3.2.7	Amination of tosylated particles	78
3.2.8	TNBS assay of polymer grafted supports	79
3.2.9	Homopolymer brush grafting of tresylated supports	80
3.2.10	Mixed polymer brush grafting of tresylated supports	80
3.2.11	Hydrolysis of grafted PTBMA chains	80
3.2.12	FTIR analysis	80
3.3	Results	81
3.3.1	Solvent testing	81
3.3.2	Studies on sulfonyl activation in acetone	81
3.3.3	Single polymer brush grafting	83
3.3.4	Mixed polymer brush grafting	90
3.4	Conclusions.....	95
4	Polymer grafting via AGE activation	97
4.1	Introduction	97
4.1.1	Controlled surface activation by partial bromination	97
4.1.2	Polymer “graft from” by ATRP.....	98
4.1.3	Polymer “graft to” by alkyl bromide substitution	102
4.1.4	Routes to mixed brushes using partial bromination	102
4.2	Materials and methods	106
4.2.1	Materials used	106
4.2.2	Absorbent preparation (washing regime).....	106
4.2.3	AGE activation	106
4.2.4	Acidified Bromine assay	107
4.2.5	Controlled bromination study	108
4.2.6	ATRP mixed brush synthesis.....	109
4.2.7	Preparation of halohydrin surface groups	111
4.2.8	Preparation of epoxide surface groups	112
4.2.9	Simultaneous bromination and polymer attack.....	112
4.2.10	Mixed brush grafting using two graft-to steps.....	113
4.2.11	Mixed brush grafting using graft-to then ATRP	113

4.2.12	Mixed brush grafting using ATRP then graft-to	113
4.2.13	Hydrolysis of PTBMA chains	114
4.2.14	FTIR analysis	114
4.3	Results	115
4.3.1	Activation of M-PVA with AGE	115
4.3.2	Dibromination of AGE activated supports	116
4.3.3	Homopolymer brush grafting by ATRP	117
4.3.4	Homopolymer brush grafting by dibromination graft to	120
4.3.5	Homopolymer grafting by other graft to approaches.....	122
4.3.6	Mixed polymer brush grafting by ATRP	123
4.3.7	Mixed polymer brush grafting by dibromination graft to	132
4.3.8	Mixed polymer brush grafting by a combining ATRP and graft to ...	136
4.4	Conclusions.....	141
5.	Binding Studies on Grafted Beads	143
5.1	Introduction	143
5.2.	Materials and methods	149
5.2.1	Materials used	149
5.2.2	Electrophoresis sample preparation	150
5.2.3	Running electrophoresis samples.....	150
5.2.4	Acidic/basic protein binding with salt elution.....	150
5.2.5	Protein binding at pH 5 with elution by pH switch	151
5.2.6	Protein binding at pH 8 with elution by pH switch	151
5.3	Results	152
5.3.1	Binding studies on ungrafted supports.....	152
5.3.2	Binding studies on homopolymer grafted supports.....	153
5.3.3	Binding studies on mixed brush products from Ce(IV) initiation method 159	
5.3.4	Binding studies on mixed brush products from tresyl activation method 165	
5.3.5	Binding studies on mixed brush products from ATRP method.....	170
5.3.6	Summary of binding data for supports modified with Ce(IV), ATRP and tresyl grafted methods	174
5.4	Conclusions.....	180
6	Conclusions and future work	181
7.	Appendix	184
7.1	Testing hydrolysis of PTBMA chains.....	184

7.1.1	Background	184
7.1.2	Method.....	184
7.1.3	Results.....	185
7.1.4	Conclusion	187
7.2	Calibration charts of monomers in DMSO (Ce(IV) reaction quantification)	188
7.2.1	Method:.....	188
7.3	Calibration charts of monomers from water into 1-butanol (ATRP)	192
7.3.1	Method:.....	192
7.4	Calibration charts of 'graft to' polymers from acetone into 1-butanol.....	196
7.4.1	Method.....	196
7.5	Comparison of bromine decay in DMSO to bromine decay in water – acidity of bromine in DMSO	200
7.5.1	Background	200
7.5.2	Method.....	200
7.5.3	Results.....	200
7.6	Comparison of bromine decay in DMSO to bromine decay in water – A_{410} of bromine in DMSO	203
7.6.1	Background	203
7.6.2	Method.....	203
7.6.3	Results.....	203
7.7	Comparison of bromine decay in DMSO to bromine decay in water – acidity of bromine in water	205
7.7.1	Background	205
7.7.2	Method.....	205
7.7.3	Results.....	205
7.8	Comparison of bromine decay in DMSO to bromine decay in water – A_{410} of bromine in water	208
7.8.1	Background	208
7.8.2	Method.....	208
7.8.3	Results.....	208
7.9	Calculation of average R_f for mixed brushes	210
7.9.1	Background	210
7.9.2	Method.....	210
7.9.2	Results.....	211
7.10	Effect of bead curvature on intergraft distances.....	215
7.10.1	Theory	215
7.10.2	Results	216

8 References..... 218

1 Introduction

1.1 Project overview

Magnetic bioseparations are gaining popularity, with great interest being seen in their application to large scale biotech and bioprocess applications. Development of magnetic separations has been hindered by a lack of economically viable functionalised supports available for use in bioseparations. There is thus a demand for low cost, robust and reusable magnetic adsorbents. The creation of Ion Exchange (IEX) supports with the aforementioned properties is preferred, due to the low cost of typical ion-exchange components and the high binding capacities possible with IEX techniques. In order to achieve such surface modifications the field of surface science has been looked to, specifically the modification of solid surfaces with polymer brush nanotechnology.

Against the above the main aims of this project/thesis have been to manufacture various types of mixed polyelectrolyte brush magnetic supports, able to perform both cation exchange (CEX) and anion exchange (AEX) protein separations. The following sections provide an introduction to the principles behind magnetic bioseparations, polymer brush nanotechnology and how the two techniques may be combined to produce new 'smart' materials for protein separations.

1.2 Magnetic separations

1.2.1 History of magnetic research

The following is a brief introduction to magnetic separations and the magnetic properties of materials which make this technique possible. It should be noted that although magnetic principles are described here, no experiments have been performed during this study to investigate magnetic properties. The discussion presented in this section is purely for background knowledge of magnetic separation techniques.

Discovery of hematite artefacts from the Olmec people of Central America, radiocarbon dated to 1400-1000 B.C., suggest that humans may have been using the directional properties of magnetic materials for over 3000 years (Carlson, 1975). Lodestone is mentioned in Greek writings from the year 800 BC (Mattis, 1965), with the first definite reference to its magnetic behaviour being made by Thales of Miletus in the 6th century B.C, who said that lodestone attracts iron “because it has a soul”. According to Carus (1st century B.C.) the word ‘magnetic’ is derived from the region of Magnesia, where lodestone was mined. Pliny the Elder, however, attributed the name and discovery of lodestone to the shepherd Magnes “the nails of whose shoes and the tip of whose staff stuck fast in a magnetic field while he pastured his flocks” (Gilbert, 1600).

Despite such early recognition of magnetic behavior in materials it was not until the publication of William Gilbert’s *De Magnete* in 1600 that the study of magnetism truly began to advance. His studies were based upon the interaction of a compass with the ‘terrella’, a sphere that he had constructed from lodestone and which bore a magnetic north and south pole. During these experiments Gilbert concluded that the earth also possessed magnetic properties and that these accounted for the directional behaviour of compass materials.

In 1845 Michael Faraday coined the term ‘diamagnetism’ after observing that a glass bar subject to a strong magnetic field would begin to orient itself

perpendicular to the field direction. This was distinctly different from the 'paramagnetism' of an iron bar, which would tend to align itself with the direction of an applied magnetic field (Fisher, 2004). This work was furthered by James Clerk Maxwell with his publication of a set of electromagnetic equations relating magnetic induction to factors such as magnetic field strength, electrical field strength and magnetic flux (Maxwell, 1861).

Developments in magnetic theory were soon being exploited by the mineral industries. Patents for devices capable of separating and handling magnetically susceptible solids were appearing by the beginning of the 20th century (Langguth et al, 1903; Koderá et al 1905; Gunther, 1909). During the last 100 years magnetic separations have become an important part of the clay/mineral/nuclear processing and waste treatment industries.

Magnetic carriers were first used for separations in the removal of organic impurities from waste water streams using electrostatic adsorption (Urbain & Steman, 1941) with the intended aims of reducing separation times; allowing removal of suspended matter from rapidly flowing water; and allowing the separation of suspended matter without first diluting the mixture. These earlier magnetic carriers were simple suspensions of magnetite which were added to waste water streams alongside flocculants (figure 1.1).

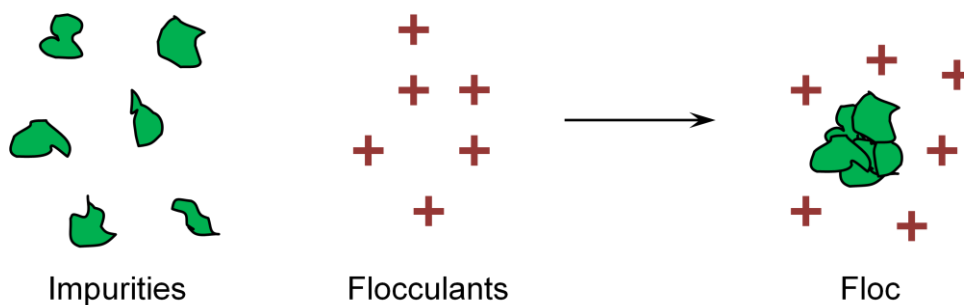


Figure 1.1. Impurities forming floc in the presence of flocculants

Once the flocculant had formed colloidal structures with impurities in the water the magnetite would aid flocculation of the colloids under the influence of a magnetic field (figure 1.2).

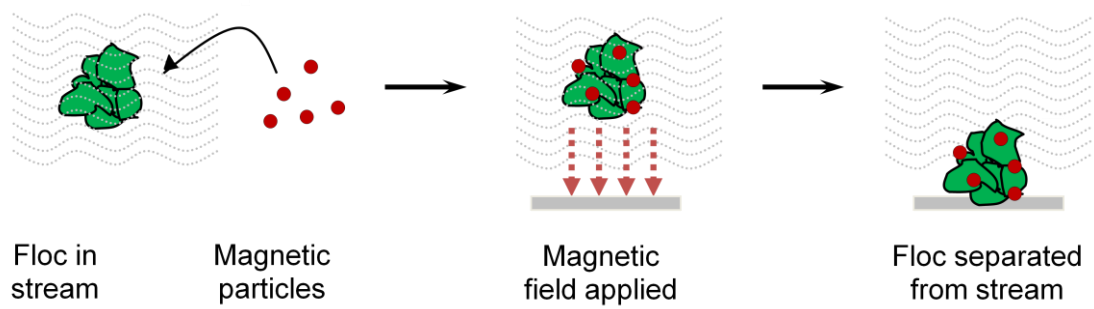


Figure 1.2. Removal of floc from stream using magnetic particles

1.2.2 Magnetic support separations

From using magnetic particles to aid the separation of colloids containing organic compounds the next development in organic magnetic separations was to replace the coagulants with magnetically responsive supports (Robinson, 1973). This development allows the convenient use of magnetic separations for primary product capture of desired products in impurity-containing feedstocks. A mixture containing magnetic supports and non magnetic impurities can easily be separated into magnetic and non-magnetic phases by the application of magnetic fields. The creation of adsorbent magnetic beads comprising magnetic particles inside a polymer matrix allowed the development of magnetic separation techniques in which stable magnetic particles can selectively bind product (figure 1.3), followed by removal of the magnetic particles plus bound product from the bulk solution using a magnetic field (figure 1.4; Munro et. al 1977, Halling and Dunnill, 1979a, 1979b, 1980).

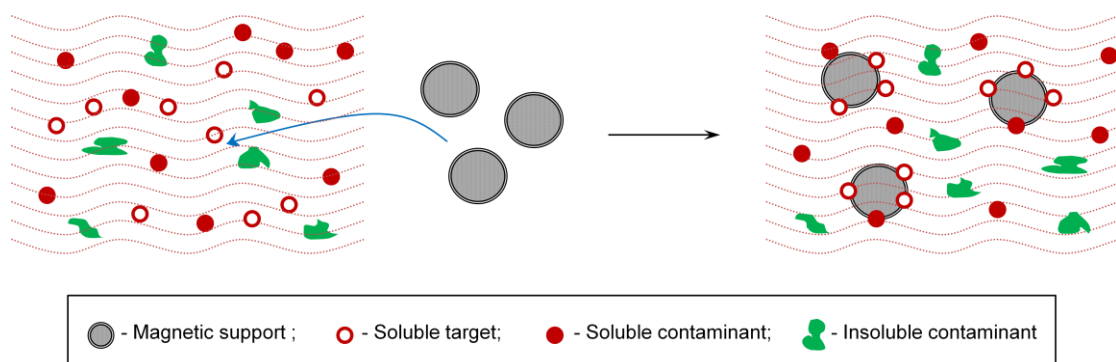


Figure 1.3. Target material adsorbed onto magnetic supports

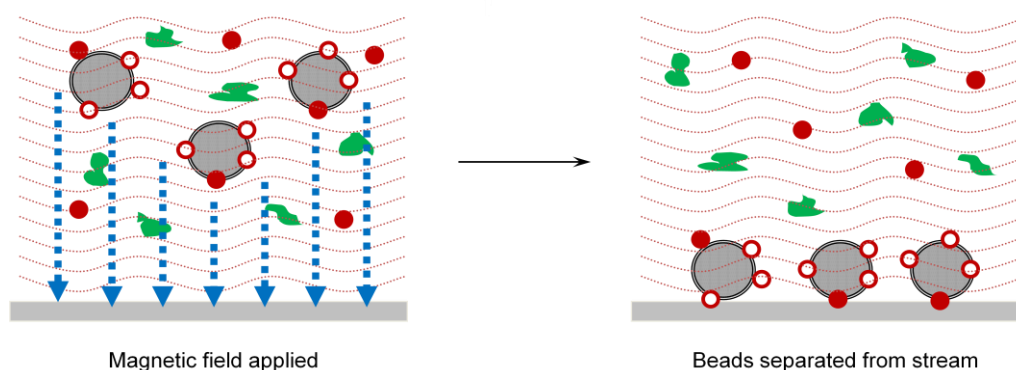


Figure 1.4. Target loaded supports magnetically separated from stream

Commercial availability of magnetic supports began during the late 1970's, with the appearance of the Enzacryl FEO-(M) and Magnogel products. These were soon replaced by improved beads from manufacturers such as BioMag, Dynabeads and Estapor M, leading to increased interest in magnetic supports for a variety of applications including cell separation; immunoassays; and the isolation of viruses and organelles. Since then magnetic nanoparticles have found use in a variety of applications including protein separations based on ion-exchange (Lee et al, 2003) and metal affinity methods (Ma et al, 2005).

Magnetic nanoparticles have also been shown to have a number of biological uses. For example, in MRI techniques for detection of specific enzymes and viruses (Perez et al., 2003; Perez et al., 2004); for in vivo detection of cancer cells (Huh et al., 2005; Song et al., 2005) and as agents to induce selective bioelectrocatalyses and amplify DNA detection (Katz and Willner, 2005; Katz et al., 2004). A variety of synthetic methods including for production of magnetic supports have been identified, including iron oxides mixed with silica (Liu et al, 2004); agar (Tong and Sun, 2009); and emulsified polymers (Odabas, 2004).

The potential of large scale protein separations based on magnetic supports has been demonstrated using the High Gradient Magnetic fishing method (HGMF) (Hubbich and Thomas, 2002). HGMF combines magnetic support properties with

the High Gradient Magnetic Separator (HGMS) techniques already available in mineral processing industries to achieve rapid separation of product-loaded supports from their suspending liquor. Compared to similar techniques used in large-scale primary product capture such as Expanded Bed Adsorption chromatography (EBA), HGMF shows advantages in terms of product selectivity, processing speed and performance in the presence of suspended solids and foulants (Hubbuck et al, 2001).

Developments in magnetic support separations lead to techniques which can avoid problems inherent to separations based on porous supports. Binding on porous supports occurs by diffusion of soluble material into the pores, followed by binding. Wash steps remove those materials which were too large to enter the support and which remain unbound, while elution steps are aimed at removing those materials which are bound within the pores (figure 1.5).

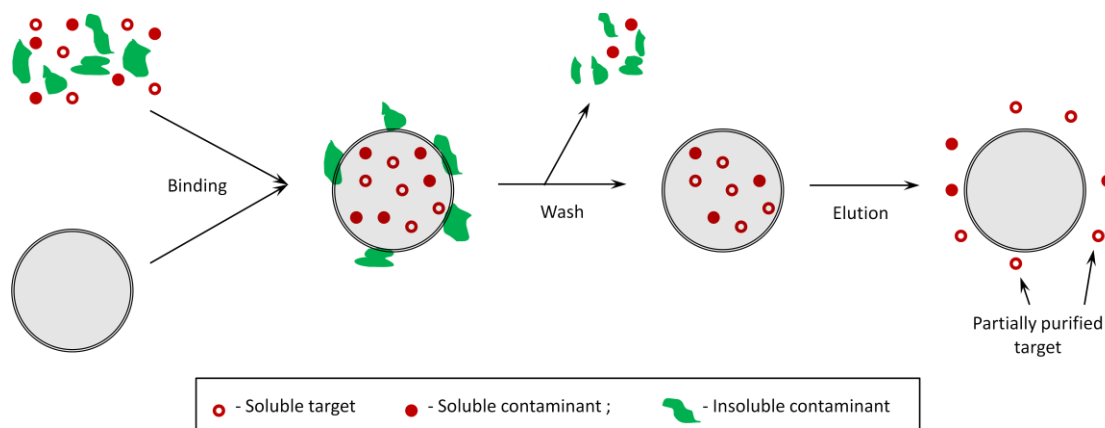


Figure 1.5. Adsorption on porous supports

The extensive framework of pores within each bead leads to a large surface area on which protein binding can occur. As most of the surface area exists within the support the surface area is largely independent of the bead size. Fouling in porous supports stems from a difficulty in removing materials which have diffused into the pore network. Biological foulants and suspended solids can become lodged in pores, making cleaning and re-use of supports difficult (Halling and Dunnill, 1980). Foulants trapped in pores are harder to remove than those which are adsorbed at the external surface of the beads. Foulants are displaced by

interaction with the surrounding fluid and experience a much weaker fluid force within the pores than on an external surface (figure 1.6).

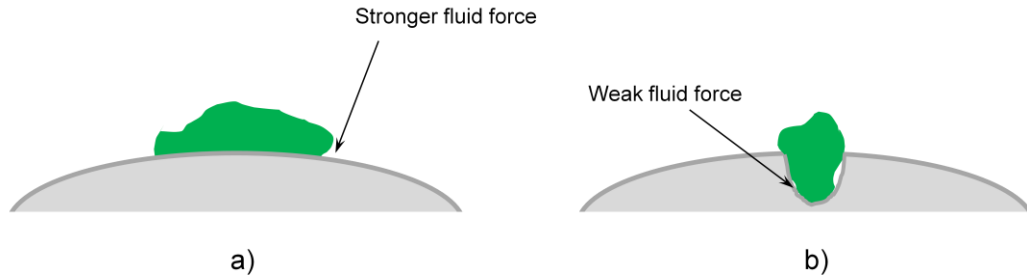


Figure 1.6. Fouling by insoluble contaminants by adsorption at an external surface (a) and by lodging within a pore (b).

The absence of this pore contamination behaviour makes non-porous supports less prone to fouling than porous supports, and easier to clean after fouling (figure 1.7.; O'Brien et al. 1996).

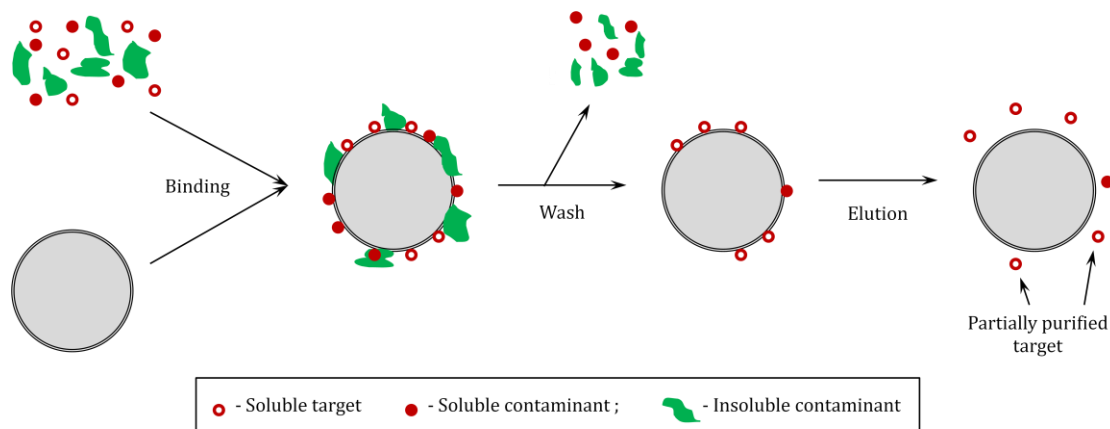


Figure 1.7. Adsorption on non-porous supports

As only the external surface of the bead is involved in binding (figure 1.7), non-porous supports have a lower surface area than the equivalent porous supports and a lower binding capacity for a certain bead size. The surface area available on non-porous supports can be maximised by using smaller bead sizes ($\sim 1 \mu\text{m}$ diameter), as smaller non-porous beads have greater surface area per unit mass. Supports of these dimensions create problems when used in fixed bed (high

pressure drops) and fluidised bed (particles are eluted too readily) techniques, so stirred tank methods must be used. Unclarified industrial feedstocks will typically contain suspended biological solids and colloids of similar size to the protein-loaded supports, making separation of the supports difficult using conventional methods. The incorporation of magnetic properties into non-porous supports allows selective removal of support and bound protein from the bulk of non-magnetic feedstock components. In this way magnetic separation techniques offer a route to protein purifications with lower rates of support fouling than are possible when using conventional methods.

1.2.3 Magnetic separation theory

Magnetic separations rely upon interactions between magnetic supports and an applied magnetic field. The theory of these interactions is described here. The force due to magnetism, F_m , experienced between two parallel wires carrying currents with strength I_1 and I_2 , is given by equation 1.1.

$$F_m = \frac{\mu I_1 I_2 L}{2\pi r}$$

Equation 1.1.

Where L is the length of the wires, r is the distance between the wires and μ is the permeability of the medium between the conductors. In the case of solids within a suspension, this force can instead be expressed by equation 1.2 (Gerber and Birrs, 1983; Svoboda, 1987):

$$F_m = \frac{1}{2} \mu_0 V_s (\chi_s - \chi_f) \nabla(H^2)$$

Equation 1.2.

Where F_m is the magnetic force that a magnetic gradient, $\nabla(H^2)$, places upon a solid of volume V_s and magnetic susceptibility χ_s , in a fluid of susceptibility χ_f . In

the case of magnetic particles suspended in a non-magnetic fluid ($\chi_s - \chi_f$) is non-zero for the supports and approximately zero for all other components. This leads to a net force acting upon the magnetic particles, allowing their selective separation from the other fluid components.

The magnetic flux density, B , experienced by a wire can be calculated from its length, L , combined with the current it carries, I , and the magnetic force which it experiences, F_m (equation 1.3).

$$B = \frac{F_m}{I \cdot L}$$

Equation 1.3.

For a wire which has been coiled to form a cylinder the flux density inside the coil is given by equation 1.4

$$B = \mu_0 \cdot \mu_r \cdot I \frac{n}{L}$$

Equation 1.4.

where n is the number of windings, μ_0 is the permeability of free space and μ_r is the permeability of a vacuum. The magnetic field intensity, H , is independent of μ_0 and μ_r and is defined by equation 1.5

$$H = I \frac{n}{L}$$

Equation 1.5.

From this it can be seen the the flux density is related to the magnetic field strength, H , by equation 1.6

$$B = \mu_0 \cdot \mu_r \cdot H$$

Equation 1.6.

When a body is subjected to an external magnetic field, the difference between the flux density inside the body, B_{inside} , and flux density outside the body, B_{outside} , is termed the magnetic polarisation, J .

$$J = B_{\text{inside}} - B_{\text{outside}}$$

Equation 1.7.

The difference between magnetic field strength inside the body, H_{inside} , and that outside, H_{outside} , is known as the magnetisation, M (equation 1.8).

$$M = H_{\text{inside}} - H_{\text{outside}}$$

Equation 1.8.

Plots of magnetisation vs. applied magnetic field strength for different materials tend to show certain characteristic responses. (see figure 1.8).

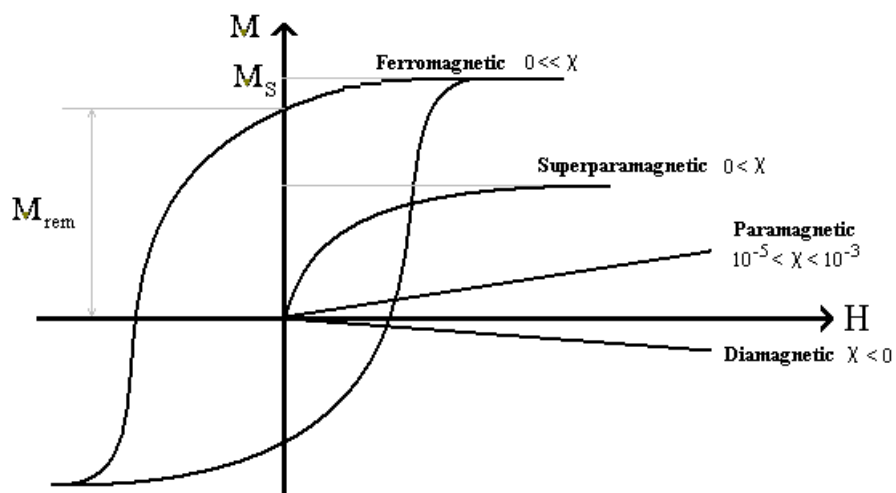


Figure 1.8: Characteristic behaviour of the general magnetic material groups, showing relationship between: applied field strength (H); magnetic susceptibility of

material (χ); magnetisation (M); saturation magnetisation (M_s) and remnant magnetisation (M_{rem}).

The relationship between M and $H_{outside}$ is related to the magnetic susceptibility, χ , of the material (equation 1.9), where the size of χ determines the responsiveness of the material in a magnetic field.

$$M = \chi \cdot H_{outside}$$

Equation 1.9.

This magnetic behaviour of materials stems from the magnetic moments of electrons within that material (West, 1988). Diamagnetic materials typically possess a small, negative χ value (-10^{-4} to -10^{-9}), due to the magnetic moment created by paired electrons as they orient against the direction of an applied magnetic field. Diamagnetic materials (e.g. water, carbon) are those which possess few unpaired electrons and appear non-magnetic in most situations, although they show repulsion in very strong magnetic fields (Simon and Geim, 2000). Paramagnetic materials have larger, positive χ values (10^{-6} to 10^{-3}) generated by unpaired electrons and their tendency to align with the applied magnetic field. Paramagnetic materials (e.g. oxygen) contain localised unpaired electrons and exhibit more obvious magnetic behaviour, being attracted to applied magnetic fields. The localisation of unpaired electrons in paramagnetic materials means that magnetisation occurs by interaction of each electron with the applied magnetic field individually. The unpaired electrons do not interact with one another and in the absence of the applied field their magnetic moments resume a random orientation.

The magnetic susceptibilities of ferro and ferromagnetic materials are significantly larger in weak fields (χ up to 10^5) but after a saturation point is reached χ may reach values of less than 1. In contrast to paramagnetic materials, the unpaired electrons in ferromagnetic materials do interact with one another, aligning not only

with the direction of an applied magnetic field but also with the magnetic moments of the unpaired electrons nearby. On the macro-scale this leads to ferromagnetic materials forming magnetic *domains* within a particle within which there is a general alignment of the magnetic moment of electrons (figure 1.9). The overall magnetisation of the particle is a result of the combined magnetisation of all domains. A change in the magnetisation of the particle by an applied field is caused by a movement of the domain boundaries. Energetic considerations result in the domain boundaries retaining some of their new structure once the magnetic field has been removed. This leads to a residual magnetisation effect, known as hysteresis (Ewing and Klaassen, 1893).

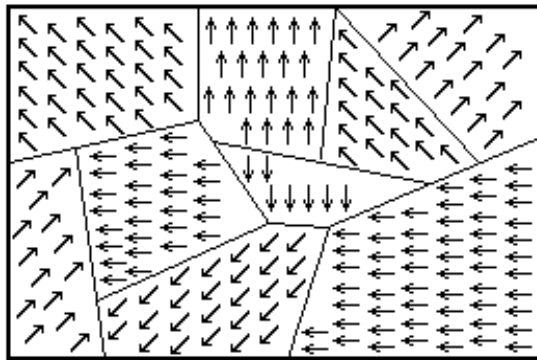


Figure 1.9: A ferromagnetic particle, containing a number of magnetic-alignment domains

For application in magnetic supports, magnetic hysteresis is not desirable. It is vital that magnetic adsorbents do not retain magnetisation, as otherwise permanent particle agglomeration would be unavoidable and desorption, cleaning and re-use of the adsorbents would be compromised. In order to take advantage of the high magnetisation possible with ferromagnetic materials without hysteresis effects, superparamagnetic particles may be formed using ferromagnetic materials with nano-scale dimensions.

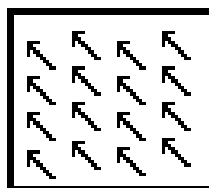


Figure 1.10: A superparamagnetic particle, containing only one domain.

In nano-scaled, ferromagnetic materials the particle is only large enough to contain one domain (figure 1.10). As a result there is no boundary movement on application of a magnetic field and no hysteresis (Elmore, 1938; Kittel, 1946; Bean et al., 1959), leading to superparamagnetic behavior.

1.3 Adapting magnetic supports for bioseparations

1.3.1 Polymer brush chemistry

Polymer chains in solution adopt a randomly coiled conformation but when they are grafted with sufficient density to a surface the chains overlap and a stretched 'polymer brush' conformation is achieved (DeGennes, 1976; Milner 1991). This conformation results from overlap and interaction between the grafted chains (Halperin et al., 1992; Jones et al, 1999) and gives the polymer brush layer significantly different behaviour to that seen for free polymers (Alexander, 1977; Klein et al., 1993;). The properties of polymer brushes have led to them finding applications in surface lubrication (Klein et al., 1994) and colloid stabilization (Fritz et al., 2002). For polymers grafted to a solid surface, three distinct types of polymer formation have been identified (figure 1.11.)

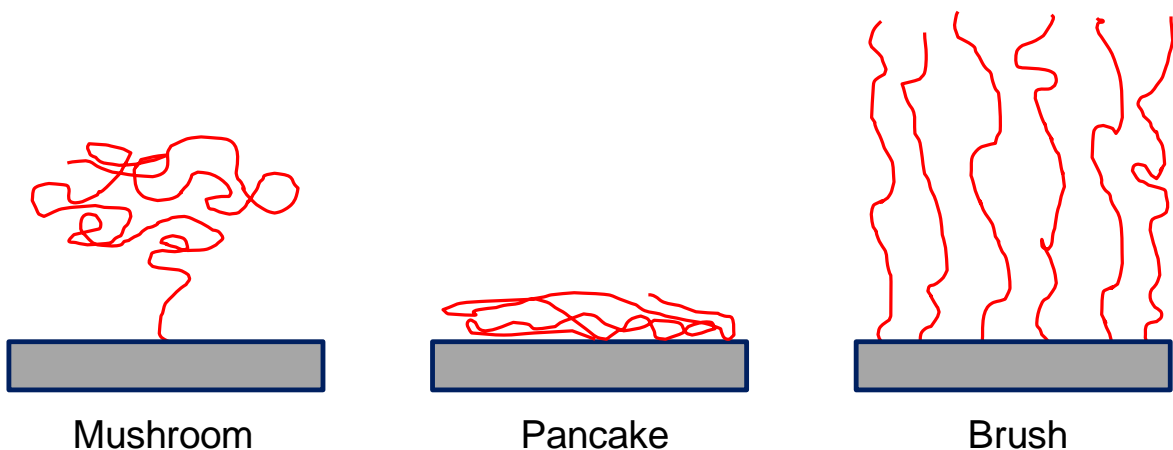


Figure 1.11. Mushroom, pancake and brush conformations of polymers attached at a surface (after Advincula et al, 2004).

1. When the spacing between graft sites is much greater than the length of the grafted polymer, interaction between polymer chains is too small to create a stretched polymer brush layer. In situations where polymer-surface interactions are favourable the polymer chains will flatten out in a 'pancake' conformation across the surface. If polymer-surface interactions are weak or unfavourable a 'mushroom' conformation is seen instead.
2. When the spacing between graft sites is significantly smaller than the polymer chain length the chains will stretch and extend away from the surface in order to minimise overlap with each other.

The relationship between brush and non-brush formations can be expressed in terms of the free energy of the grafted polymer system. The preferred polymer conformation is that which produces the lowest free energy state (Alexander, 1977). The overall free energy is a combination of the elastic energy F_{el} and the interaction energy F_{int} (equation 1.10).

$$F = F_{el} + F_{int}$$

Equation 1.10.

F_{el} is higher in polymer brush formations, where the rigid, stretched chain conformation results in a loss of entropy. F_{int} is higher for non-brush formations, where chain overlap has not been minimised. As graft density and chain length increase so does the favourability of minimising F_{int} by adopting a brush formation.

The Flory radius of a grafted polymer relates to the expected 'random walk' of the polymer chain end from its point of attachment (Bartucci et al, 2002). This radius can be calculated from the length of the chains in monomer units, L , the monomer size, A_m , and the Flory exponent, ν , which is dependent upon solvent-polymer interactions (equation 1.11).

$$R_f \approx A_m L^\nu$$

Equation 1.11.

The transition from a collapsed structure begins as the value of $2R_f$ reaches that of the intergraft distance, D . At this value it becomes possible for adjacent polymer chains to overlap with one another, promoting chain extension. As the value of R_f rises compared to D chain overlap and extension increase, resulting in highly extended brush structures at values of $R_f \gg D$ (Unsworth et al., 2005) (figure 1.12).

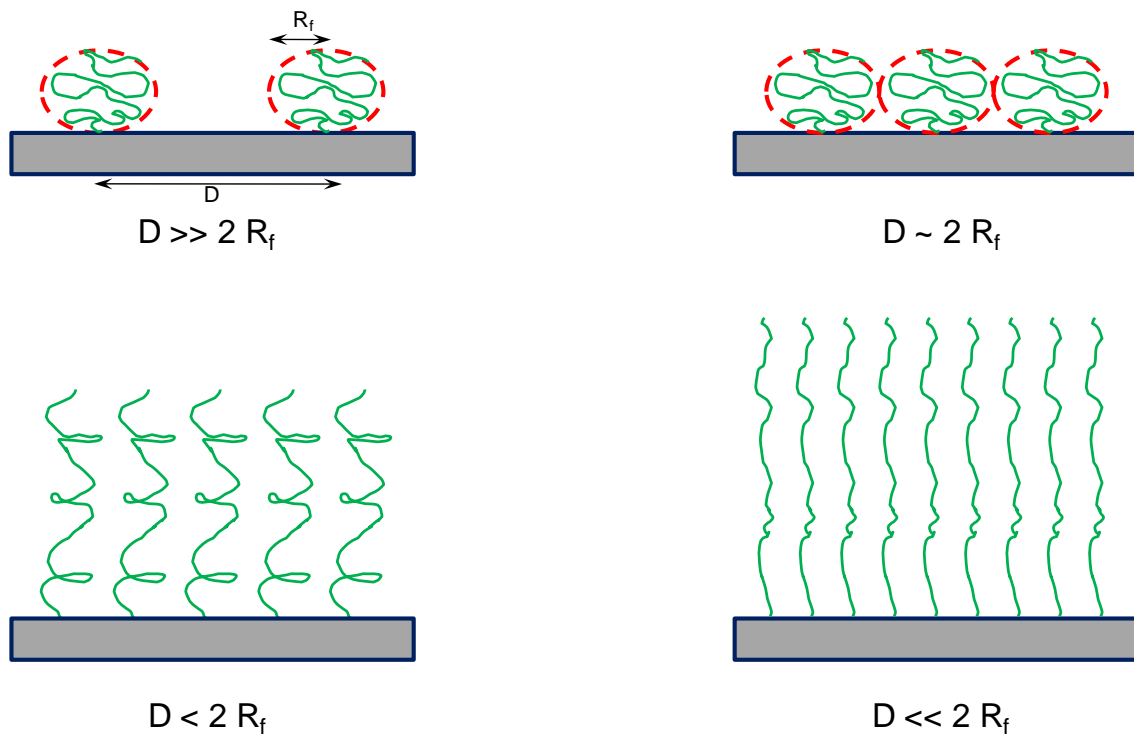


Figure 1.12. Relationship between grafted polymer structure, R_f and D (from Unsworth et al., 2005)

1.3.2 Switchable behavior in polymer brushes

Polymer brushes show height and density variations when exposed to different solvent conditions (Sidorenko et al, 1999; Minko et al., 2002). The presence of a good solvent for a grafted polymer promotes extension of polymer chains, while the presence of a poor solvent promotes collapse of the chains (figure 1.13).

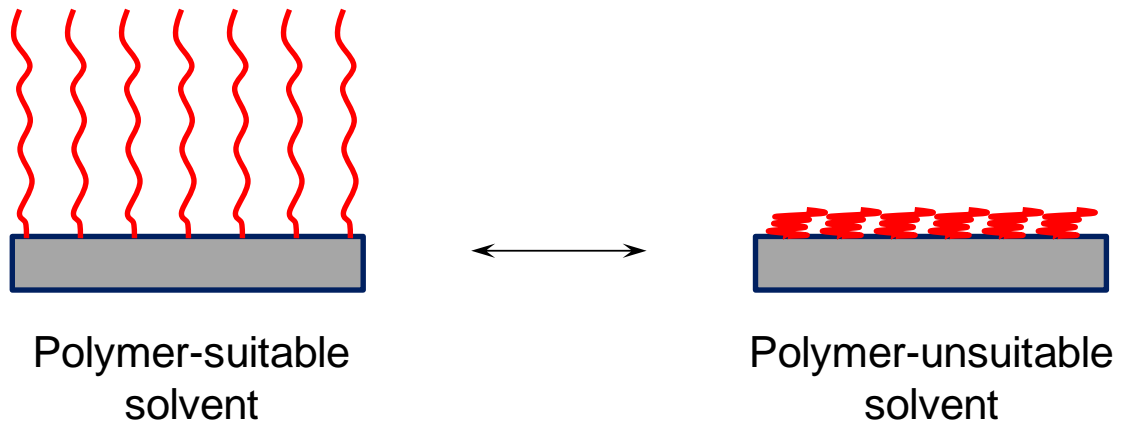


Figure 1.13. Polymer brushes may expand or collapse depending upon solvent conditions

Mixed polymer brushes are those consisting of two or more different polymers grafted onto the same surface. These polymers segregate laterally into nanoscopic phases across the surface (Draper and Luzinov, 2004). Due to layered and lateral segregation effects mixed polymer brushes also show surface composition variations under different solvent conditions. When exposed to a nonselective solvent, each type of polymer will be exposed on the top of the brush. In selective solvents a layered segregation may also be seen, with preferential segregation of one particular polymer to the top of the brush while another polymer segregates close to the grafted surface ((figure 1.14; Ionov, Houbenov et al, 2004). In this way the surface composition properties of a mixed brush can be controlled by altering its environment.

Using silica wafers as a grafting surface, electrolytic polymer brushes have been made which respond controllably to environmental effects such as pH or temperature (Ionov, Sidorenko et al., 2004; Balamurugan et al., 2003). These include brushes formed with an acidic polymer such as poly(acrylic acid) (PAA) grafted beside a basic polymer such as poly(2-vinyl pyridine) (P2VP) creating a mixed polyelectrolyte brush layer.

Switchable behaviour in the PAA/P2VP mixed brush results from the electrostatic repulsions which occur between the units in P2VP at low pH, or the repulsions between units in PAA at high pH. Previous studies on mixed brushes composed of P2VP and PAA grafted at a silica surface (Houbenov et al, 2003) indicate that the mixed brush surface is predominantly P2VP below pH 3.2 and predominantly PAA above pH 6.7, with ellipsometric measurements showing that the brush layer is much thicker above pH 6.7 and below pH 3.2 than at the intermediary pH values. This behaviour stems from the response of the P2VP and PAA polymer side-units to changing pH conditions.

P2VP has a pK_b of 7.1 (Imanishi et al., 1973) where K_b is give by equation 1.12:

$$K_b = \frac{[H^+][P2VP \text{ (neutral)}]}{[P2VP \text{ (protonated)}]}$$

Equation 1.12.

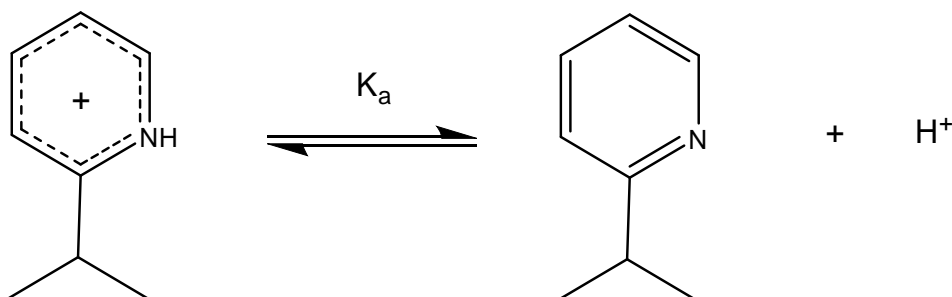


Fig 1.16. Neutral and protonated forms of P2VP side group.

P2VP side groups become increasingly positively charged as the environmental pH is lowered, with protonation of P2VP side units approaching 100% at pH values below 7 (figure 1.16).

PAA has pK_a 4.5 (Govender et al., 1999), with K_a given by equation 1.13:

$$K_a = \frac{[H^+][\text{PAA (deprotonated)}]}{[\text{PAA (neutral)}]}$$

Equation 1.13.

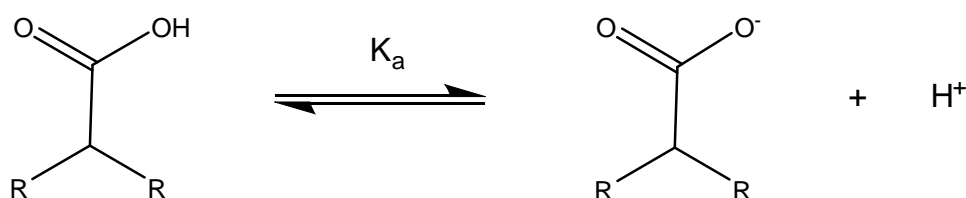


Figure 1.17. Neutral and deprotonated forms of PAA side group.

PAA side groups become deprotonated as the environmental pH increases, with deprotonation of the side units approaching 100% at pH values above 5.

The combined effect of P2VP and PAA chains grafted in a mixed brush layer is that at pH 4.9 the positive charge on P2VP and the negative charge on PAA compensate for each other and create a surface with no overall charge (Houbenov et al, 2003). At higher pH values a larger proportion of negatively charged PAA side groups are present. The presence of more charged side groups causes the layer thickness to increase compared to pH 4.9, as repulsion between like-charged side groups cause the chains to expand (figure 1.18). Similarly, at low pH values a higher proportion of positively charged P2VP side groups are present and the brush layer is thicker than at pH 4.9.

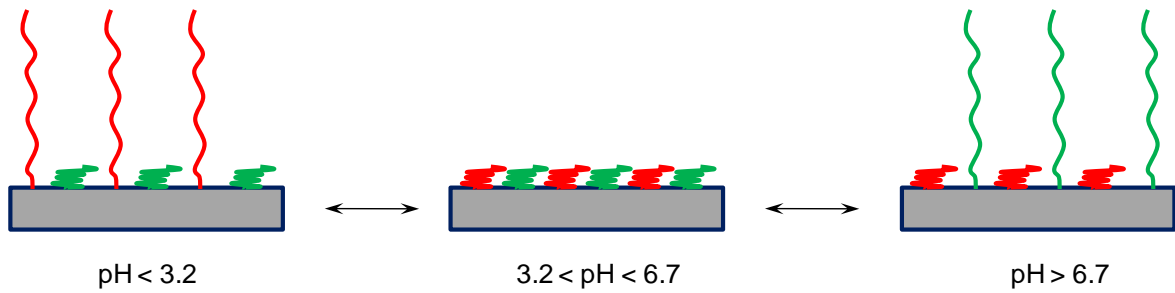


Figure 1.18: Mixed polymer consisting of P2VP (red lines) and PAA (green lines) showing brush expansion and collapse at different solvent pH values.

1.3.3 Ion exchange

Separation of proteins using ion-exchange (IEX) methods has been performed since the late 1940s (Janson and Ryden, 1998) and has since become, due to the prevalence of ion-exchange chromatography (IEC), the most commonly found technique in protein purification. IEC is included in approximately 75% of purification protocols (Bonnerjea et al., 1986) and accounts for about 40% of all purification steps found in these protocols (Janson and Ryden, 1998). This widespread usage of IEX methods stem from the high binding capacities, versatility and straightforward principles of operation.

The principle of IEX is based upon competition between charged proteins and salts for binding sites on the ion exchange material. The energy of these interactions can be approximated using Coulomb's law (equation 1.14).

$$\Delta E \propto \frac{Z_A Z_B e^2}{r_{AB}}$$

Equation 1.14.

where ΔE is the energy difference in charge interactions between two point charges, Z_A and Z_B , when they are brought from points of infinite separation to a

distance r_{AB} from each other (Ladisch, 2001). Coulomb's law indicates that the strength of binding is proportional to the charge on the molecule and for ΔE to be favourable Z_A and Z_B must be oppositely charged. In reality ion-exchange interactions are more complex than the simple model of Coulomb's law. The protein and support are not point charges (Kopaciewicz et al., 1983) and each charge interacts with a number of other charges simultaneously (Chicz and Regnier, 1988). However, the overall principle of Coulomb's law is correct for ionic binding of proteins.

The supports used for IEX separations are insoluble matrices with covalently attached charged groups. The presence of charged groups allows the support to bind charged protein groups, with the binding behavior being dependent on the pK_a of the support groups and pI of the protein. A protein with a positive net charge will bind to a support containing carboxylate groups, or other anion-generating groups which give the support a net negative charge (figure 1.19). Similarly, a protein with a negative net charge will bind to a support which has a net positive charge on its surface. Supports which carry many cationic groups and have a strong positive charge at neutral pH are anion exchangers and can be used to separate anionic proteins from mixtures. Supports with a strong negative charge at neutral pH are cation exchangers and can be used to separate cationic proteins (Haddad and Jackson, 2000).

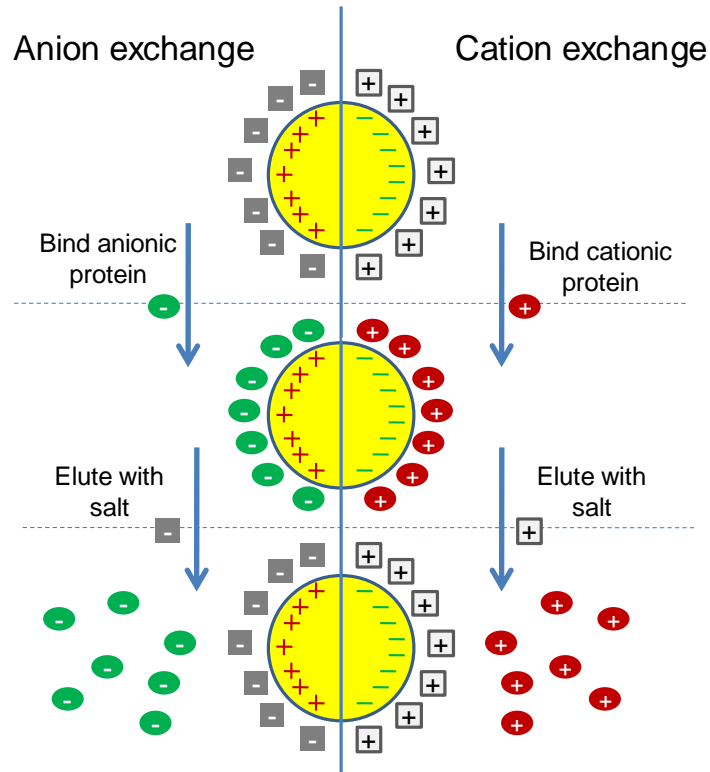


Figure 1.19. IEX binding and salt elution principle

IEX separations are based on charge-charge interactions between immobilized charges on an exchange support and charges found on the protein surface (Ladisich, 2001). IEX can take the form of anion exchange, with a positively charged support binding negatively charged proteins; or cation exchange, with a negatively charged support binding positively charged proteins. The protein mixture which is to be separated is adjusted to a suitable pH using a low ionic strength buffer. The chosen pH is one at which the support and the desired protein are oppositely charged and will share an ionic attraction. A binding step is followed by washing to remove weakly bound material and then elution stages designed to break charge-charge attractions between the protein and the support surface. This elution can involve reversing the pH to make charge interactions between the support and protein unfavourable, or using an elution buffer with salt concentration suitable for causing the release of bound proteins (figure 1.20).

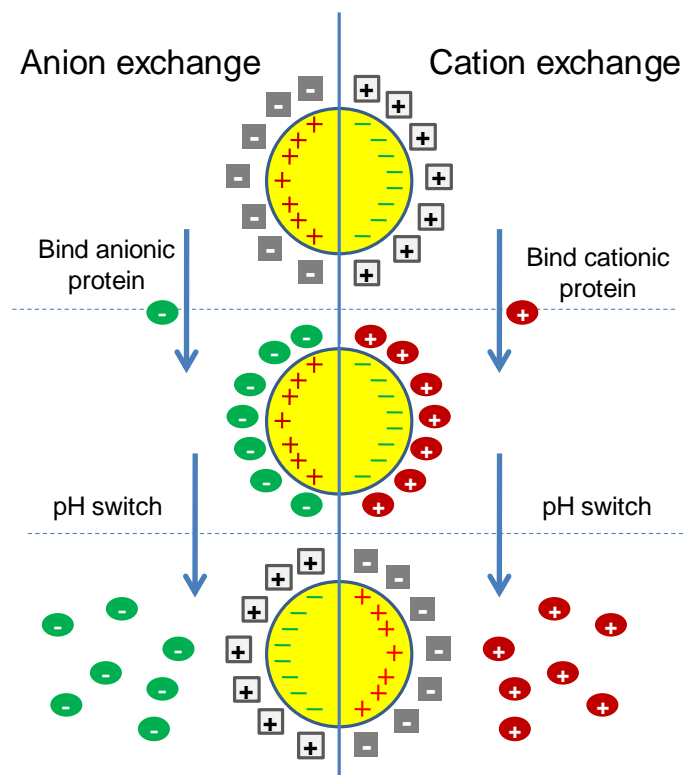


Figure 1.20. IEX binding and pH switching principle (pH switch during elution reverses charge on protein)

1.3.4 Switchable polymer brushes as ion exchange surfaces

Polyelectrolyte brushes grafted onto a surface are a source of IEX interactions (Ballauff and Borisov, 2006) with previous studies showing that charged polymer brushes can act as suitable ligands for protein binding by both cation and anion exchange (Kawai et al., 2003; Savina et al., 2006; Bayramoglu et al., 2007).

By combining responsive polymer brushes with the currently available superparamagnetic adsorbents it may be possible to produce adsorbents which are capable of not only selectively binding proteins, but also of enhanced pH elutions and self-cleaning behaviour (figure 1.21).

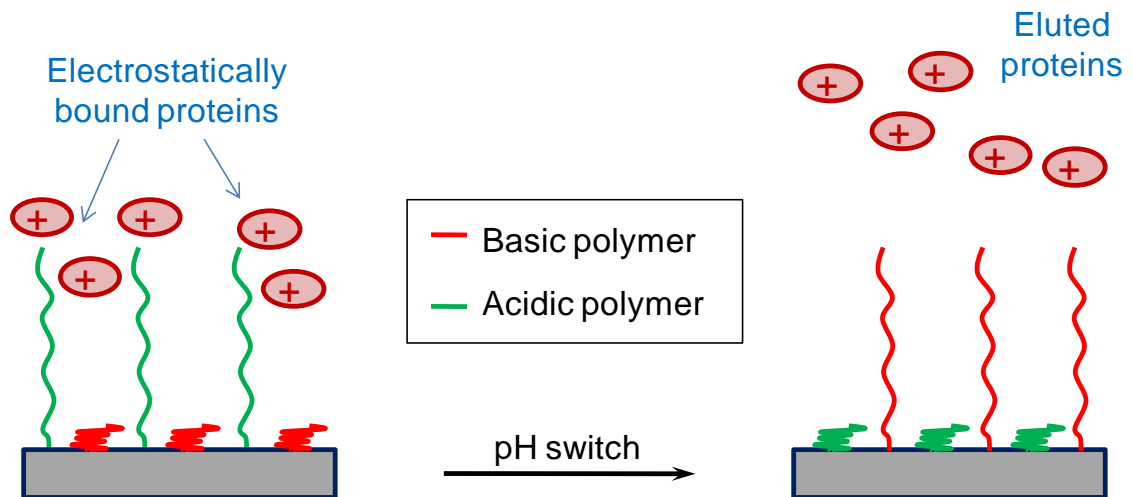


Figure 1.21: Release of basic proteins from acidic, deprotonated polymer by increasing pH (neutralisation of acidic polymer and protonation of basic polymer).

This elution technique is based around two properties of mixed polyelectrolyte brushes (Houbenov et al, 2003).

1. Switching of pH results in collapse/extension behaviour of the polymer brush. Under binding pH conditions, proteins at the surface undergo attractive interactions with the extended polymer brush layer. Following a switch to elution pH conditions the charge repulsion between bound protein and polymer brush are accompanied by a physical 'push' as the proteins uncounters a like-charged polymer brush extending out from the surface (figure 1.21).
2. The presence of both basic and acidic polymers at the surface allows the adsorbent to carry a strong negative or strong positive charge, depending upon the pH. This enhances the charge-repulsion aspect of pH elutions.

1.3.5 Synthesis of polymer brushes on magnetic supports

Polymer brushes are generally tethered by either physisorption or covalent grafting techniques. In physisorption methods the polymer may be tethered by a functionalized end-group or the polymer itself may be a diblock copolymer, in which one block adheres to the surface while the other block is extended (Belder et al., 1997). The absence of chemical bonding between polymer and surface in physisorption techniques leads to the creation of polymer brushes which are unstable to both thermal and solvent effects.

Covalent grafting techniques, on the other hand, form polymer brushes which display significantly higher stability. Covalent grafting of polymer brushes can be performed using either a 'graft to' or 'graft from' approach. 'Graft to' involves the reaction of polymer chain end-groups with the surface leading to formation of a covalent bridge between the polymer and surface (Mansky et al., 1997). This method allows for good control of the polymer chain structure, as the attached polymer is preformed prior to the grafting reaction. Polymer brushes created by covalent graft-to methods typically have low grafting density and brush thickness. These limitations relate to the difficulty of large polymer chains to diffuse to sterically hindered reactive sites (figure 1.22).

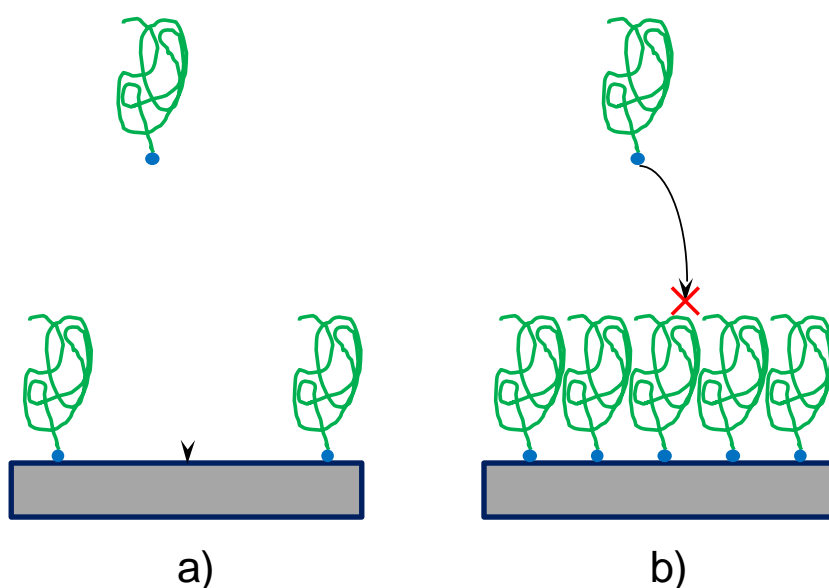


Figure 1.22. 'Graft-to' mechanism: a) Attack by reactive end-group at surface; b) Hinderance to further attack by surface grafted polymers. (Adapted from Advincula, et al., 2004)

Degrading of graft-to polymer brushes has been observed, due to low grafting density allowing small, reactive molecules to attack the brush grafting points (Tran, Auroy, 2001). This problem can be overcome by using graft-to techniques which lead to the creation of a polymer-surface bond which is not susceptible to attack by nucleophiles or electrophiles. For example the formation of stable ether, sulfonyl ether or amine links through attack by hydroxyl, sulfonyl or amine groups at surface carbon sites which have been activated to nucleophilic attack.

'Graft from' techniques involve synthesis of the grafted polymer from an initiator on the grafting surface (figure 1.23; Manksky et al., 1997). The initiation and subsequent synthesis can be based on radical, ionic or metathesis techniques. As each step in a graft-from synthesis involves reaction of a small group with the surface or grafted polymer chain end the steric limitations are much less than those seen for graft-to methods, making higher graft densities possible (Advincula et al., 2004).

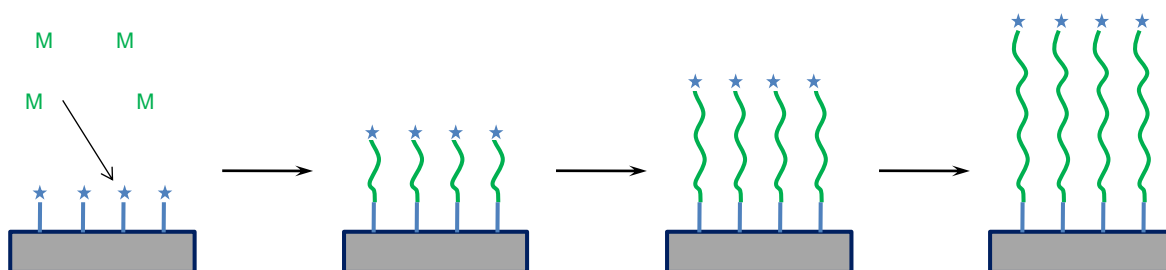


Figure 1.23. Graft from synthesis by propogation from a surface initiator site

'Graft from' synthetic techniques include free radical polymerisation (Zhao and Brittain, 2000), in which a radical is generated on a group at the surface leading to propagation from the surface by reaction with vinyl or allyl monomers. 'Living' radical polymerisation methods, such as reversible addition-fragmentation transfer

(RAFT) (Tsuji et al., 2001) and atom transfer radical polymerisation (ATRP) (Ejaz et al., 1998), offer a route to higher monodispersity of grafted chains through control of radical concentration. In the case of RAFT this involves exchange of radicals between propagating polymer chains and a dithioester compound. For ATRP this exchange is performed by a copper halide catalyst.

Non-radical graft from techniques such as cationic (Jordan and Ulman, 1998), anionic (Advincula et al., 2002) and ring-opening metathesis polymerisation (ROMP) (Weck et al., 1999) have also been used to create surface tethered polymer layers with dimensions well within the brush regime.

1.3.6 Characterisation of polymer brushes

A variety of characterization techniques have been applied to polymer brushes synthesized on flat surface. These include:

Infrared (IR) spectroscopy, which can be used to monitor IR responsive functional groups, even at monolayer thickness (Kawaguchi et al., 1988).

X-ray and neutron diffraction, used to find the distance between polymer graft points at the surface (Mendelsohn et al., 1995; Levy et al., 1998).

X-ray and neutron reflectometry, to find the thickness of grafted polymer brush layers (Kawaguchi et al., 1988).

UV-vis spectroscopy, which allows polymer film build-up to be followed (Advincula et al., 2004). Fluorescence spectroscopy is also suitable for following the build-up of polymer brushes which contain fluorescent probes.

X-ray photoelectron spectroscopy: has been used to monitor abundances and oxidation states of atoms within the polymer brush (Kong et al., 2001).

Ellipsometry is commonly used to find the polymer brush layer thickness and can be used to estimate the molecular weight of graft-from polymer brush chains (Habicht et al., 1999; Jordan et al., 1999).

Scanning electron microscopy (SEM), atom force microscopy (AFM), optical microscopy and scanning tunneling microscopy (STM) can be used to characterize polymer brushes by mapping the topology and morphology of the surface (Iwata et al., 1997); identifying polymer phase segregations and patterning (Boyes et al., 2002); measuring surface forces (Yamamoto et al., 2000) and estimating molecular weights of grafted chains (Al-Maawali et al., 2001).

Contact angle measurements allow analysis of surface energy, providing information on surface morphology, composition and wetting behavior (Juthongpiput et al., 2003).

Electrochemical methods can be used to determine the redox activity and ion mobility within the polymer brush (Anne and Moiroux, 1999).

These techniques are well suited to the investigation of polymer brushes on flat, fixed surfaces. The application of such techniques to polymer brushes on suspended magnetic particles such as those used in magnetic separations is limited. Microscopy, reflectometry and diffraction techniques rely upon the base material being held in place, which is not possible for microscale magnetic particles. On-support characterisation of polymer brush layers is largely limited to techniques which can identify and quantify the presence of certain functional groups. The low vis/UV absorbance by the graft polymers of interest (P2VP/PTBMA) in comparison to higher absorbances from typical magnetic particles and other reagents which may be used in grafting, makes vis/UV analysis ineffective. Due to various other limitations, the most obvious technique for characterizing the composition of polymer brush grafted magnetic particles is Infrared spectroscopy.

The term infrared describes a region of the electromagnetic spectrum with frequencies lower than those of visible light but higher than those of microwave radiation (figure 1.24).

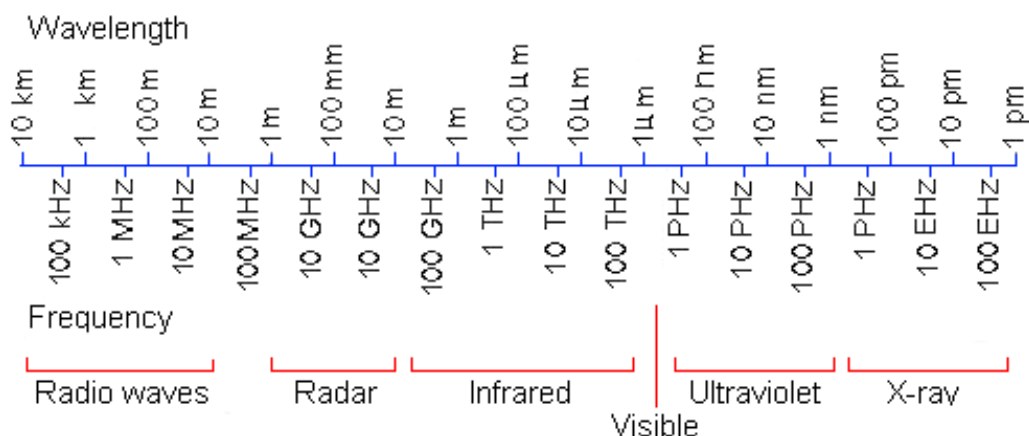


Figure 1.24. The electromagnetic spectrum

Infrared radiation can be further divided into three subsections; near-, mid- and far-infrared, so called because of their proximity to the visible spectrum. Near-infrared ($14000\text{-}4000\text{ cm}^{-1}$) is highest in energy and is useful for spectral analysis of overtone or harmonic vibrations in chemical bonds (Blanco et. Al, 2002; Shilli et al., 2002); mid-infrared is in the region $4000\text{-}400\text{ cm}^{-1}$ and can be used to identify fundamental vibrations in chemical groups (figure 1.25; Su et al, 2002; Bajaj et al., 1996); and far-infrared ($400\text{-}100\text{ cm}^{-1}$) measures the rotational spectrum of a sample (Bershtein and Ryzhov, 1994).

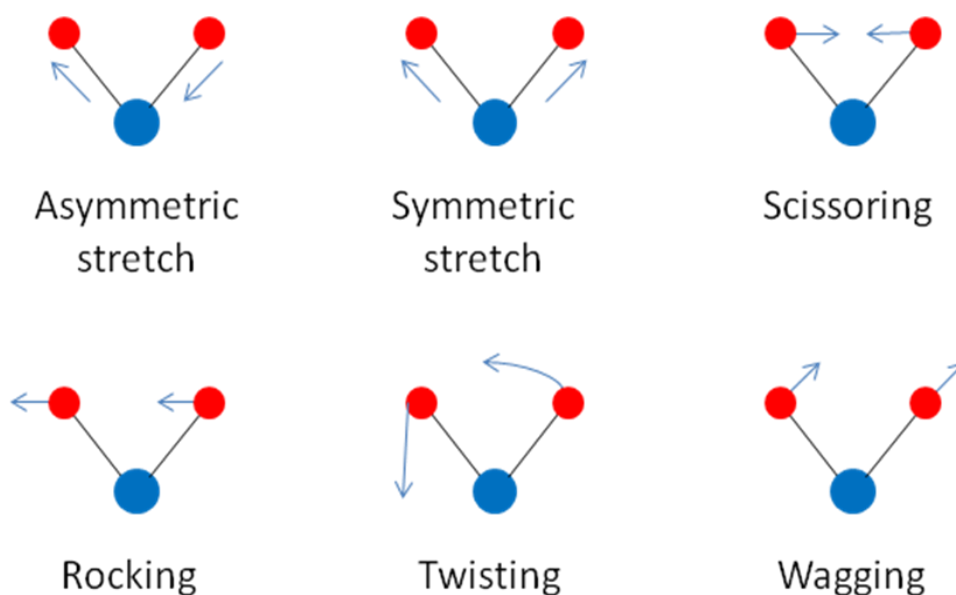


Figure 1.25. Vibrational modes which contribute to mid-IR spectra.

Infrared radiation can interact with molecules to cause rotations and vibrations within those molecules. Different molecules have different specific frequencies at which they will rotate or vibrate. These frequencies correspond to discrete vibrational/rotational energy levels which are specific to the structure and composition of the molecule (figure 1.26).

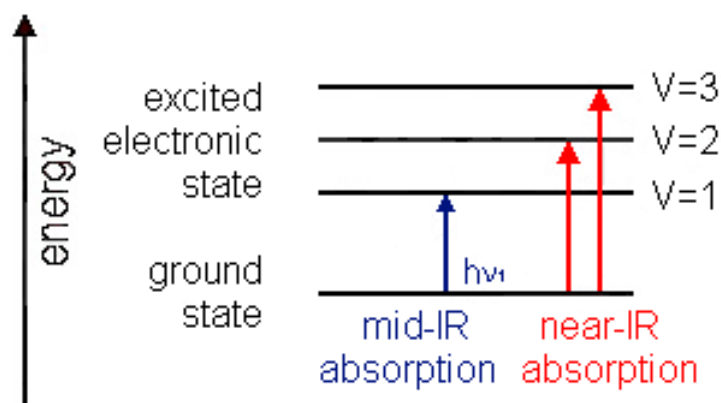


Figure 1.26. Absorbance of IR radiation leads to discrete electronic energy level shifts, with the difference in energy between ground state and excited state matching the energy of the absorbed photon.

For a vibrational mode to absorb infrared radiation the vibrational motion must be associated with a change in a permanent dipole. For this reason, vibrational modes typically indicate the presence of heteroatomic functional groups containing an electronegative atom. The resulting vibrational frequency will be related to both the strength of the bond and the mass of the atoms at either end. This means that bond frequencies can be assigned to particular bond types. Through infrared spectroscopy the specific frequencies at which a molecule absorbs can be found and from this vibrational modes and the chemical groups which cause them can be identified.

In Fourier Transform IR spectroscopy (FTIR) a spectrum is collected by passing pulses of infrared radiation through a sample and onto a detector. These pulses, called interferograms, are created by the out-of-phase combination of two infrared beams split from the same source. An interferogram contains all infrared frequencies in the range of interest and once passed through the sample, the beam and the original interferogram are used by a Fourier Transform program to calculate the infrared spectra of the sample. This spectra contains all of the frequencies from which the original interferogram was created. This fast 'pulsing' approach to obtaining an IR spectra allows multiple scans to be taken for each sample within a short timescale.

Quantification of sample composition can be performed using FTIR by comparing samples absorbance to the absorbance of calibration samples. The Beer-Lambert law relates the absorption of light following a certain path to the properties of the material it passes through on that path (figure 1.27).

$$\frac{I}{I_0} = 10^{-\alpha c}$$

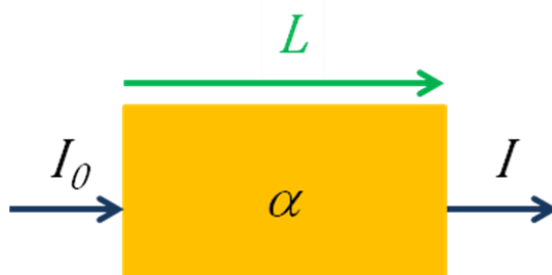


Figure 1.27. According to the Beer-Lambert law (above) the relationship between light intensity going into (I_0) and coming out of (I) a substance depends upon the concentration of the absorbing species (c) and the absorption coefficient of the absorbing species (α).

When passing radiation through samples containing a known set of absorbing materials with known absorption coefficients, it is possible to calculate the concentration of the materials based on the Beer-Lambert law. If extended to FTIR samples, the Beer-Lambert law suggests that quantification of polymer or monomer concentrations in FTIR samples can be determined by analysis of peak heights/areas using IR extinction coefficients obtained from samples containing known polymer or monomer concentrations.

Previous studies (Chen et al, 1998; Painter, 1981) have indicated that FTIR can be used for quantitative analysis of both liquid and solid samples. Grinding samples with KBr and pressing into discs allows each sample to be measured homogeneously, so that path lengths are consistent and the Beer-Lambert law can apply. Similarly, a liquid sample measured with an Attenuated Total Reflectance (ATR) method has a fixed path length in a given solvent so the Beer-Lambert law is also appropriate here. This method has been demonstrated to be useful in the quantification of polymer groups in samples (Johnck et al., 2000; Xu et al., 2001)

1.4 Choice of support

One suitable choice of non-porous beads for surface modification is M-PVA, available from Chemagen. These supports are available in large quantities at an affordable price. M-PVA consists of nano-sized magnetite/maghemite ($\text{Fe}_3\text{O}_4/\text{Fe}_2\text{O}_3$) particles encapsulated within a PVA matrix to form monodisperse, stable beads with a diameter of approximately $2\ \mu\text{m}$ (figure 1.28).

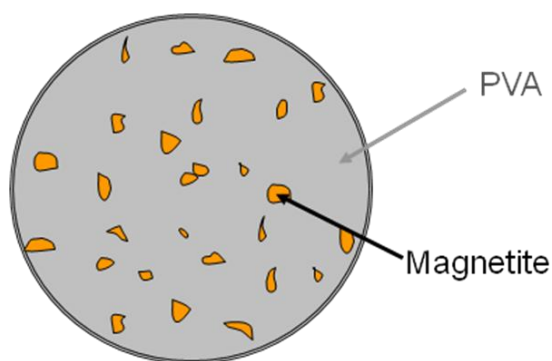


Figure 1.28. M-PVA: magnetite encapsulated in a PVA matrix.

Magnetite (the scientific name for lodestone) is an iron oxide with the chemical formula Fe_3O_4 . The atoms of magnetite are arranged in a spinel structure, which supports the presence of both the Fe(II) and Fe(III) states within the same crystal (figure 1.29).

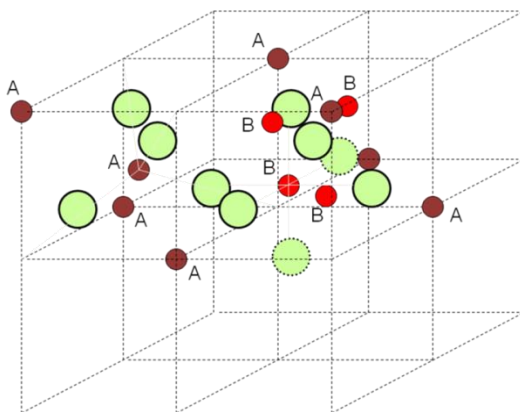


Figure 1.29: crystal structure of magnetite showing tetrahedral Fe sites (A), octahedral sites (B) and oxygen sites (green circles) (after Banerjee and Moskowitz, 1985)

Magnetite is a ferrimagnetic material. The properties of ferrimagnetic materials are largely the same as ferromagnetic materials, displaying high χ values when subjected to a low external magnetic field and saturation behaviour at higher magnetic fields. As with ferromagnetic materials, magnetite displays hysteresis behaviour, with multi-domain particles maintaining a residual magnetisation in the absence of a magnetic field. The nanosized particles used in M-PVA are sub-domain sized and do not display hysteresis effect. This gives the encapsulated particles superparamagnetic behaviour giving M-PVA a strong, hysteresis-free response to applied magnetic fields.

Poly(vinyl alcohol) (PVA) is a polymer consisting of a C-C bond backbone and 1 hydroxyl side group for every 2 backbone carbons. Although composed of vinyl alcohol subunits, PVA is not formed by polymerization of vinyl alcohol. Vinyl alcohol generally exists as its more stable keto tautomer, acetaldehyde (figure 1.30; Clayden et al., 2001) and is unsuitable for use in polymerisation reactions.

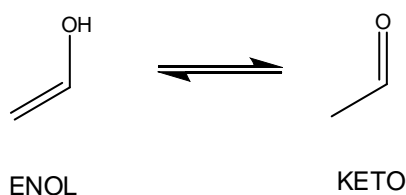


Figure 1.30. Tautomerisation of vinyl alcohol (enol) and acetaldehyde (keto).

PVA is instead synthesized via polymerization of vinyl acetate to produce poly(vinyl acetate) (figure 1.31).

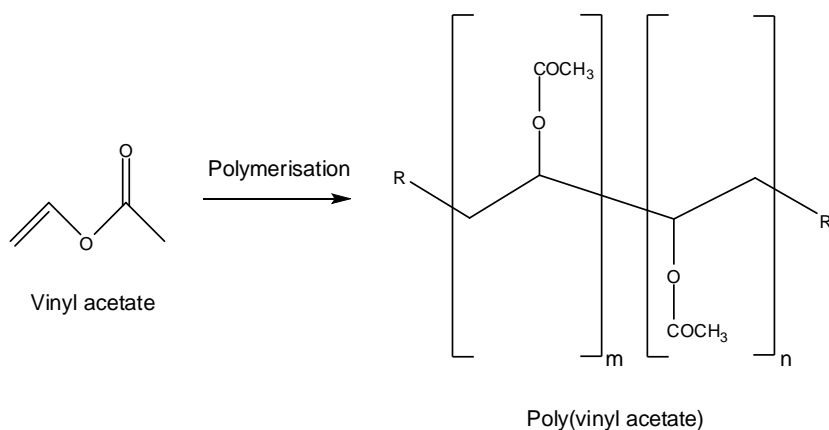


Figure 1.31. Synthesis of poly(vinyl acetate)

The ester side groups of poly(vinyl acetate) are then hydrolysed, producing PVA (figure 1.32).

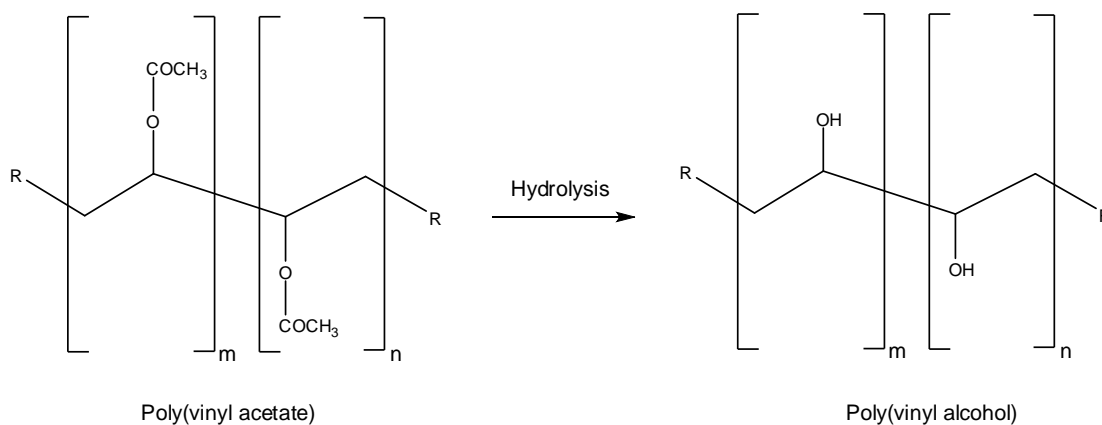


Figure 1.32. Hydrolysis of poly(vinyl acetate) to give poly(vinyl alcohol)

The typical FTIR spectra of PVA shows the presence of some remaining acetate groups, as this hydrolysis process does not achieve 100% conversion (figure 1.33).

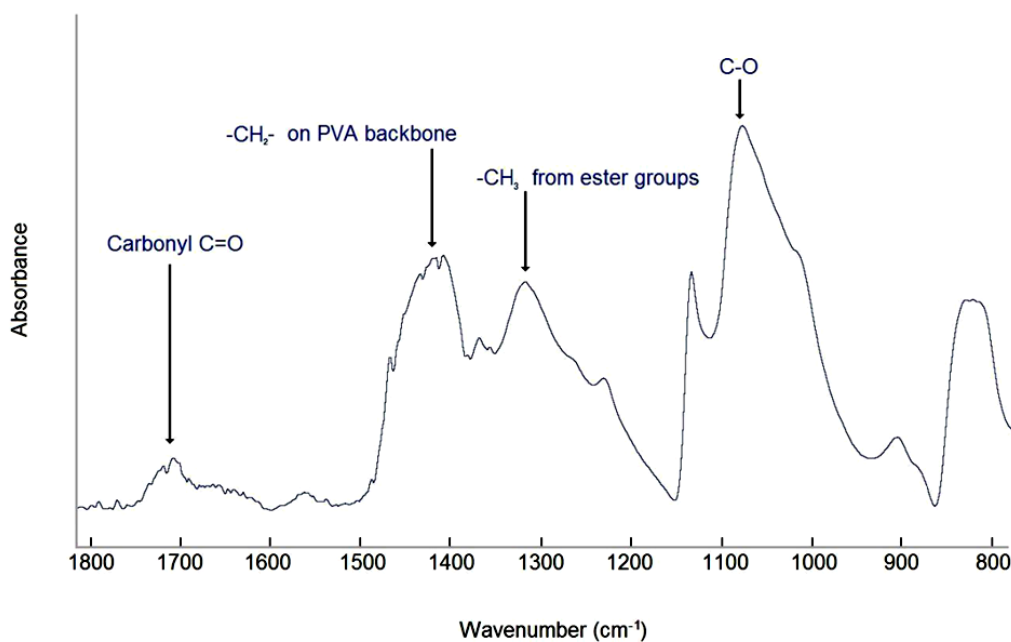


Figure 1.33. FTIR spectra of PVA between 1800 and 800 cm^{-1} .

The simple chemical structure of PVA makes it attractive as a basis for stable emulsions, as is the case with M-PVA. The number of possible side reactions which can occur from the surface secondary hydroxyls are relatively small and the carbon-carbon linked backbone is mostly unreactive. This unreactive behaviour makes M-PVA difficult to functionalise using conventional methods, posing a challenge for the synthesis of polymer brushes at the M-PVA surface.

1.5 Outline of thesis

Against all this, the subsequent chapters describe the methods used to manufacture M-PVA with polyelectrolyte homopolymer and heteropolymer mixed brush grafted surfaces. As mentioned in section 1.4, non-porous M-PVA particles are comparatively cheap, readily available and good properties in terms of magnetism, stability and resistance to fouling compared to other magnetic adsorbents. In order to improve the binding properties of these particles a number of polymer grafting methods have been investigated, with the intention of grafting

P2VP and PMAA polyelectrolytes to the typically unreactive M-PVA surface, ultimately leading to the creation of adsorbents with 'switchable' ion-exchange surfaces.

Chapter 2 describes how cerium (IV) initiation of the M-PVA surface has been used to achieve a free-radical "graft from" polymerization to form polyelectrolyte homopolymer and heteropolymer layers at the M-PVA surface with suitable dimensions for brush behavior. In Chapter 3 the synthesis of polyelectrolyte brushes is performed using a "graft to" method via sulfonyl activation of M-PVA, with calculated polymer brush dimensions distinctly different to those produced by cerium (IV) initiation. Chapter 4 cover the partial activation of the M-PVA surface with brominated sites, which are then used as activators in ATRP "graft from" brush syntheses and "graft to" reactions involving bromine substitution by nucleophilic polymer end-groups.

Chapter 5 covers binding studies performed on the modified M-PVA supports produced in Chapters 2 to 4. These binding studies use a model protein system consisting of acidic, neutral and basic proteins to identify the cation exchange and anion exchange properties of each support type under a range of pH conditions. The composition and brush properties of modified M-PVA surfaces are then compared to their binding behavior and response to salt and pH based elutions.

Further areas of research, based on the results of this study, are suggested in Chapter 6.

2 Polymer grafting by Ce(IV) initiated 'graft from'

2.1 Introduction

The "graft from" method of polymer brush synthesis involves synthesis of a polymer from an initiator attached to a surface. This generates a polymer which is attached to the surface through the initiator group. Graft from synthesis is an attractive route to the creation of ion exchange (IEX) polymer brushes, as the high brush density possible with graft from techniques translates to higher densities of charged polymer subunits within the brush and hence to improved ionic binding capacity and binding strength. In addition, the intergraft distance, D , seen at higher brush density results in more pronounced brush behaviour for chains of a given Flory Radius, R_f . This follows from the condition for brush behavior defined for R_f and D values (equation. 2.1) (Unsworth et al., 2005).

$$\frac{2R_f}{D} \gg 1$$

Equation 2.1

For the creation of IEX ligands with switchable brush behaviour, the combination of high charge density and low D values make 'graft from' polymerisation a very useful technique.

One 'graft from' technique of interest is the Ce(IV) initiated free-radical polymerisation of vinyl and allyl monomers (Mino and Kaizermann, 1958). Salts of Ce(IV) show high reactivity as initiators of free-radical vinyl polymerisations in the presence of reducing agents such as alcohols, aldehydes, ketones, acid and amines (Nagarajan and Srinivassan, 1994). Previous studies in to Ce(IV) initiation have shown it to be a useful method for the generation of radicals on polymer hydroxyl sites, providing a route to the synthesis of graft-polymers by a free-radical mechanism (Reddy et al., 1995; Lagos et al., 1992; Tsubokawa et al., 1988; Vera-Pacheco et al., 1993). Of particular interest are studies which have shown the ability of Ce(IV) to initiate radical polymerisation from the PVA backbone (Oadian and Kho, 1970; Story and Goff, 1989; Müller, 1986). The behaviour of PVA as a

free-radical initiator in the presence of Ce(IV) leads to the possibility of free-radical graft from polymerisation from the PVA matrix of M-PVA. Previous studies have shown that 'graft from' polymerisation by free-radical Ce(IV) activation can be used to improve protein binding capacities on chromatography supports (Muller, 1990), poly(vinyl acetate-divinyl benzene) particles (Guan et al., 2005) and PVA surfaces (Pitfield, 1992).

Initiation by Ce(IV) occurs through complex formation between Ce(IV) and the reducing agents, followed by single electron transfer from the reducing agent to the ceric ion. This results in reduction of Ce(IV) to Ce(III) and the production of a free radical functionality on the reducing agent. Mechanisms of PVA oxidation by Ce(IV) have been studied in the presence of polymerisable monomers (Mino and Kaizermann, 1958; Iwakura and Imai, 1966; Ogiwara and Uchiyama, 1969; Narita et al., 1969) and in their absence (Mino et al., 1959).

Initiation of PVA by Ce(IV) occurs at hydroxyl sites, with interaction between the hydroxyl group and ceric ion allowing radical initiation to occur from the adjacent carbon atom. The major product of PVA synthesis is isolated hydroxyl units, formed by head-to-tail reaction between vinyl acetate groups (figure 2.1).

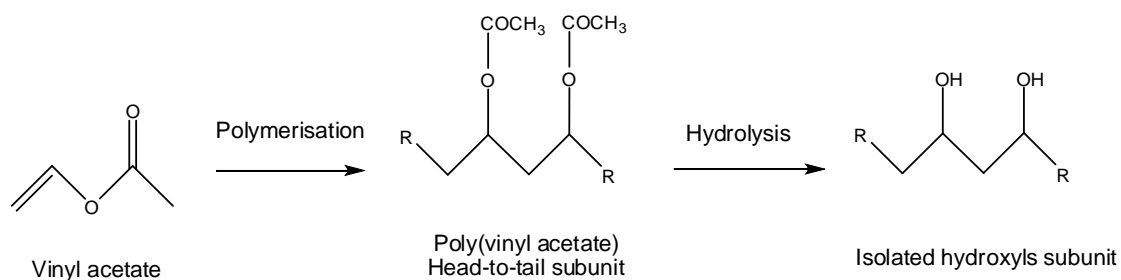


Figure 2.1. Head-to-tail reaction between vinyl acetate monomers leading to PVA isolated hydroxyls subunit

Reaction between isolated hydroxyl groups and Ce(IV) leads to initiation from the hydroxyl carbon site with loss of a hydrogen atom (figure 2.2).

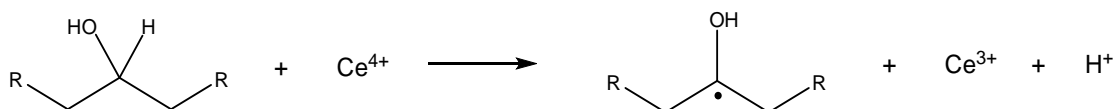


Figure 2.2. Oxidative initiation of hydroxyl subunit by Ce(IV)

1-2% of subunit linkages in PVA are in the form of diol groups, formed by head-to-head reaction between vinyl acetate monomers (figure 2.3; Finch, 1973).

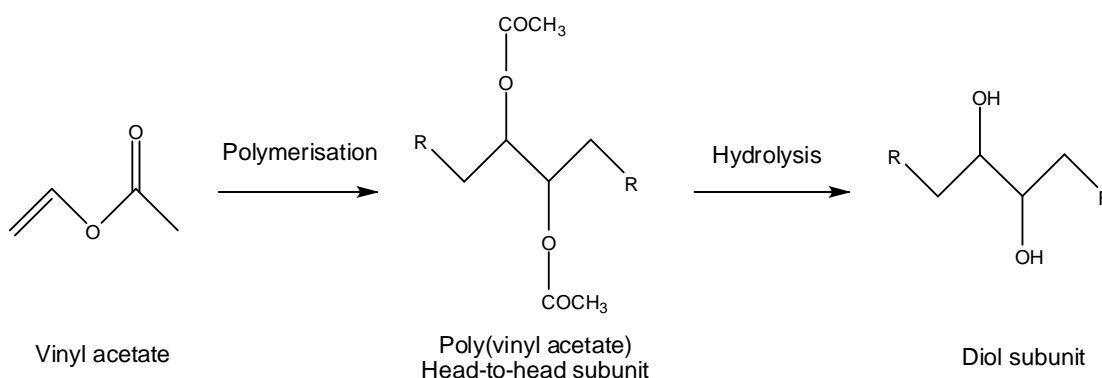


Figure 2.3. Head-to-head reaction between vinyl acetate monomers leading to PVA diol subunit

Initiation from the PVA diol subunit occurs at a significantly faster rate than reaction from isolated hydroxyls (Iwakura and Imai, 1966). The mechanism for initiation at diol sites results in cleavage of the C-C bond which joins the two hydroxyl groups (figure 2.4). This produces a terminal alcohol radical and an aldehyde. Subsequent polymerisation reactions can occur from the terminal radical group.

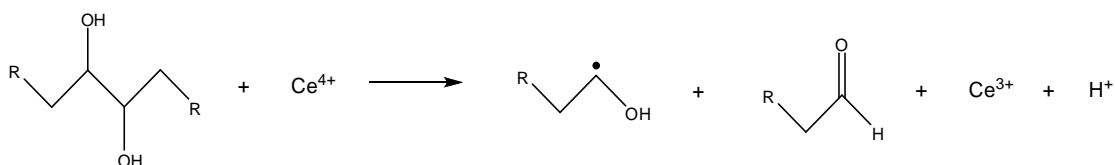


Figure 2.4. Oxidative initiation of diol subunit by Ce(IV)

Ce(IV) oxidations are typically performed in the presence of nitric acid, as acidic conditions favour the more reactive Ce^{4+} form. In neutral solution Ce(IV) is found

as $(\text{Ce-O-Ce})^{6+}$ and CeOH^{3+} , the presence of which correspond to significantly reduced rates of initiation (O dian and Kho, 1970). The kinetics of reduction of Ce(IV) by PVA have been investigated and the progress of Ce(IV) reduction by PVA proposed as a three stage process, with three different rates of reduction (Ogiwara and Uchiyama, 1969). Initially, a rapid reduction of Ce(IV) by 1,2-diols is seen. This is followed by a second stage of slower rate and a third stages with very slow rate. Chain cleavage of PVA is observed during the first stage, with polymerization from the radicals here producing a block copolymer between PVA and the polymerizing monomer. The second and third stages involve radical generation at isolated hydroxyl sites along the PVA backbone and involve no cleavage. Polymerizations which are initiated by uncleaved PVA units produce true graft polymers.

Radical polymerisations initiated from the M-PVA surface with Ce(IV) have the advantage of being 'one pot' procedures. This makes the adjustment of reagent conditions for optimum grafting easier than for polymerisation techniques which require multiple activation steps. Grafted polymers are attached to the M-PVA surface by a covalent C-C bond, leading to grafted layers which are resistant to most forms of chemical attack. As the amount of complexed Ce(IV) present directly effects the extent of initiation it is possible to control the extent of surface initiation by the use of controlled amounts of Ce(IV). In this way modification of M-PVA surfaces by grafting two polymer species to form a 'mixed brush' grafted surface may be achieved through two consecutive partial initiation/polymerisation steps (figure 2.5).

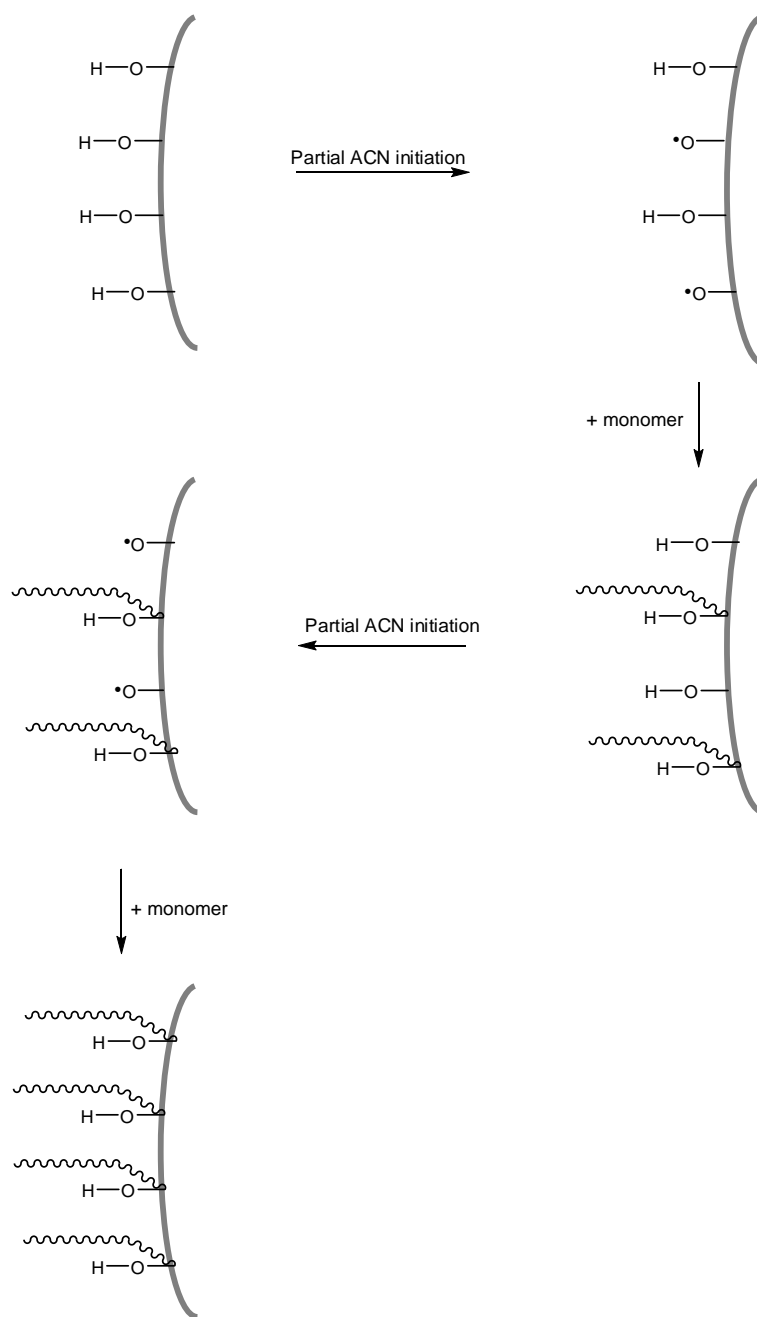


Figure 2.5. Overall synthetic route for mixed brush grafting by Ce(IV) initiation.

This method may be used to create a mixed polyelectrolyte grafted layer with switchable polymer brush properties (Houbenov et al., 2003). Such a brush composed of basic polymers grafted alongside acidic polymers can lead to a dense surface charge, capable of IEX binding followed by elution assisted by pH change wherein both the sign of the surface charge and the surface-dominating

polymer are switched (figure 2.6). Elution in this case can occur by both charge repulsion and the physical push of expanding polymer chains.

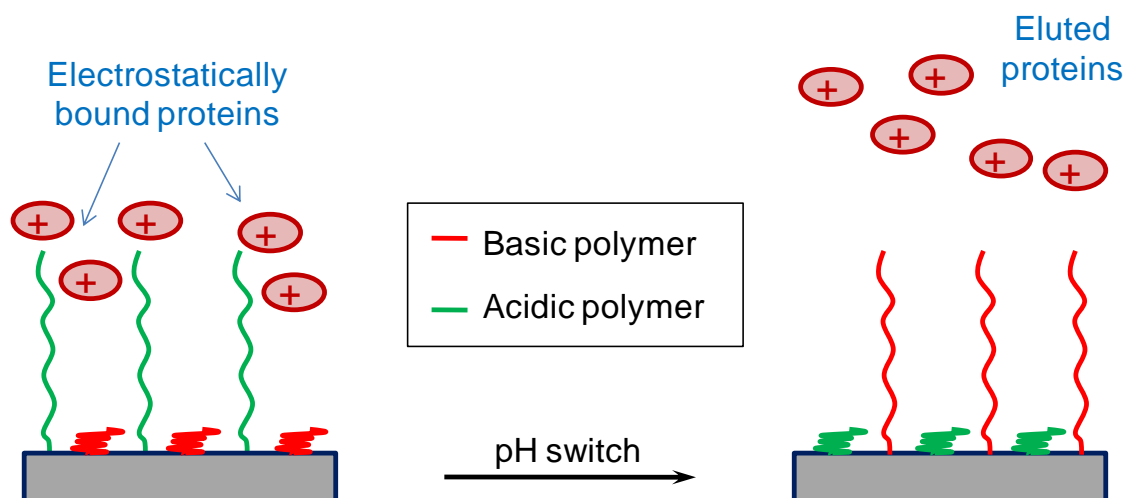


Figure 2.6. Release of basic proteins from acidic polymer by increasing pH.

Work by Houbenov et al. (2003) showed that a polymer brush layer comprised of P2VP and PAA exhibits switchable behaviour with full expansion of P2VP below pH 3.2 and expansion of PAA above pH 6.7. For this brush the minimum charge and layer expansion exists at pH 4.9. However, as this pH value is lower than the desired binding range of pH 5-8 (see Chapter 5) a more suitable choice of acidic polymer may be PMAA, whose pK_a of 5.5 (Ryan et al., 2005) may result in the uncharged state of a PMAA/P2VP mixed brush layer being at a higher pH than is seen for a PAA/P2VP mixed brush layer. For comparison, the pK_a of PAA is 4.5 (Govender et al., 1999).

The synthesis of mixed polyelectrolyte layers as described by Houbenov et al. (2003) involves the grafting of P2VP and poly(*tert*-butyl acrylate) (PTBAA). PTBAA is a protected form of PAA containing ester side groups. This grafting is followed by a hydrolysis of the PTBAA chains to produce the PAA carboxylic acid side groups (figure 2.7). The acidic polymer here is grafted in its protected form to reduce interaction between acidic and basic polymer chains during the grafting reactions.

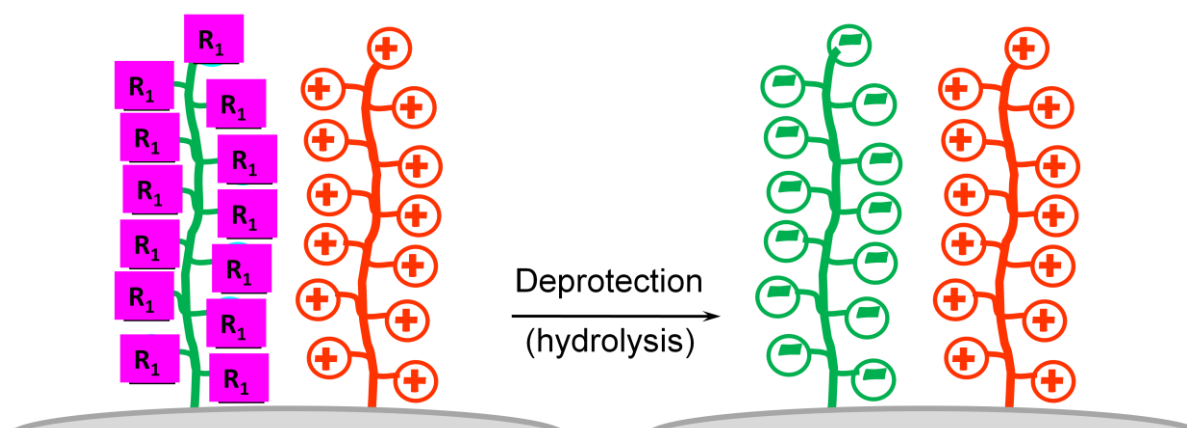


Figure 2.7. Grafted P2VP/PBAA mixed brush undergoes hydrolysis to form P2VP/PAA mixed brush.

In the case of grafting a P2VP/PMAA mixed brush with a Ce(IV) initiated “graft from” method, the same principle involves the use of the protected tert-butyl methacrylate (TBMA) monomer alongside 2-vinyl pyridine (2VP). Surface initiated polymerisation of TBMA and 2VP produces a grafted layer composed of P2VP and poly(tert-butyl methacrylate) (PTBMA). This layer can then be hydrolysed to give a mixed PMAA/P2VP grafted surface.

Against the above, the following sections describe the development of a technique for creating a mixed brush layer composed of both P2VP and PMAA chains via Ce(IV) initiated grafting of 2VP and TBMA monomers. This includes with a discussion of the layer dimensions calculated from FTIR data and the implications of these dimensions for potential brush properties.

2.2 Materials and methods

2.2.1 Materials used

M-PVA (batch R2-0105096; V_m ; 3.4 cm³/g; specific surface area 59.2 m² per g) was obtained from Chemagen (Baesweiler, Germany). t-butyl methacrylate (CAS 585-07-9); 2-vinyl pyridine (CAS 100-69-6); 4-ethoxyphenol (CAS 622-62-8); dimethyl sulfoxide (CAS 68-78-5); acetone (67-64-1); ammonium cerium (IV) nitrate, Ce(NH₄)₂(NO₃)₆ (CAS 16774-21-3); HCl solution (CAS 7647-01-0); nitric acid (CAS 7697-37-2); acetic acid (CAS 64-19-7); sodium sulphate (CAS 7757-82-6); sodium chloride (CAS 7657-14-5); sodium hydroxide (CAS 1310-73-2); potassium bromide (CAS 7758-02-3); and methanol (CAS 67-56-1) were obtained from Sigma Aldrich (Poole, Dorset).

Cuvettes, 2 ml screw-cap micro test tubes, 15 ml screw-cap centrifuge tubes and 50 ml screw-cap centrifuge tubes were obtained from Sarstedt (Leicester, UK). 1.5 ml hinged-lid micro test tubes were obtained from Eppendorf (Cambridge, UK). All unheated mixing was performed with a VM20 vortex mixer or a IKA Vibrax VXR basic mixer with attachments for 15 ml centrifuge tubes and micro test tubes. Heated mixing was performed in a Grant OLS water bath with shaker rack. Samples were dried on watchglasses in a Gallenkamp size 2 hotbox oven. Chemicals were weighed on Mettler AE160 and AT261 balances. Pipetting was performed with 20 ml, 200 ml, 1 ml and 5 ml adjustable pipettes.

2.2.2 Base matrix preparation

M-PVA stock was washed thoroughly before use to remove potential contaminants. 1.5 g M-PVA was washed in a succession of solvents (30 ml, 60 s) these were: water; 50% acetone in water; 100% acetone; 50% acetone / 50% methanol; 100% methanol; 50% methanol in water; water (x2); 1 M NaCl in water; water (x3). The washed M-PVA was then suspended in water (30 ml).

2.2.3 Quenched Ce(IV) polymer grafting

The effect of an additional radical quenching agent, 4-ethoxyphenol, upon Ce(IV) initiated graft from was tested (figure 2.8).

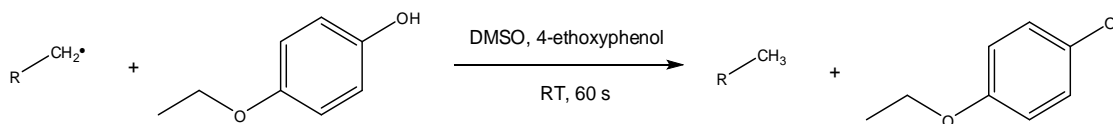


Fig 2.8. Quenching of radical chain by 4-ethoxyphenol

For the first grafting step a degassed solution of nitric acid (150 μ l, 2 M) containing ammonium cerium (IV) nitrate (ACN) was added to a degassed suspension of M-PVA (50 mg) in dimethyl sulfoxide (DMSO, 5 ml). The mixture was mixed under nitrogen (600 s). Degassed monomer was then added and the mixture was kept under nitrogen for (3 h) with good mixing. With the system still under nitrogen the supernatant was removed and the supports were mixed (60 s) with DMSO (5 ml) containing 4-ethoxyphenol (10 mg). The reaction was then opened to the air and washed (60 s, 2 ml) with the following solvents: 0.2 M Na_2SO_3 in 10% (v/v) acetic acid; DMSO (x 2); 1 M $\text{NaCl}_{(\text{aq})}$; water; DMSO.

For mixed brush synthesis a second grafting step was used. A degassed solution of nitric acid (75 μ l, 2 M) containing ACN was added to a a degassed suspension of DMSO (2.5 ml) containing half of the total product from the first grafting step (assumed to include 25 mg of M-PVA). The mixture was mixed under nitrogen (600 s). The second monomer (degassed) was then added and the mixture was kept under nitrogen with good mixing (3 h). With the system still under nitrogen the supernatant was removed and the supports were mixed (60 s) with water (2.5 ml) containing 4-ethoxyphenol (5 mg). The reaction was then opened to the air and washed (60 s, 1 ml) with the following solvents: 0.2 M Na_2SO_3 in 10% (v/v) acetic acid; DMSO (x 2); 1 M $\text{NaCl}_{(\text{aq})}$; water; DMSO.

2.2.4 Unquenched Ce(IV) polymer grafting

Grafting was performed as described in 2.2.3, without the 4-ethoxyphenol wash step.

2.2.5 Ce(IV) mixed polymer grafting without second initiation

Quenched and unquenched Ce(IV) initiated polymerisations were performed as in method 2.2.3 and 2.2.4, without a second addition of ACN/nitric solution before the second monomer grafting step. These reactions were performed to identify diblock copolymer formation from unterminated polymer end groups produced during the first grafting stage.

2.2.6 Hydrolysis of PTBMA grafted products

Supports grafted with PTBMA brushes were hydrolysed using a 50/50 (v/v) aqueous solution of trifluoroacetic acid (TFA, see appendix 7.1 for details of this reagent choice).

PTBMA grafted single and mixed brush supports were reacted with a 50/50 (v/v) mixture of TFA and water (5 ml, 60°C, 24 h) followed by washing with water (5 ml, 60s, x 2).

2.2.7 FTIR solid analysis

For solid samples an aliquot of aqueous particle suspension was pipetted onto a watchglass and dried in an oven (100 °C, 2 h). A portion of the dry sample was taken and ground with 300 mg of KBr until a fine, homogenous powder was produced. Using a Specac 15 ton manual press the KBr-sample powder was pressed in a 13 mm die to a pressure of 10 bar, producing FTIR suitable discs. Samples were run on a Thermo Nicolet 380 FTIR in direct beam mode for 64 scans per sample at a resolution of 2 cm⁻¹.

FTIR samples were prepared from reaction supernatants and quantified as described in Appendix 7.2. FTIR samples were analysed using a Nicolet Smart

Orbit diamond ATR apparatus at a resolution of 2 cm^{-1} , with $50\ \mu\text{l}$ aliquots of the sample liquid pipetted onto the ATR crystal.

2.3 Results

2.3.1 FTIR peak assignments for grafted polymers

Peak assignments for ungrafted P2VP are expected to show wavenumbers values similar to grafted P2VP. An awareness of the expected peak values for P2VP allows identification of grafted P2VP through the presence of new peaks in the FTIR spectra of M-PVA beads. As a basis for grafted support analysis, spectra of solid P2VP and PTBMA were obtained (figure 2.9).

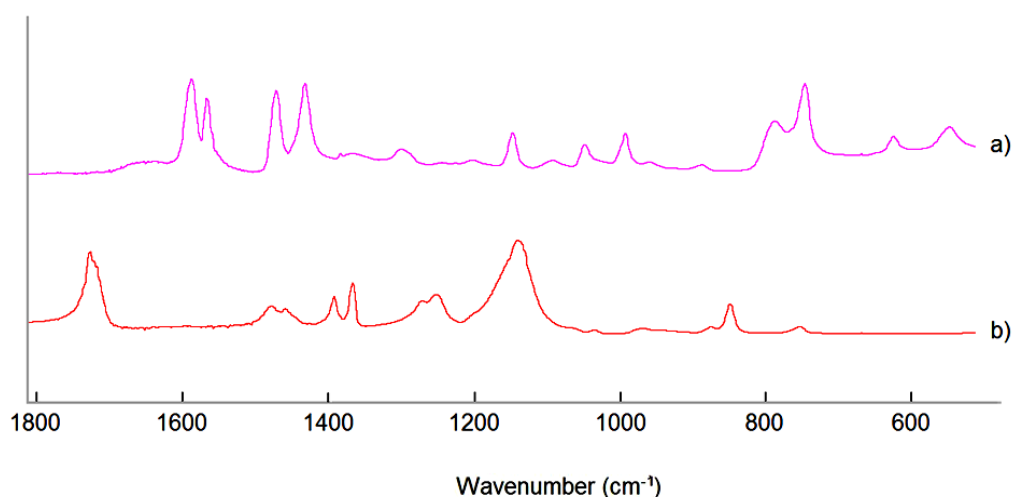


Fig 2.9. Spectra. FTIR spectra for pure P2VP (a) and PTBMA (b)

Based upon these spectra, wavenumbers were assigned to the various bonds which are expected in each polymer (Tables 2.1 and 2.2).

Table 2.1. FTIR peak assignments for P2VP (Clayden et al., 2001; Solomons and Fryhle, 2007)

Wavenumber (cm ⁻¹)	Assignment
1588	Aromatic C-C
1567	Aromatic C-C
1472	Aromatic C-C
1433	Aromatic C-C
1301	Methyl, CH ₃
1147	Pyridine C-N
787	Aromatic C-H
746	Aromatic C-H

Table 2.2. FTIR peak assignments for PTBMA (Clayden et al., 2001; Solomons and Fryhle, 2007)

Wavenumber (cm ⁻¹)	Assignment
1727	Carbonyl group (ester)
1478	Methylene, -CH ₂ -
1460	Methylene, -CH ₂ -
1393	Methyl, -CH ₃
1367	Methyl, -CH ₃
1251	Methyl, -CH ₃
1139	C-O, (ester)

2.3.2 Ce(IV) initiated homopolymer brush grafting

The presence of P2VP following ACN activation and reaction with 2VP monomer was confirmed using FTIR spectroscopy on solid samples (figure 2.10).

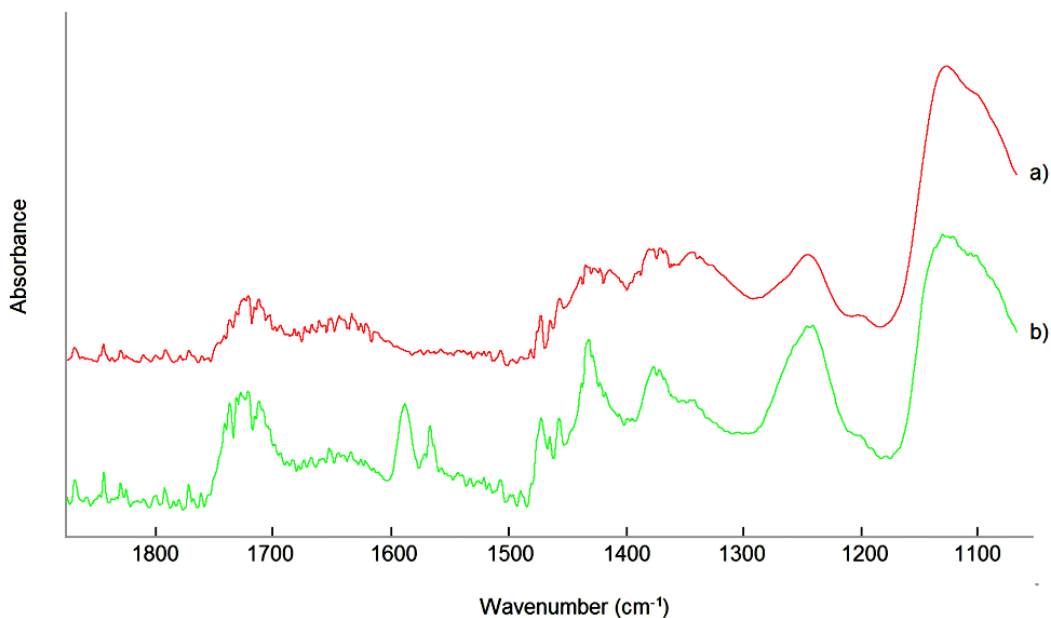


Figure 2.10. a) M-PVA; b) M-PVA (50 mg) following activation with 4 mg ACN and 237 ml 2VP in DMSO

Following P2VP grafting new peaks are seen 1590 and 1570 cm⁻¹ accompanied by a noticeable increase in peak heights at 1490 and 1430 cm⁻¹. These indicate presence of the 2VP aromatic C-H bonds on the supports and show that grafting was successful. FTIR of supernatant for the reactions (figure 2.11) also indicate consumption of 2VP, with loss in peak height is observed at all 2VP wavenumbers (1590, 1570, 1480 and 1430 cm⁻¹)

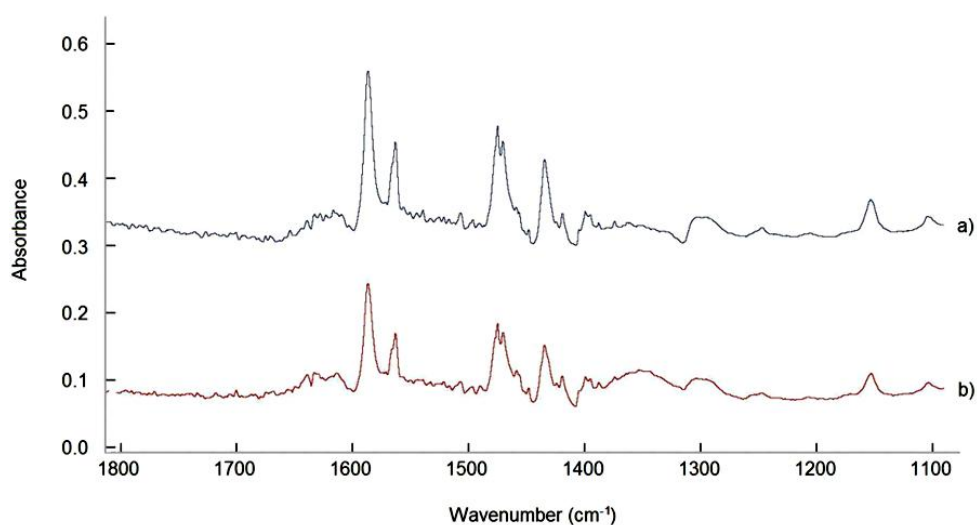


Figure 2.11. Supernatant a) before and b) after reaction of 50 mg M-PVA with 4 mg ACN and 237 ml 2VP in DMSO

Brush dimensions were compared for graft reactions which used varied amounts of Ce(IV) per g M-PVA and consistent amount of monomer (44 mmol 2VP per g M-PVA), showing a maximum yield of 8.75 mmol polymer units grafted per g M-PVA when 294 mmol Ce(IV) initiator per g M-PVA was used (Table). The total mass of P2VP grafted at this point is 0.92 g P2VP per g M-PVA, which means that 48% of the final support mass is P2VP. This means that although the average radius of the M-PVA bead is approximately 1 μm the grafted support mass is concentrated in the outermost 10 nm, where the polymer brush layer is found.

Intergraft spacing (D) was calculated from the molar quantity of Ce(IV) initiator present and the M-PVA surface area ($59.2 \text{ m}^2 \text{ g}^{-1}$). The intergraft distance along the bead surface is predicted to be the same as the 'true' distance between adjacent graft sites (see appendix 7.10), so relevant intergraft distances can be calculated directly from the M-PVA surface area. R_f for each graft product was calculated from equation 2.2 using a monomer size, A_m , of 0.67 nm for P2VP (Seo et al., 2004) and chain length, L , calculated by dividing the molar quantity of Ce(IV) by the molar quantity of grafted monomer). The Flory exponent, ν , was taken to be 0.6 (Katao and Wadati, 2007).

$$R_f \approx A_m L^v$$

Equation 2.2

Values of $2R_f/D$ were also calculated from this data. These values are important in predicting the behaviour of tethered polymer layers, as the relationship between $2R_f$ and D determines the extent of overlap between neighbouring polymer chains. When $2R_f$ is in excess of D there will be significant overlap between chains and extended brush behaviour will be favoured. Hence the relationship for expecting a brush phase is $2R_f/D \gg 1$ (Unsworth et al., 2005).

Table 2.3. Comparison of grafting yield to Ce(IV) initiator presence (50 mg m-PVA, 2.2 mmol 2VP)

Polymer grafted	Ce(IV) (μmol) per g M-PVA	Monomer presented (mmol) per g M-PVA	Monomer grafted (mmol) per g M-PVA	Yield (%)	D (nm)	R_f (nm)	$2R_f/D$	$n(\text{poly})/n(\text{init})$
P2VP	36.8	43.96	0.61	1.4	16.36	3.60	4.4	16.6
P2VP	73.5	43.96	2.91	6.6	11.57	6.09	10.5	39.6
P2VP	110.3	43.96	4.23	9.6	9.44	5.98	12.7	38.3
P2VP	147.0	43.96	5.77	13.1	8.18	6.06	14.8	39.3
P2VP	183.8	43.96	5.87	13.4	7.32	5.36	14.6	31.9
P2VP	220.5	43.96	6.20	14.1	6.68	4.96	14.9	28.1
P2VP	257.3	43.96	7.08	16.1	6.18	4.90	15.8	27.5
P2VP	294.0	43.96	8.75	19.9	5.78	5.13	17.7	29.8
P2VP	330.8	43.96	8.62	19.6	5.45	4.74	17.4	26.1
P2VP	367.5	43.96	8.51	19.4	5.17	4.41	17.1	23.2
P2VP	404.3	43.96	8.23	18.7	4.93	4.09	16.6	20.4
P2VP	441.0	43.96	8.52	19.4	4.72	3.96	16.8	19.3

Higher R_f values tend to be reached with lower amounts of Ce(IV) added, which is as expected. The use of a constant monomer concentration means that the

number of units available per initiator is much higher when [Ce(IV)] is lower. Values of $2R_f/D$ suggest extended brush behaviour for all grafted layers, with the maximum $2R_f/D$ value of 17.7 at 294 mmol Ce(IV) per g M-PVA corresponding to the maximum grafting yield (figure 2.12).

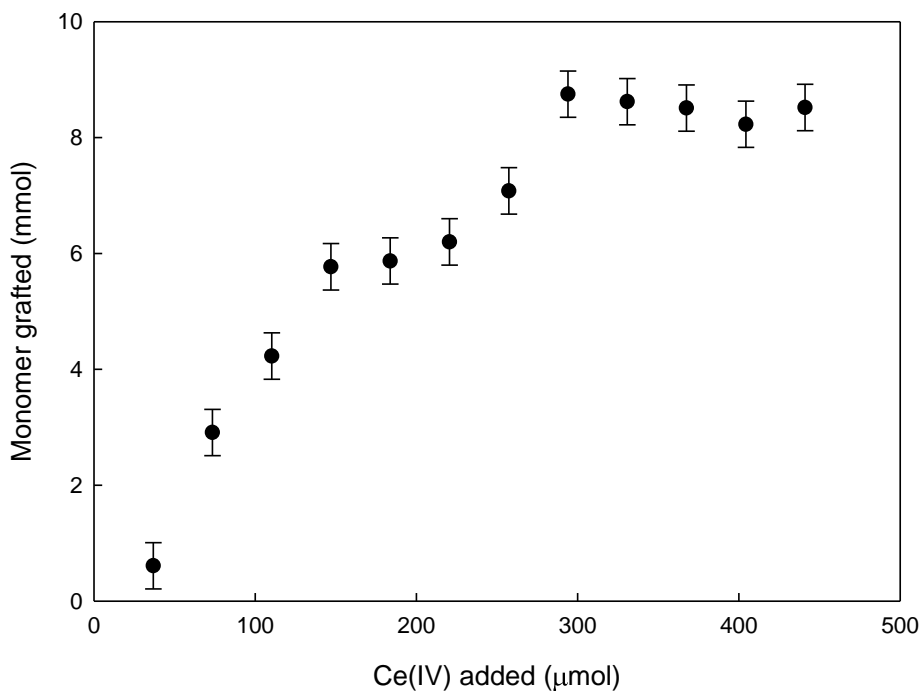


Figure 2.12. Comparison of 2VP grafted to Ce(IV) initiator presence (50 mg m-PVA, 2.2 mmol 2VP)

The same set of experiments was performed with TBMA grafting by Ce(IV) activation. The presence of PTBMA on M-PVA following Ce(IV) initiated reaction with tBmA was confirmed using FTIR (figure 2.13).

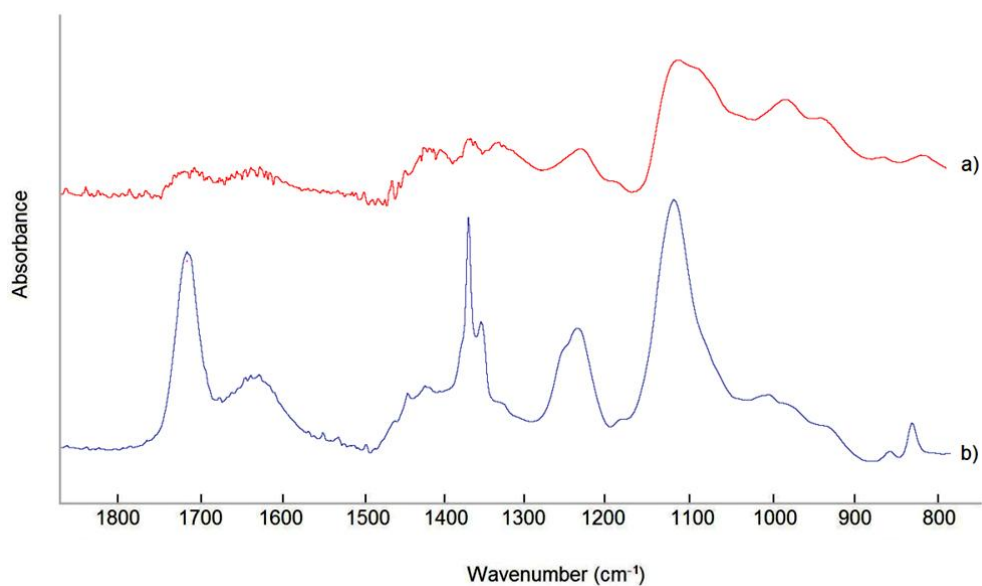


Figure 2.13. a) M-PVA; b) M-PVA (50 mg) following reaction with ACN (4 mg) and TBMA (301 μl) in DMSO

Large increases in peak height at 1720 (carbonyl), 1390 (methyl), 1370 (methyl), 1250 (methyl) and 1140 (ester C-O) cm⁻¹ indicate the presence of grafted PTBMA following ACN initiated grafting. Similarly, FTIR spectra of supernatants for the PTBMA grafting reaction (figure 2.14) show consumption of TBMA monomer.

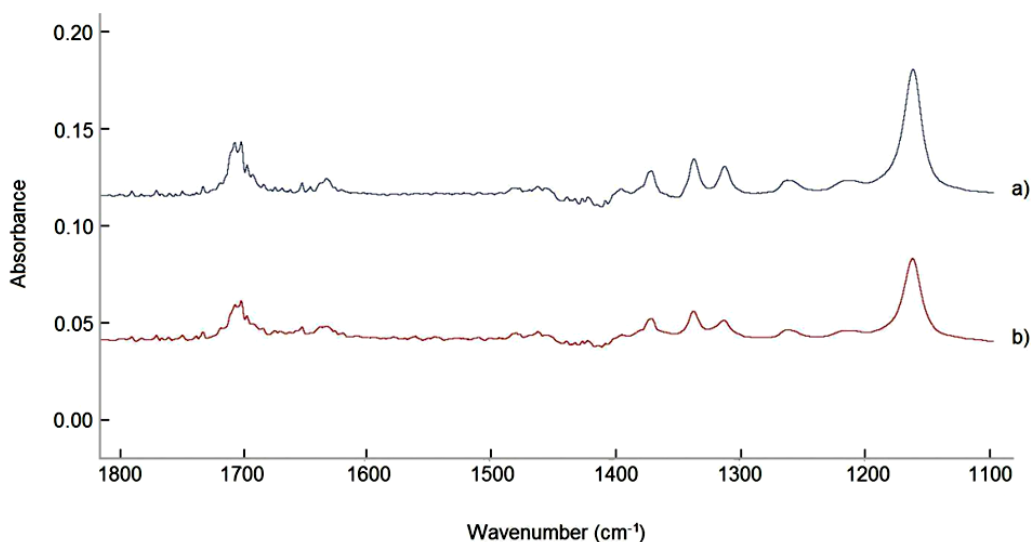


Figure 2.14. Supernatant a) before and b) after reaction of 50 mg M-PVA with 4 mg ACN and 301 ml TBMA in DMSO

As with P2VP grafting, ACN initiation procures larger graft-polymer peaks in the support FTIR spectrum than tresyl-initiated grafting, indicating a larger number of tBmA subunits compared to the tresyl grafting product. The comparison of brush dimensions following reaction of varied amounts of Ce(IV) and consistent amount of monomer (37 mmol TBMA per g M-PVA) with M-PVA showed an increase in polymer yield with increasing Ce(IV) addition, until a maximum monomer consumption of 9.25 mmol per g M-PVA was achieved with Ce(IV) addition of 330.8 μmol per g M-PVA (table 2.4, figure 2.15). As with P2VP grafted chains this represents a concentration of mass in the grafted layer, with 1.32 g PTBMA per g M-PVA grafted (69% of total grafted support mass). Following hydrolysis, this becomes 0.80 g PMAA per g M-PVA (44% of total grafted support mass).

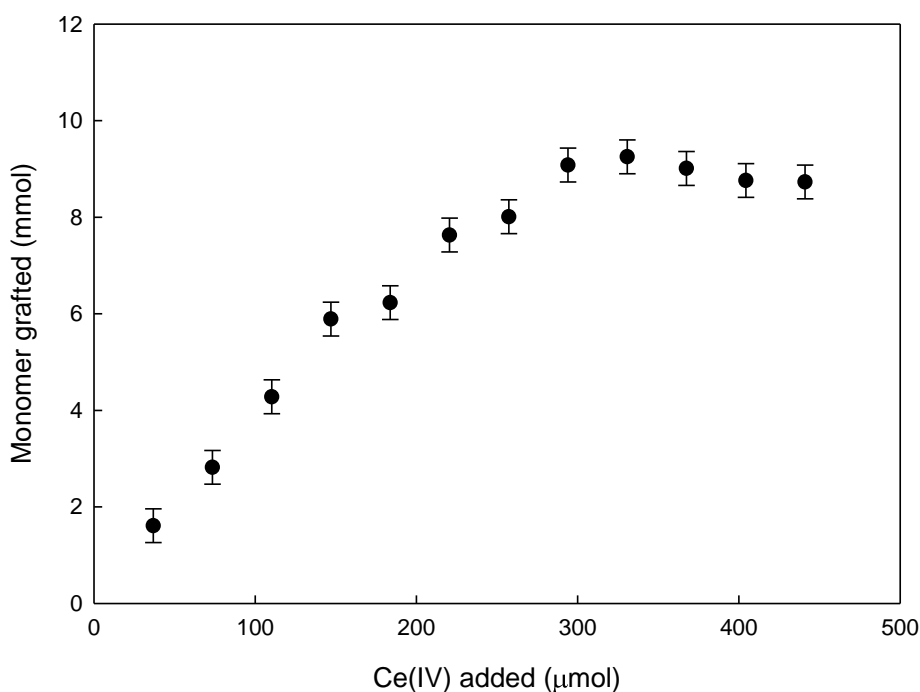


Figure 2.15. Comparison of TMBA grafted to Ce(IV) initiator presence (50 mg m-PVA, 1.85 mmol TBMA)

D values were calculated as described for P2VP grafted supports. Calculation of R_f used a monomer size of 0.33 nm for PMAA (Hester et al., 2002). Although quantification data was based upon analysis of PTBMA, the monomer size of

PMAA was used in R_f calculations as it is the brush properties of the hydrolysed polymer product which are of most interest for IEX behavior (figure 2.16).

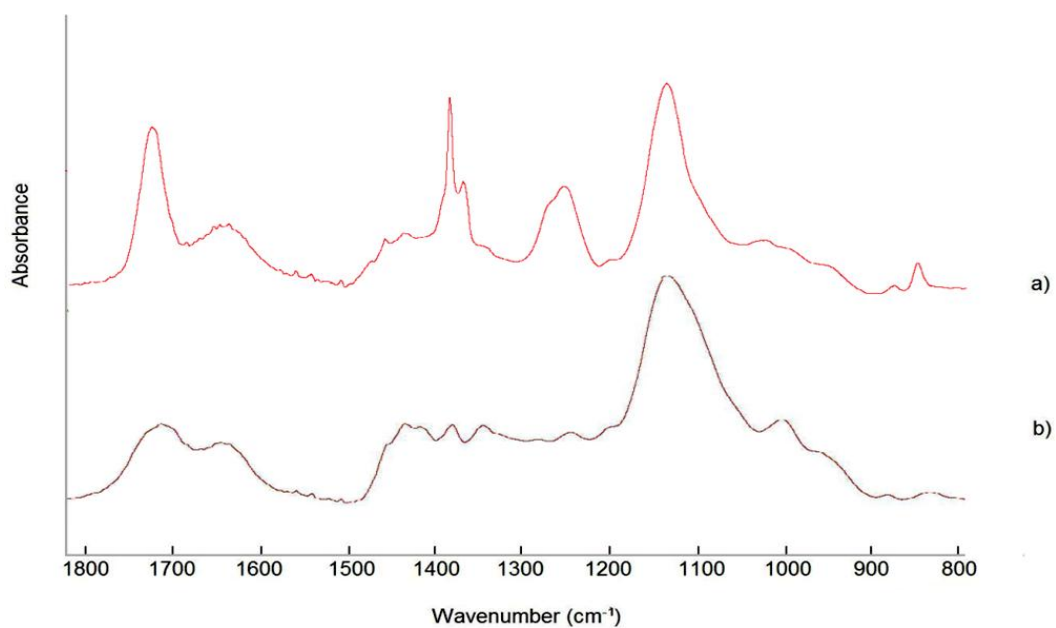


Figure 2.16. a) M-PVA (50 mg) following reaction with ACN (4 mg) and TBMA (301 μ l) in DMSO; b) PTBMA grafted support following hydrolysis with TFA solution

Table 2.4. Comparison of grafting yield to Ce(IV) initiator presence (50 mg m-PVA, 1.85 mmol TBMA)

Polymer grafted	Ce(IV) (μmol) per g M-PVA	Monomer presented (mmol) per g M-PVA	Monomer grafted (mmol) per g M-PVA	Yield (%)	D (nm)	R_f (nm)	$2R_f/D$	$n(\text{poly})/n(\text{init})$
PMAA	36.8	37.04	1.61	4.3	16.36	3.18	3.9	43.8
PMAA	73.5	37.04	2.82	7.6	11.57	2.94	5.1	38.4
PMAA	110.3	37.04	4.28	11.6	9.44	2.97	6.3	38.8
PMAA	147.0	37.04	5.89	15.9	8.18	3.02	7.4	40.1
PMAA	183.8	37.04	6.23	16.8	7.32	2.73	7.5	33.9
PMAA	220.5	37.04	7.63	20.6	6.68	2.77	8.3	34.6
PMAA	257.3	37.04	8.01	21.6	6.18	2.60	8.4	31.1
PMAA	294.0	37.04	9.08	24.5	5.78	2.58	8.9	30.9
PMAA	330.8	37.04	9.25	25.0	5.45	2.44	8.9	28.0
PMAA	367.5	37.04	9.01	24.3	5.17	2.25	8.7	24.5
PMAA	404.3	37.04	8.76	23.7	4.93	2.09	8.5	21.7
PMAA	441.0	37.04	8.73	23.6	4.72	1.98	8.4	19.8

Calculated R_f values achieved during PMAA grafting are lower than those seen for P2VP grafting. This is because of the much greater size of P2VP units (0.67 nm) than PMAA units (0.33 nm). In terms of average number of units per chain the PMAA result is similar to that for P2VP, suggesting that tBmA and 2VP share similar abilities as propagating monomers under these conditions. The lower R_f values seen for PMAA grafted products and the corresponding lower $2R_f/D$ indicate that the surfaces of these supports will show weaker brush behaviour than the analogous P2VP grafted surfaces.

2.3.3 Ce(IV) initiated mixed polymer brush grafting

Following reaction of TBMA with 2VP grafted M-PVA and ACN, new support peaks were visible at 1390 cm^{-1} and 850 cm^{-1} . Peaks at 1720 and 1140 cm^{-1} also became noticeably larger. These results suggest successful grafting of tBmA, with

the clear presence of PTBMA groups alongside M-PVA and P2VP peaks (figure 2.17).

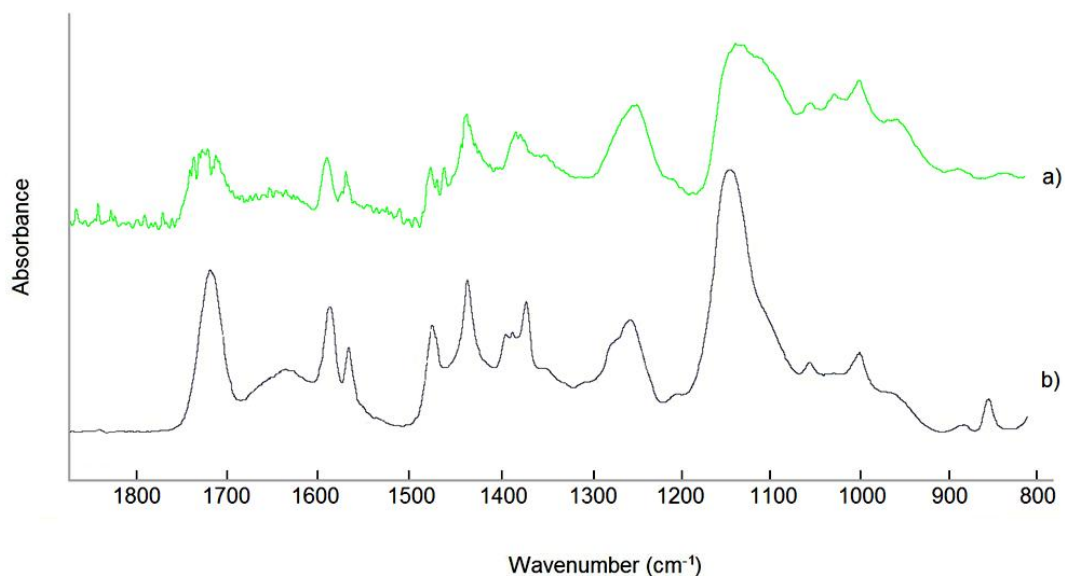


Figure 2.17. a) M-PVA (50 mg) following reaction with ACN (4 mg) and 2VP (237 μ l) in DMSO, followed by quenching with 4-ethoxyphenol; b) P2VP grafted support (50 mg) following reaction with ACN (2 mg) and tBmA (150.5 μ l) in DMSO then quenching.

Hydrolysis of the mixed brush product with TFA led to loss of characteristic t-butyl ester peaks while P2VP peaks were retained (figure 2.18).

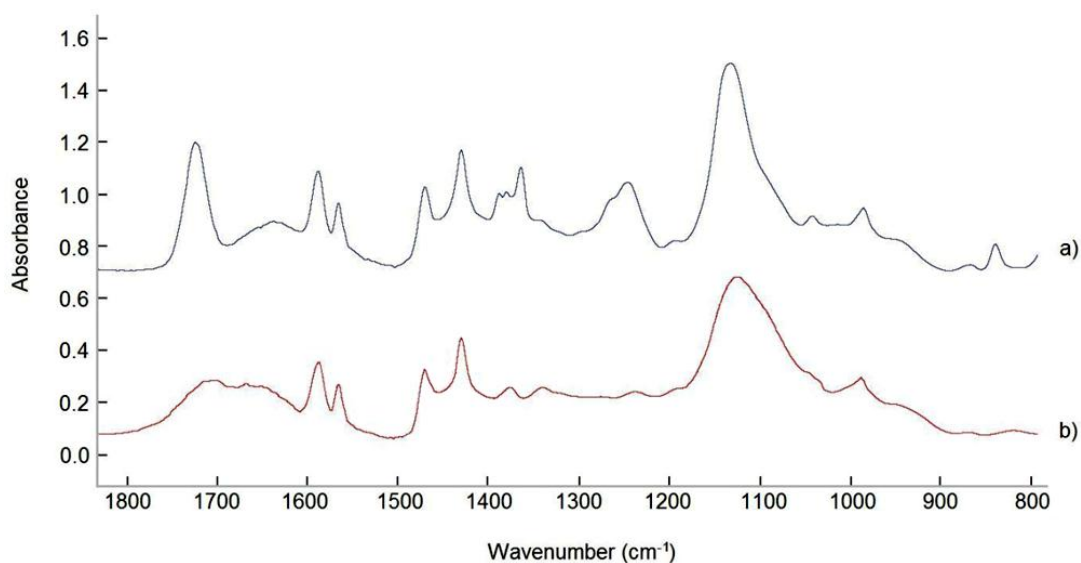


Figure 2.18. a) P2VP grafted support (50 mg) following reaction with ACN (2 mg) and TBMA (150.5 μ l) in DMSO; b) P2VP + PTBMA grafted support following hydrolysis with TFA

Mixed brush synthesis by polymerisation of 2VP from the PTBMA grafted support was also successful, with the appearance of new P2VP peak in the product spectrum at 1590 and 1570 cm^{-1} (aromatic C-H) and a significant peak increase at 1430 cm^{-1} (figure 2.19). A new peak is also seen at 990 cm^{-1} which may correspond to C-H on the P2VP backbone. These results indicate the successful grafting of 2VP onto PTBMA grafted M-PVA using the ACN activation method.

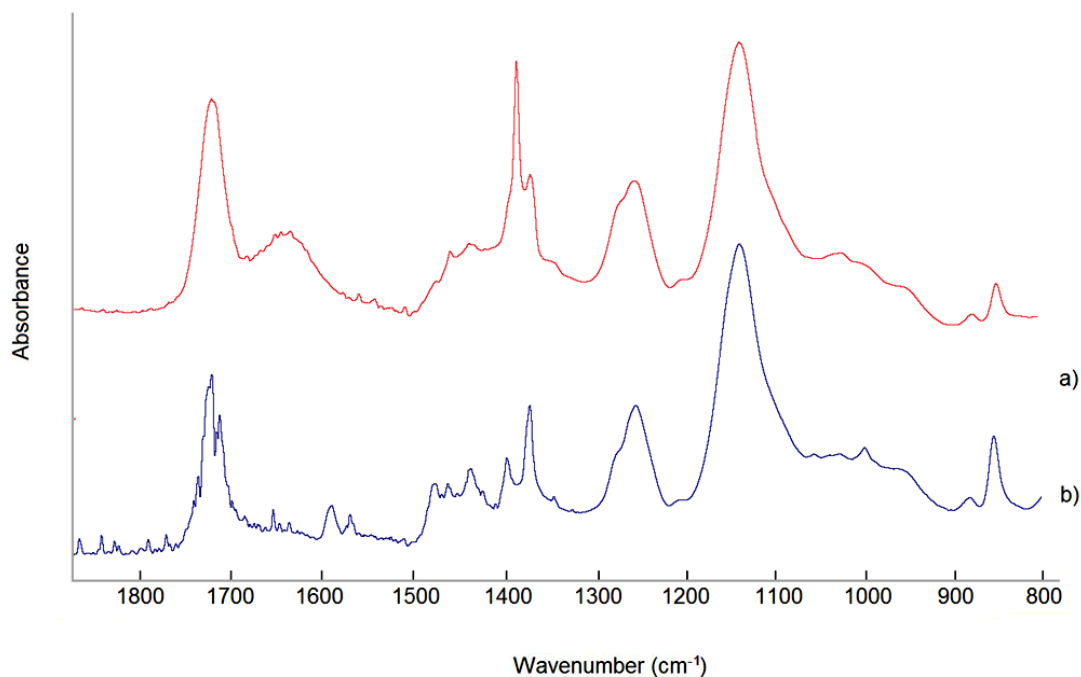


Figure 2.19. a) M-PVA (50 mg) following reaction with ACN (4 mg) and TBMA (301 μ l) in DMSO, with quenching; b) PTBMA grafted support (50 mg) following reaction with ACN (2 mg) and 2VP (118.5 μ l) in DMSO then quenching

The effect of quenching by 4-ethoxyphenol upon the addition of the second brush during a mixed-polymer brush synthesis was quantified (tables 2.5 and 2.6; figure 2.20). It was observed that in the absence of both a quenching step and new activation with Ce(IV) some polymerisation was seen between a 2nd monomer and the homopolymer grafted support (samples 5 and 6, table 2.6 and figure 2.20). Such polymerisation was not seen when quencher was used after 1st grafting with no subsequent activation step (samples 7 and 8). This indicates the continuation of a radical functionality in the absence of a quenching step. As this radical functionality is likely to exist at the chain ends of the 1st grafted polymer, it is vital that a quenching step is included in mixed-polymer synthesis to avoid the creation of diblock copolymers incorporating the 1st and 2nd monomer types.

FTIR quantification for the mixed brush support reaction (table 2.5), showed that up to 9.74 mmol of monomer was grafted per g of M-PVA. This was equivalent to 1.167 g of P2VP/PTBMAA per g M-PVA (54 % of total support mass), or 0.951 g P2VP/PMAA per g M-PVA (49% of total support mass).

As shown in table 2.6 average R_f values for the mixed brush [(P2VP) $_x$ + (PMAA) $_y$] layers were calculated from values of R_f for the component P2VP and PMAA grafts using equation 2.3. The background to this calculation is explained in Appendix 7.7.

$$R_f(av) = \frac{R_f(P2VP)^2 \cdot N(P2VP) + R_f(PMAA)^2 \cdot N(PMAA)}{R_f(P2VP) \cdot N(P2VP) + R_f(PMAA) \cdot N(PMAA)}$$

Equation 2.3.

$R_f(P2VP)$ and $R_f(PMAA)$ are the Flory radii of P2VP and PMAA chains respectively and $N(P2VP)$ and $N(PMAA)$ refer to the number of grafted chains present, which are calculated from the amount of Ce(IV) used during grafting.

Average R_f values for support 5 and 6 in table 2.6 were calculated using the assumption that without a second addition of Ce(IV) initiators the grafting of a second polymer species will occur from the chain ends of polymers grafted during the first stage. The R_f value here (equation 2.4) was derived from the average monomer size, A , the total chain length of (P2VP + PTBMA), L , and the molar quantities of monomer grafted to the support, n .

$$R_f(av) = \left(\frac{A(P2VP) \cdot n(P2VP) + A(PMAA) \cdot n(PMAA)}{n(P2VP) + n(PMAA)} \right) \cdot (L(P2VP) \cdot L(PMAA))^{0.6}$$

Equation 2.4

The presence of diblock copolymers is ignored for R_f calculations on supports 1-4 (table 2.5) for simplicity. This simplification assumes that the number of radical

PVA sites created during the second Ce(IV) addition is much higher than the number of radical functionalities remaining at the ends of grafted chains. This is reasonable, as the relatively low monomer conversion (typically 10-15% during the first graft step) indicates that most radical chain ends have been terminated by the end of the first graft stage. R_f calculations for supports 5 and 6 are based upon initiation from all grafted chain ends, as the extent of termination is not known. In this case the individual R_f values of chains grafted to 5 and 6 are expected to have a large deviation from this average, with a small number of long diblock chains extending beyond the polymers grafted during the first graft step.

Calculated values of $2R_f/D$ indicate that all grafted layers fall within the brush regime. Mixed brush layers show higher R_f values for P2VP than PMAA in all cases, as a result of larger P2VP monomer size. This indicates that the maximum extension of P2VP chains in the mixed brush is greater than that of PMAA. As the calculated R_f values do not factor for charge-charge interactions it is likely that the effective R_f values are considerably higher than those tabulated. Repulsion between charge sidegroups within the polymer chains will lead to more extended chain behaviour, rather than the 'random walk' seen for uncharged polymers chains. In this case it may be expected that electrostatic effects outweigh the influence of sterics on chain extension, leading to more similar effective R_f values for P2VP and PMAA chains.

The efficiency of Ce(IV) activation also has an effect upon the properties of the polymer layer. Lower Ce(IV) efficiencies lead to a lower number of activation sites and hence a lower number of grafted chains, with a longer average chain length for a given polymer grafting yield. Previous studies have indicated that Ce(IV) activation from PVA has an efficiency of 70% (Gupta and Sahoo, 2001), which would correspond to 147 μmol Ce(IV) leading to initiation from 103 μmol of PVA sites. An example of the effect of this grafting efficiency upon mixed brush properties can be given using support 3 in Table 2.5. 100% Ce(IV) efficiency would give calculated values of $D = 0.58$ nm, $R_f = 4.55$ nm and $2R_f/D = 15.7$ for the mixed brush, whereas 70% Ce(IV) efficiency gives $D = 0.69$ nm, $R_f = 5.64$ nm

and $2R_f/D = 16.3$. 2% Ce(IV) efficiency has also been reported (Hrictu et al., 1999), which would correspond to $D = 4.09$ nm, $R_f = 47.59$ and $2R_f/D = 23.3$. In both cases it can be seen that lower Ce(IV) activation efficiencies correspond to longer polymer chains, higher $2R_f/D$ values and hence the expectation of more pronounced brush regime behavior.

2.4 Conclusions

The work described in this chapter demonstrates the relevance of Ce(IV) as a method for creating tethered polymers at the M-PVA surface. Successful grafting of polyelectrolytes constituting up to 49% of the total product mass shows Ce(IV) initiation can be used to create a dense, chargeable polymer layer on the M-PVA surface, with dimensions indicating brush behavior ($2R_f/D > 15$). The direct initiation mechanism of Ce(IV) based grafting methods gives some control of surface grafting density. This allows synthesis of mixed polymer brush layer by sequential Ce(IV) grafting steps, separated by a quenching step to prevent diblock polymer formation.

Table 2.5. M-PVA mixed brush grafting with 147 mmol Ce(IV) added per g M-PVA before each polymer addition.

Prior to second graft step, quenching was performed on support 3 and 4

Support	Stage	Polymer grafted	Ce(IV) (μmol) per g M-PVA	Quench	Monomer presented (mmol) per g M-PVA	Monomer grafted (mmol) per g M-PVA	Yield (%)	D (nm)	Mol % P2VP	Mol % PTBMA	R_f (nm)	2 R_f /D	n(pol)/ n(init.)
1	Step 1	P2VP	147	No	43.96	5.89	13.4	0.82			6.13	15.0	80.1
1	Step 2	PMAA	147	No	37.04	3.85	10.4	0.82			2.34	5.7	52.4
1	Finished	[(P2VP) x + (PMAA) y]				9.74		0.58	60	40	5.09	17.6	
2	Step 1	PMAA	147	No	37.04	5.41	14.6	0.82			2.87	7.0	73.6
2	Step 2	P2VP	147	No	43.96	3.47	7.9	0.82			4.47	10.9	47.2
2	Finished	[(P2VP) x + (PMAA) y]				8.88		0.58	39	61	3.84	13.3	
3	Step 1	P2VP	147	Yes	43.96	4.88	11.1	0.82			5.48	13.4	66.4
3	Step 2	PMAA	147	Yes	37.04	4.56	12.3	0.82			2.59	6.3	62.0
3	Finished	[(P2VP) x + (PMAA) y]				9.44		0.58	52	48	4.55	15.7	
4	Step 1	PMAA	147	Yes	37.04	6.11	16.5	0.82			3.09	7.6	83.1
4	Step 2	P2VP	147	Yes	43.96	3.34	7.6	0.82			4.36	10.7	45.4
4	Finished	[(P2VP) x + (PMAA) y]				9.45		0.58	35	65	3.84	13.3	

Table 2.6. M-PVA grafting with 147 mmol Ce(IV) added per g M-PVA before first polymer addition, but no Ce(IV) present during second polymer addition, leading to formation of potential diblock polymers. Prior to second graft step, quenching was performed on support 7 and 8.

Support	Stage	Polymer grafted	Ce ⁴⁺ (μ mol) per g M-PVA	Quench	Monomer presented (mmol) per g M-PVA	Monomer grafted (mmol) per g M-PVA	Yield (%)	D (nm)	Mol % P2VP	Mol % PTBMA	R _f (nm)	2R _f /D	n(pol)/ n(init.)
5	Step 1	P2VP	147	No	43.96	5.98	13.6	0.82			6.19	15.1	81.4
5	Step 2	PMAA	0.0	No	37.04	1.41	3.8	-			1.28	-	
5	Finished	[(P2VP) _x + (PMAA) _y]				7.39		0.82	81	19	6.35	21.9	
6	Step 1	PMAA	147	No	37.04	5.82	15.7	0.82			3.00	7.3	79.2
6	Step 2	P2VP	0.0	No	43.96	1.05	2.4	-			2.19	-	
6	Finished	[(P2VP) _x + (PMAA) _y]				6.87		0.82	15	85	3.84	9.4	
7	Step 1	P2VP	147	Yes	43.96	5.89	13.4	0.82			6.13	15.0	5.89
7	Step 2	PMAA	0.0	Yes	37.04	0.00	0	-			-	-	
7	Finished	[(P2VP) _x + (PMAA) _y]				5.89		0.82	100	0			
8	Step 1	PMAA	147	Yes	37.04	6.04	16.3	0.82			3.07	7.5	6.04
8	Step 2	P2VP	0.0	Yes	43.96	0.00	0	-			-	-	
8	Finished	[(P2VP) _x + (PMAA) _y]				6.04		0.82	0	100			

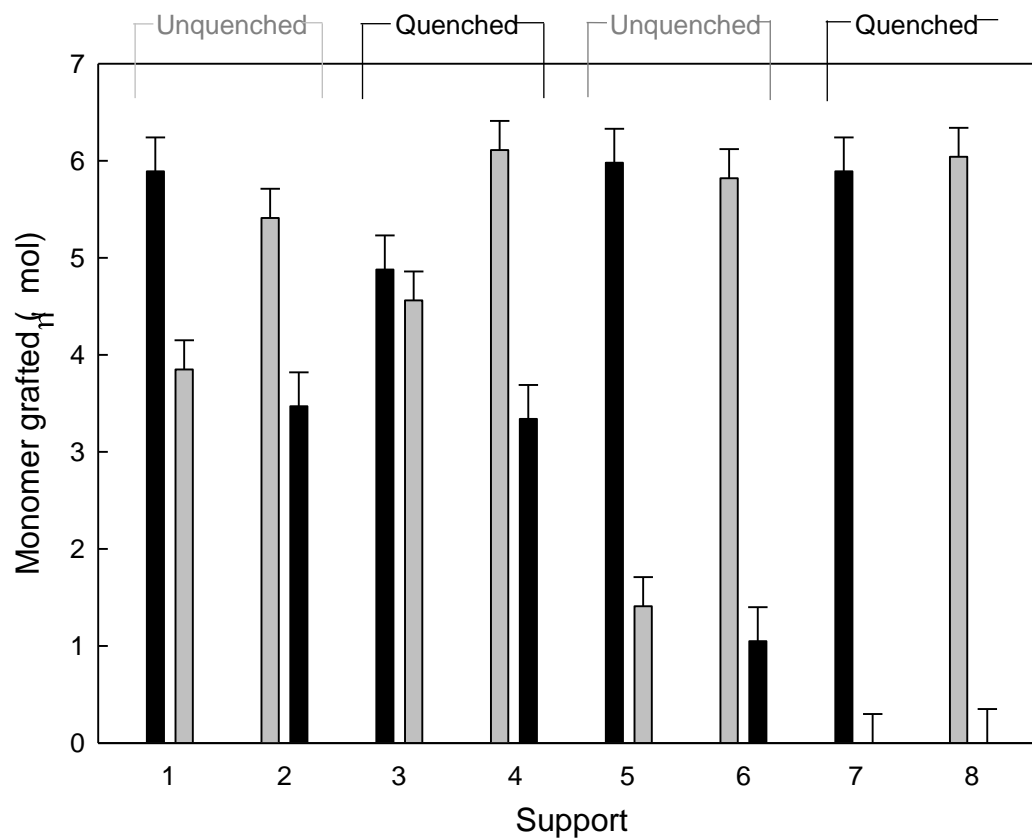


Figure 2.20. Monomer grafting results for supports as described in tables 2.5 and 2.6. Supports 1-4 have Ce(IV) addition before both polymer additions. Supports 5-8 have Ce(IV) addition before first polymer addition only. Supports 3, 4, 7 and 8 have polymerisation quenched by 4-ethoxyphenol addition after 3 hours. Black bars represent P2VP, grey bars represent PTBMA/PMAA.

3. Polymer grafting sulfonyl chloride activated ‘graft to’

3.1 Introduction

“Graft to” polymer brush syntheses are based upon traditional techniques for ligand attachment to solid surfaces, with a nucleophilic or electrophilic polymer end group being used to graft that polymer by reaction with a surface site. Graft to techniques offer various benefits over graft from methods. As polymerisation in graft to techniques is performed before the grafting stage, polymerisation reactions for graft to products are not constrained by grafting conditions. This means that the grafting reaction does not need optimisation to produce polymers of specific M_w and composition, as this is controlled during the pre-grafting polymerisation step. Another benefit of graft to techniques is the possibility of synthesising a mixed polymer brush through a “one-pot” grafting step, in which two polymer species are present and participate in graft to reactions simultaneously. This technique is not possible with most graft reactions as the presence of two monomer species will typically result in creation of grafted copolymers.

One suitable route to graft to synthesis on hydroxyl bearing surfaces is hydroxyl activation with sulfonyl chlorides. Sulfonyl chlorides are derivatives of sulfonic acid which contain a SO_2Cl functional group attached to an aromatic or aliphatic molecule. Attack by a hydroxyl group upon a sulfonyl chloride group leads to replacement of the chlorine atom by the hydroxyl, leading to formation of a sulfonyl ester group (figure 3.1; Hermanson et al., 1992). The improved performance of this reaction in the presence of pyridine was first noted in 1944 (Tipson, 1944) and this improvement contributed to the wide use of sulfonyl esters as leaving groups in organic syntheses.

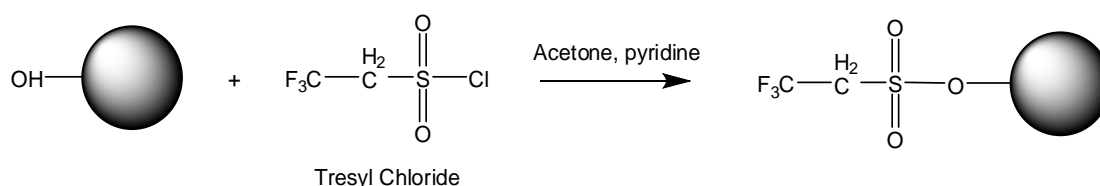


Figure 3.1. Activation of hydroxylated surface with tresyl chloride

Reaction between nucleophiles and sulfonyl activated surfaces leads to the creation of stable, covalent bonds between the nucleophile and surface (figure 3.2).

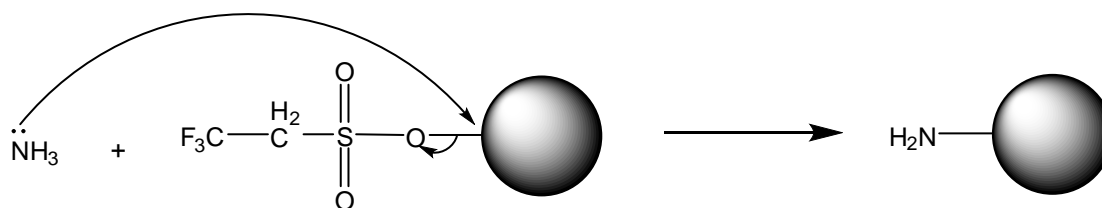


Figure 3.2. Nucleophilic attack upon tresyl activated surface.

2,2,2-trifluoroethanesulfonyl chloride (tresyl) chloride (Oesterling, 1961; Truce and Norell, 1963) is one of the most commonly used sulfonyl chloride activating agents. The use of tresyl chloride as an agent for nucleophilic substitutions was first reported in 1971 (Crossland et al., 1971). Many subsequent studies have used tresyl esters as a route to couple nucleophilic ligands onto hydroxyl-bearing supports (Mosbach and Nilsson, 1981; Demiroglou et al, 1994). These studies have shown tresyl chloride to be an effective agent for activating surfaces for the coupling of nucleophilic ligands. An alternative sulfonyl chloride activation route is with the use of 4-toluenesulfonyl (tosyl) chloride (Hermanson et al., 1992). Tosyl chloride activation works by the same principles as tresyl chloride activation but the tosyl chloride reagent is considerably lower in cost than tresyl chloride.

The preparation of polymer brushes on the hydroxylated M-PVA surface can be performed using the sulfonyl chloride activation technique mentioned above. Polymer chains bearing nucleophilic end groups can be attached to the bead via reaction of the polymer end groups with the activated surface (figure 3.3).

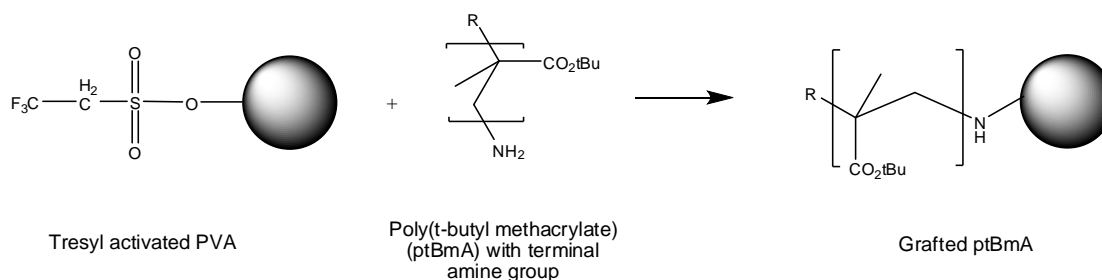


Figure 3.3. Grafting of nucleophile terminated polymer to tresyl activated surface

This method can be extended to the creation of mixed polymer brush surfaces. Grafting of two separate polymer species may be achieved by a two-step synthesis involving reaction of one polymer species with a limited number of surface sites, followed by reaction of a second polymer species with the remaining surface sites (figure 3.4).

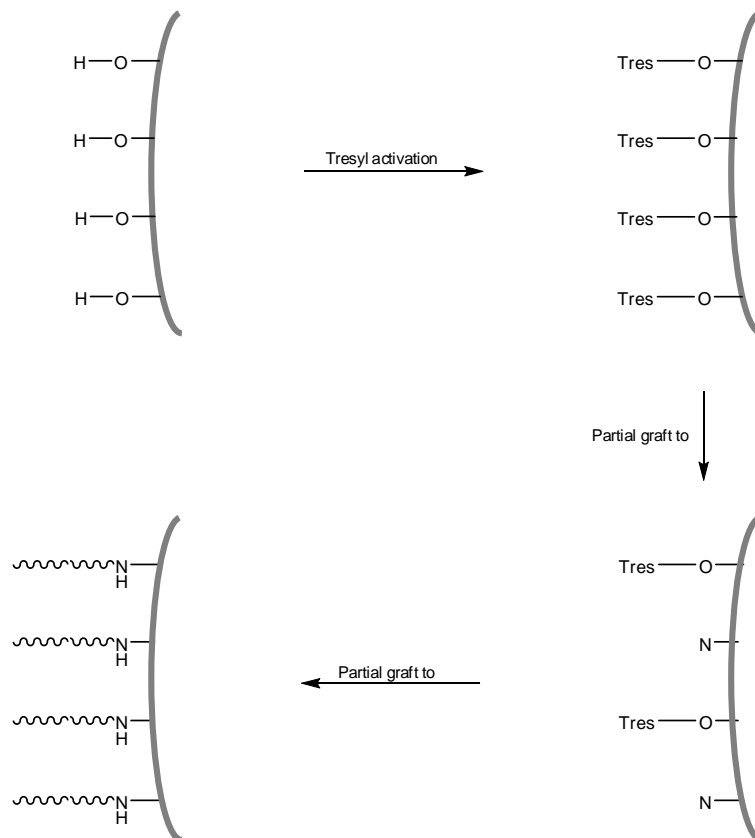


Figure 3.4. Consecutive grafting of polymer species to form a mixed polymer brush layer

Alternatively, a mixed polymer layer may be generated by the simultaneous coupling of two polymer species from the same mixture (figure 3.5).

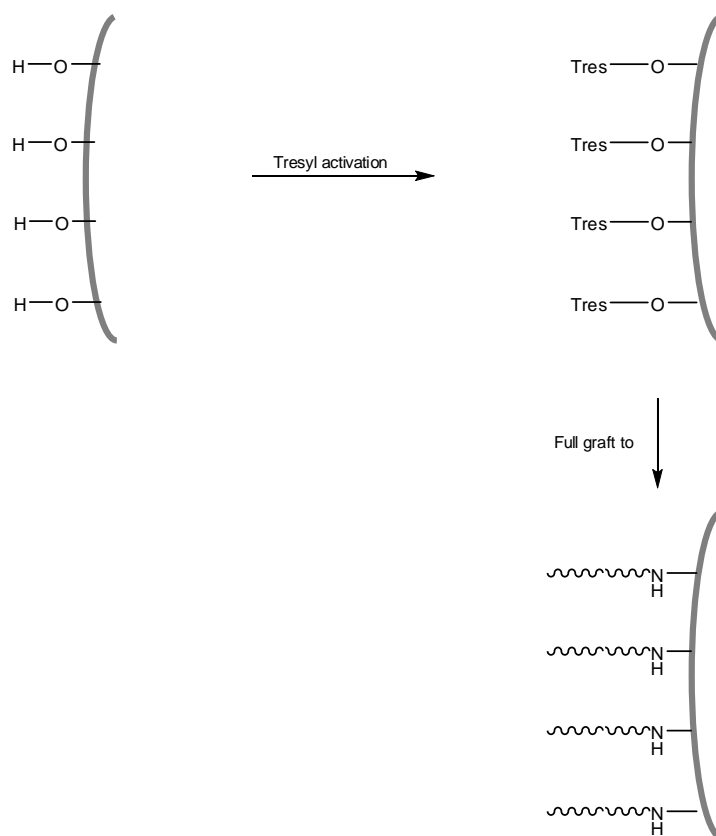


Figure 3.5. Simultaneous grafting of polymer species to form a mixed polymer brush layer

Against the above, this chapter describes sulfonyl activation techniques as applied to the surfaces of M-PVA beads. This includes initial tests of the reactivity of tresyl and tosyl ester surface groups to ammonia and polymer end group, to find a suitable approach for controlled grafting of polymer. These tests were followed by the synthesis of polymer brush layers composed of both P2VP and PMAA chains via initiated grafting of P2VP and PTBMA amine-terminated polymers. The choice of these two polymers is explained in more detail in Chapter 2. Grafted polymer layers are analysed by FTIR including a discussion of the calculated layer dimensions and the implications of these dimensions in potential brush properties.

3.2 Materials and methods

3.2.1 Materials used

M-PVA (batch R2-0105096; V_m ; 3.4 cm³/g; specific surface area 59.2 m² per g) was obtained from Chemagen (Baesweiler, Germany). Amine-terminated poly(2-vinyl pyridine) ($M_w = 113,100$; $M_w = 14,800$) and amine-terminated poly(t-butyl methacrylate) ($M_w = 143,400$; $M_w = 14,500$) were purchased from Polymersource inc. (Montreal, Canada). Tosyl chloride (CAS 98-59-9); 2,2,2-Trifluoroethanesulfonyl chloride (CAS 1648-99-3); pyridine (CAS 110-86-1); acetone (67-64-1); HCl solution (37%, CAS 7647-01-0); sodium hydroxide (CAS 1310-73-2); ammonia solution (37%, CAS 1336-21-6); monobasic sodium phosphate (NaH₂PO₄, CAS 7558-80-7); dibasic sodium phosphate (Na₂HPO₄, CAS 7558-74-9); picrylsulfonic acid (1M, CAS 2508-19-2)); sodium tetraborate (Na₂B₄O₇, CAS 1330-43-4); potassium bromide (CAS 7758-02-3); and methanol (CAS 67-56-1) were obtained from Sigma Aldrich (Poole, Dorset).

Cuvettes, 2 ml screw-cap micro test tubes, 15 ml screw-cap centrifuge tubes and 50 ml screw-cap centrifuge tubes were obtained from Sarstedt (Leicester, UK). 1.5 ml hinged-lid micro test tubes were obtained from Eppendorf (Cambridge, UK).

All unheated mixing was performed with a VM20 vortex mixer or a IKA Vibrax VXR basic mixer with attachments for 15 ml centrifuge tubes and micro test tubes. Heated mixing was performed in a Grant OLS water bath with shaker rack. Samples were dried on watchglasses in a Gallenkamp size 2 hotbox oven. Chemicals were weighed on Mettler AE160 and AT261 balances. Pipetting was performed with 20 ml, 200 ml, 1 ml and 5 ml adjustable pipettes.

3.2.2 Solvent testing

A range of solvents were tested for usefulness in the graft to synthesis. It was necessary for the reaction solvent to suspend M-PVA well and to dissolve both P2VP and PTBMA fully.

Solubility tests were carried out for each sample as follows: 5 ml of solvent was pipetted into a 15 ml screw cap tube and 10 mg of polymer was then added to the tube. This mixture was mixed on a vortex mixer at RT for 15 seconds. If all polymer was dissolved at this point, step i) was followed. If some polymer remained undissolved, step ii) was followed.

- i) A further 20 mg of polymer was added and the mixture mixed for 2 minutes. If the extra polymer was fully dissolved a “*****” value was assigned, if not a “****” was assigned.
- ii) If all polymer was not dissolved during step i), the mixture was mixed on a vortex mixer at RT for 2 more minutes. If all polymer was dissolved at this point, the table was marked with a “****” value. If there had been a significant decrease in the amount of precipitated polymer, the table was marked with a “**” value. If the amount of precipitated polymer had decreased only a small amount the table was marked with a “*” value. If there had been no visible solvation of polymer the table was marked with a “0” value.

3.2.3 Base matrix preparation

Prior to experimentation M-PVA stock was washed thoroughly to remove contaminants from the support manufacture. 1.5 g M-PVA was washed (30 ml, 60 s) with: water; 50% acetone in water; 100% acetone; 50% acetone / 50% methanol; 100% methanol; 50% methanol in water; water (x2); 1 M NaCl in water; water (x3). The washed M-PVA was then suspended in water (30 ml).

3.2.4 Tresyl chloride activation

Following a method described by Hermanson et. al. (1992), tresyl chloride was added to suspensions of M-PVA (5 mg) in acetone (1 ml) with pyridine (50 μ l) and mixed for 600 s at RT. Supports were then separated from the solution and washed four times in washing solutions made of, respectively, 30%, 50%, 70% and 100% 1 μ M aqueous HCl in acetone. Particles were then stored in 1 ml of 1 mM HCl at 4°C.

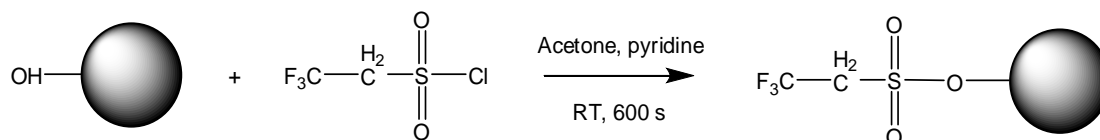


Figure 3.6. Activation of M-PVA hydroxyl sites by tresyl chloride

3.2.5 Tosyl chloride activation

Following Hermanson et. al. (1992), tosyl chloride was added to suspensions of M-PVA (5 mg) in acetone (1 ml) with pyridine (50 μl) and mixed for 1 hour at RT. Supports were then separated from the solution and washed four times in washing solutions made of, respectively, 30%, 50%, 70% and 100% 1 μM aqueous HCl in acetone. Particles were then stored in 1 ml of 1 mM HCl at 4°C.

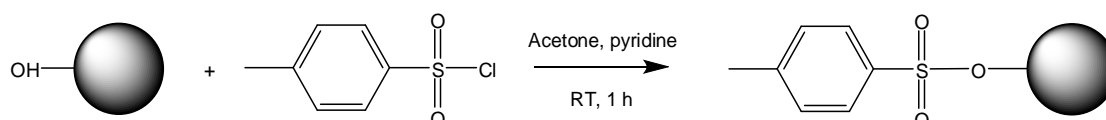


Figure 3.7. Activation of M-PVA hydroxyl sites by tosyl chloride

3.2.6 Amination of tresylated particles

Tresyl activated support (5 mg) was reacted with conc. ammonia solution (50 μl) in acetone (1 ml, 24 h). Supports were then separated from the supernatant and washed (1 ml, 60s) with water; 50% acetone in water; 100% acetone; 100% methanol; water (x2).

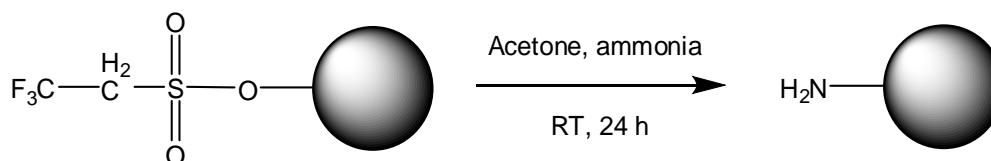


Figure 3.8. Amination of tresylated M-PVA sites with ammonia

3.2.7 Amination of tosylated particles

Tosyl activated support (5 mg) was reacted with conc. ammonia solution (50 μl) in acetone (1 ml, 24 h). The supports were then separated from the supernatant and washed (1 ml, 60s) with water; 50% acetone in water; 100% acetone; 100% methanol; water (x2).

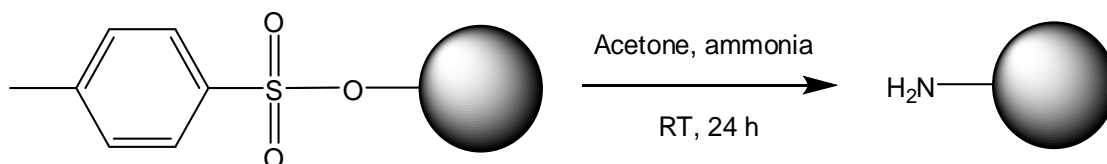


Figure 3.9. Amination of tresylated M-PVA sites with ammonia

3.2.8 TNBS assay of polymer grafted supports

Sulfonyl activated M-PVA particles (5 mg) were mixed with a solution of amine-terminated polymer in acetone (1 ml, 24 h). Supports were then washed with acetone (1 ml, 60 s, x2) followed by reaction with conc. ammonia solution (50 μ l) in acetone (1 ml, 24 h). The supports were then separated from the supernatant and washed (1 ml, 60s) with water; 50% acetone in water; 100% acetone; 100% methanol; water (x2).

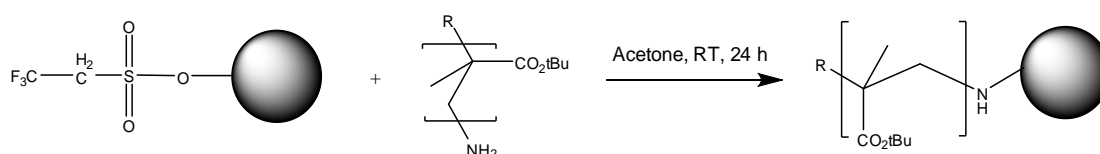


Figure 3.10. Reaction of amine terminated polymer at sulfonated surface site

Following a method described by Halling and Dunnill (1979), an aqueous mixture comprising picrylsulfonic acid (TNBS, 1 M, 10 μ l) and $\text{Na}_2\text{B}_4\text{O}_7$ (0.05 M, 1.5 ml) was added to a sample of aminated support (5 mg). The suspension was heated with mixing (70°C, 600 s) then allowed to cool to room temperature (600 s). The supports were then separated from the supernatant and washed (1 ml, 60s) with water; 50% acetone in water; 100% acetone; water (x2).

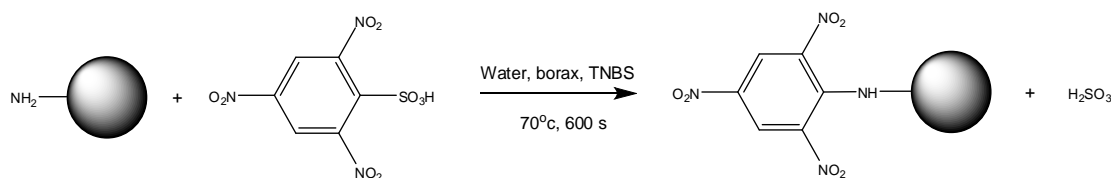


Figure 3.11. Coupling of picrylsulfonic acid to aminated M-PVA sites

The supports were then suspended in 5 ml of $\text{NaOH}_{(\text{aq})}$ solution (1 M, 5 ml) and heated to 70°C with mixing. The suspension was heated with mixing (70°C, 600 s) then allowed to cool to room temperature (600 s). A sample of the supernatant

containing no particle was then taken and its absorbance read at 410 nm. Samples were calibrated against standards containing picric acid in 1 M NaOH.

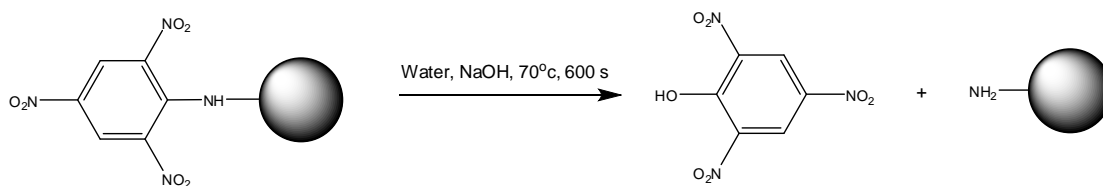


Figure 3.12. Release of picric acid (absorbance at 410 nm)

3.2.9 Homopolymer brush grafting of tresylated supports

50 mg of tresyl activated M-PVA was reacted with amine-terminated polymer (8 mg) in acetone (5 ml, 24 h). Supports were then washed with acetone (5 ml, 60 s, x3).

3.2.10 Mixed polymer brush grafting of tresylated supports

25 mg of tresyl activated, single-brush grafted M-PVA was reacted with a second amine-terminated polymer (30 mg) in acetone (2.5 ml, 24 h). Supports were then washed with acetone (2.5 ml, 60 s, x3).

3.2.11 Hydrolysis of grafted PTBMA chains

Hydrolysis of PTBMA grafted supports to give PMAA chains was achieved using a 50/50 (v/v) aqueous solution of trifluoroacetic acid (TFA, see appendix 7.1 for details of this reaction and reagent choice). PTBMA grafted single and mixed brush supports were reacted with a 50/50 (v/v) mixture of TFA and water (5 ml, 60°C, 24 h) followed by washing with water (5 ml, 60s, x 2).

3.2.12 FTIR analysis

Dry solid samples were pressed with KBr to form 13 mm discs as described in Chapter 2. Samples discs were analysed using a Thermo Nicolet 380 FTIR with 64 scans per sample at a resolution of 2 cm⁻¹.

Liquid FTIR samples were prepared from supernatant and quantified as described in Appendix 7.4. FTIR samples were run on a Nicolet Smart Orbit diamond ATR apparatus, using 50 µl aliquots of the sample liquid at a resolution of 2 cm⁻¹.

3.3 Results

3.3.1 Solvent testing

Solubility tests for P2VP and PTBMA samples with long ($M_r \sim 100,000$) and shorter ($M_r \sim 15,000$) polymer chain lengths showed that for all samples pure acetone solubilised polymers to a significantly greater extent than water, DMSO or mixtures of these solvents 3.1. The noticeable change in polymer solubility between 100% acetone solvent and 80% acetone/20% water solvent also indicated that addition of aqueous components to a solution of polymer in acetone should be avoided if polymer solvation is to be maintained.

Table 3.1. Solubility tests on short chain P2VP (M_w : 14,800), short chain PTBMA (M_w : 14,500), long chain P2VP (M_w : 113,100), long chain P2VP (M_w : 143,400). 0 indicates poor polymer solubility, **** indicates complete solvation of polymer under the experimental conditions (see method 3.2.2 for further details).

Solvent Composition.	p2VP, short chain. Solubility	ptBmA, short chain. Solubility	p2VP, long chain. Solubility	ptBmA, long chain. Solubility
Water	*	*	0	0
20% Acetone/ 80% Water	**	*	*	0
50% Acetone/ 50% Water	****	***	***	*
80% Acetone/ 20% Water	****	***	***	*
100% Acetone	*****	*****	****	***
50% DMSO/ 50% Water	*	0	0	0
100% DMSO	***	**	***	*

3.3.2 Studies on sulfonyl activation in acetone

In order to achieve mixed brush grafting using a graft to method it is especially important not to saturate the surface with grafted polymer during the first step, as this will result in the a second polymer species being unable to reach the surface due to hinderance from the previously grafted polymers. One method investigated for controlling sulfonyl activated mixed brush graftings was partial sulfonyl activations,

with the intention of using two separate activation steps in which the initial grafting produces a graft with low enough density to allow a second activation and graft step with space for the second polymer species to graft at the surface.

To test the relationship between sulfonyl chloride concentration and density of surface activation surfaces samples of M-PVA were activated using a range of tresyl chloride concentrations. These tresyl activated samples were then reacted with ammonia and the results assayed using the TNBS method. A plot of tresyl chloride concentration vs. extent of amination shows that tresylation followed by amination is not a stoichiometric reaction (figure 3.13). From these results the maximum number of sites activated to amine attack using tresyl ester was calculated as 57.8 μmol per g of support.

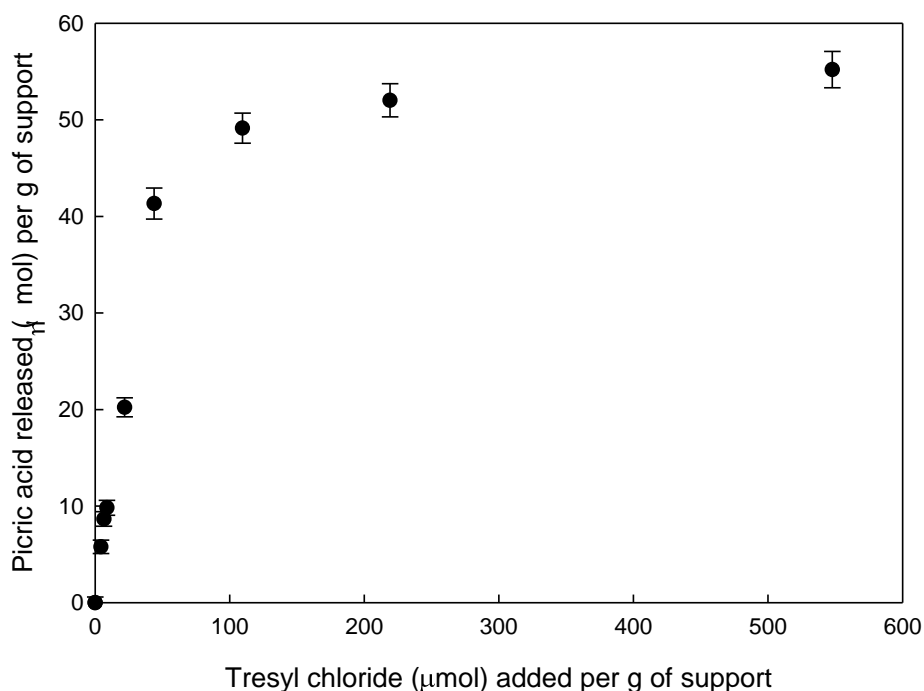


Figure 3.13. Test for amination of activated M-PVA vs. tresyl chloride present during activation (TNBS assay)

Samples of M-PVA were also activated using a range of tosyl chloride concentrations in the original tresylation step. The activated samples were reacted with ammonia and the results assayed using the TNBS method (figure 3.14).

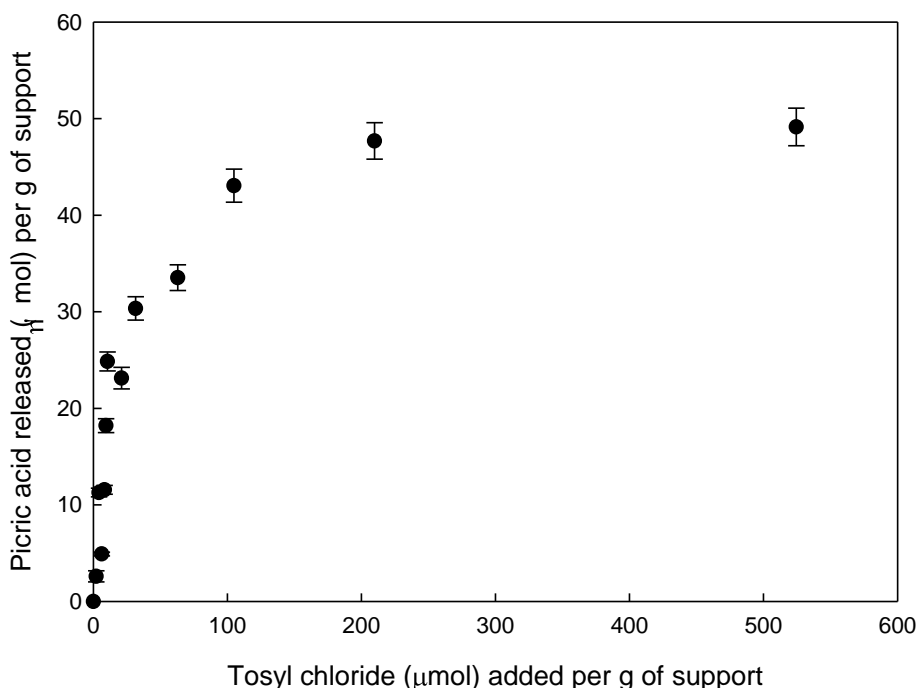


Figure 3.14. Test for amination of activated M-PVA vs. tosyl chloride present during activation (TNBS assay)

The plot of tosyl chloride concentration vs. extent of amination shows similar behaviour to that for tresyl chloride activation. The maximum tosyl activation to amine attack was calculated as $49.4 \mu\text{mol}$ per g of support. Tresyl chloride appears to be a slightly better activator for nucleophilic attack with a greater maximum amination value. The relationship between amount of sulfonyl chloride added and the activation as measured by the TNBS assay indicates that controlling graft density through measured use of sulfonyl chloride would be extremely difficult. For simplicity, all subsequent grafting experiments were based around a maximum sulfonyl chloride activation with control of graft density through the polymer concentration used.

3.3.3 Single polymer brush grafting

Grafting was attempted with both long-chain (P2VP M_w : 113,100; PTBMA M_w : 143,400) and short-chain (P2VP M_w : 14,800; PTBMA M_w : 14,500) polymers. Although grafting of long-chain polymers was successful, interactions between the grafted particles resulted in clumping of the supports. In the case of P2VP the

product was a single continuous mass of M-PVA which could not be broken down without loss of magnetic properties. This behaviour may be attributed to interactions between the grafted polymer chains on separate M-PVA beads leading to chain entanglement and other formed of physical bonding between beads. Consequently, all subsequent grafting experiments and brush syntheses were performed with the short-chain polymers.

The presence of P2VP following activation with tresyl and tosyl chlorides was confirmed using FTIR spectroscopy on solid samples (figure 3.15).

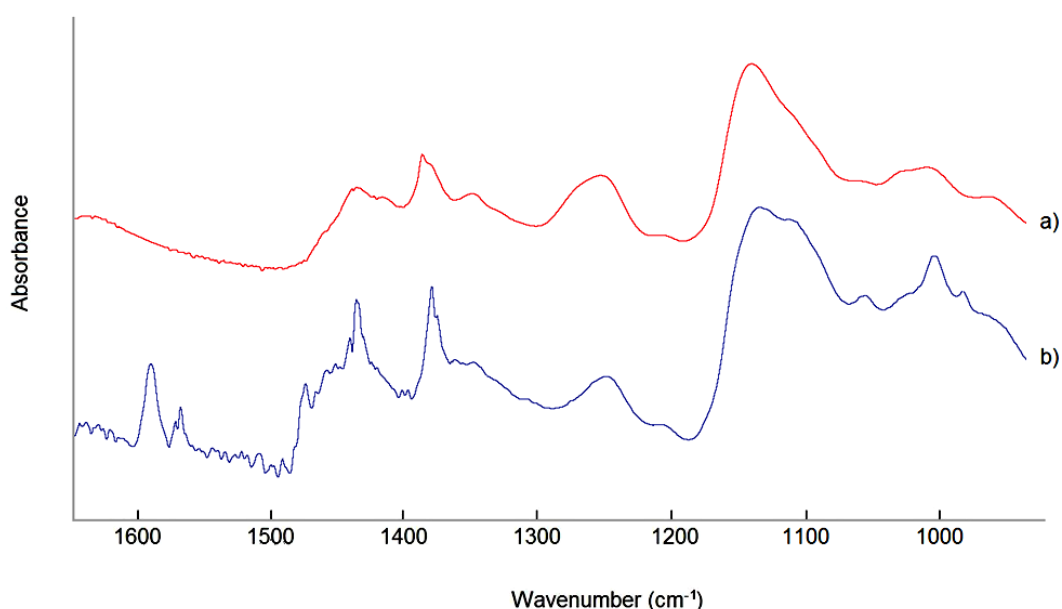


Figure 3.15. a) Tresyl activated M-PVA; b) Tresyl activated m-PVA following reaction of support (50 mg) with P2VP (5 mg) in ACETONE

Peaks for P2VP are clearly visible following graft-to reaction, New peaks appear between 1600 and 1400 cm^{-1} , corresponding to the presence of additional aromatic C-H bonds. This indicates the presence of 2-pyridine groups due to grafted P2VP on the M-PVA. A similar spectra was obtained following P2VP reaction with the tosyl activated support.

P2VP grafting reactions followed by amination and TNBS assay was performed over a range of initial polymer solution concentrations, in order to show how the presence

of grafted P2VP affects further amination at sulfonated surface sites. Picric acid release during the TNBS assay was plotted against P2VP concentration in the polymer grafting step (figure 3.16).

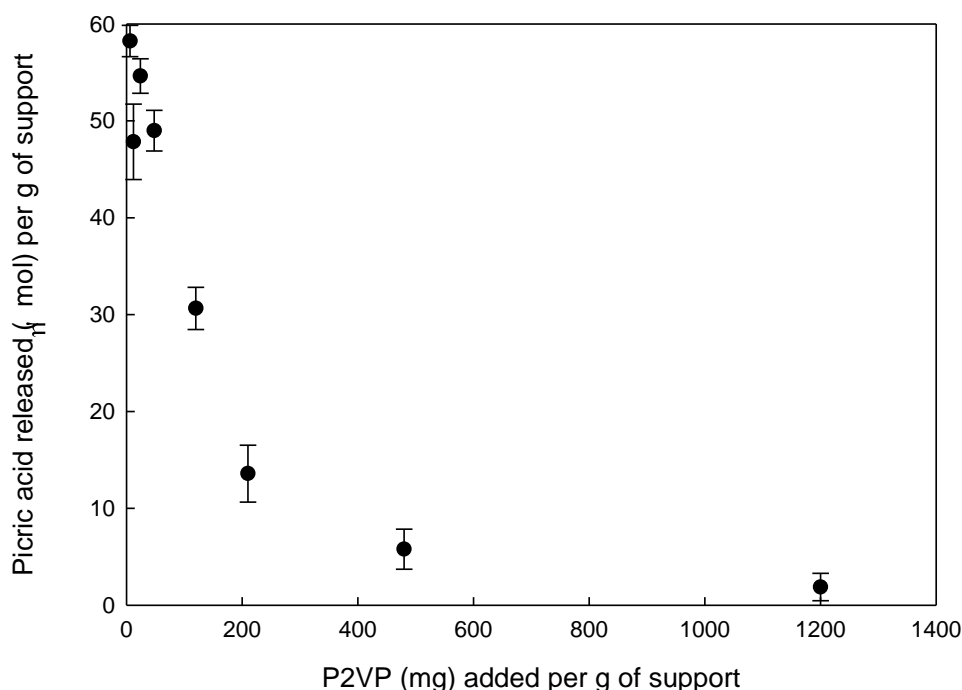


Figure 3.16. TNBS test results on support reacted with ammonia after tresyl chloride led reaction with amine-terminated P2VP.

Increased P2VP concentration in the polymer grafting step corresponds to a decreased availability of activated surface sites in the subsequent ammonia attack stage. It was estimated that consumption of 50% of the originally available sites ($23.9 \mu\text{mol}$ per g of support) requires a polymer concentration of approximately 160 mg per g of support. This was based on the observation that 50% amination (based on TNBS assay, compared to 100% amination with the ungrafted, sulfonated surface) was possible when reacted with tresylated M-PVA which had been reacted with 160 mg P2VP per g of support. For stepwise addition of binary mixed brush polymers, 50% consumption of sites is desired at the first step followed by maximum consumption of the remaining sites during the second step. Similar behaviour was seen for reaction of P2VP with the tosyl activated support (figure 3.17).

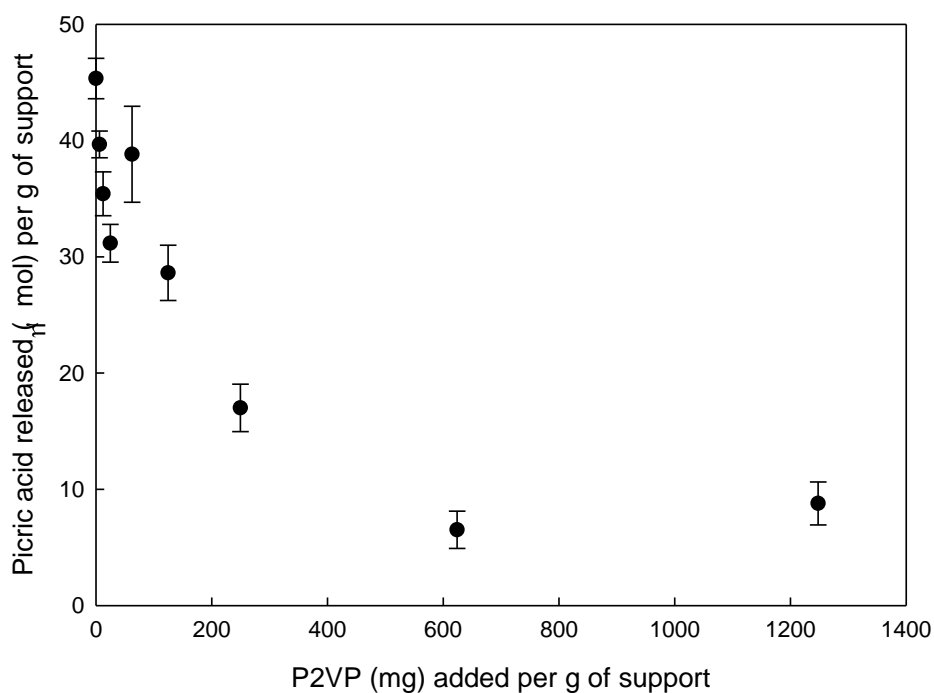


Figure 3.17. TNBS test results on support reacted with ammonia after tosyl chloride led reaction with amine-terminated P2VP.

As can be seen for figures 3.16 and 3.17, some degree of error may be present in this assay due to interaction of the P2VP chain with TNBS. In particular steric hindrance of TNBS reaction at, and release from, the aminated surface is expected due to the presence of P2VP chains.

Liquid spectra for these reactions showed consumption of P2VP from the reaction supernatant, with a significant decrease in polymer peak heights when low polymer concentrations were used (figure 3.18). This is indicative of a high conversion from free polymer to grafted form at lower grafting densities.

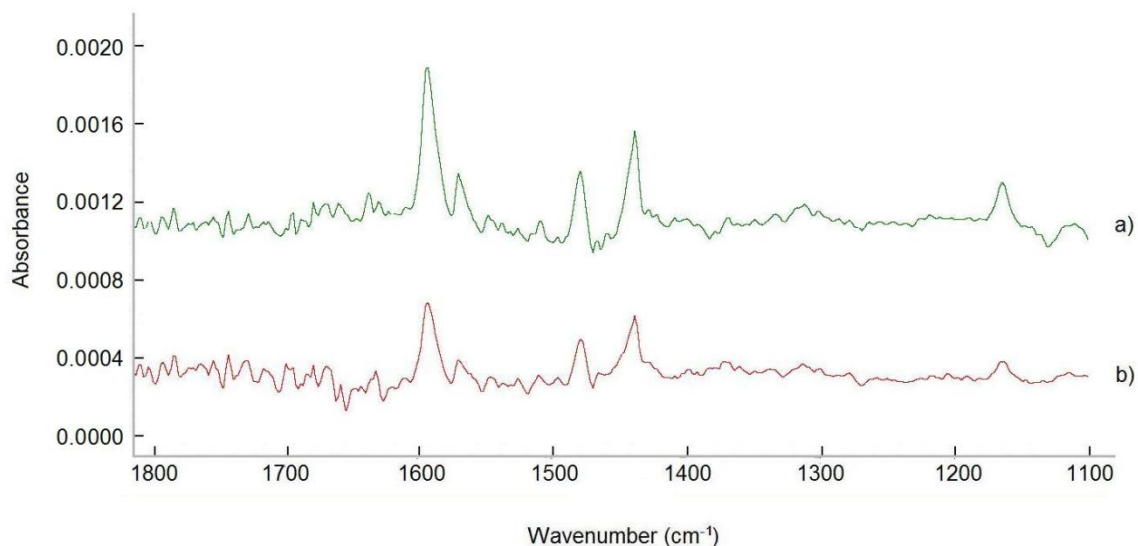


Figure 3.18. Supernatant FTIR sample from before (a) and after (b) reaction of tresyl activated M-PVA (50 mg) with P2VP (5 mg).

The presence of PTBMA following activation with tresyl and tosyl chloride was confirmed using FTIR spectroscopy on solid samples (figure 3.19).

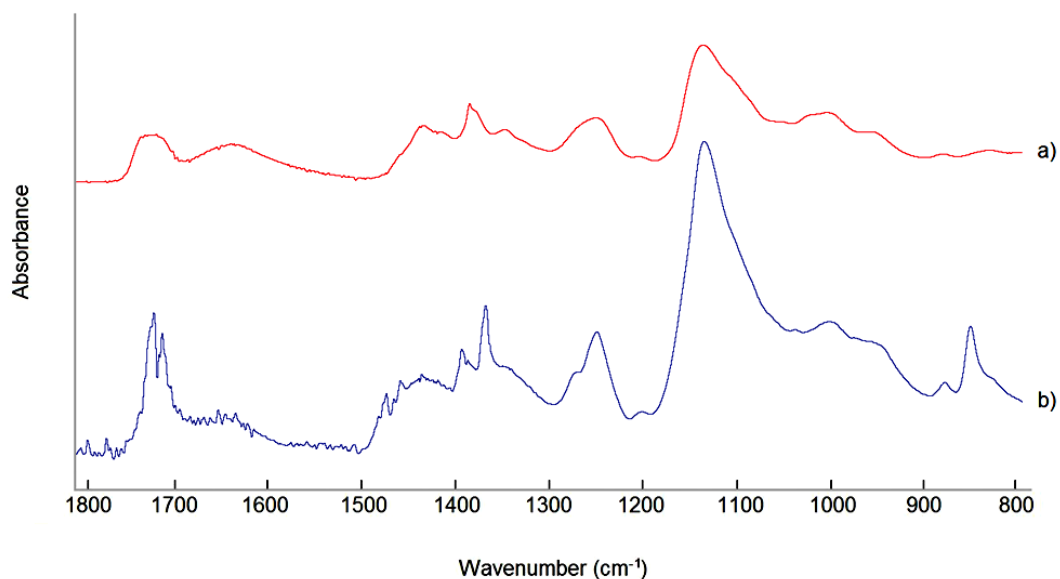


Figure 3.19. a) Tresyl activated M-PVA; b) Tresyl activated M-PVA following reaction of support (50 mg) with PTBMA (5 mg).

Peak changes between the two spectra indicate the presence of anchored PTBMA following graft to reaction. A significant increase in peak height at around 1720 cm^{-1} is observed, corresponding to the additional carbonyl bonds provided by ptBmA ester groups. Small peaks at 1480 cm^{-1} and 1460 cm^{-1} indicate the addition of methylene groups, associated with grafted polymer backbone. A sharp methyl C-H peak visible at around 1370 cm^{-1} is not present in the ungrafted M-PVA and is probably due to the multiple methyl groups present on the graft polymer t-butyl esters. These new peaks were also visible in solid spectra following reaction of the tosyl activated supports with PTBMA. Increases in peak heights at 1250 (additional methyl groups) and 1140 cm^{-1} (ester C-O) also give evidence of successful grafting, although similarly placed peaks were already present prior to grafting.

PTBMA grafting reactions followed by amination and TNBS assay were performed over a range of initial polymer solution concentrations. Picric acid release during the TNBS assay was plotted against PTBMA concentration in the polymer grafting step (figure 3.20).

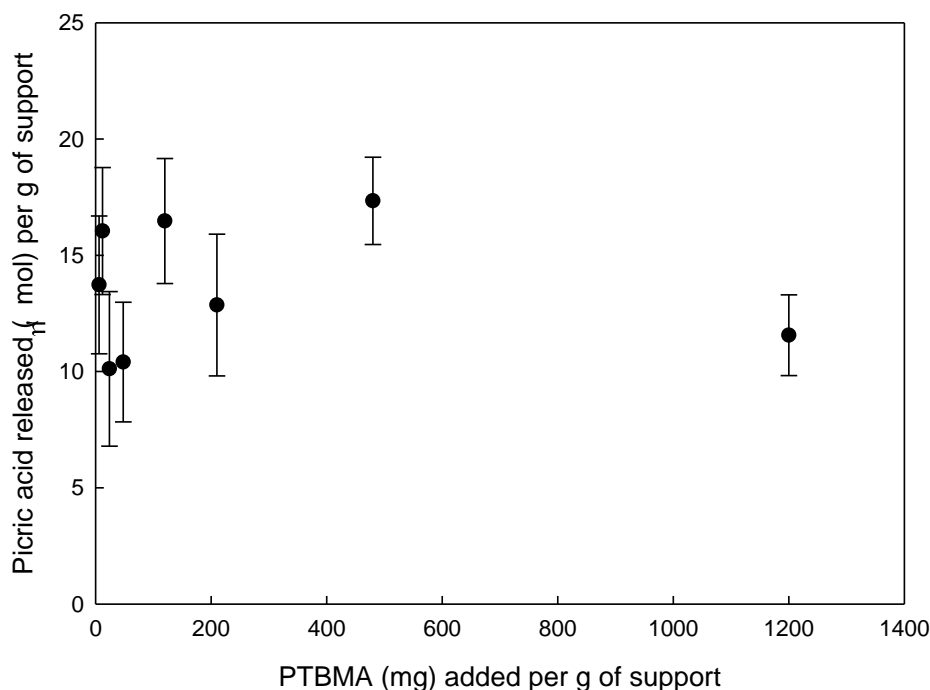


Figure 3.20. TNBS test results on support reacted with ammonia after tresyl chloride led reaction with amine-terminated PTBMA.

Picric acid release in the final step showed no clear relationship to initial polymer graft solution concentration. This may be due to reaction between ammonia and butyl ester side groups, leading to interference with the TNBS assay. Concentrated ammonia may engage in nucleophilic attack upon butyl ester groups to create amide groups, which may in turn interfere with later stages in the assay either directly or by releasing ammonia when conditions are altered.

Due to interference in the TNBS assay of PTBMA graft products it was assumed that the consumption of activated sites during PTBMA grafting followed a similar pattern to sulfonyl site consumption with the amount of polymer required for 50 % sulfonyl sites consumption (160 mg polymer per g tresyl activated M-PVA; 200 mg polymer per g tosyl activated M-PVA) and 100 % site consumption (1200 mg polymer per g tresyl activated M-PVA; 1500 mg polymer per g tosyl activated M-PVA) during P2VP grafting were assumed to be correct for PTBMA grafting for the purpose of mixed brush syntheses.

Liquid spectra results showed loss of PTBMA from reaction supernatants (figure 3.21), as evidenced by the loss in height for all PTBMA absorbance peaks.

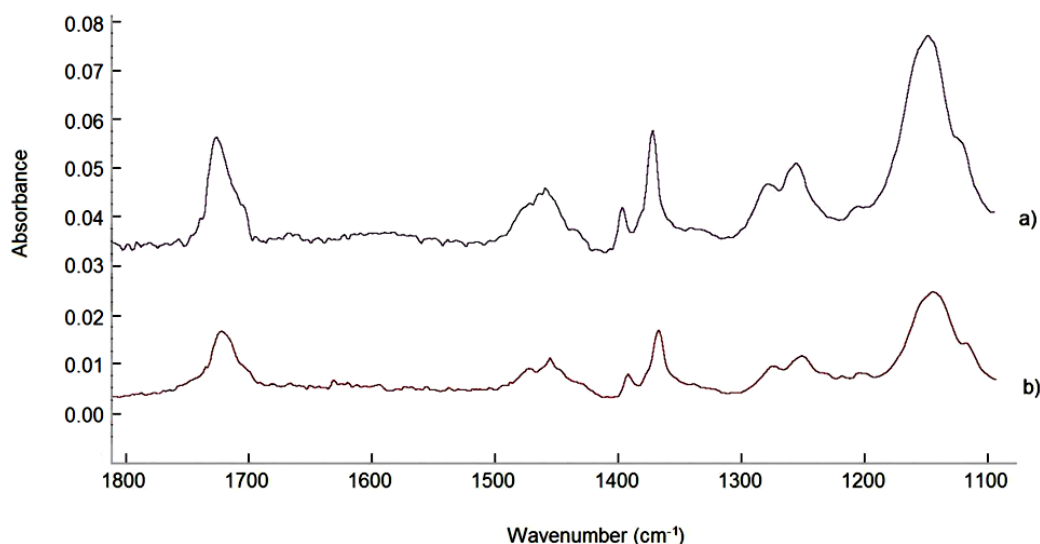


Figure 3.21. Supernatant FTIR sample from before (a) and after (b) reaction of tresyl activated M-PVA (50 mg) with PTBMA (5 mg).

These results show that tresyl and tosyl activations are both suitable methods for grafting amine-terminated polymers to the M-PVA surfaces. Based upon the higher activation densities seen with tresyl activation (see section 3.3.2) it was decided to pursue tresyl activation as a route for mixed brush grafting. The higher activation densities seen with tresyl grafting are expected to lead to higher polymer grafting densities than would be possible with tosyl activation. Although tresyl chloride is a considerably more expensive reagent than tosyl chloride the improvements in grafting properties are expected to make tresyl chloride the more desirable reagent for polymer grafting in this case.

3.3.4 Mixed polymer brush grafting

Reaction of polymer grafted M-PVA (tresyl route) with a second polymer was performed to create supports with mixed brush surfaces. Spectra of the product following P2VP then PTBMA grafting indicate that a mixed polymer P2VP/PTBMA layer has been successfully grafted, with the appearance of a new peak at 1390 cm^{-1} and significant increases in peak height at 1720 , 1370 and 1140 cm^{-1} , corresponding to PTBMA addition on the P2VP grafted surface (figure 3.22)

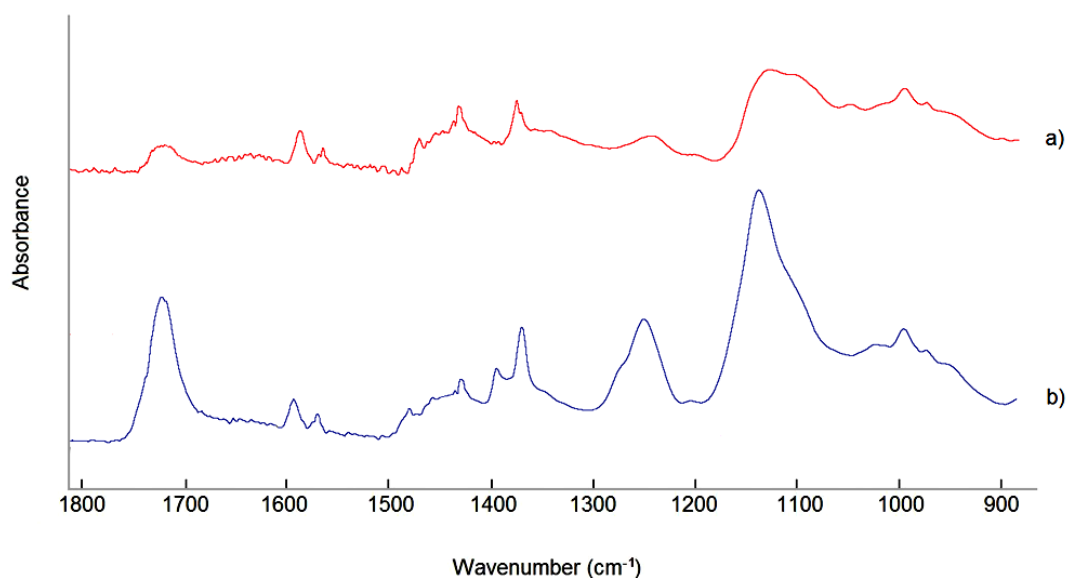


Figure 3.22. a) Tresyl activated M-PVA (50 mg) following reaction with P2VP (5 mg);
b) P2VP grafted support (25 mg) with PTBMA (30 mg)

Mixed brush grafting of PTBMA then P2VP produced similar results (figure 3.23).

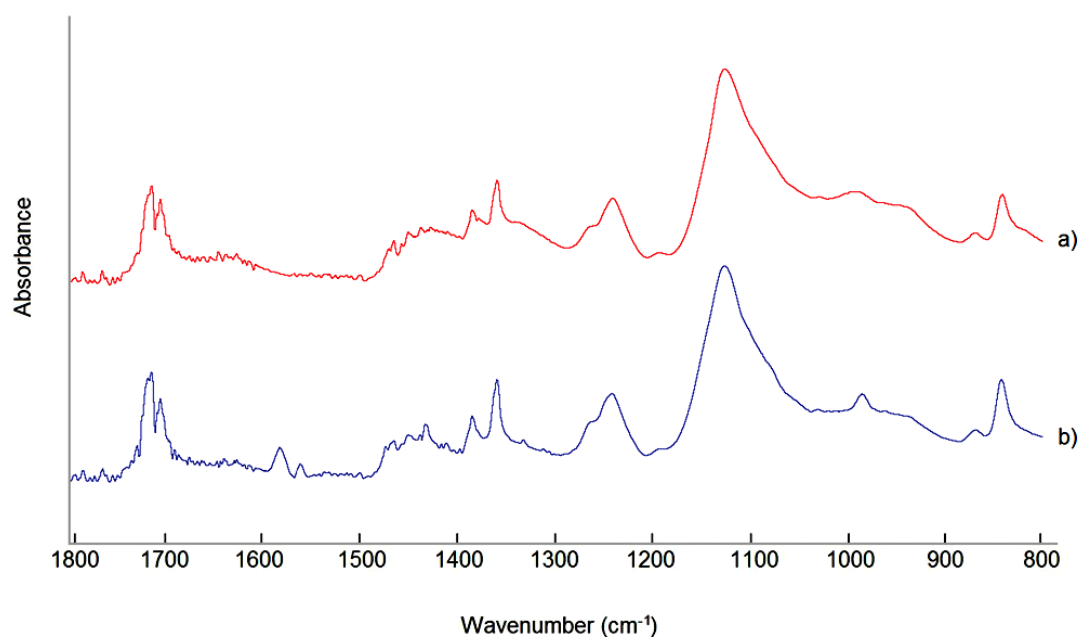


Figure 3.23. a) Tresyl activated M-PVA (50 mg) following reaction with PTBMA (5 mg); b) PTBMA grafted support (25 mg) with P2VP (30 mg)

The appearance of new peaks at 1590 and 1570 cm^{-1} (aromatic C-H) and an increase in the peak height at 980 cm^{-1} are good evidence of P2VP addition in the second grafting step. Peaks at 1470 and 1430 cm^{-1} are also expected for grafted P2VP, however absorbance at these wavelengths already has contributions from the M-PVA/PTBMA support and the additional P2VP peaks are not clearly visible. Similar results were seen for supports grafted by simultaneous addition of P2VP and PTBMA, with peaks for both polymers appearing following the combined polymer grafting stage.

Following mixed brush grafting, hydrolysis of the supports with TFA solution led to loss of characteristic PTBMA peaks at 1370, 1250 and 850 cm^{-1} (figure 3.24). These peaks correspond to methyl C-H peaks found in the t-butyl alcohol group which is removed during hydrolysis.

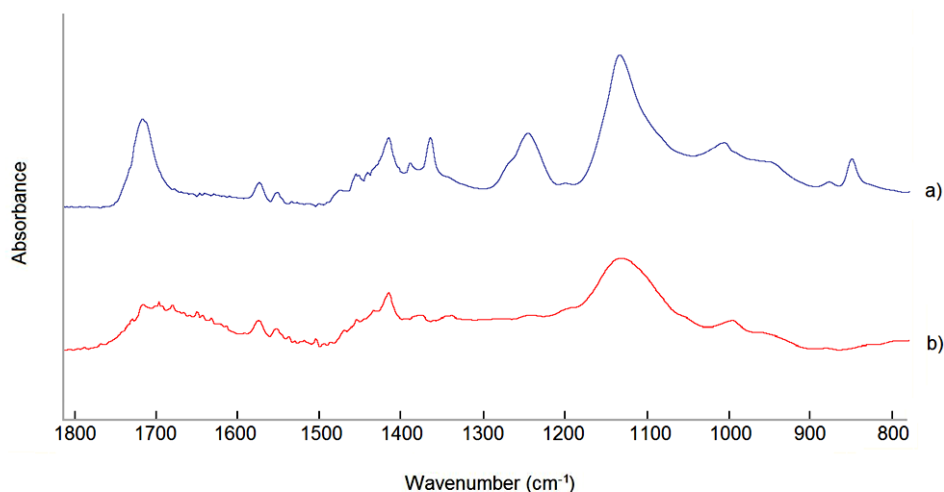


Figure 3.24. a) P2VP grafted support (25 mg) with PTBMA (30 mg) in acetone; b) P2VP + PTBMA grafted support following hydrolysis with TFA solution

Mixed graft products were quantified for M-PVA and graft polymer composition by liquid state FTIR analysis of the reaction supernatants, as shown in table 3.2. Brush spacing for graft-to methods was calculated from the grafted polymer yield plus the polymer chain lengths as given by polymersource and an M-PVA surface area of 59.2 m² per g. R_f and $2R_f/D$ values for homopolymer and mixed brush layer were calculated using the method described in Chapter 2, with an average R_f value calculated for the mixed brush from the R_f values of its component P2VP and PMAA phases. R_f values remained consistent for each species, as is obvious for graft to approaches using known polymer chain lengths.

Table 3.2. Quantification results for supports modified by tresyl graft-to grafting technique, using consecutive addition of polymers (supports 1 and 2) and simultaneous addition of polymers (supports 3 and 4).

Support	Stage	Polymer grafted	Monomer presented (mmol) per g M-PVA	Monomer grafted (mmol) per g M-PVA	Yield (%)	D (nm)	Mol % P2VP	Mol % PMAA	R _f (nm)	2R _f /D	n(poly)/n(init.)
1	Step 1	P2VP	1.52	1.35	88.8	3.20			13.04	8.1	141
1	Step 2	PMAA	4.22	1.81	42.9	2.36			5.29	4.5	102
1	Finished	[(P2VP) _x + (PMAA) _y]		3.16		1.90	43	57	9.72	10.2	
2	Step 1	PMAA	1.13	0.94	83.2	3.26			5.29	4.1	102
2	Step 2	P2VP	5.71	2.44	42.7	2.38			13.04	11.0	141
2	Finished	[(P2VP) _x + (PMAA) _y]		3.39		1.92	72	28	11.66	12.1	
3	Step 1	P2VP	1.52	0.93	61.2	3.85			13.04	6.8	141
3	Step 1	PMAA	1.13	0.77	68.1	3.62			5.29	2.9	102
3	Finished	[(P2VP) _x + (PMAA) _y]		1.70		2.64	55	45	10.59	8.0	
4	Step 1	P2VP	5.71	1.92	33.6	2.68			13.04	9.7	141
4	Step 1	PMAA	4.22	1.34	31.8	2.73			5.29	3.9	102
4	Finished	[(P2VP) _x + (PMAA) _y]		3.26		1.91	59	41	10.86	11.3	

A maximum grafting of 3.39 mmol polymer was seen, equivalent to 25 % of the total mass of final hydrolysed support (0.399 g polymer per g M-PVA). This value is low in comparison to Ce(IV) grafted mixed brush product, in which up to 49 % of support was graft polymer, but still represents a high density of chargeable groups at the support surface.

$2R_f/D > 1$ for all products from the tresyl graft to reactions. Support 3 shows a comparatively low R_f/D value ($2R_f/D = 2.9$) for the grafted PMAA phase, although the overall R_f/D value of 8.0 for this mixed brush product suggests that brush behaviour will be seen. All other supports also show lower $2R_f/D$ values for PMAA chains, but values for the mixed brush which suggest significant brush behaviour. By comparison with Ce(IV) grafting products from Chapter 2 it is predicted that tresyl grafted products from this chapter will display weaker brush responses, resulting from lower $2R_f/D$ values. However, the much higher R_f values seen for tresyl grafted products suggest that height variations seen during brush switching will be much more significant for tresyl grafted products than for those grafted by Ce(IV).

Total grafted amounts are low in comparison with Ce(IV) initiated grafting, with a maximum of 3.39 mmol (0.391 g) polymer grafted per g M-PVA. This is equal to 28% of total product mass. Graft density for simultaneous grafting was similar to that achieved with consecutive grafting steps when a higher polymer concentration was used for both polymers in the simultaneous grafting mixture (table 3.2/figure 3.25 support 4). When both polymers were at concentrations suitable for partial polymer addition (table 3.2/figure 3.25 support 3) a lower graft density was achieved. This indicates the requirement for a higher polymer concentration in order to produce extra grafting at a heavily grafted surface.

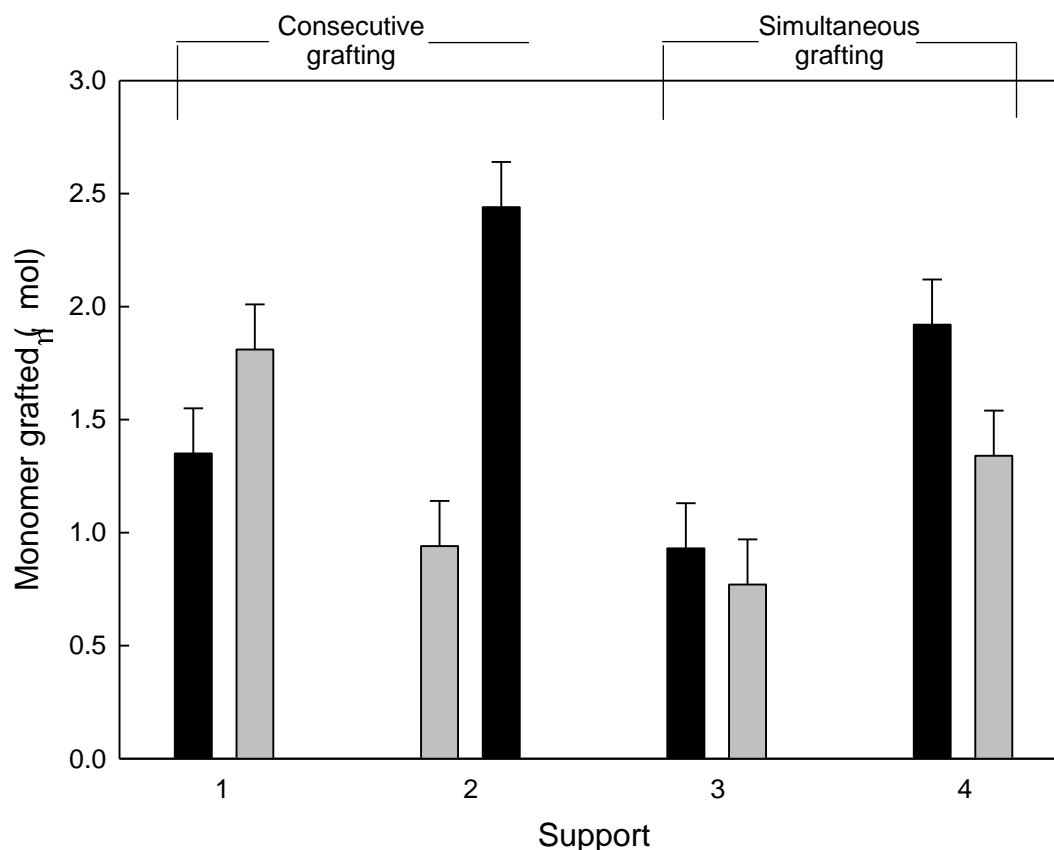


Figure 3.25. Polymer grafting results for supports as described in table 3.2. Black bars represent P2VP, grey bars represent PTBMA/PMAA.

3.4 Conclusions

Synthesis based upon sulfonyl chloride activation has been shown to be a useful method for the grafting of amine-terminated polymers to M-PVA. Successful activation of the M-PVA surface to nucleophilic attack has been achieved using tresyl and tosyl chloride activating agents. Of these two methods tresyl chloride shows superior activating ability, with activation of 57.8 μmol of sites per g M-PVA. Grafting density can be controlled by limiting the concentration of polymer during the graft to reaction, which has allowed the successful synthesis of mixed brush surfaces on M-PVA by limiting polymer concentration during the first grafting step. Equal success has been achieved with the simultaneous addition of higher polymer concentrations, showing that both simultaneous and consecutive grafting methods are suitable for tresyl activated mixed brush formation. Comparison with Ce(IV) initiated techniques described in Chapter 2 indicate that sulfonyl activation produces lower overall grafting than Ce(IV), with tresyl activated mixed brush grafting giving a maximum of 0.338 g

polyelectrolyte per g M-PVA (25 % of total support mass), compared to 0.951 g per g M-PVA for CE(IV) initiation. Flory radius calculations for tresyl grafted products indicate brush behavior, with mixed brush $2R_f/D$ values > 10 produced when higher polymer concentrations are used during the grafting reaction.

4 Polymer grafting via AGE activation

4.1 Introduction

4.1.1 Controlled surface activation by partial bromination

A requirement for the successful synthesis of a mixed polymer brush is the ability to distribute potential graft sites between two polymer species. During sequential addition of polymers, too high a grafting density of one polymer may lead to a low presence of the other polymer species. In the case of mixed polyelectrolyte brushes this behaviour is undesirable if switchable surface properties are to be achieved, as it must be possible for either polymer species to dominate at the surface under appropriate conditions (Sidorenko et al., 1999; Houbenov et al., 2003; Ionov et al., 2005).

As shown in the previous chapters, an even distribution of polymer graft sites may be attempted by inferring activation behaviour from overall polymer yields (Chapter 2) or by controlling the concentration of polymer in the grafting mixture (Chapter 3). However, there are also possibilities for more direct stoichiometric creation of activated surface sites for both graft from and graft to techniques. One such possibility is partial bromination of surface allyl groups followed by ATRP graft from synthesis or polymer graft to based on bromide substitution reactions.

Partial bromination is based upon electrophilic addition controlled amounts of Br_2 to a surface containing allyl double bonds, for example an M-PVA surface activated with allyl glycidyl ether (AGE). In non-nucleophilic solvents this leads to the formation of brominated sites (figure 4.1).

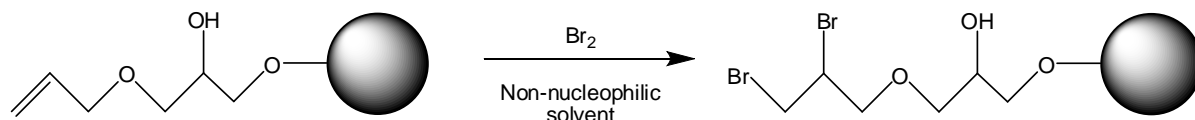


Figure 4.1. Dibromination of allyl sites on AGE activated M-PVA.

This reaction is stoichiometric and under suitable conditions all Br_2 present in a mixture containing allyl groups will participate in electrophilic addition at the allyl sites. This means that the number of brominated sites is expected to be roughly equal to the amount of Br_2 added until all allyl groups are consumed. Hence it is

possible to achieve a controlled partial bromination of the allyl groups containing surface in which only a proportion of the C=C bonds undergo electrophilic addition of Br_2 (figure 4.2).

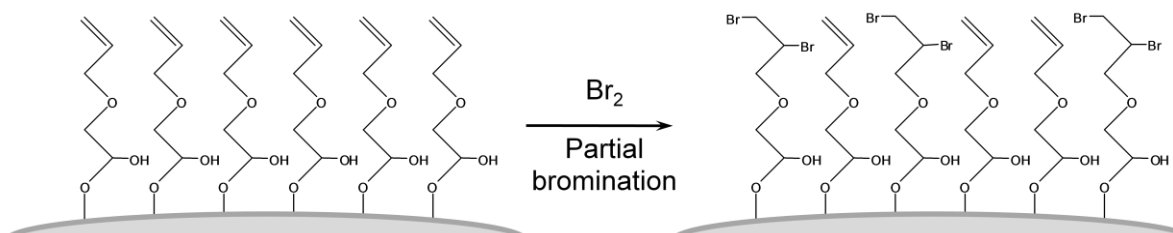


Figure 4.2. Partial bromination of an AGE activated surface using a controlled amount of Br_2 .

By combining partial bromination techniques with approaches for grafting at brominated sites it is possible to create polymer brushes with greater control of graft density. Two techniques which are suitable for grafting through brominated sites are Atom Transfer Radical Polymerisation (ATRP) (Matyjaszewski and Spanswick, 2005), a radical graft from technique, and alkyl bromide substitution, a graft to technique. These two techniques are described in the following pages.

4.1.2 Polymer “graft from” by ATRP

Atom transfer radical polymerisation (ATRP) is a living polymerisation technique which is based on the generation of a carbon-based radicals by the interaction of a halogenate initiator with a transition metal-halide catalyst (Wang and Matyjaszewski, 1995; Matyjaszewski and Xia, 2001). It can be used to create polymers with specific compositions and functionalities as it allows a controlled amount of radical to be created in equilibrium with an added catalyst system. The concentration of radicals generated can be controlled by altering both the concentration and type of catalyst system used. ATRP can be used with a wide range of functional monomers and does not require harsh or impractical reaction conditions (Jeyaprakash, 2002). ATRP has been regularly used as a technique for synthesis of polymer brushes. ATRP initiation from surfaces has been used to graft polymers for biological application (Kurosawa, 2004; Xu, 2001) and for making polymer layers with switchable brush (Wang et al., 2008) and ion-exchange (Singh et al., 2005) capacities.

The ATRP mechanism involves an inner sphere electron transfer with exchange of a halide atom between a halogenated alkyl site and a transition metal complex in its low oxidation state (figure 4.3). This exchange produces a radical group and a transition metal complex in a higher oxidation state with an extra coordinated halide (Singleton et al., 2003).



Figure 4.3. ATRP initiation/deinitiation through equilibrium reaction of copper bromide with alkyl bromide and alkyl radical sites

In the presence of monomer this radical can create a propagation reaction, generating a polymer grafted at the original alkyl initiator site (figure 4.4).

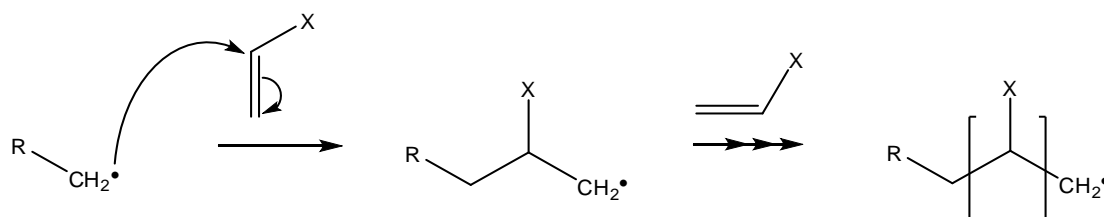


Figure 4.4. Propagation reaction following initiation by CuBr.

As polymerization occurs the concentration of propagating radical is controlled through continued exchange of halide atoms between propagating chains and the transition metal complex (figure 4.5).

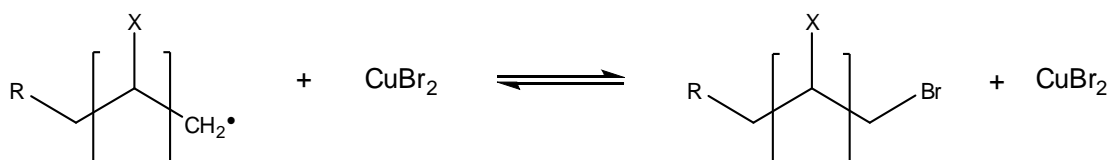


Figure 4.5. Exchange of bromine atom between polymer chain and copper bromide, leading to deactivation or initiation.

The concentration of radicals is a function of both the concentration of initiator and the concentration of catalyst. Low concentrations of radical are beneficial in many polymerisation reactions, as higher concentrations lead to higher rates of termination. Radical termination occurs through coupling or disproportionation reactions, as well as through equilibrium reactions between the radical and catalyst. Coupling involves the direct reaction of two radicals on separate polymer chains with each other (figure 4.6), leading to loss of radical reactivity from both chains and the formation of a covalent C-C bond between the two chains.

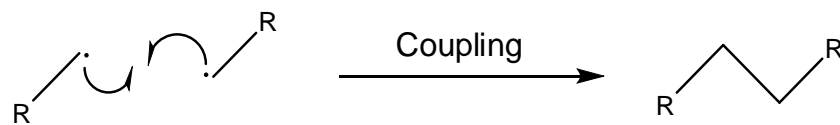


Figure 4.6. Coupling reaction between two radical end groups.

Disproportionation involves transfer of a hydrogen atom from one radical chain to the other (figure 4.7). This leads to loss of two radical groups and the creation of a new allyl group on one of the chains. Unlike coupling reactions, disproportionation does not involve the creation of a new C-C bond between the two chains.

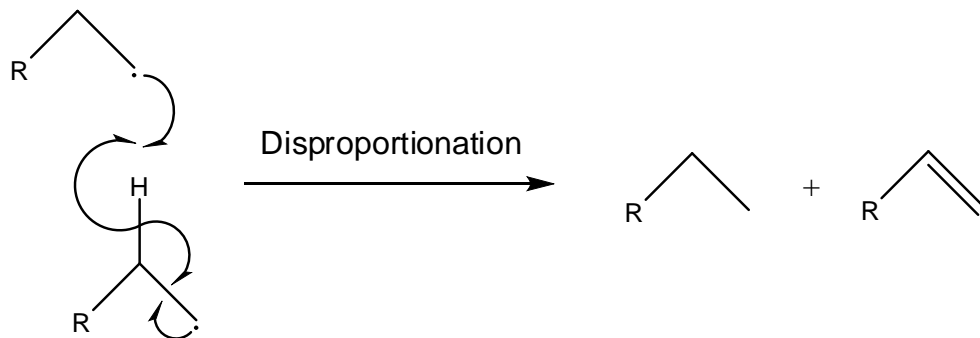


Figure 4.7. Disproportionation reaction between two radical end groups.

The equilibria which exist between catalyst, halogenated end-groups and radical chains leads to the constant presence of a low radical concentration in a so-called 'persistent radical effect' (Fischer, 1999). Lowering the concentration of radical sites causes a decrease in rate of termination which is greater than the accompanying decrease in rate of polymerization. This is because the rate of termination in free polymerisation is proportional to $[\text{radical}]^2$, whereas the rate of propagation is

proportional to [radical]. In effective ATRP reactions the continual low concentration of radicals leads to high polymer yields and low polydispersity (Patten, 1996).

An ATRP catalyst is a transition metal complex comprising of a low oxidation state metal, complexing ligands and halogen counterions. Copper is the most common choice of metal, forming versatile complexes which work in a range of environments. A variety of other transition metals have been used in successful ATRP catalysts, including molybdenum, rhenium, ruthenium, iron and palladium (Matyjaszewski and Xia, 2001). An important feature of these mid and later transition series metals is their ability to expand their coordination spheres and increase their oxidation number in order to accommodate extra halide atoms during catalysis (Braunecker and Matyjaszewski, 2006).

For a group to be a suitable ATRP initiator it must contain a halogenated carbon which is able to lose its halogen atom to the catalyst in order to produce a radical (Matyjaszewski and Xia, 2001; Wang and Matyjaszewski, 1995). The efficiency with which a group is able to undergo dehalogenation is important as this determines the total number of chains from which initiation can occur. For an initiator to be suitable for use in ATRP its reaction with the ATRP catalyst must have an apparent rate constant greater than that of the radical propagation reaction. This ensures that the polymer chains are all initiated early in the reaction, with no 'runaway' propagations occurring while other initiators remain unreacted. Initiation of ATRP systems can be encouraged by the presence of groups which can participate in inductive or resonance stabilization with the alkyl halide group.

During ATRP synthesis the original initiator alkyl group is incorporated at one end of the polymer, making ATRP an obvious method for the preparation of surface-grafted polymers. The synthesis of polymer brush layers from ATRP macroinitiators at a solid surface has been demonstrated on numerous occasions, with ATRP polymerisation from a variety of surface types. These include silicon wafers (Ejaz et al., 1998), gold surfaces (Kim et al., 2000), dendrimers (Leduc et al., 1996), colloids (Zhang et al., 2006), latexes (Guerrini et al., 2000) and a variety of polymers (Beers et al., 1998; Cheng et al., 2001; Boerner et al., 2002). Polymers grafted using ATRP have been shown to have potential for biochemical application including protein

adsorption (Feng et al., 2004; Feng et al., 2005) and enzyme immobilization (Tugulu, 2005).

4.1.3 Polymer “graft to” by alkyl bromide substitution

Alkyl bromide groups are commonly used in syntheses as alkylating agents for molecules containing nucleophilic groups (Hardcastle et al., 2001; Jannasch and Wesslen, 2003). Reaction of amine groups with alkyl bromides are a simple route to higher orders of alkylation, with no additional reagents required to achieve amine attack at the brominated site (Wakeman et al., 1965; Sanchez et al., 2000). As with sulfonyl ester activation, the presence of alkyl bromide groups at a surface offers a route to the grafting of nucleophile terminated polymers by attack of polymer end groups at alkyl bromide surface sites (figure 4.8).

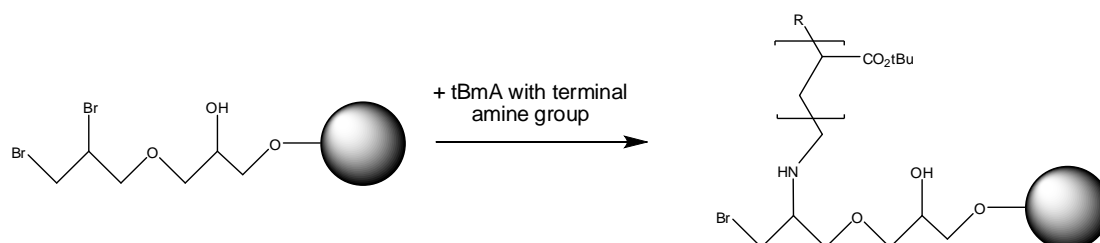


Figure 4.8. Grafting of nucleophile terminated polymer following activation of surface with AGE and bromination

4.1.4 Routes to mixed brushes using partial bromination

As both ATRP and alkyl bromide substitution may afford polymer grafting at brominated sites, the possibility of creating mixed polymer brushes by combining partial bromination of AGE activated M-PVA with either technique can be explored. Examples of routes to mixed brushes utilising these techniques include two-stage ATRP synthesis of mixed brush with generation of new surface initiator by partial bromination before each stage (figure 4.9).

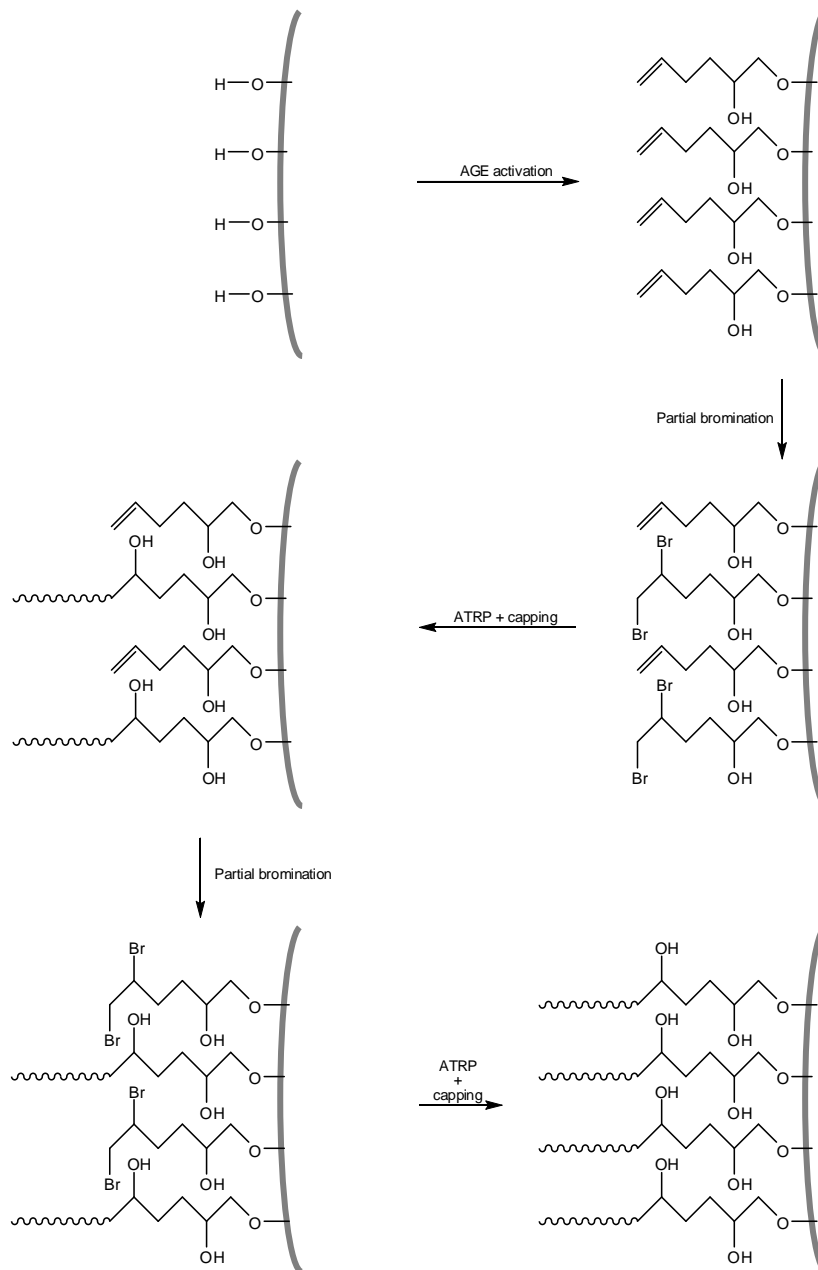


Figure 4.9. ATRP mixed brush synthesis by sequential partial brominations of M-PVA surface

A similar technique can be used to create a grafted layer by a combination of graft from and graft to. For example, partial bromination can be followed by ATRP from the brominated sites then another bromination stage and graft to of amine terminated polymers at the second set of brominated sites (figure 4.10). Similarly, sequential partial brominations can be used to achieve graft to then ATRP, or graft to then a second graft to.

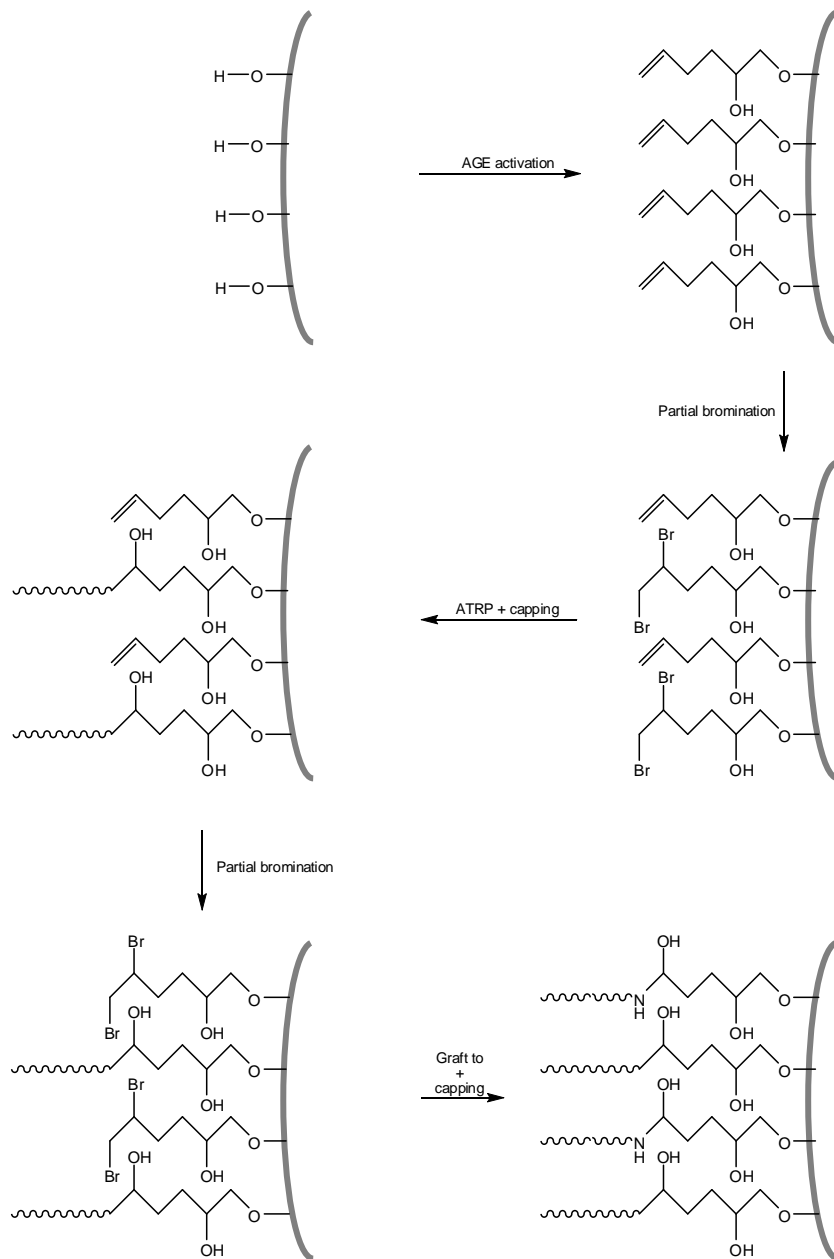


Figure 4.10. Mixed brush synthesis by ATRP then GT through sequential partial bromination of M-PVA surface.

Finally, mixed brush grafting at a brominated surface may be achieved by the graft to approach shown in Chapter 2, with sequential or simultaneous additions of controlled amounts of polymer to a brominated surface without the need for additional bromination steps (figure 4.11).

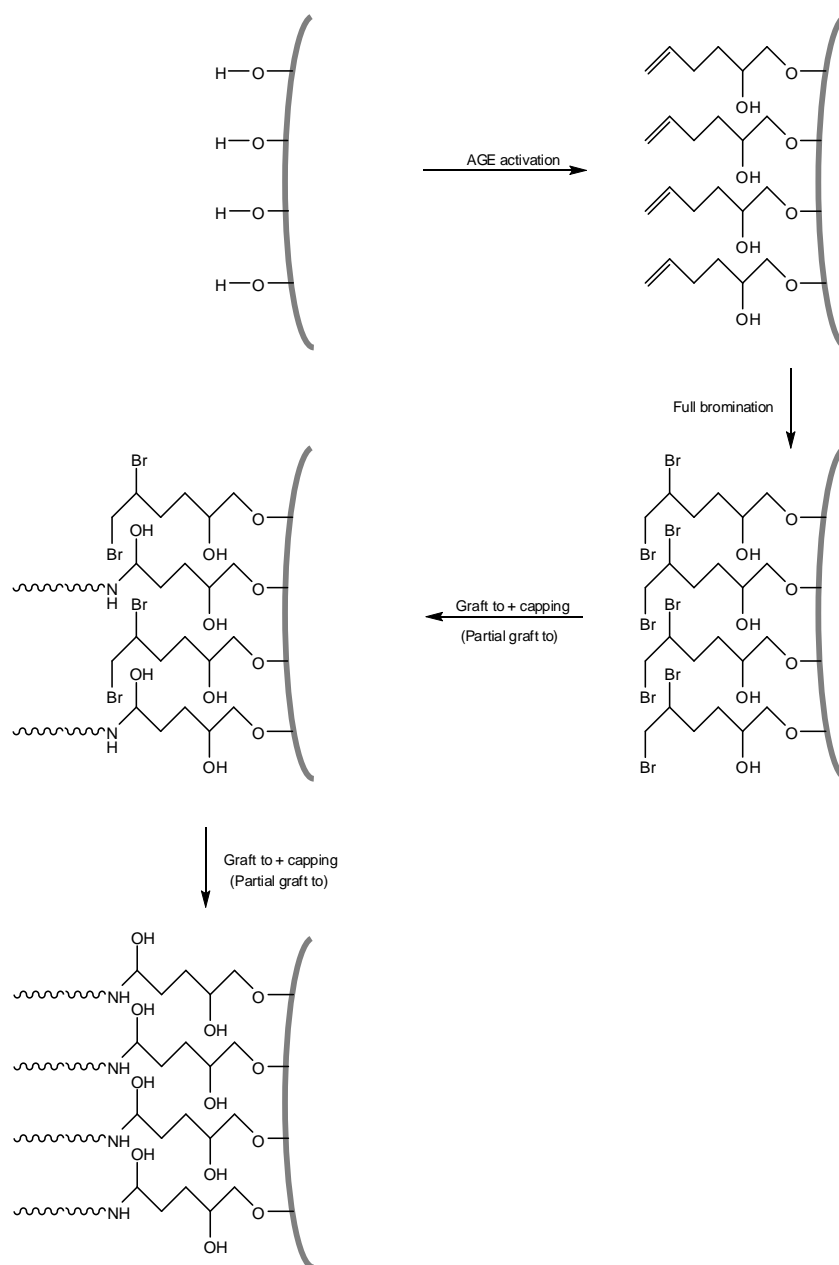


Figure 4.11. Mixed brush synthesis through controlled addition of amine terminated polymers to a fully brominated M-PVA surface

Against all of the above, the following chapter describes the preparation and quantification of brominated sites on the M-PVA surface, followed by grafting of brush surfaces with polyelectrolyte brushes composed of P2VP and PMAA (as described in Chapter 2). These brushes are synthesised via ATRP reactions of 2VP and TBMA and GT of amine terminated P2VP and PTBMA, with the reaction progress and resultant brush properties being quantified using FTIR techniques.

4.2 Materials and methods

4.2.1 Materials used

M-PVA (batch R2-0126067; V_m ; 3.3 cm³/g; specific surface area 56.7 m² per g) was obtained from Chemagen (Baesweiler, Germany). Allyl glycidyl ether (CAS 106-92-3); sodium borohydride (CAS 16940-66-2); sodium sulfate (CAS 7757-82-6); sodium hydroxide (CAS 1310-73-2); bromine (CAS 7726-95-6); bromide-bromate solution (0.1 N in H₂O); dimethyl sulfoxide (CAS 68-78-5); copper(I) bromide (CAS 778-70-4) and 2,2-bipyridine (CAS 366-18-7) were obtained from Sigma Aldrich (Poole, Dorset). Cuvettes, 2 ml screw-cap micro test tubes, 15 ml screw-cap centrifuge tubes and 50 ml screw-cap centrifuge tubes were obtained from Sarstedt (Leicester, UK). 1.5 ml hinged-lid micro test tubes were obtained from Eppendorf (Cambridge, UK).

All unheated mixing was performed with a VM20 vortex mixer or a IKA Vibrax VXR basic mixer with attachments for 15 ml centrifuge tubes and micro test tubes. Heated mixing was performed in a Grant OLS water bath with shaker rack. Samples were dried on watchglasses in a Gallenkamp size 2 hotbox oven. Chemicals were weighed on Mettler AE160 and AT261 balances. Pipetting was performed with 20 ml, 200 ml, 1 ml and 5 ml adjustable pipettes.

4.2.2 Absorbent preparation (washing regime)

M-PVA stock was washed before use to minimize reaction contamination. 1.5 g M-PVA was washed in a succession of solvents (30 ml, 60 s): water; 50% acetone in water; 100% acetone; 50% acetone / 50% methanol; 100% methanol; 50% methanol in water; water (x2); 1 M NaCl in water; water (x3). Following washing, M-PVA was suspended in water (30 ml).

4.2.3 AGE activation

M-PVA (2000 mg) was washed twice with water (20 ml). Water (10 ml) containing NaOH (16.0 g), NaBH₄ (333 mg) and Na₂SO₄ (8.93 g) was added and the suspension was allowed to react with stirring (50°C, 1 h, 150 rpm).

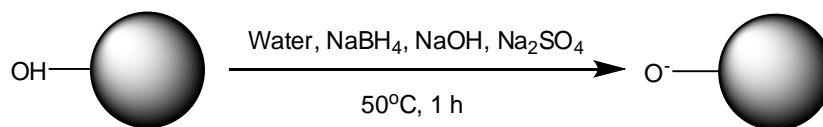


Figure 4.12. Deprotonation of M-PVA hydroxyls

The temperature was then lowered (40°C), AGE (10 ml) was added and the reaction continued (15 h, 170 rpm).

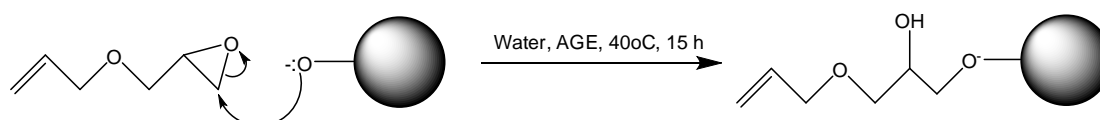


Figure 4.13. Reaction of AGE at deprotonated hydroxyl sites

Following reaction the supports were allowed to cool to room temperature and washed with 20 ml aliquots of water, ethanol (70 %) and water. Beads were then suspended in water (10 ml) and stored at 4°C.

4.2.4 Acidified Bromine assay

The acidified bromine assay allows calculation of the number of C=C bonds present in a sample. It is based upon a rapid stoichiometric reaction between Br₂ and C=C double bond, in which one Br₂ molecule is consumed per C=C double bond present. Br₂ molecules absorb strongly at 410 nm, allowing calculation of the amount of Br₂ consumed by measuring ΔA₄₁₀ in the bromine solution during reaction.

An acidified KBr/KBrO₃ stock solution was prepared by mixing KBr/KBrO₃ solution (0.1 M, 2.5 ml) with dilute sulphuric acid (0.2 M, 5 ml, 120 s) and taking its absorbance at 410 nm. A sample of this stock solution (150 μl) was mixed with H₂SO₄ (0.18 M, 1.35 ml, 5 s). The absorbance of this solution was then taken at 410 nm. Samples were taken until a constant absorbance value was seen for successive samples, corresponding to a stable Br concentration in the stock.

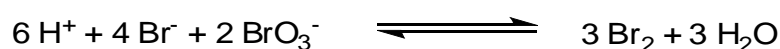


Figure 4.14. Release of Br₂ by acidification of BrO₃/Br⁻ solution

A sample of the stable acidified mixture (1.5 ml) was mixed with dried support (5 mg, 10 s). A sample of the resulting supernatant (150 μ l) was mixed with H_2SO_4 (0.18 M, 1.35 ml, 5 s). The absorbance of this solution was then taken at 410 nm. Following reaction of the stock with samples a final reading was taken for the stock solution to confirm the stability of its absorbance during the experiment.

4.2.5 Controlled bromination study

Dibromo surface groups were synthesised on AGE activated M-PVA by reaction with Br_2 in DMSO. In non-nucleophilic solvent, Br_2 reacts across a C=C bond to create a cationic bromonium intermediate (Clayden et al, 2001) with simultaneous release of a bromide ion (figure 4.15).

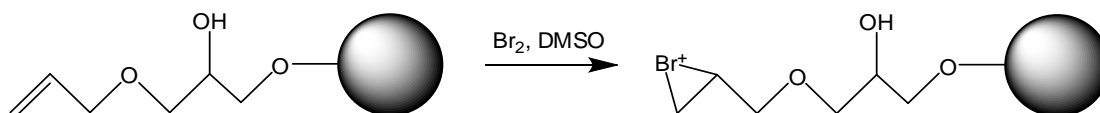


Figure 4.15. Formation of bromonium ion intermediate by electrophilic addition at allyl group

The two carbon atoms of the bromonium group are susceptible to nucleophilic attack and undergo rapid reaction with a nucleophile. In the absence of other nucleophilic groups this results in nucleophilic attack by bromide ions and the creation of a dibromide group (figure 4.16).

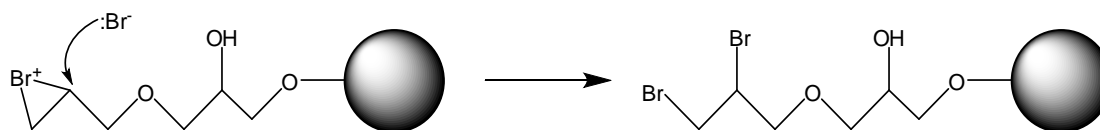


Figure 4.16. Formation of bromonium ion intermediate by electrophilic addition at allyl group

The creation of a controlled amount of dibromo groups at the AGE activated M-PVA surface was tested by mixing a dilute solutions of Br_2 in DMSO (1 ml) with AGE activated M-PVA (5 mg, 60 s). The acidified bromine assay was then performed on the dibrominated supports to test for the presence of unreacted C=C groups.

4.2.6 ATRP mixed brush synthesis

ATRP syntheses of grafted brushes were performed on halogenated M-PVA surfaces produced by dibromination of AGE sites (figure 4.17).

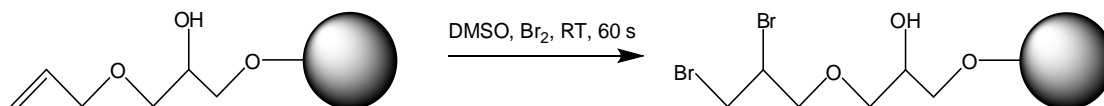


Figure 4.17. Dibromination of AGE allyl group by Br_2 in DMSO

Masses of catalyst and monomer were scaled according to the amount of bromine used during the M-PVA dibromination step. For 50% activation of 50 mg M-PVA a volume of 31 μl Br_2 was used during the activation step, followed by ATRP reaction using 9.7 mg CuBr , 23.1 mg dipyriddy and 0.727 ml 2VP or 1.096 ml tBmA. Quantities of Br_2 , catalysts and monomer were scaled according to the percentage activation and mass of M-PVA used, with the ratio Br_2 :catalyst:monomer remaining constant for all subsequent ATRP reactions.

AGE modified M-PVA (50 mg) was mixed with the desired concentration of bromine in DMSO (60 s), followed by washing 5 times in DMSO (5 ml, 60 s). The brominated supports were then suspended in 5 ml solvent and purged with nitrogen (0.5 h). CuBr and dipyriddy catalysts were added to a 15 ml eppendorf tube and the tube was purged with nitrogen (300 s). The M-PVA/monomer mixtures were then added to the degassed tube under a nitrogen blanket. The tube was then sealed and allowed to react under mixing (12 h). The component steps of this ATRP reaction are shown in figures 4.18-4.20, with the overall reaction described by figure 4.21.

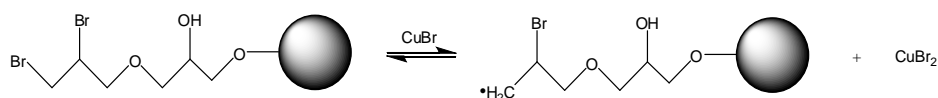


Figure 4.18. Initiation of ATRP system by CuBr catalyst

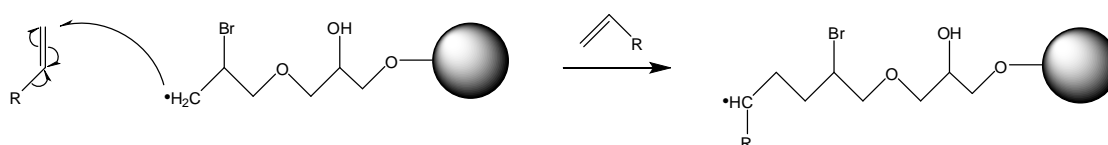


Figure 4.19. Propagation of initiated ATRP system

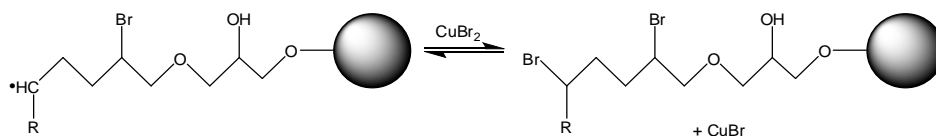


Figure 4.20. Termination of radical by CuBr catalyst

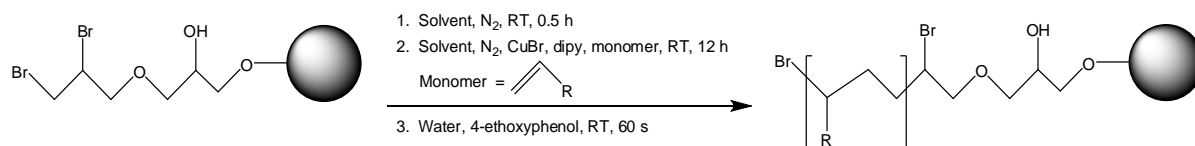


Figure 4.21. Overall ATRP reaction

Following reaction the supernatant was separated under a nitrogen blanket and mixed with 4-ethoxyphenol_(aq) (5 ml, 0.3 M, 60 s). The supports were washed twice with DMSO (5 ml), twice with water (5 ml) and then mixed with NaOH(aq) (1M, 5 ml, 1 h). Following NaOH reaction, supports were washed three times with water (5 ml).

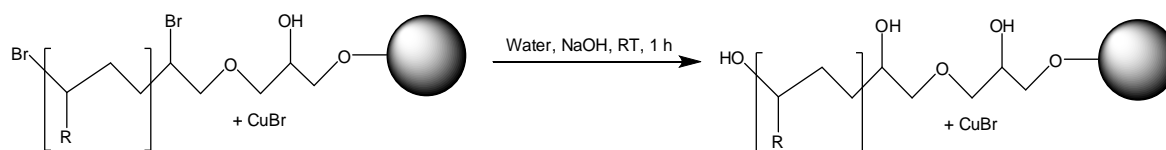


Figure 4.22. Substitution of bromide sites by hydroxide during capping reaction

Single brush grafted M-PVA supports (25 mg) were mixed with the desired concentration of bromine in DMSO (60 s), followed by washing 5 times in DMSO (2.5 ml, 60 s). The brominated support were then suspended in solvent (2.5 ml) and purged with nitrogen (0.5 h). CuBr and dipyrindyl were added to a 15 ml eppendorf tube and the tube was purged with nitrogen (300 s). The M-PVA/monomer mixtures were then added to the degassed tube under a nitrogen blanket. The tube was then sealed and allowed to react under mixing (12 h). Following reaction the supernatant was separated under a nitrogen blanket and 4-ethoxyphenol_(aq) (2.5 ml, 0.3 M) solution was added followed by mixing for 1 minute. The supports were washed twice with DMSO (2.5 ml), twice with water (2.5 ml) and then mixed with NaOH(aq) (1M, 2.5 ml, 1 h). Following NaOH reaction, supports were washed three times with water (2.5 ml).

4.2.7 Preparation of halohydrin surface groups

In an aqueous bromine solution bromonium groups will react with water, leading to the creation of halohydrin groups. (figures 4.23 and 4.24; Clayden et al, 2001). In the case of reaction with AGE the halohydrin formed will typically have a bromine atom on the terminal carbon. This is because charge stabilisation within the bromonium group means that small nucleophiles prefer to attack at the more substituted carbon.

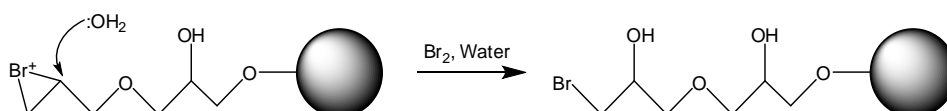


Figure 4.23. Formation of halohydrin by water attack on bromonium ion

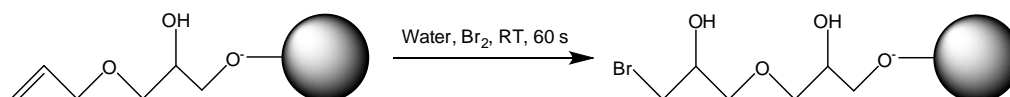


Figure 4.24. Overall halohydrin formation reaction

AGE activated M-PVA (5 mg) was activated with Br_2 (0.31 μl) in water (1 ml) for 60 s at RT. The activated supports were then washed 5 times with DMSO (1 ml) followed by reaction with NH_2 terminated polymer (6 mg) in acetone (1 ml, RT, 24 h).

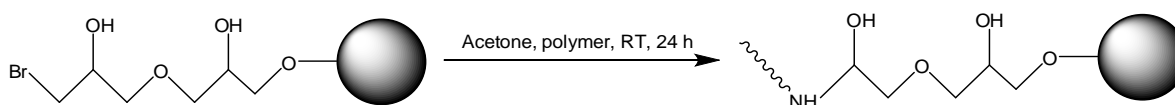


Figure 4.25. Attack by amine terminated polymer on halohydrin brominated site

4.2.8 Preparation of epoxide surface groups

Under alkali conditions deprotonation of the halohydrin reagent leads to a slow intramolecular nucleophilic attack of the hydroxyl group upon the adjacent bromide site and subsequent formation of an epoxide group (figure 4.26; Clayden et al., 2001).

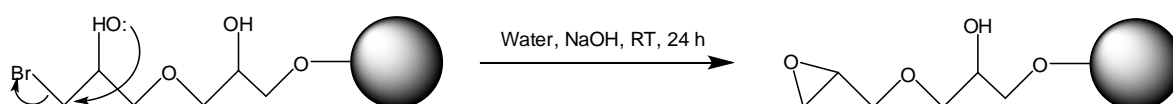


Figure 4.26. Deprotonation of halohydrin group leading to epoxide formation under basic conditions

AGE activated M-PVA (5 mg) was activated with Br_2 (0.31 μl) in water (1 ml) for 60 s at RT. The activated supports were then washed twice with DMSO (1 ml) and twice with water (1 ml) before being mixed with an aqueous solution of NaOH for 24 h at RT. Supernatant was then removed and the supports reacted with amine-terminated polymer (6 mg) in acetone (1 ml, RT, 24 h).

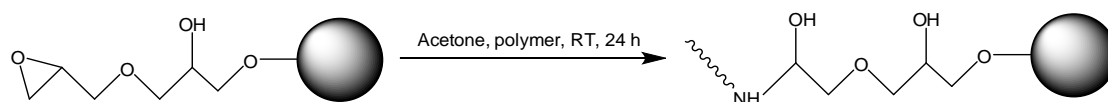


Figure 4.27. Attack by amine terminated polymer on epoxide site

4.2.9 Simultaneous bromination and polymer attack

When Br_2 addition across a double bond is performed in the presence of amine-terminated polymer the intermediate bromonium ion provides a possible site for graft-to attack by the polymer end group.

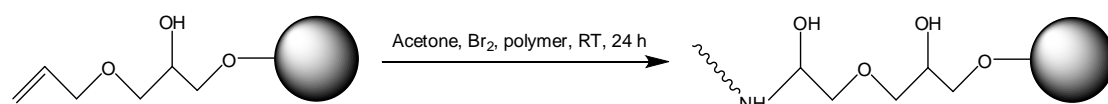


Figure 4.28. Attack by amine terminated polymer on bromonium ion

AGE activated M-PVA (5 mg) was reacted with Br_2 (0.31 μl) and amine-terminated polymer (3 mg) in acetone (1 ml, 24 h). Supports were then washed twice with acetone (1 ml) and twice with water (1 ml).

4.2.10 Mixed brush grafting using two graft-to steps

AGE activated M-PVA (50 mg) was activated with Br₂ (6.2 μl) in DMSO (5 ml). The activated supports were then washed 5 times with DMSO (5 ml) followed by reaction with 8 mg amine terminated in acetone (5 ml, 24 h) and two acetone washes (5 ml, 60 s, x 3).

Single brush graft M-PVA was then reacted with a 30 mg of the second amine-terminated polymer in acetone (2.5 ml) followed by washing with acetone (2.5 ml, 60 s x 3).

4.2.11 Mixed brush grafting using graft-to then ATRP

AGE activated M-PVA (50 mg) was activated with Br₂ (3.1 μl) in DMSO (5 ml). The activated supports were then washed 5 times with DMSO (5 ml) followed by reaction with 8 mg amine terminated polymer in acetone or DMSO solvent (5 ml).

ATRP single brush grafted M-PVA (25 mg) was activated with Br₂ (1.55 μl) in DMSO (2.5 ml) and then washed 5 times with DMSO (2.5 ml). The supports were then suspended in 2.5 ml water and purged with nitrogen (0.5 h). CuBr (4.84 mg) and dipyriddy (11.56 mg) were added to a 15 ml eppendorf tube and the tube was purged with nitrogen (300 s). The M-PVA/monomer mixtures were then added to the degassed tube under a nitrogen blanket. The tube was sealed and allowed to react under mixing (12 h). Following reaction the supernatant was separated under a nitrogen blanket and 4-ethoxyphenol_(aq) (2.5 ml, 0.3 M) solution was added followed by mixing for 1 minute. The supports were washed twice with DMSO (5 ml), twice with water (2.5 ml) and then mixed with NaOH(aq) (1M, 2.5 ml, 1 h). Following NaOH reaction, supports were washed three times with water (2.5 ml).

4.2.12 Mixed brush grafting using ATRP then graft-to

AGE activated M-PVA (50 mg) was activated with Br₂ (1.55 μl) in DMSO (5 ml) and then washed 5 times with DMSO (5 ml). The supports were then suspended in 5 ml water and purged with nitrogen (0.5 h). CuBr (9.68 mg) and dipyriddy (23.11 mg) were added to a 15 ml eppendorf tube and the tube was purged with nitrogen (300

s). The M-PVA/monomer mixtures were then added to the degassed tube under a nitrogen blanket. The tube was sealed and allowed to react under mixing (12 h). Following reaction the supernatant was separated under a nitrogen blanket and 4-ethoxyphenol_(aq) (5 ml, 0.3 M) solution was added followed by mixing for 1 minute. The supports were washed twice with DMSO (5 ml), twice with water (5 ml) and then mixed with NaOH(aq) (1M, 5 ml, 1 h). Following NaOH reaction, supports were washed three times with water (5 ml).

ATRP single brush grafted M-PVA (25 mg) was activated with Br₂ (7.2 µl) in DMSO (2.5 ml). The activated supports were then washed 5 times with DMSO (2.5 ml) followed by reaction with 30 mg amine terminated polymer in acetone or DMSO solvent (5 ml).

4.2.13 Hydrolysis of PTBMA chains

PTBMA brushes were hydrolysed using a 50/50 (v/v) aqueous solution of trifluoroacetic acid. Supports were reacted with a 50/50 (v/v) mixture of TFA and water (5 ml, 60°C, 24 h) followed by washing with water (5 ml, 60s, x 2).

4.2.14 FTIR analysis

Dry solid samples were pressed with KBr to form 13 mm discs as described in Chapter 2. Samples discs were analysed using a Thermo Nicolet 380 FTIR with 64 scans per sample at a resolution of 2 cm⁻¹.

Liquid FTIR samples for graft to reactions were prepared and quantified as described in Appendix 7.4, while liquid samples from ATRP reactions used the method described in Appendix 7.3. FTIR samples were run on a Nicolet Smart Orbit diamond ATR apparatus, using 50 µl aliquots of the sample liquid at a resolution of 2 cm⁻¹.

4.3 Results

4.3.1 Activation of M-PVA with AGE

M-PVA supports before and after activation with AGE were assayed using the bromine water method and FTIR spectroscopy. Reduction of carbonyl groups on the M-PVA surface during the initial reaction with sodium borohydride resulted in a change on the FTIR spectrum, with disappearance of carbonyl peak at 1720 cm^{-1} . Activation of the reduced surface with AGE did not produce a visible change in the FTIR spectrum (figure 4.28).

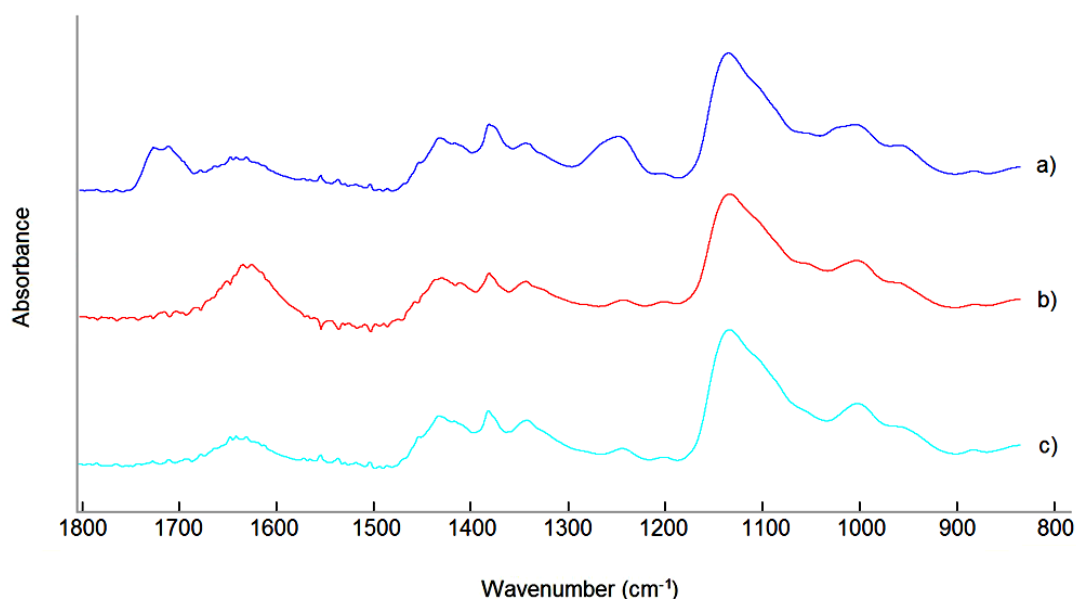


Figure 4.28. a) Unmodified M-PVA; b) AGE activated M-PVA; c) AGE activated M-PVA following dibromination

Although the sodium borohydride reduction reaction and the AGE attachment reaction both occur at the M-PVA surface, only the reduction reaction is visible in FTIR spectra (disappearance of peak at 1720 cm^{-1}). The reduction reaction appears to reduce almost all of the carbonyl groups present. As it is unlikely that the sodium borohydride reacts throughout the structure of the non-porous M-PVA support it may be assumed that the carbonyl peaks on the unmodified M-PVA supports are found at the support surface. These carbonyl groups were generated by oxidation of hydroxyl groups on the M-PVA surface during or after synthesis of the supports.

Alternatively, as residual carbonyl groups are expected following the synthesis of M-PVA from poly(vinyl acetate) it is possible that the emulsification process used

positions the unhydrolysed acetate groups at the support surface. This is likely as the main interatomic force holding together the M-PVA matrix is expected to be hydrogen bonds between the PVA hydroxyl groups and the presence of acetate groups within the matrix is unfavourable. Acidified bromine assays upon the same three samples indicated the presence of 2.97 mmol double bonds per g support for the AGE reacted sample. The unreacted M-PVA and the reduced samples both showed ~0 mols of double bond per g support.

4.3.2 Dibromination of AGE activated supports

AGE activated supports were partially brominated and then assayed using the bromine water method to assess the number of double bonds remaining following partial bromination (figure 4.29). It is assumed that disappearance of double bonds is caused by bromine attack at double bonds, leading to the formation of dibromo groups at the double bond site.

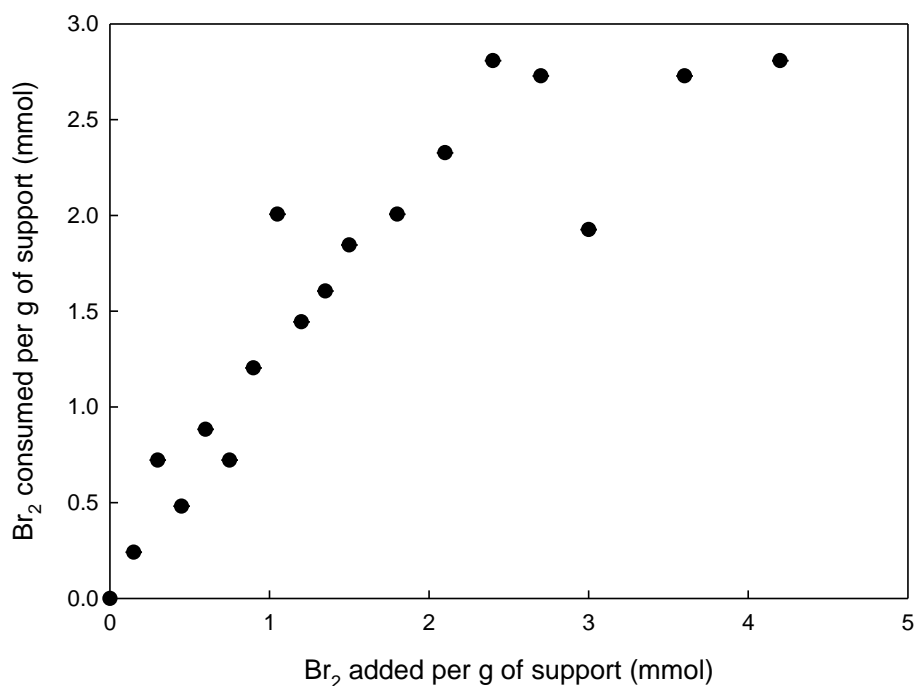


Figure 4.29. Formation of dibrominated groups vs. mols Br₂ added in controlled bromination

Dibromination of surface double bonds occurred in an approximately stoichiometric fashion, with each mol of bromine added during the dibromination step consuming

approximately one mol of double bond to create one mol of dibromo groups. Saturation of C=C addition was seen with addition of 2.70 mmol bromine added per g of support.

The corresponding minimum spacing of dibromo groups at the M-PVA surface was found to have a minimum distance of 1.86 Angstroms (figure 4.30). For polymer grafting purposes, this value would be the minimum intergraft distance which might be possible although in reality the intergraft distance may be considerably greater.

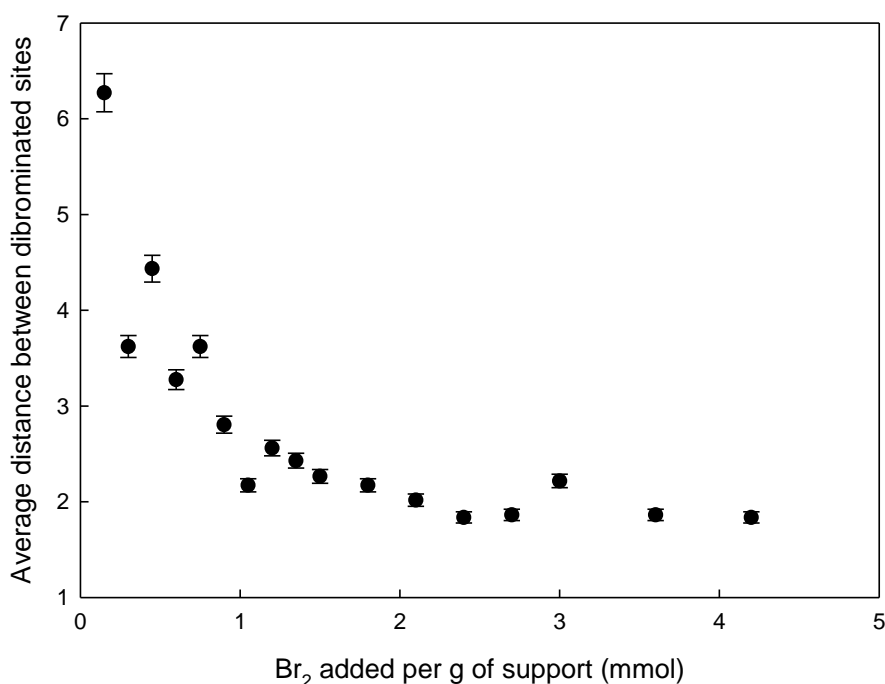


Figure 4.30. Spacing of dibrominated groups vs. mols Br₂ added in controlled bromination.

4.3.3 Homopolymer brush grafting by ATRP

Grafting of single-brush layers following ATRP reaction was observed using FTIR spectroscopy. The appearance of new peaks corresponding to grafted P2VP were both observed in FTIR spectra following reaction of M-PVA with 2VP under ATRP conditions (figure 4.31).

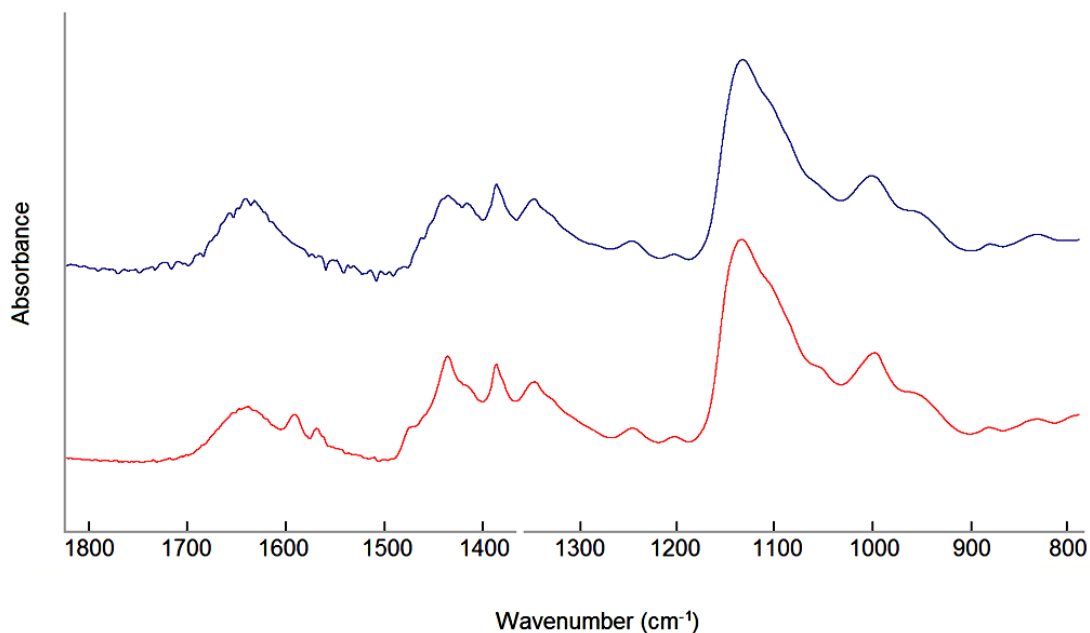


Figure 4.31. a) AGE activated M-PVA; b) AGE activated M-PVA following 50% dibromination and ATRP reaction with 2VP.

Small peaks at 1590 and 1570 cm⁻¹ are seen, along with a small increase in the peak height and sharpness at 1430 cm⁻¹. This is evidence of P2VP grafting on M-PVA, although peak heights suggest that the total mass of 2VP grafted per g of M-PVA is lower for ATRP than that achieved with ACN initiated grafting. A related consumption of 2VP monomer was seen in the supernatant spectrum, with losses in height seen for all 2VP peaks (figure 4.32).

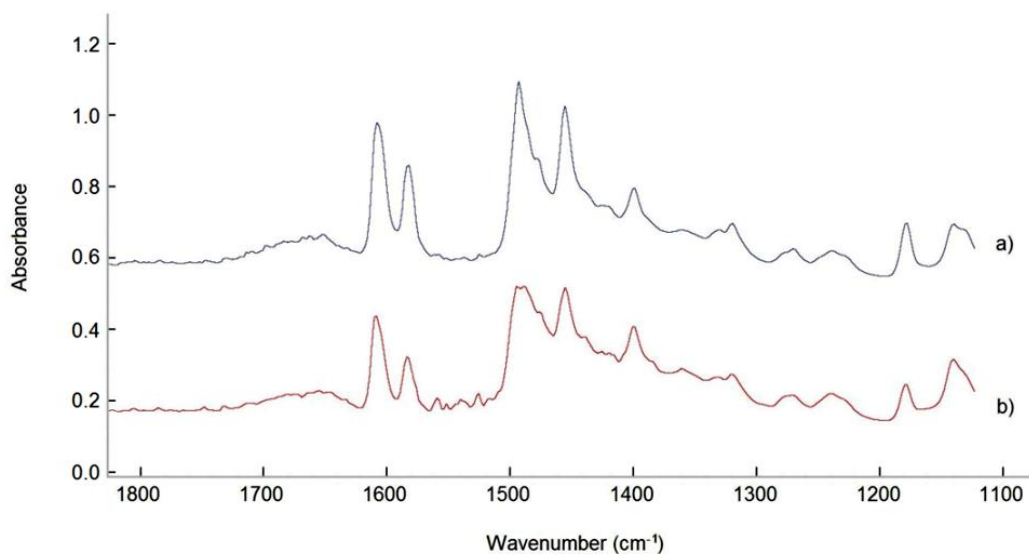


Figure 4.32. a) ATRP supernatant before grafting 2VP to 50% activated M-PVA (quantification spec.); b) ATRP supernatant after grafting 2VP to 50% activated M-PVA (quantification spec).

Likewise, the appearance of PTBMA peaks was observed in the solid FTIR spectra of M-PVA supports following ATRP reaction with tBmA (figure 4.33).

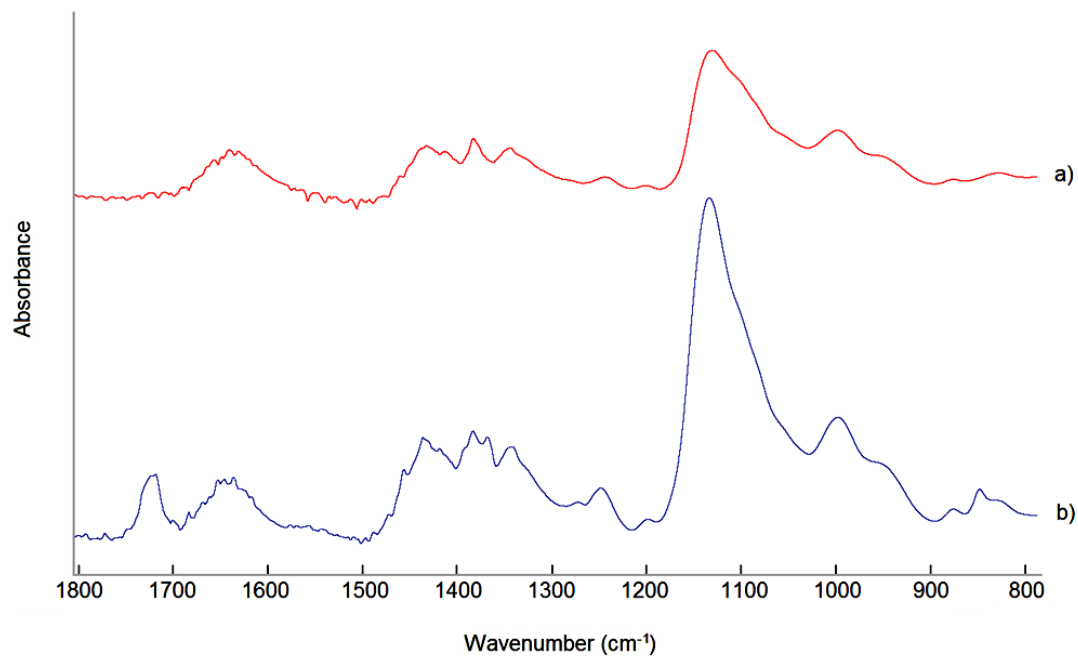


Figure 4.33. a) AGE activated M-PVA; b) AGE activated M-PVA following 50% dibromination and ATRP reaction with tBmA.

The presence of new peaks at 1720, 1370 and 850 cm^{-1} and an increase in peak height at 1140 cm^{-1} indicated successful grafting of PTBMA by ATRP. The presence of a carbonyl peak at 1720 cm^{-1} is a particularly useful indicator for ATRP grafting of PTBMA, as AGE activation removes the carbonyl peak from the ungrafted support spectra. The presence of a new peak at this wavenumber corresponds to t-butyl ester groups on the grafted polymer. This was accompanied by consumption of the tBmA monomer in the liquid FTIR spectra (figure 4.34). All tBmA peaks showed some loss of peak height following ATRP reaction, although the total consumptions were low compared to the total amount of monomer used.

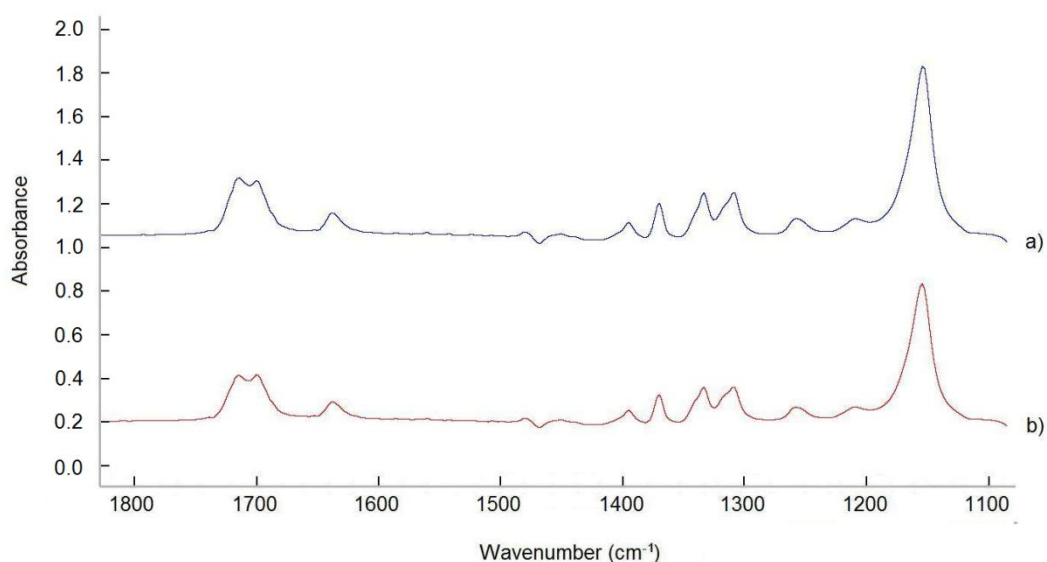


Figure 4.34. a) ATRP supernatant before grafting TBMA to 50% activated M-PVA (quantification spec.); b) ATRP supernatant after grafting TBMA to 50% activated m-PVA (quantification spec.)

4.3.4 Homopolymer brush grafting by dibromination graft to

Grafting of single-brush layers by graft to reaction at dibrominated sites was observed using FTIR spectroscopy. The disappearance of carbonyl peaks from reaction with borohydride and the appearance of new peaks corresponding to grafted polymers were both observed in FTIR spectra of the solid products (figures 4.35 and 4.36).

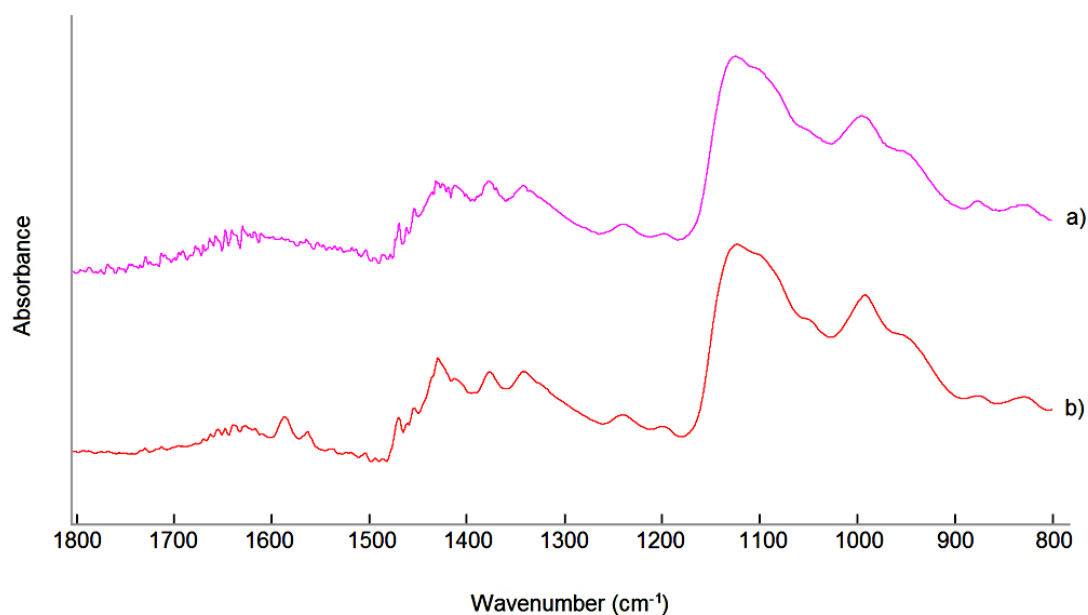


Figure 4.35. a) AGE activated M-PVA; b) AGE activated M-PVA following 100% dibromination and graft-to with P2VP.

Peaks in figure 4.35 spectrum b) appear at 1590 and 1570 cm⁻¹, along with a small increase in the peak height and sharpness at 1430 cm⁻¹. No other major peak changes are noticeable. The presence of aromatic C-H peaks is evidence of P2VP grafting on M-PVA by the AGE/Br₂ graft-to method.

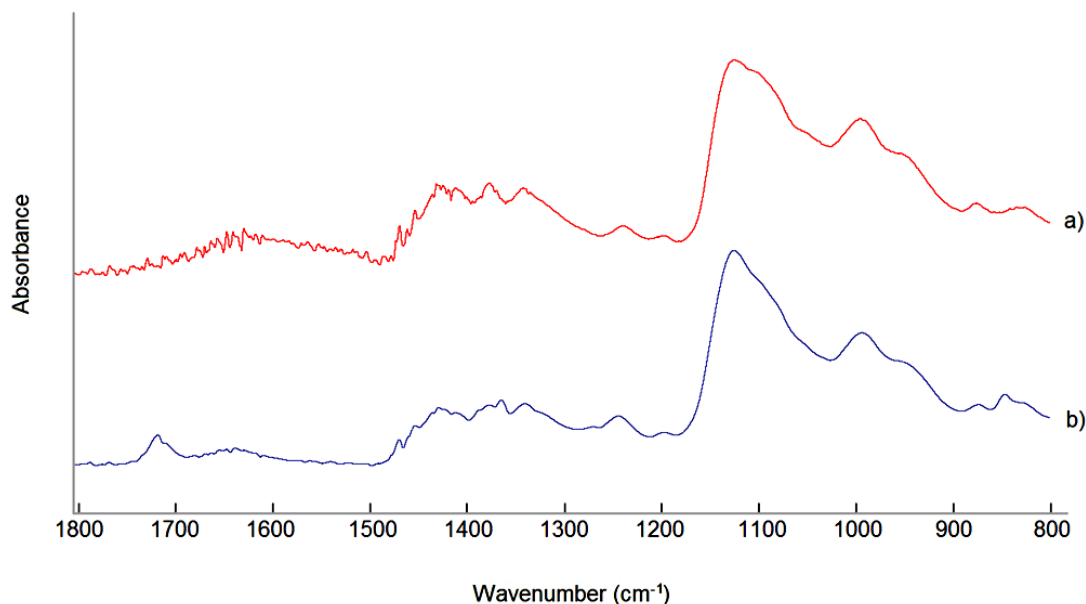


Figure 4.36. a) AGE activated M-PVA; b) AGE activated M-PVA following 100% dibromination and graft-to with PTBMA.

The presence of new peaks at 1720 and 850 cm^{-1} in figure 4.36 and the increase in peak height at 1140 cm^{-1} indicates successful grafting of PTBMA by AGE/ Br_2 graft-to. A small peak is also seen at 1370 cm^{-1} .

4.3.5 Homopolymer grafting by other graft to approaches

Grafting reactions with P2VP upon halohydrinated supports showed no polymer grafting under otherwise identical conditions to those which achieved polymer grafting for dibrominated supports, with the appearance of no characteristic P2VP peaks in the solid spectra (figure 4.37, spectrum b).

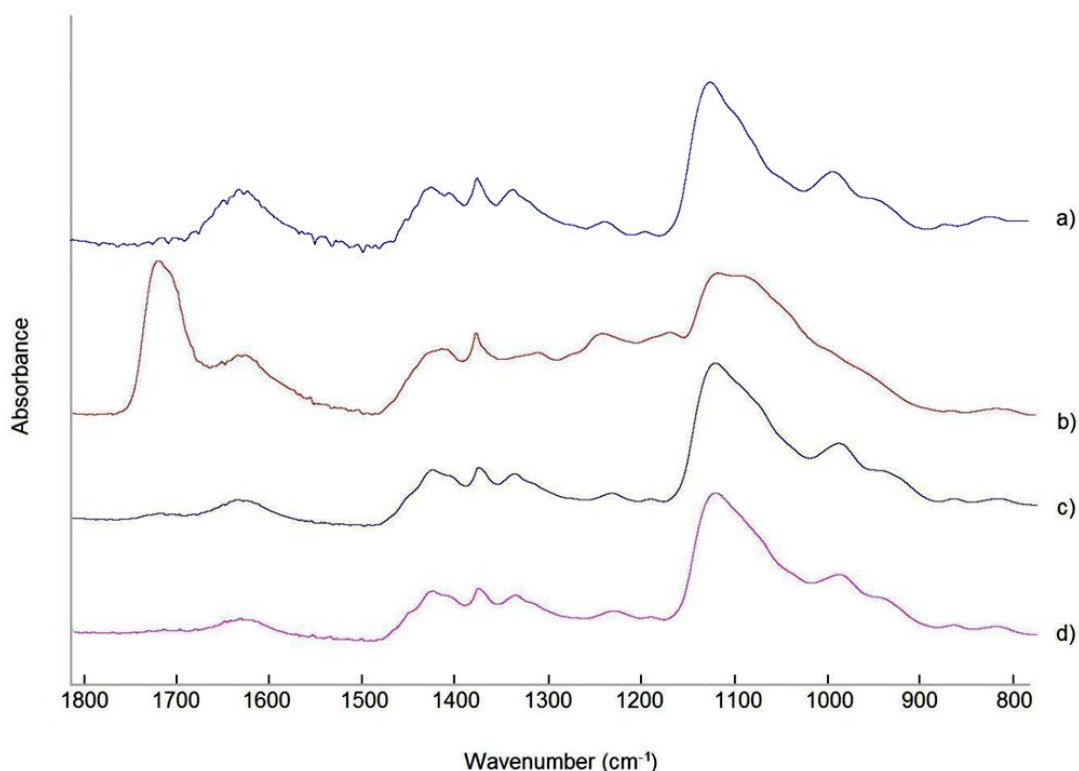


Figure 4.37. a) AGE activated M-PVA; b) P2VP/halohydrin reaction product; c) P2VP/ NaOH epoxidation reaction product; d) P2VP/ Br_2 simultaneous reaction product.

No significant changes were seen in the products from the NaOH epoxidation method or the simultaneous Br_2 /polymer attack method, indicating that neither approach is effective for P2VP grafting. A similar set of results were seen for PTBMA reactions (figure 4.38.). Appearance of a new peak at 1720 cm^{-1} , as seen in fig spectra, is characteristic of PTBMA addition. However, the absence of any other characteristic PTBMA peaks suggests that this peak is not due to PTBMA

addition. Results from the liquid spectra support this, with no significant loss of PTBMA peak heights observed following reaction.

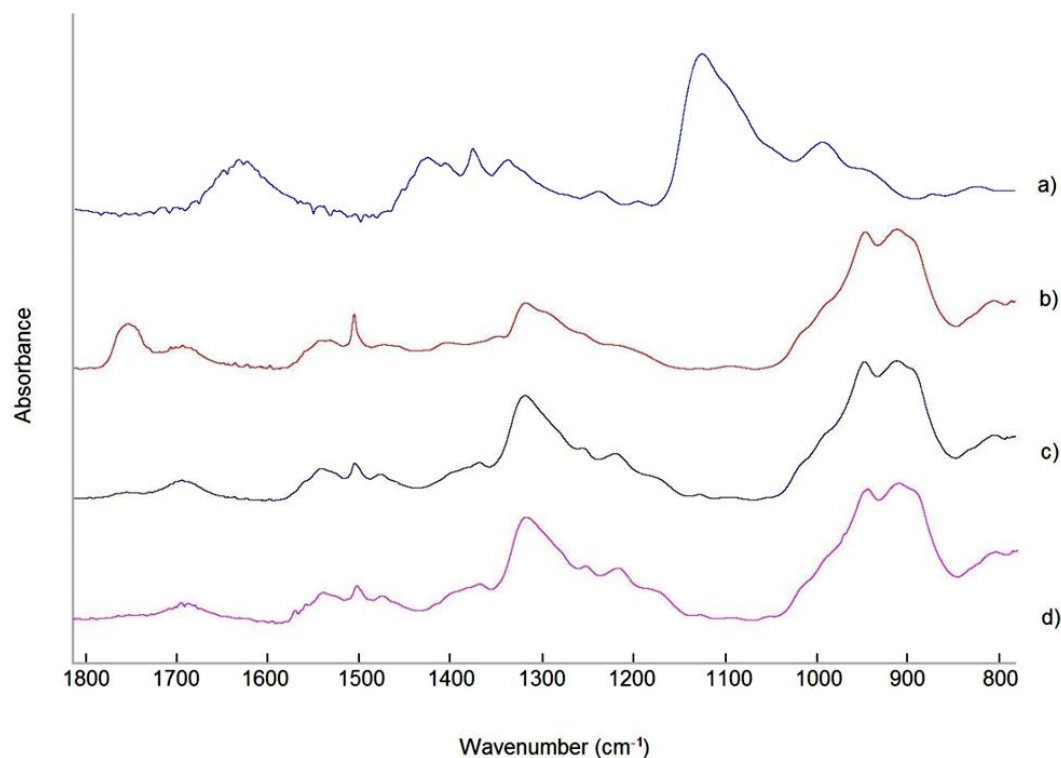


Figure 4.38. a) AGE activated M-PVA; a) PTBMA/halohydrin reaction product; b) PTBMA/epoxidation reaction product; c) PTBMA/Br₂ simultaneous reaction product.

4.3.6 Mixed polymer brush grafting by ATRP

The dibromination method was chosen as a route to mixed brush synthesis. Dibrominations of the AGE activated surfaces for mixed brush grafting were performed in two stages. Initial dibrominations were performed using the mass of bromine required to brominate 10, 20, 30, 40 and 50% of the available AGE groups. The first polymer grafting was then performed and the products analysed using FTIR.

A second bromination step was then performed on the grafted products, using the mass of bromine required to brominate the unbrominated AGE groups. It was assumed at this point that the presence of grafted polymers would not interfere with the dibromination reaction. Following the second dibromination step, a second polymer grafting was performed and the final mixed brush support was analysed using FTIR.

FTIR spectra of solid products show the presence of new polymer peaks corresponding to PTBMA and P2VP, indicating successful grafting of a mixed brush by the ATRP method (figures 4.39).

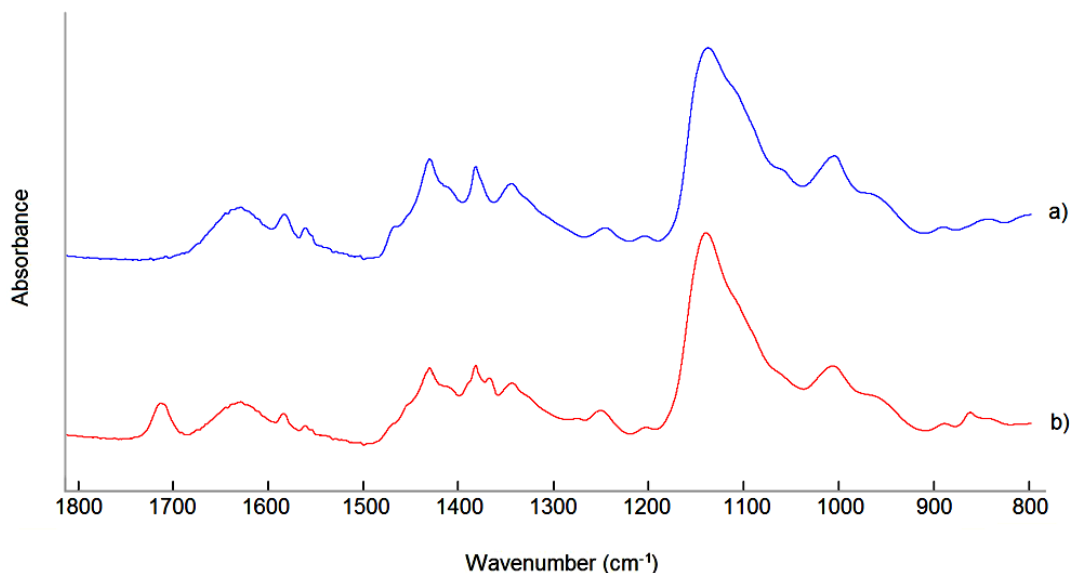


Figure 4.39. a) AGE activated M-PVA following 50% dibromination and ATRP reaction with 2VP; b) 2VP grafted support following 50% dibromination and ATRP reaction with TBMA.

Reaction of PTBMA with 2VP grafted M-PVA using the AGE/Br₂ method leads to the appearance of new peaks at 1720, 1390 and 850 cm⁻¹ (figure 4.39). These results suggest successful grafting of tBmA to create a mixed polymer layer on the support surface.

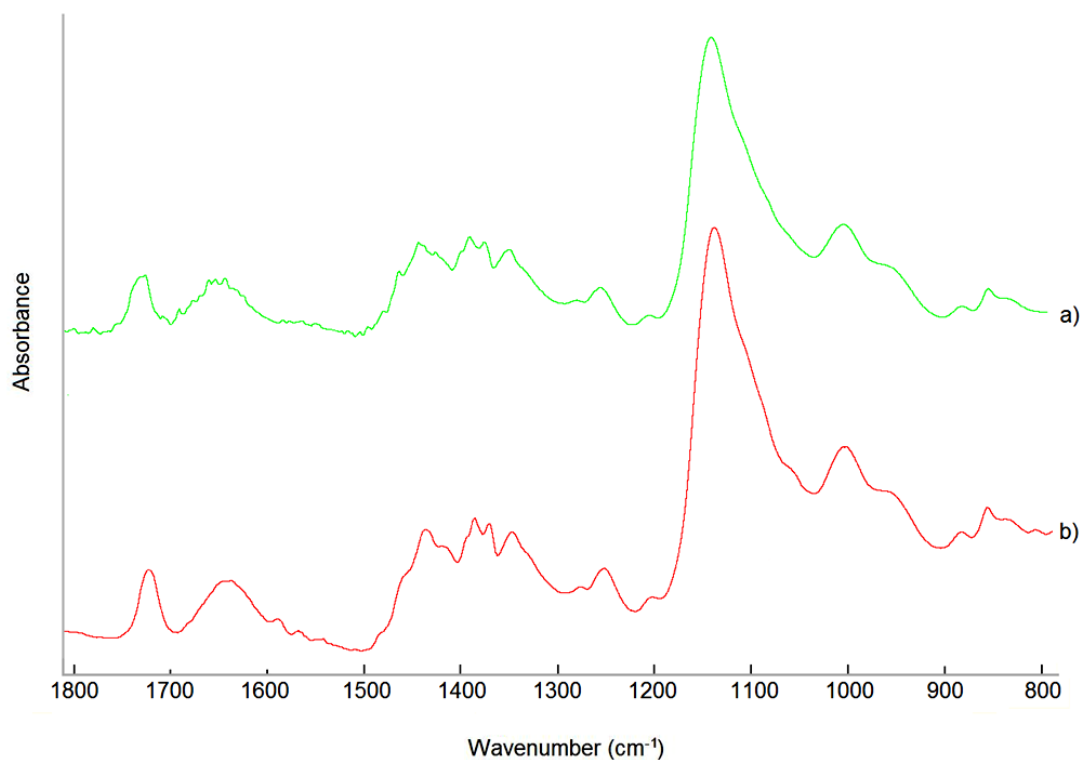


Figure 4.40. a) AGE activated M-PVA following 50% dibromination and ATRP reaction with TBMA; b) TBMA grafted support following 50% dibromination and ATRP reaction with 2VP.

Small peaks appear at 1590 and 1570 cm⁻¹ (aromatic C-H) indicating the grafting of some P2VP onto the PTBMA grafted support (figure 4.40).

Hydrolysis of ATRP grafted mixed brushes resulted in conversion of t-butyl ester side chains to give PMAA, as evidenced by FTIR spectra of the hydrolysed product (figure 4.41). Loss of peaks at 1720, 1390, 1250 and 850 is observed, indicating removal of the t-butyl alcohol group during hydrolysis.

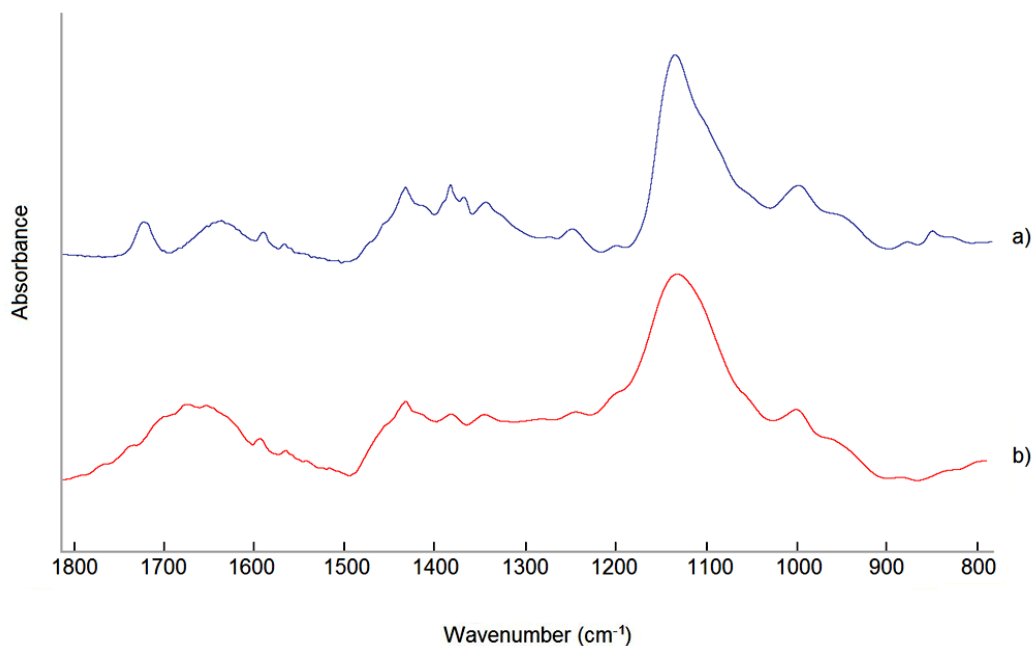


Figure 4.41. a) 2VP grafted support following 50% dibromination and ATRP reaction with TBMA; b) P2VP + PTBMA grafted support following hydrolysis with TFA solution.

Quantification of product compositions was calculated via liquid state FTIR analysis of the reaction supernatants (tables 4.1 and 4.2). Intergraft spacing, D , was calculated from the amount of Br_2 used during initiation and an M-PVA surface area of 56.7 m^2 per g. Brush length was calculated from the monomer consumption divided by the amount of Br_2 used during initiation and from this the Flory Radius, R_f , of each brush was found. Average Flory Radii for mixed brushes were calculated as described in Chapter 2. From these values $2R_f/D$ values were also calculated to allow estimation of the extent of brush behaviour that will be seen in the grafted layer.

Total grafting yields for mixed brush synthesis were $<4\%$, which is far less than expected for an ATRP 'living radical' polymerisation. This may result from the poor solubility of 2VP and TBMA monomers in the water solvent which is required to dissolve the ATRP catalyst system alongside well suspended M-PVA supports. A higher number of brominated sites during the first graft step leads to a higher grafting yield. This behaviour is not seen during the second graft step, leading to a maximum

polymer grafting of 0.887 g polymer per g M-PVA (41 % of total mass) with 1.35 mmol Br₂ added per g M-PVA for each step.

Calculated R_f values for ATRP grafted polymers are low (<2.3) but due to very small values of D (<0.59 nm) the values of $2R_f/D$ calculated for mixed brushes are similar to those seen for tresyl grafted supports in Chapter 3 and are suitable for brush behaviour. The very low values of R_f suggest a low brush height, which may limit the switchable steric behaviour hoped for with these mixed brushes.

It is worth noting that previous studies (Wu et al., 2008) have indicated that ATRP initiation is might only be expected on ~16% of activated surface sites. Based upon that information, it might be expected that both the D and R_f values calculated here are much smaller than the real values. $2R_f/D$ values calculated from this revised model would be higher, leading to increased brush behaviour.

Table 4.1. ATRP grafting of mixed polymer brushes from M-PVA following partial bromination (100% = 2.7 mmol Br₂ per g M-PVA).

Support	Stage	Polymer grafted	% bromination	Monomer presented (mmol) per g M-PVA	Monomer grafted (mmol) per g M-PVA	Yield (%)	D (nm)	Mol % P2VP	Mol % PTBMA	R _f (nm)	2R _f /D	n(poy)/n(init.)
1	Step 1	PMAA	10	27	1.69	6.3	0.59			0.99	3.4	6.3
1	Step 2	P2VP	90	243	3.29	1.4	0.20			0.80	8.2	1.4
1	Finished	[(P2VP) _x + (PMAA) _y]			4.99		0.19	34	66	0.83	8.9	
2	Step 1	PMAA	20	54	1.91	3.5	0.42			0.70	3.4	3.5
2	Step 2	P2VP	80	216	3.07	1.4	0.21			0.83	7.9	1.4
2	Finished	[(P2VP) _x + (PMAA) _y]			3.07		0.19	62	38	0.81	8.6	
3	Step 1	PMAA	30	81	2.33	2.9	0.34			0.62	3.6	2.9
3	Step 2	P2VP	70	189	3.63	1.9	0.22			0.99	8.9	1.9
3	Finished	[(P2VP) _x + (PMAA) _y]			5.96		0.19	39	61	0.91	9.8	
4	Step 1	PMAA	40	108	2.84	2.6	0.30			0.59	4.0	2.6
4	Step 2	P2VP	60	162	3.69	2.3	0.24			1.10	9.1	2.3
4	Finished	[(P2VP) _x + (PMAA) _y]			6.53		0.19	57	43	0.91	9.8	
5	Step 1	PMAA	50	135	3.40	2.5	0.26			0.59	4.0	2.5
5	Step 2	P2VP	50	135	3.84	2.8	0.26			1.10	9.1	2.9
5	Finished	[(P2VP) _x + (PMAA) _y]			7.24		0.19	53	47	0.96	10.3	

Table 4.2. ATRP grafting of mixed polymer brushes from M-PVA following partial bromination (100% = 2.7 mmol Br₂ per g M-PVA).

Support	Stage	Polymer grafted	% bromination	Monomer presented (mmol) per g M-PVA	Monomer grafted (mmol) per g M-PVA	Yield (5)	D (nm)	Mol % P2VP	Mol % PMAA	R _f (nm)	2R _f /D	n(poy)/n(init.)
6	Step 1	P2VP	10	27	2.05	7.6	0.59			2.26	7.7	7.6
6	Step 2	PMAA	90	243	2.67	1.1	0.20			0.35	3.5	1.1
6	Finished	[(P2VP) _x + (PMAA) _y]			4.73		0.19	43	57	1.15	12.3	
7	Step 1	P2VP	20	54	2.59	4.8	0.42			1.72	8.2	4.8
7	Step 2	PMAA	80	216	3.00	1.4	0.21			0.40	3.8	1.4
7	Finished	[(P2VP) _x + (PMAA) _y]			5.58		0.19	46	54	1.08	11.6	
8	Step 1	P2VP	30	81	3.20	3.9	0.34			1.53	9.0	4.0
8	Step 2	PMAA	70	189	2.83	1.5	0.22			0.42	3.8	1.5
8	Finished	[(P2VP) _x + (PMAA) _y]			6.02	3.6	0.19	53	47	1.09	11.7	
9	Step 1	P2VP	40	108	3.86	1.7	0.30			1.44	9.7	3.6
9	Step 2	PMAA	60	162	2.76		0.24			0.45	3.8	1.7
9	Finished	[(P2VP) _x + (PMAA) _y]			6.62	3.0	0.19	58	42	1.12	12.0	
10	Step 1	P2VP	50	135	4.03	2.0	0.26			1.29	9.8	3.0
10	Step 2	PMAA	50	135	2.67		0.26			0.50	3.8	2.0
10	Finished	[(P2VP) _x + (PMAA) _y]			6.70		0.19	60	40	1.07	11.5	

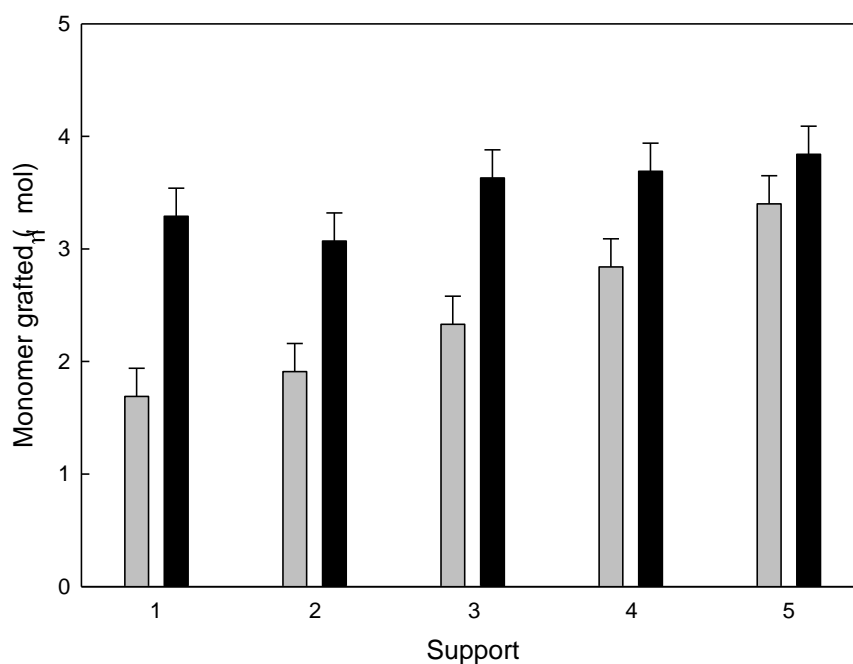


Figure 4.42 (above). Grafting results for ATRP route supports as described in table 4.1. Black bars represent P2VP grafted, grey bars represent PTBMA/PMAA.

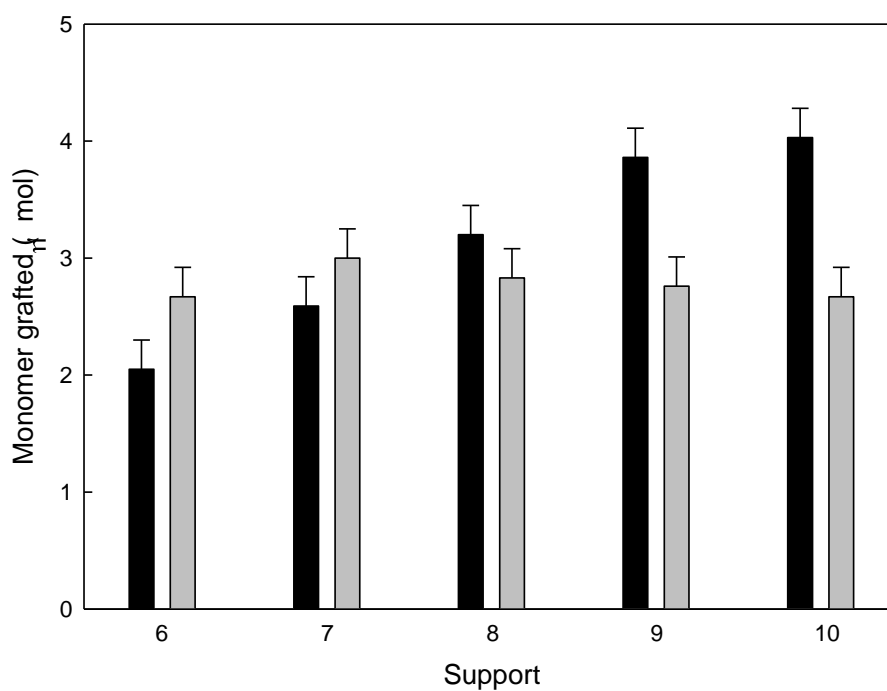


Figure 4.43 (above). Grafting results for ATRP route supports as described in table 4.2. Black bars represent P2VP grafted, grey bars represent PTBMA/PMAA.

The effect of ATRP solvent upon TBMA and 2VP grafting was also investigated by performing ATRP synthesis of homopolymer brush grafted supports in three different solvent systems: water; water/DMSO 50/50 mix; and DMSO. This experiment followed the observation that TBMA and 2VP monomers both showed better miscibility in DMSO than water, whereas the solubility of the CuBr/dipy catalyst and dispersion of M-PVA were better in water. It was observed that ATRP grafting in DMSO and water/DMSO solvent led to grafting yields that were lower than those achieved with water as solvent (table 4.3)

Table 4.3. Grafting yield following ATRP reaction with 50% brominated M-PVA (50 mg, 1.35 mmol Br₂ per g M-PVA) in a variety of solvents.

Support	Polymer grafted	Solvent	Monomer presented (mmol) per g M-PVA	Monomer grafted (mmol) per g M-PVA	Yield (%)	D (nm)	R _f (nm)	2R _f /D
1	PMAA	Water	135	3.40	2.5	0.26	0.57	4.3
2	P2VP	Water	135	4.03	3.0	0.26	1.29	9.8
3	PMAA	Water/DMSO 50/50	135	2.19	1.6	0.26	0.44	3.3
4	P2VP	Water/DMSO 50/50	135	2.64	2.0	0.26	1.00	7.6
5	PMAA	DMSO	135	0.28	0.2	0.26	0.13	1.0
6	P2VP	DMSO	135	0.85	0.6	0.26	0.51	3.8

Use of an acidified water solvent during ATRP grafting of 2VP was investigated in a similar manner. Increased acidity leads to an increased concentration of the protonated form of 2VP, which is more favourably solvated in water than the neutral form (table 4.4).

Table 4.4. Grafting yield following ATRP reaction with 50% brominated M-PVA (50 mg, 1.35 mmol Br₂ per g M-PVA) in aqueous HCl solutions at pH 0-4.

Support	Polymer grafted	Solvent pH	Monomer presented (mmol) per g M-PVA	Monomer grafted (mmol) per g M-PVA	Yield (5)	D (nm)	R _f (nm)	2R _f /D
1	P2VP	0	135	1.54	1.1	0.26	0.73	5.5
2	P2VP	1	135	1.18	0.8	0.26	0.62	4.7
3	P2VP	2	135	2.91	2.2	0.26	1.06	8.0
4	P2VP	3	135	2.48	1.8	0.26	0.97	7.3
5	P2VP	4	135	2.70	2.0	0.26	1.02	7.7

Improved ATRP grafting of 2VP is not seen under acidified conditions. Although full solvation of 2VP was observed at lower pH values, it is likely that these conditions also interfere with the ATRP reaction.

4.3.7 Mixed polymer brush grafting by dibromination graft to

The dibromination method was chosen as a route to mixed brush synthesis. Consecutive grafting steps were tested, with grafting onto a 100% dibrominated support followed by full dibromination and grafting of the second polymer. FTIR spectra of the solid products and reactions solutions show that grafting was successful for both polymer types in all of the dibromination techniques, showing the presence of new polymer peaks corresponding to PTBMA and P2VP (figures 4.44 and 4.45).

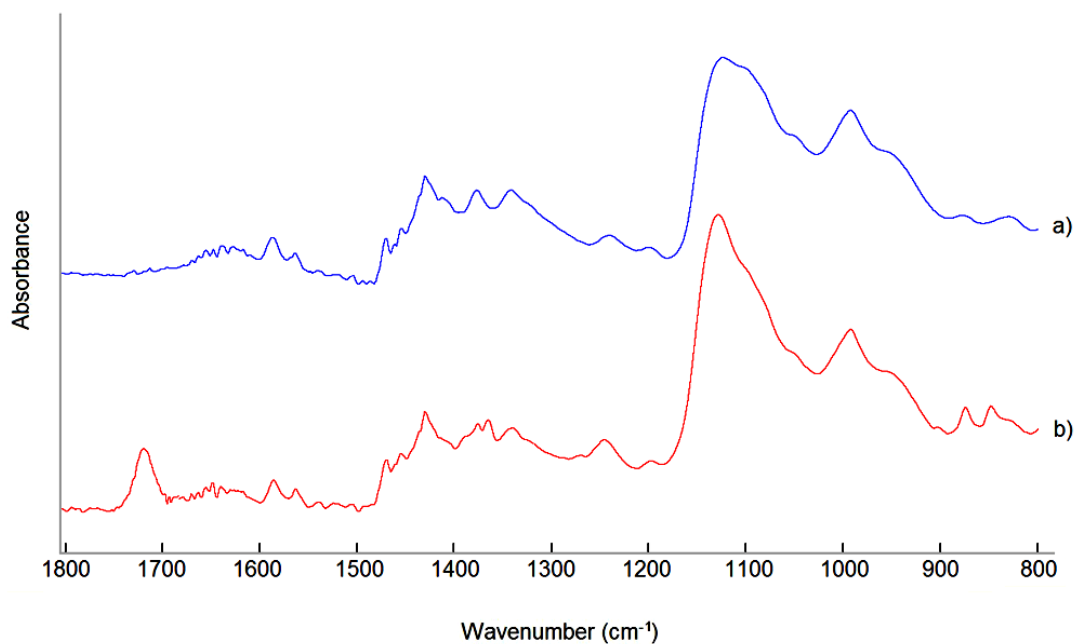


Figure 4.44. a) AGE activated M-PVA following 100% dibromination and graft-to reaction with P2VP; b) P2VP grafted M-PVA following graft-to reaction with PTBMA.

Reaction of PTBMA with 2VP grafted M-PVA using the AGE/Br₂ method leads to the appearance of new peaks at 1720, 1390 and 850 cm⁻¹ (figure 4.42). Peak height at 1140 cm⁻¹ also is seen to increase. These results suggest successful grafting of TBMA to create a mixed polymer layer on the support surface.

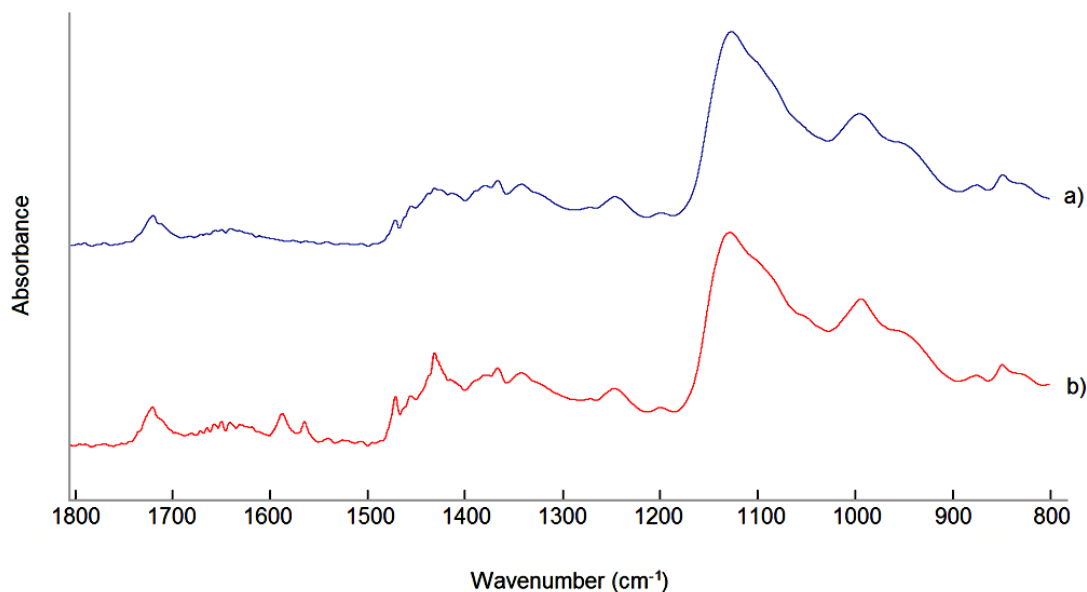


Figure 4.45. a) AGE activated M-PVA following 100% dibromination and graft-to reaction with PTBMA; b) PTBMA grafted M-PVA following graft-to reaction with P2VP.

New peaks are visible at 1590 and 1570 cm^{-1} (aromatic C-H) and peak height at 1430 cm^{-1} increases, indicating the grafting of P2VP onto the PTBMA grafted support (figure 4.45).

Brush quantification and dimensions were calculated as for tresyl graft to supports (Chapter 3), with mixed brush average R_f values calculated as described in Chapter 2. Total polymer grafted was slightly less than observed for tresyl graft to (table 4.5), with up to 0.280 g polyelectrolyte present per g M-PVA (22 % of final product mass). This indicates that alkyl bromide substitution is a less effective activation method for amine-terminated polymer graft to. This may be surprising as the total number of brominated sites (2.7 mmol per g M-PVA) is much higher than the calculated number of tresylated sites (57.8 μmol s per g M-PVA) and indicates the effectiveness of the tresyl activation described in Chapter 3 as a precursor to nucleophilic attack.

Table 4.5 Grafting yield following graft-to reaction between amine terminated polymer and 100% brominated M-PVA (50 mg, 1.35 mmol Br₂ per g M-PVA) in acetone.

Support	Stage	Polymer grafted	Monomer presented (mmol) per g M-PVA	Monomer grafted (mmol) per g M-PVA	Yield (%)	D (nm)	Mol % P2VP	Mol % PMAA	R _f (nm)	2R _f /D	n(poly)/n(init.)
1	Step 1	P2VP	1.52	1.18	77.6	3.35			13.04	7.8	141
1	Step 2	PMAA	4.22	1.25	29.6	3.56			5.29	3.0	102
1	Finished	[(P2VP) _x + (PMAA) _y]		2.43		2.44	49	51	11.00	9.0	
2	Step 1	PMAA	1.13	0.67	59.3	4.87			5.29	2.8	102
2	Step 2	P2VP	5.71	2.11	37.0	2.51			13.04	10.4	141
2	Finished	[(P2VP) _x + (PMAA) _y]		2.78		2.23	76	24	12.30	11.0	

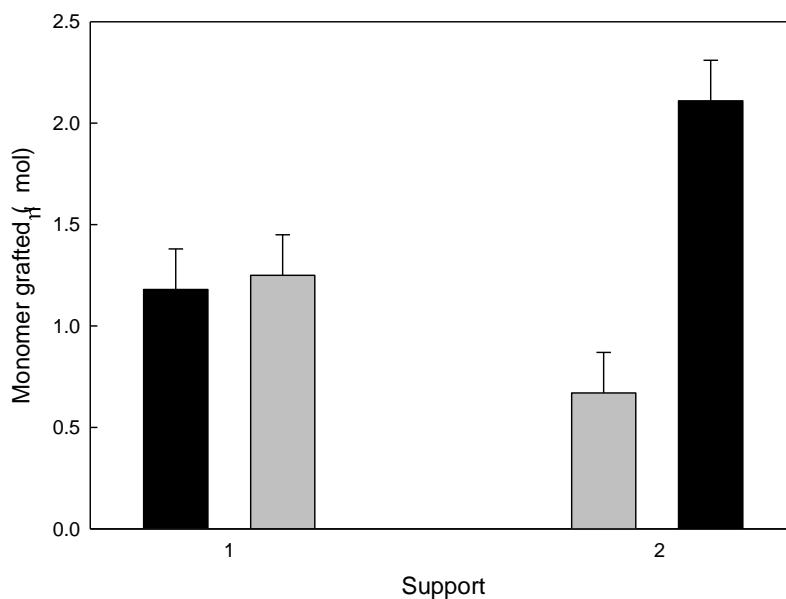


Figure 4.46. Grafting results for graft-to supports as described in table 4.5. Black bars represent P2VP grafted, grey bars represent PTBMA/PMAA.

4.3.8 Mixed polymer brush grafting by a combining ATRP and graft to

A third route to mixed brushes via dibromination involved using one graft-to step and one ATRP step on the same supports. For example, AGE activated supports underwent 50% bromination and graft-to reaction of P2VP at the surface. The remaining AGE groups of these P2VP grafted supports were then brominated and ATRP was performed with tBmA to produce supports with mixed P2VP/PTBMA brush layers. FTIR analysis shows the presence of both P2VP and PTBMA on all final products (figures 4.47-4.50).

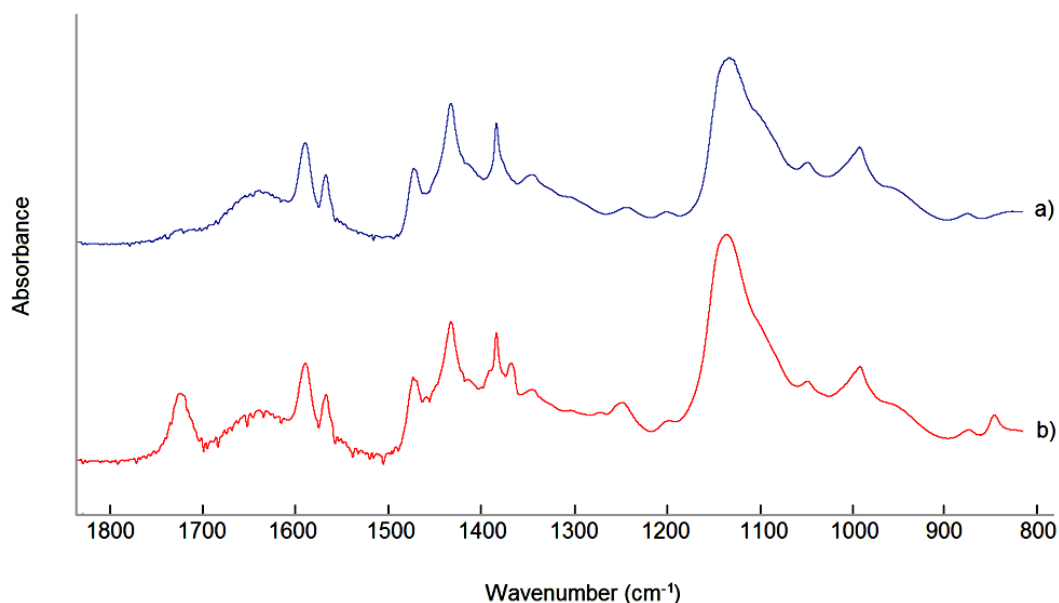


Figure 4.47. a) AGE activated M-PVA following 50% dibromination and ATRP reaction with 2VP; b) 2VP grafted M-PVA following 50% dibromination and graft-to reaction with PTBMA.

The appearance of new peaks at 1720, 1370 and 850 cm^{-1} and increase in peak height at 1140 cm^{-1} indicate the presence of PTBMA on the support following ATRP grafting (figure 4.47). Comparison of grafted P2VP peaks in the solid spectra here (figure 4.47) suggest that ATRP grafting of P2VP has been more successful than the previous P2VP-ATRP graft shown in figure 4.31. However, liquid spectra quantification does not suggest any such difference (see tables 4.2 and 4.6) which suggests that the difference in solid spectra may result from variation between solid FTIR samples. In the case of figure 4.44 it is likely that a 'P2VP rich' portion has been used leading to larger P2VP peaks than would be expected from the liquid data. This result suggests that a certain degree of localization is to be seen within the grafted M-PVA samples, with some beads being far richer in P2VP and others richer in PMAA.

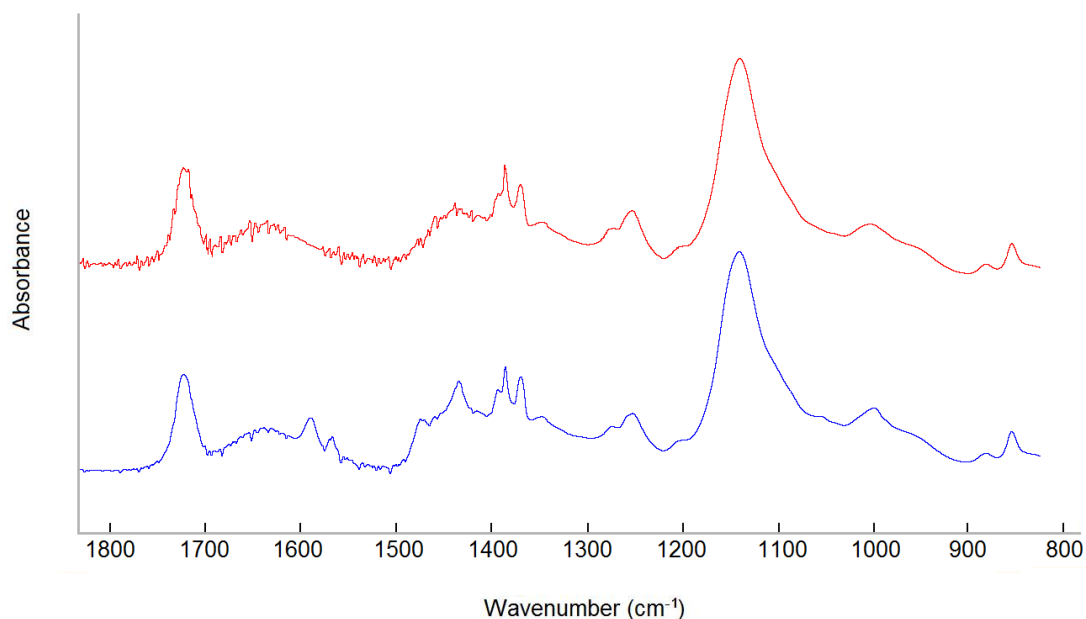


Fig 4.48. a) AGE activated M-PVA following 50% dibromination and ATRP reaction with TBMA; b) TBMA grafted M-PVA following 50% dibromination and graft-to reaction with P2VP.

The appearance of new peaks at 1590, 1570 and 1430 cm^{-1} indicate successful grafting of P2VP using ATRP (figure 4.48)

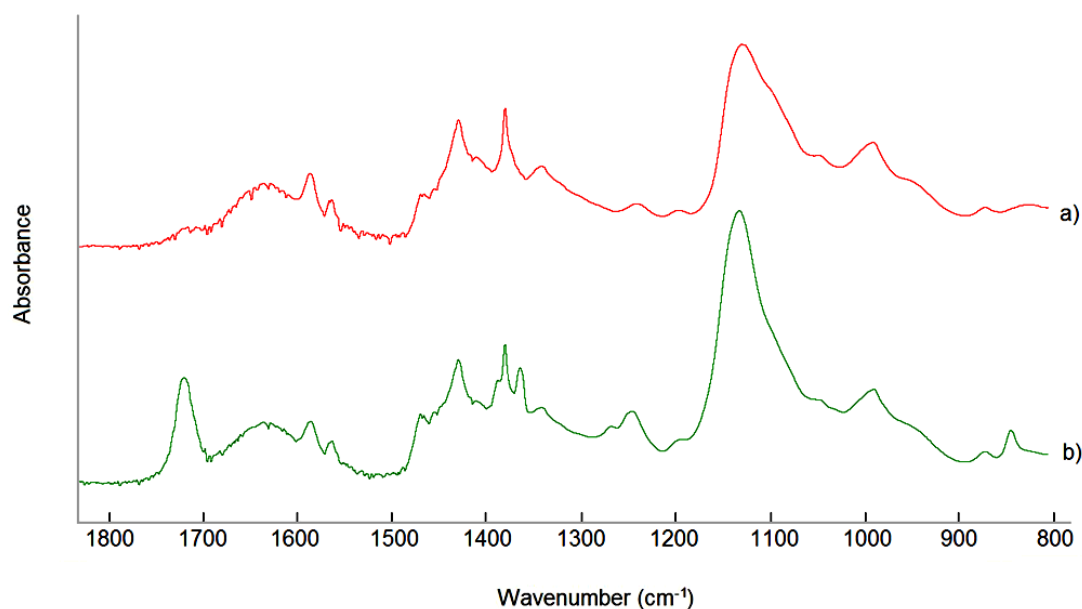


Fig 4.49. a) AGE activated M-PVA following 50% dibromination and graft-to reaction with P2VP; b) P2VP grafted M-PVA following 50% dibromination and ATRP reaction with TBMA.

The appearance of new peaks at 1720, 1370 and 850 cm^{-1} , and a significant increase in peak height at 1140 cm^{-1} , show that grafting of PTBMA using AGE/ Br_2 activated graft-to has been successful (figure 4.49).

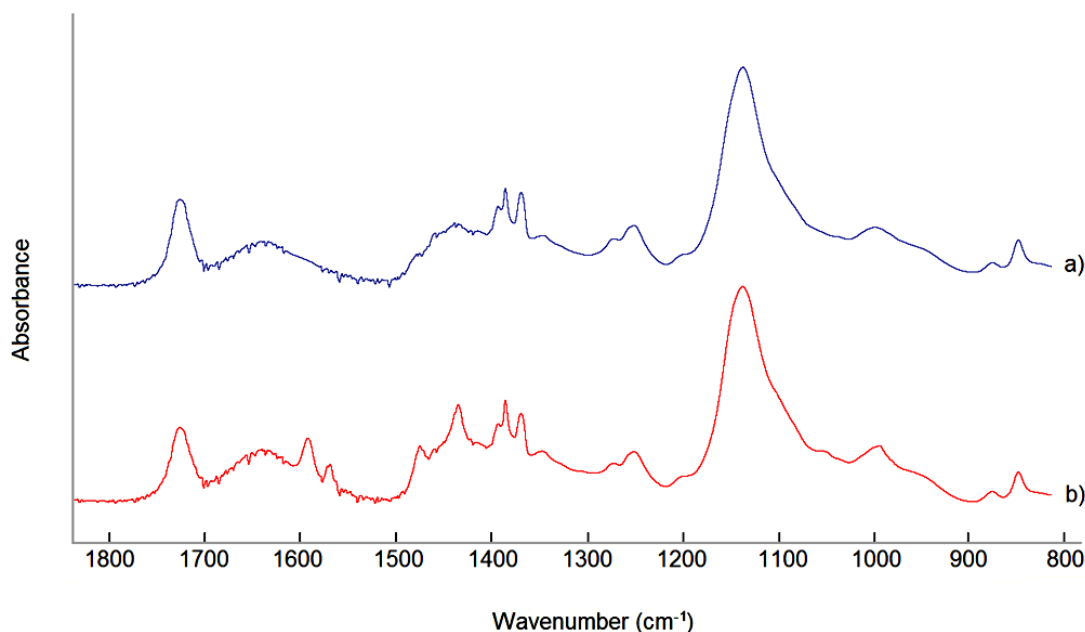


Fig 4.50. a) AGE activated M-PVA following 50% dibromination and graft-to reaction with PTBMA; b) PTBMA grafted M-PVA following 50% dibromination and ATRP reaction with 2VP.

New peaks can be seen at 1590, 1570, 1490 and 1430 cm^{-1} , indicating the presence of grafted P2VP following AGE/ Br_2 activated graft-to (figure 4.50).

Mixed brush quantification and dimension calculations were performed as described for the previous ATRP and graft to methods, with R_f averaging as described in Chapter 2 (table 4.6). As seen for previous supports, all $2R_f/D$ values indicate some degree of brush regime behaviour. Average $2R_f/D$ values for the mixed brush may be misleading, as these are influenced by the high R_f values of the graft to brushes and low D values of the ATRP brushes, meaning that the expected brush behaviour is unlikely to be more strict than for the mixed brushes synthesised by graft to or ATRP alone. The differences in D and R_f between the two methods do suggest that this method produces grafted polymer layers composed of tightly spaced, short ATRP-grafted chains between longer, less tightly packed graft to chains.

Table 4.6. Grafting yield following graft-to and ATRP reactions between amine terminated polymer and 50% brominated M-PVA (50 mg, 1.35 mmol Br₂ per g M-PVA) in acetone.

Support	Stage	Method	Polymer grafted	Monomer presented (mmol) per g M-PVA	Monomer grafted (mmol) per g M-PVA	Yield (%)	D (nm)	Mol % P2VP	Mol % PMAA	R _f (nm)	2R _f /D	n(poly)/n(init.)
1	Step 1	ATRP	P2VP	135	2.88	2.1	0.26			1.06	8.0	2.1
1	Step 2	Graft-to	PMAA	4.22	1.86	44.1	2.92			5.29	3.6	102
1	Finished		[(P2VP) _x + (PMAA) _y]		4.75		0.26	61	39	1.33	9.3	
2	Step 1	ATRP	PMAA	135	2.69	2.0	0.26			0.50	3.8	2.0
2	Step 2	Graft-to	P2VP	5.71	2.43	42.6	2.33			13.04	11.2	141
2	Finished		[(P2VP) _x + (PMAA) _y]		5.12		0.26	48	52	3.64	27.8	
3	Step 1	Graft-to	P2VP	5.71	1.97	34.5	2.60			13.04	10.1	141
3	Step 2	ATRP	PMAA	135	2.53	1.9	0.26			0.48	2.7	1.1
3	Finished		[(P2VP) _x + (PMAA) _y]		4.50		0.26	44	56	3.23	24.6	
4	Step 1	Graft-to	PMAA	4.22	1.34	31.7	3.44			5.29	3.1	102
4	Step 2	ATRP	P2VP	135	3.12	2.3	0.26			1.11	8.4	2.3
4	Finished		[(P2VP) _x + (PMAA) _y]		4.46		0.26	70	30	1.29	9.3	

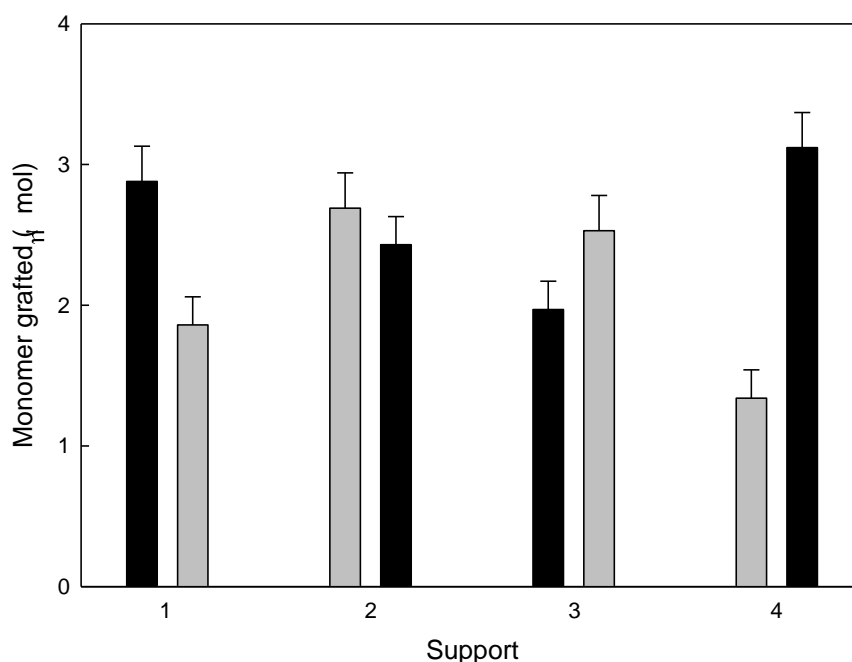


Figure 4.51. Grafting results for graft-to supports as described in table 4.6. Black bars represent P2VP grafted, grey bars represent PTBMA/PMAA.

4.4 Conclusions

Partial brominations of M-PVA surface sites have been achieved through AGE activation followed by quantitative Br_2 addition to AGE double bonds, with a maximum Br_2 consumption of 2.7 mmol per g of AGE activated M-PVA. This technique has allowed controlled generation of sites suitable for polymer graft to and graft from synthetic techniques. Using these sites successful synthesis of mixed polymer brush layers has been achieved through ATRP graft from; amine terminated polymer graft to; and combinations of the two techniques. Total grafted masses for ATRP techniques (up to 0.696 g polyelectrolyte per g M-PVA) are higher than those seen for the tresyl graft to method described in Chapter 3, but lower than the Ce(IV) initiated graft from described in Chapter 2. Masses grafted using nucleophilic attack by amine-terminated polymers (up to 0.280 g per g M-PVA) were lower than those achieved with tresyl activated graft to reactions. This is as expected, given the lower reactivity of alkyl bromides than sulfonyl chlorides to nucleophilic substitution reactions

and the typical requirement for significant excesses of (even small) nucleophile required to achieve successful substitutions at alkyl bromide sites. The use of a combined ATRP/graft from approach has led to the possibility of mixed brushes composed of short, tightly packed polymers past which a separate species of much longer, more widely spaced polymer chains extending from the same surface. All techniques produced grafted layers with Flory Radius values of $2R_f/D > 10$, indicating brush regime behavior.

Overall, the patterned activation possible by partial bromination to the M-PVA surface is of great interest, although the graft masses seen here for partial bromination methods are lower than those achieved using with the analogous Ce(IV) and tresyl grafting approaches.

5. Binding Studies on Grafted Beads

5.1 Introduction

Ionic exchange (IEX) constitutes one of the most commonly applied protein separation techniques, being used in about 75% of protein purification protocols, compared to affinity (60%) and gel (50%) separation methods (Bonnerjea et al., 1986).

IEX is widely used for a number of reasons, these include.

- 1) High binding capacities.
- 2) High resolving power for proteins with different pI values.
- 3) Easy process to operate and adapt, based on simple binding principles (Janson and Ryden, 1998).

Polyelectrolyte grafted magnetic supports, as described in Chapters 2-4, have potential IEX applications due to the chargeable nature of their graft polymer sideunits. Supports grafted with a mixed brush comprising P2VP and PMAA may display both cation and anion binding behaviour, depending upon the pH of operation. At low pH values the positive charge of P2VP chains is expected to lead to a positive surface charge (Houbenov et al., 2003), which is associated with anion binding behaviour. At higher pH values the negative charge on PMAA sideunits is expected to dominate, leading to cation binding behaviour (figure 5.1).

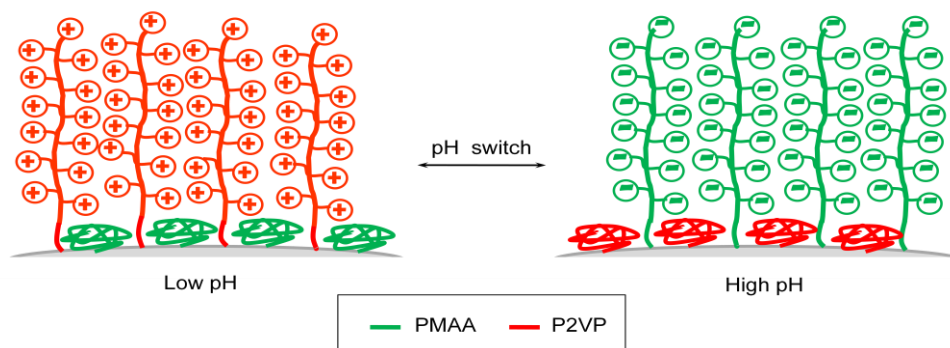


Figure 5.1. Switchable charge properties of a PMAA/P2VP mixed brush grafted surface.

The dominant protein binding behaviour of a surface can be tested with the used of a model protein solution containing a selection of proteins with known isoelectric point (pI). The availability of proteins with a variety of pI values means that cationic and anionic binding of proteins can be tested over a range of pH (Table 5.1).

Table 5.1. Molecular weight values, M_w , and isoelectric points, pI, of proteins of interest.

Protein	pI	M_w (kDa)	Reference
Lysozyme	11.0	14.4	(Ekstrand, 1989)
LPO	9.8	77	(Ekstrand, 1989)
Myoglobin	6.9	17	(Graf and Watzig, 2004)
Carbonic Anhydrase	6.6	29.5	(Righetti, 1976)
β -lactoglobulin	5.3	18.6	(Dumetz et al., 2008)
BSA	5.1	66.3	(Kinsella and Whitehead, 1989)
Ovalbumin	4.7	45	(Moritz & Simpson, 2005)

A suitable technique for use in analysis of protein binding is reducing SDS-PAGE, a form of gel electrophoresis (Laemmli, 1970). During gel electrophoresis sample protein solutions are prepared and loaded onto a gel through which an electrical current is passed. Sample preparation involves treatment with sodium dodecyl sulphate (SDS) and β -mercaptoethanol to denature the protein structures (Weber and Osborn, 1969; Huggins et al., 1950). The presence of SDS also leads to each protein acquiring a negative charge proportional to its mass. Under an electric field, the molecules move towards the anode at a rate proportional to their mass. For a protein solution containing proteins of different sizes, this results in the separation of the proteins according to their molecular weight. In addition, proteins of the same molecular weight will travel at approximately the same rate through the gel and resolve into distinct bands which correspond to the most common molecular weights in the gel. Visualisation of SDS-page gels is achieved

through the use of protein stains. Protein stains contain dye molecules which can bind specifically to proteins and allow the protein distribution on the gel to be visualised (figure 5.2).

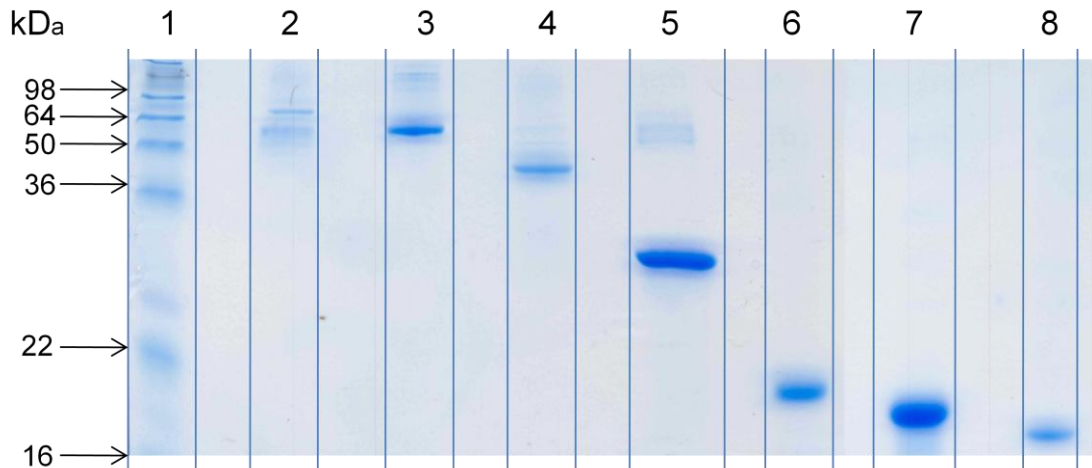


Fig 5.2. SDS-page loaded with samples from table 4.1. Lane 1: SeeBluePlus2 Marker.; Lane 2: LPO.; Lane 3: BSA.; Lane 4: Ovalbumin.; Lane 5: Carbonic anhydrase.; Lane 6.: β -lactoglobulin.; Lane 7: Myoglobin.; Lane 8: Lysozyme.

Computer based imaging and quantification of these dyed gel bands are then possible with the use of scanning methods. In the past scanning densitometry was the method of choice (Andrews, 1986), however, recent developments such as the US National Institute of Health's ImageJ computer program allow analysis of band intensities from high-resolution gel images (Girish and Vijayalakshmi, 2004). The wide availability of high-resolution scanners has resulted in the rapid uptake of the ImageJ technology for use in bioscientific research (Hausera, 2007; Le Saux et al., 2008) due to its cost effectiveness and convenience. As with a densitometer, the ImageJ program measures band intensity within designated lanes. Output data is plotted as lane distance vs. intensity, with protein bands appearing as peaks. The area under each such peak is proportional to the gel band intensity. As band intensity is proportional to the amount of protein present, protein loads of individual bands can be calculated by comparing band intensities.

Against the above, this Chapter describes protein binding studies based upon a selection of polyelectrolyte grafted M-PVA supports (table 5.3). CE-AX is M-PVA grafted with PMAA and CE-CX is M-PVA grafted with P2VP, both synthesized using Ce(IV) activation. These supports are presented for comparison with mixed brush supports created using Ce(IV), ATRP and tresyl graft-to methods. Of these mixed brush supports CE-MX1/CE-MX2 have been grafted using Ce(IV) activation; TR-MX1/TR-MX2 using tresyl activation and AT-MX1/AT-MX2 using ATRP from dibrminated AGE groups at the M-PVA surface. For more details on these methods see chapters 2-4 of this study, and for the specific order of polymer grafting and brush composition see table 5.3.

The studies in this chapter utilize a model protein binding mixture containing the following proteins (table 5.2) and include basic, neutral and acidic species with distinct M_w values.

Table 5.2. Component proteins for model protein mixture.

Protein	pI	M_w
Ovalbumin	4.7	45
Carbonic Anhydrase	6.6	29.5
β -lactoglobulin	5.3	18.6
Lysozyme	11.0	14.4

This model protein system is used in conjunction with SDS-PAGE and ImageJ gel analyses to obtain qualitative and quantitative information about the nature of IEX protein binding behaviour on P2VP and PMAA grafted supports under a range of pH conditions. Finally, the relationship between brush composition and dimensions is discussed in terms of the observed protein binding properties.

Table 5.3. Data for polyelectrolyte grafted supports. Table shows name as used in this chapter, grafting method, order of polymer grafting and amount of polymer per g of M-PVA. Graft dimensions are also shown, these are: Chain length, L; Intergraft distance, D; and a ratio of Flory Radius to intergraft distance, $2R_f/D$.

Name	Method	Graft order	P2VP (mol/g)	P2VP R_f (nm)	P2VP D (nm)	P2VP $2R_f/D$	n(P2VP)/n(init.)	PMAA (mol/g)	PMAA R_f (nm)	PMAA D (nm)	PMAA $2R_f/D$	n(PMAA)/n(init.)	MIX R_f (nm)	MIX D (nm)	MIX $2R_f/D$
CE-AX	Ce(IV) (Ch. 2)	P2VP only	4.88	5.48	0.82	13.4	66.4	-	-	-	-	-	-	-	-
CE-CX	Ce(IV) (Ch. 2)	PMAA only	-	-	-	-	-	6.11	3.09	0.82	7.6	83.1	-	-	-
CE-MX1	Ce(IV) (Ch. 2)	1.P2VP 2.PMAA	4.88	5.48	0.82	13.4	66.4	4.56	2.59	0.82	6.3	62.0	4.55	0.58	15.7
CE-MX2	Ce(IV) (Ch. 2)	1.PMAA 2.P2VP	3.34	4.36	0.82	15.1	45.4	6.11	3.09	0.82	7.6	83.1	3.84	0.58	13.3
TR-MX1	Tresyl (Ch. 3)	1.P2VP 2.PMAA	1.35	13.04	3.20	8.1	141	1.81	5.29	2.36	4.5	102	9.72	1.90	10.2
TR-MX2	Tresyl (Ch. 3)	1.PMAA 2.P2VP	2.44	13.04	2.38	11.2	141	1.50	5.29	3.26	4.1	102	11.66	1.92	12.1
AT-MX1	ATRP (Ch. 4)	1.P2VP 2.PMAA	3.84	1.10	0.26	9.1	3.0	3.40	0.59	0.26	4.0	2.0	0.96	0.19	10.3
AT-MX2	ATRP (Ch. 4)	1.PMAA 2.P2VP	2.67	1.29	0.26	9.8	2.9	4.03	0.50	0.26	3.8	2.5	1.07	0.19	11.5

5.2. Materials and methods

5.2.1 Materials used

Modified M-PVA supports were obtained from the syntheses described in Chapters 2-4. Citric acid (CAS 5949-29-1); sodium citrate (CAS 18996-35-5); sodium phosphate (CAS 7558-80-7); sodium carbonate (CAS 497-19-8); trizma hydrochloride (CAS 1185-53-1); trizma base (CAS 77-86-1) and sodium chloride (CAS 7647-14-5) were obtained from Sigma Aldrich (Poole, Dorset). Cuvettes, 2 ml screw-cap micro test tubes, 15 ml screw-cap centrifuge tubes and 50 ml screw-cap centrifuge tubes were obtained from Sarstedt (Leicester, UK). 1.5 ml hinged-lid micro test tubes were obtained from Eppendorf (Cambridge, UK). Deionised water was re-filtered using 0.2 µm Minisart filters obtained from Sartorius (Epsom, UK).

All unheated mixing was performed with a VM20 vortex mixer or a IKA Vibrax VXR basic mixer with attachments for 15 ml centrifuge tubes and micro test tubes. Electrophoresis samples were heated in a Grant GP3 heating rack. Chemicals were weighed on Mettler AE160 and AT261 balances. Pipetting was performed with 20 ml, 200 ml, 1 ml and 5 ml adjustable pipettes. All proteins were obtained from Sigma-Aldrich (Poole, Dorset).

Electrophoresis was performed using precast polyacrylamide Tris-HCl gels (15% gels and 4-20% gradient gels) obtained from Bio-Rad (California, US). Electrophoresis samples were prepared with Laemmli sample buffer (Bio-Rad, US) and β-mercaptoethanol (Sigma-Aldrich, CAS 60-24-2). Electrophoresis tank and MP-250V power pack were purchased from Cleaver Scientific (Rugby, Warwickshire). Protein molecular weight standards were provided by Seebue Plus 2 prestained protein standard mixture (Invitrogen, UK). Gel staining was performed using Seebue Safestain or Novex Colloidal Blue stain kit (Invitrogen, UK).

5.2.2 Electrophoresis sample preparation

Protein composition in binding and elution solutions was performed using reducing SDS-PAGE (Laemmli, 1970). Running buffer was prepared from laemmli sample buffer (975 μ l) and β -mercaptoethanol (25 μ l). Each protein solution (25 μ l) was mixed with running buffer (25 μ l, heated (70°C, 600 s) and then allowed to cool (RT, 600 s).

5.2.3 Running electrophoresis samples

Electrophoresis samples (10 μ l) were loaded onto gels alongside the prestained protein standard mixture. Samples were ran in a refrigerated room (6°C) at lowered voltage (45 V, 60 mA, 0.5 h) until all samples has passed through the stacking phase. Following the stacking phase the voltage was increased and samples allowed to pass through to the end of the gel (80 V). Electrical current was removed once running buffer colour had exited the far end of the gel.

The gel was then removed from the electrophoresis setup and shaken in water (25 ml, 5 min, x 3). The water was removed and the gel was shaken in Simply Blue Safe Stain solution (25 ml, 1h). The staining solution was then removed and the gel was washed in water (25 ml, 5 min, x 2). The gel was then washed with NaCl solution (25 ml, 1M, 24 h, x 2) before being stored in ammonium sulphate solution (25 ml, 10% (w/v), 4°C).

Prior to scanning the gels were washed in water (25 ml, 1 min). Washing solvent was removed and the damp gel was scanned at 2400 dpi using a high-resolution HP ImageJet scanner.

5.2.4 Acidic/basic protein binding with salt elution

The ability of supports to bind selections of basic and acidic proteins was analysed in buffered solutions at pH 5, 6, 7 and 8. Buffer solutions (20 mM) were prepared at the experimental pH and the same buffer pH was used throughout each experiment. Citrate buffer was used at pH 5; sodium phosphate buffer at pH 6 and 7; Tris-HCl buffer at pH 8. Binding solution comprised of buffer (20 mM) plus ovalbumin (CAS

9006-59-1); carbonic anhydrase (CAS 9001-03-0); β -lactoglobulin (CAS 9045-23-2) and lysozyme (52219-07-5). Each protein was present at 0.25 mg/ml, making a total protein conc. of 1 mg/ml.

1 mg of support was washed twice with buffer solution (20 mM, 100 μ l, 0.25 h). The supports were then separated and mixed with binding solution. (100 μ l, 0.25 h). Binding supernatant was stored for analysis. The supports were then washed twice with buffer (100 μ l, 0.25 h). After washing protein was eluted from support by mixing with a solution of NaCl in buffer (1 M, 100 μ l, 0.25 h). Binding and elution supernatants were tested by electrophoresis using 15 % polyacrylamide gels.

5.2.5 Protein binding at pH 5 with elution by pH switch

The ability of supports to bind selections of basic and acidic proteins was analysed in buffered solutions at pH 5. Buffer solutions were prepared as in section 5.2.4 and used to make binding solution comprising of pH 5 buffer (20 mM) plus ovalbumin; carbonic anhydrase; β -lactoglobulin and lysozyme with each protein present at 0.25 mg/ml. 1 mg of support was washed twice with pH 5 buffer solution (20 mM, 100 μ l, 0.25 h). The supports were then separated and mixed with binding solution (1 mg/ml, 100 μ l, 0.25 h). Binding supernatant was stored for analysis. The supports were then washed twice with pH 5 buffer (100 μ l, 0.25 h). After washing proteins were eluted from support by mixing in buffers at pH 6, 7 or 8 (100 μ l, 0.25 h). Binding/elution gels were obtained by running electrophoresis samples of binding and elution supernatants on 15 % polyacrylamide gels.

5.2.6 Protein binding at pH 8 with elution by pH switch

The method described for pH elution in section 5.2.5 was adapted by using binding/washing solutions buffered at pH 8 and elution buffers at pH 5, 6 and 7. All concentrations and conditions were otherwise the same.

5.3 Results

5.3.1 Binding studies on ungrafted supports

Binding and salt elution behaviour of the 4 protein mixture (ovalbumin; carbonic anhydrase; β -lactoglobulin; lysozyme) was first studied for unmodified M-PVA supports over the range pH 5-8. Neither binding nor elution were observed on unmodified M-PVA supports (figure 5.3; table 5.4)

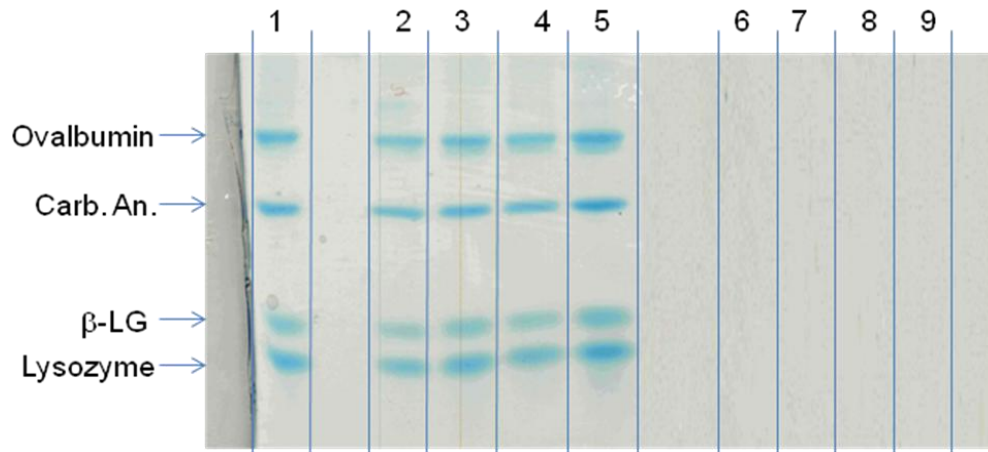


Figure 5.3. Binding of 4 protein solution on unmodified M-PVA, with salt elution. Lane 1: Challenge; Lanes 2 to 5: Binding supernatants at pH 5-8; Lanes 6 to 9. Elution supernatants at pH 5-8.

Table 5.4. Binding study for unmodified M-PVA with salt elution

	Unbound @				Elution @			
	pH 5	pH 6	pH 7	pH 8	pH 5	pH 6	pH 7	pH 8
OVA	115	105	102	109	0	0	0	0
CA	93	94	93	102	0	0	0	0
β LG	104	108	98	97	0	0	0	0
LYS	109	110	105	108	0	0	0	0

Binding and elution studies performed on the ungrafted M-PVA beads showed no binding or elution of proteins under any of the conditions tested. Although the hydroxyl groups of PVA might be expected to become deprotonated and gain cation exchange properties at higher pH values, the pH ranges required for this behaviour are more basic than those tested here.

5.3.2 Binding studies on homopolymer grafted supports

Prior to analysis of anion-exchanger grafted supports, the binding and elution behaviour of the unhydrolysed PTBMA grafted supports was tested. These supports had been synthesised as described in Chapter 2, by reaction of 50 mg M-PVA with 4 mg ACN and 301 μ l tBmA and without a subsequent hydrolysis step. As with unmodified supports, binding and elution on PTBMA grafted supports were not observed under any of the conditions used (figure 5.4; table 5.5).

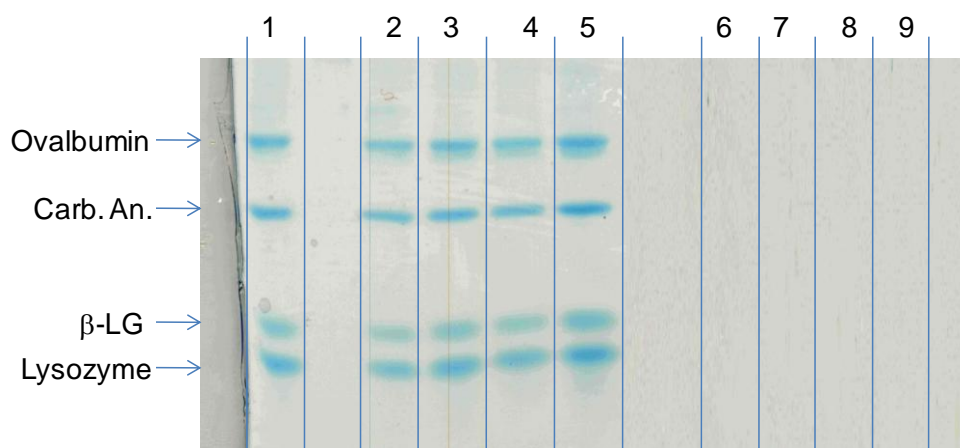


Figure 5.4. Binding of 4 protein solution on unhydrolysed PTBMA (ACN) grafted M-PVA, with salt elution. Lane 1: Challenge; lanes 2 to 5: Binding supernatants at pH 5-8; lanes 6 to 9. Elution supernatants at pH 5-8.

Table 5.5. Binding study for PTBMA grafted M-PVA with salt elution

	Unbound @				Elution @			
	pH 5	pH 6	pH 7	pH 8	pH 5	pH 6	pH 7	pH 8
OVA	101	98	97	89	0	0	0	0
CA	104	94	92	86	0	0	0	0
β LG	105	98	87	84	0	0	0	0
LYS	104	103	92	86	0	0	0	0

Band intensities showed that protein concentration in binding supernatants decreased slightly as the binding pH was increased, indicative of protein binding at higher pH. The changes were, however, consistent for all proteins in solution which suggests that the change is due to experimental error in gel loading or quantification although this was not verified. The lack of binding is further evidenced by the absence of eluted protein in the salt elution supernatants.

The hydrolysed equivalent, CE-CX, showed effective binding of lysozyme (figure 5.5; table 5.6). This demonstrates cationic binding abilities resulting from the grafted PMAA in the pH 5-8 range, as lysozyme ($pI > 10$) is positively charged at those pH values.

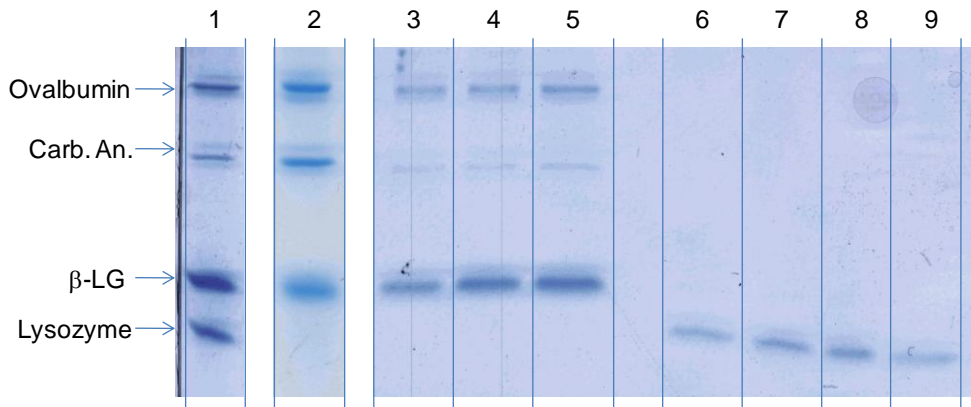


Fig 5.5 Binding of 4 protein solution on CE-CX, with salt elution. Lane 1: Challenge; lanes 2 to 5: Binding supernatants at pH 5-8; lanes 6 to 9. Elution supernatants at pH 5-8.

Table 5.6. Binding study data for CE-CX, with salt elution. Values show band intensity as a percentage of intensity seen in challenge band.

	Unbound @				Elution @			
	pH 5	pH 6	pH 7	pH 8	pH 5	pH 6	pH 7	pH 8
OVA	103	82	90	93	0	0	0	0
CA	86	36	49	83	0	0	0	0
βLG	101	71	86	89	2	0	0	0
LYS	0	0	0	0	62	72	78	75

All lysozyme present in the challenge was bound at pH 5-8, which corresponds to a cationic binding capacity of at least 25 mg/g. Elution values show that the amount of lysozyme released during the 1 M NaCl elution step is some way below 25 mg/g. This indicates that either some lysozyme is released during the wash steps before elution due to this lysozyme being weakly bound, or that some lysozyme is too strongly bound to be released during the salt elution.

For CE-CX, pH shift following protein binding at pH 5 produced no protein elution (figure. 5.6; table 5.7). Although binding supernatants show that all lysozyme is bound at pH 5, no bound lysozyme is eluted on shifting to pH 6-8. This is to be expected as it has already been demonstrated that the CE-CX have a lysozyme binding capacity of over 25 mg/ml for pH 6-8.

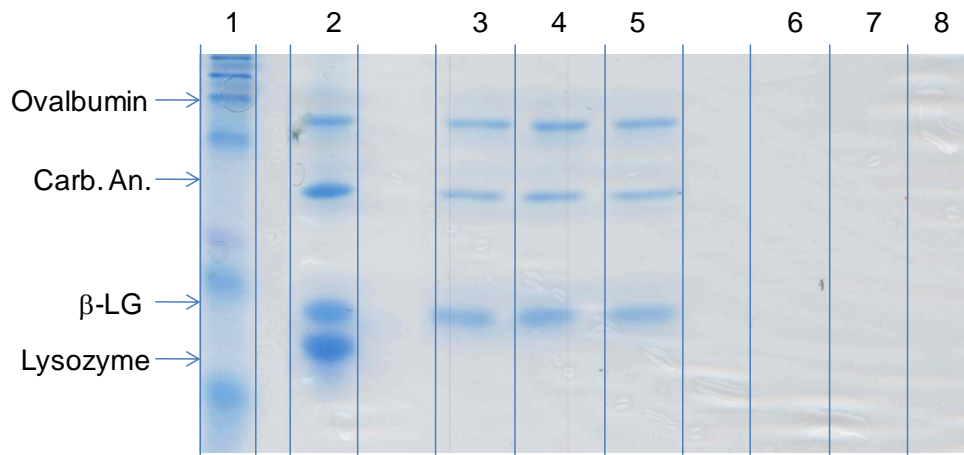


Fig 5.6. Binding of 4 protein solution on CE-CX, with pH elution. Lane 1: Marker; lane 2: Challenge; lanes 3 to 5: Binding supernatants at pH 5; lanes 7 to 9: Elution supernatants at pH 6-8.

Table 5.7. Binding study data for CE-CX, with pH elution. Values show band intensity as a percentage of intensity seen in challenge band.

	U	Elution @		
	pH 5	pH 6	pH 7	pH 8
OVA	103	0	0	0
CA	86	0	0	0
βLG	101	0	0	0
LYS	0	0	0	0

The P2VP grafted CE-AX supports showed some binding of β -lactoglobulin (β -LG) and ovalbumin at pH 5, while binding of >25 mg/g was seen for both proteins at pH 6-8 (figure. 5.7; table 5.8). No significant carbonic anhydrase or lysozyme binding was observed under these pH conditions. This agrees with the expected anionic binding properties of the grafted P2VP layer, as β -LG ($pI = 5.3$) and ovalbumin ($pI = 4.7$) are negatively charged at pH 6-8. Salt elutions show that both proteins are eluted to similar extents. As with elution from CE-CX the mass of protein eluted is lower than original mass bound, suggesting that loss during washing or retention due to strong binding is occurring.

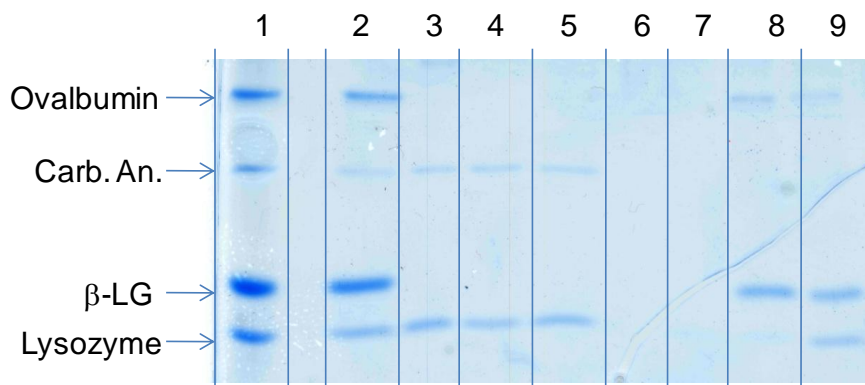


Figure 5.7. Binding of 4 protein solution on CE-AX, with salt elution.

Lane 1: Challenge; lanes 2 to 5: Binding supernatants at pH 5-8; lanes 6 to 9.

Elution supernatants at pH 5-8.

Table 5.8. Binding study data for CE-AX, with salt elution. Values show band intensity as a percentage of intensity seen in challenge band.

	Unbound @				Elution @			
	pH 5	pH 6	pH 7	pH 8	pH 5	pH 6	pH 7	pH 8
OVA	75	0	0	0	0	0	46	42
CA	74	87	84	84	0	0	0	0
β LG	92	0	0	0	0	0	55	52
LYS	95	93	87	91	0	0	0	32

For CE-AX, pH shift following protein binding at pH 8 produced varying degrees of ovalbumin elution (fig. 5.8; table 5.9). Shifting to pH 5 produced a large amount of ovalbumin elution, the mass eluted being similar to that seen during salt elution. Shifting to pH 6 or 7 resulted in comparatively little ovalbumin elution. No β -LG elution was observed following pH shift.

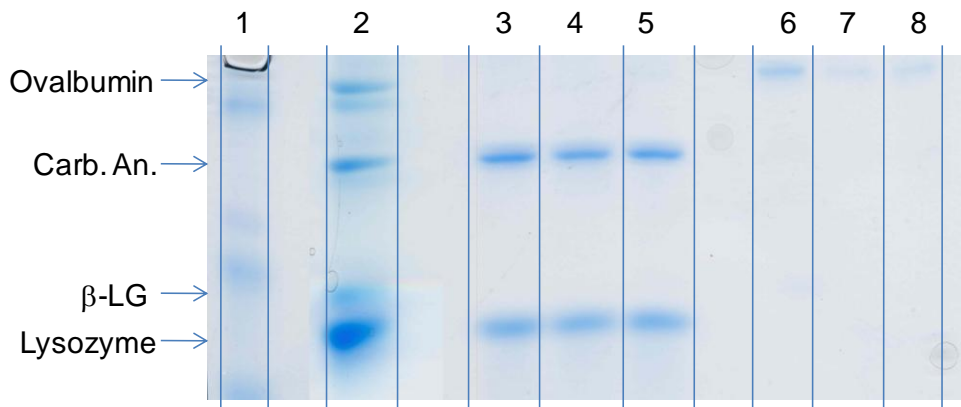


Fig. 5.8. Binding of 4 protein solution on CE-AX, with pH elution. Lane 1: Marker; lane 2: Challenge; lanes 3 to 5: Binding supernatants at pH 8; lanes 7 to 9: Elution supernatants at pH 5-7.

Table 5.9. Binding study data for CE-AX, with pH elution. Values show band intensity as a percentage of intensity seen in challenge band.

	U	Elution @		
	pH 8	pH 5	pH 6	pH 7
OVA	0	44	4	6
CA	98	0	0	0
β LG	0	0	0	0
LYS	86	0	0	0

5.3.3 Binding studies on mixed brush products from Ce(IV) initiation method

CE-MX1 showed a lysozyme binding (>25 mg/g) at pH 7-8, indicating cation binding properties at these pH values (figure. 5.9; table 5.10).

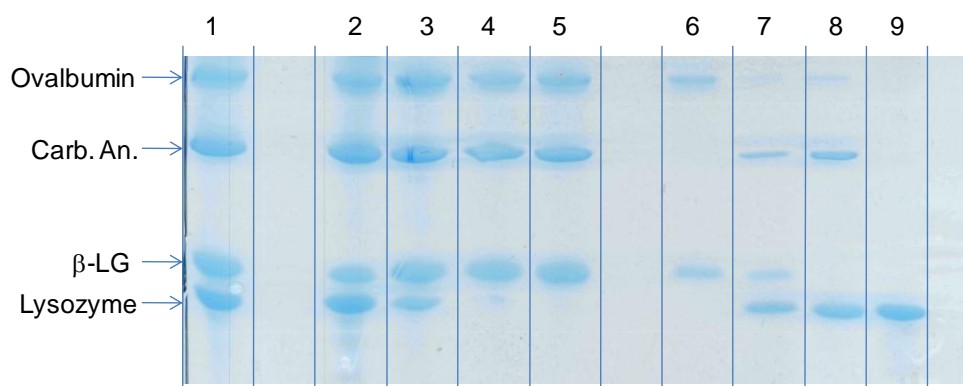


Figure 5.9. Binding of 4 protein solution on mixed brush grafted CE-MX1 with salt elution. Lane 1: Challenge; lanes 2 to 5: Binding supernatants at pH 5-8; lanes 6 to 9. Elution supernatants at pH 5-8.

Table 5.10. Binding study data for CE-MX1, with salt elution. Values show band intensity as a percentage of intensity seen in challenge band.

	Unbound @				Elution @			
	pH 5	pH 6	pH 7	pH 8	pH 5	pH 6	pH 7	pH 8
OVA	86	104	99	107	23	2	4	0
CA	94	104	96	91	0	11	23	0
β LG	63	97	94	104	29	8	0	0
LYS	108	36	0	0	0	26	72	77

Lysozyme binding was slightly lower at pH 6 and not seen for pH 5. Some binding of β -LG and ovalbumin was seen at pH 5 (anionic binding) and binding of carbonic anhydrase was measured at pH 7. For this experiment elution data is perhaps clearer. Salt elution after binding at pH 5 released a significant amount of β -LG and ovalbumin and salt elution at pH 8 released lysozyme. This indicates that CE-MX1 supports can behave as anion or cation exchangers, with the observed behaviour depending upon pH conditions. This agrees with CEX and AEX properties seen for P2VP/PAA mixed brushes in previous studies (Uhlmann et al., 2007).

At pH 6-7 all 4 proteins were observed to varying degrees in the elution supernatant. As salt elutions follow two washing steps, these results may suggest that both cation and anion exchange behaviour is present at pH 6 and 7. This is suggested because β -LG and ovalbumin are anionic species at pH 6-7, while lysozyme is cationic yet all are bound. As the cation or anion exchange properties of mixed brush grafted M-PVA should depend upon the number of charged P2VP and PMAA groups on the surface. An uneven distribution of P2VP and PMAA groups between individual supports may lead to a mix of cation and anion exchange supports being present at certain intermediate solution pH values. At lower pH values more anion exchange groups would be expected while at higher pH values more cation exchange groups would be expected, as is seen at pH 5 and 8 here respectively.

pH elution from CE-MX1 showed improved protein release compared to homopolymer grafted brushes (figure. 5.10; table 5.11). Binding at pH 5 followed by shift to pH 7-8 resulted in release of β -LG and ovalbumin. Binding at pH 8 followed by shift to pH 5-7 resulted in release of lysozyme.

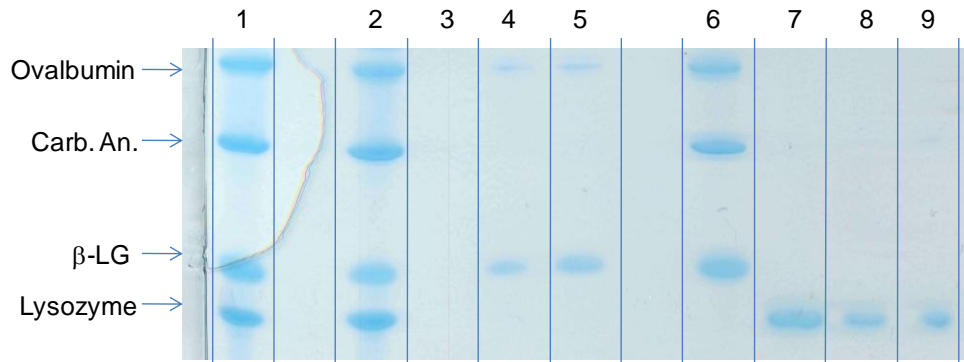


Figure 5.10. Binding of 4 protein solution on mixed CE-MX1 with pH elution. Lane 1: Challenge; lanes 2 to 5: Binding at pH 5 (lane 2), elution at pH 6-8 (lanes 3 to 5). lanes 6 to 9: Binding at pH 8 (lane 6), elution at pH 5-7 (lanes 7 to 9).

Table 5.11. Binding study data for CE-MX1, with pH elution. Values show band intensity as a percentage of intensity seen in challenge band.

	U pH 5	Elution @			U pH 8	Elution @		
		pH 6	pH 7	pH 8		pH 5	pH 6	pH 7
OVA	84	0	11	16	90	0	0	0
CA	91	0	0	2	76	0	0	4
β LG	66	0	18	28	79	0	0	0
LYS	98	0	0	0	0	68	32	23

The mass of protein eluted increased when larger pH shifts were used (shifting from pH 5 to 8 and from pH 8 to 5 released the most bound protein). This is expected as a larger pH shift moves the system further away from original binding conditions.

Within the switchable charged polymer brush model a larger pH shift would result in a larger change in electrostatic forces between polymer subunits, leading to a more pronounced switch and the potential for a greater steric push against bound proteins.

Alongside these potential steric effects, a larger shift in pH is more likely to disrupt the charge compatibility between the support surface and bound proteins. Using the example of lysozyme elution by pH shift, lysozyme is a cationic species at pH values below 11. At all experimental pHs used here lysozyme will only engage in ionic binding with cation exchangers. Lysozyme binding is seen at pH 8, indicating the presence of cation exchangers. Lysozyme binding is not seen at pH 5, which indicates the absence of cation exchangers as the conditions are otherwise the same as those at pH 8. Furthermore, the elution seen with binding at pH 8 and elution at pH 5 indicates a significant presence of positively charged groups at pH 5. The changing number of cation and anion exchangers between pH 5 and 8 can be explained as a change in the charge on the support surface. For example at pH 8 positively charged P2VP groups still exist on the mixed polymer surface but a greater number of negatively charged PMAA groups are present, resulting in an overall negative charge. Switchable behaviour is also seen for CE-MX2, with strong lysozyme binding evident at pH 6-8 and binding of ovalbumin and β -LG at pH 5 (figure 5.11; table 5.12).

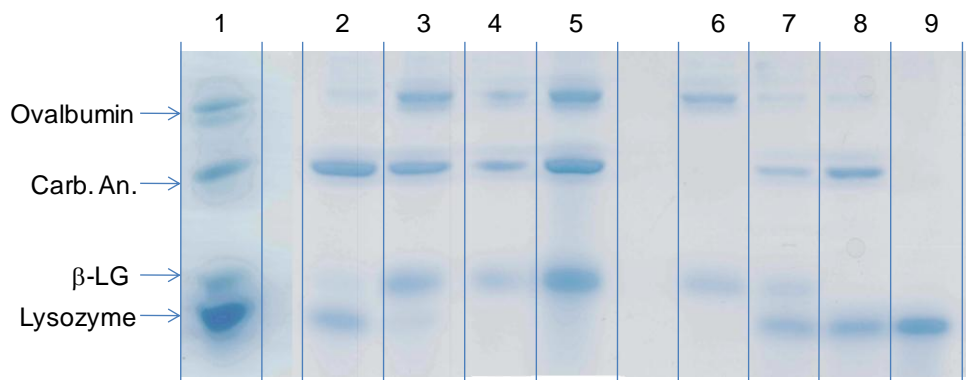


Figure 5.11. Binding of 4 protein solution on CE-MX2 with salt elution. Lane 1: Challenge; lanes 2 to 5: Binding supernatants at pH 5-8; lanes 6 to 9. Elution supernatants at pH 5-8.

Table 5.12. Binding study data for CE-MX2, with salt elution. Values show band intensity as a percentage of intensity seen in challenge band.

	Unbound @				Elution @			
	pH 5	pH 6	pH 7	pH 8	pH 5	pH 6	pH 7	pH 8
OVA	10	82	71	101	74	17	12	0
CA	106	69	38	112	0	33	59	0
β LG	7	86	36	97	57	25	0	0
LYS	59	30	0	0	0	53	68	86

pH elution from CE-MX2 shows elution of lysozyme following pH shift from 8 to 5-7 (figure 5.12; table 5.13). This behaviour is similar to CE-MX1.

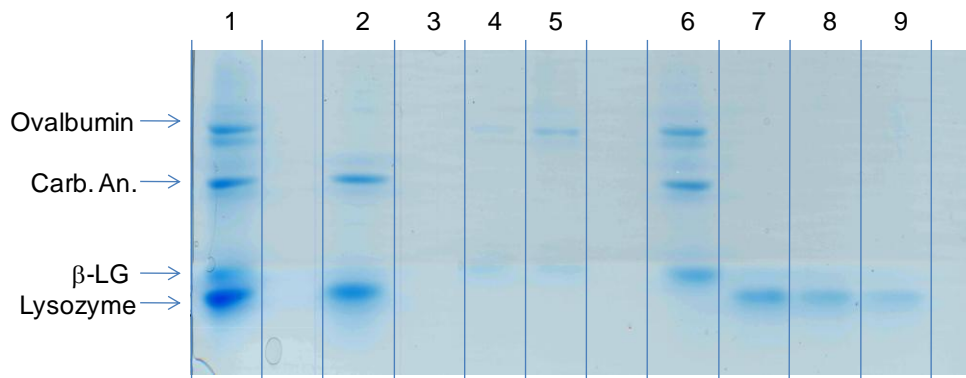


Fig 5.12. Binding of 4 protein solution on CE-MX2 with pH elution. Lane 1: Challenge; lanes 2 to 5: Binding at pH 5 (lane 2), elution at pH 6-8 (lanes 3 to 5); lanes 6 to 9: Binding at pH 8 (lane 6), elution at pH 5-7 (lanes 7 to 9).

Table 5.13. Binding study data for CE-MX2, with pH elution. Values show band intensity as a percentage of intensity seen in challenge band.

	U pH 5	Elution @			U pH 8	Elution @		
		pH 6	pH 7	pH 8		pH 5	pH 6	pH 7
OVA	0	0	5	14	98	0	0	0
CA	96	0	0	0	99	0	0	0
β LG	0	0	3	7	105	0	0	0
LYS	98	0	0	0	0	73	35	28

Both mixed brush supports grafted by ACN show similar behaviour. Binding of lysozyme is effective at higher pH although elution of the bound lysozyme is not complete. At pH 7-8 complete binding of lysozyme is observed, with a larger mass of lysozyme being salt eluted from the support bound at pH 8. This is unexpected as the binding supernatants indicate that the same amount of lysozyme was bound at pH 7 and 8. In this case less elution would be expected at pH 8 due to a higher negative charge on the support surface. Binding behaviour of β -LG and ovalbumin to CE-MX2 differs to that seen with CE-MX1. Binding of these proteins to CE-MX2 at pH 5 appears to be stronger than binding to CE-MX1 although the final eluted amounts are similar.

CE-MX1 and CE-MX2 both display cation and anion binding properties under suitable conditions, indicating the presence of a polyelectrolyte brush layer with a 'switchable' net charge. CE-MX2 in particular displays the ability to bind > 25 mg lysozyme at pH 8 and to bind > 25 mg of both ovalbumin and β -lactoglobulin at pH 5, indicating switchable behavior which sees it act as an anion exchanger at lower pH values and cation exchanger at higher values. In terms of mass eluted, pH elution of lysozyme appears more successful than the equivalent elution of acidic proteins. One explanation for this phenomenon is the stricter brush behaviour expected from the grafted P2VP chains, as $2R_{f/D}$ values for the P2VP phase in CE-MX1/CE-MX2 are higher than those for the PMAA phase. Higher $2R_{f/D}$ values relate to more

pronounced brush behaviour with higher forces involved in brush extension etc. The higher level of brush behaviour expected for grafted P2VP in CE-MX1/CE-MX2 may translate to a great steric 'push' behind the elution of lysozyme when pH is decreased.

5.3.4 Binding studies on mixed brush products from tresyl activation method

TR-MX1 showed some binding of lysozyme at pH 6-8 with the highest binding at pH 8. No other binding was seen, however, the salt elutions which followed binding at pH 6-7 released some carbonic anhydrase. Salt elution also released lysozyme from products bound at pH 6-8 (figure 5.13; table 5.14).

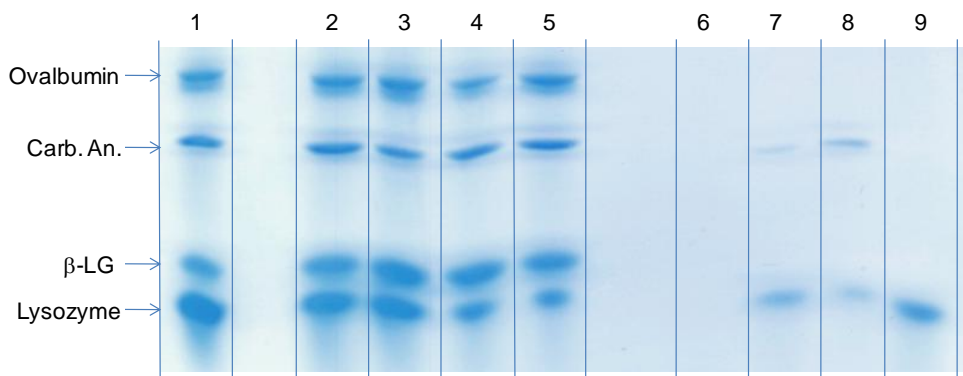


Figure 5.13. Binding of 4 protein solution on TR-MX1, with salt elution. Lane 1: Challenge; Lanes 2 to 5: Binding supernatants at pH 5-8; Lanes 6 to 9. Elution supernatants at pH 5-8.

Table 5.14. Binding study data for TR-MX1, with salt elution. Values show band intensity as a percentage of intensity seen in challenge band.

	Unbound @				Elution @			
	pH 5	pH 6	pH 7	pH 8	pH 5	pH 6	pH 7	pH 8
OVA	96	108	80	112	0	0	0	0
CA	109	93	101	101	0	7	13	0
β LG	97	107	102	94	0	0	0	0
LYS	96	89	50	39	0	19	14	43

Binding at pH 5 followed by switch to pH 6-8 resulted in no protein elution (figure 5.14; table 5.15). Binding at pH 8 followed by switch to pH 5-7 resulted in lysozyme elution at pH 5 and 6. This data shows only cation binding, with no anion binding behaviour demonstrated over the pH 5-8 range.

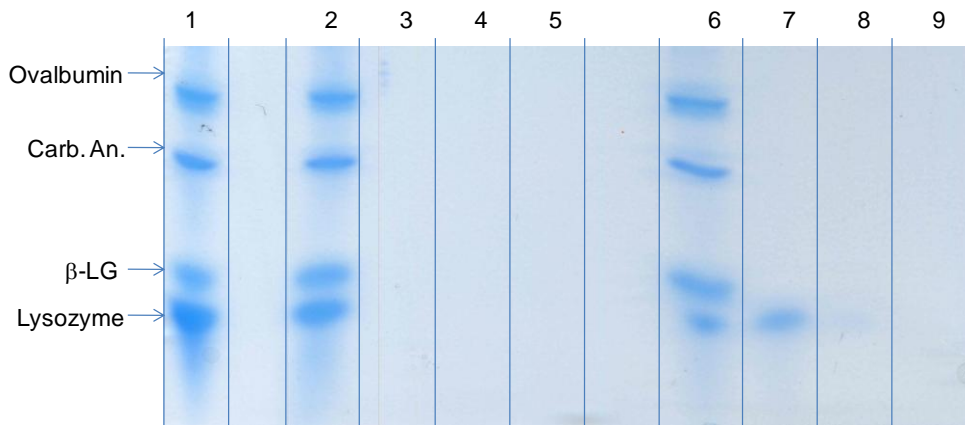


Fig 5.14. Binding of 4 protein solution on TR-MX1 with pH elution. Lane 1: Challenge; lanes 2 to 5: Binding at pH 5 (lane 2), elution at pH 6-8 (lanes 3 to 5); lanes 6 to 9: Binding at pH 8 (lane 6), elution at pH 5-7 (lanes 7 to 9).

Table 5.15. Binding study data for TR-MX1 with pH elution. Values show band intensity as a percentage of intensity seen in challenge band.

	U	Elution @			U	Elution @		
	pH 5	pH 6	pH 7	pH 8	pH 8	pH 5	pH 6	pH 7
OVA	89	0	0	0	103	0	0	0
CA	97	0	0	0	93	0	0	0
β LG	89	0	0	0	99	0	0	0
LYS	95	0	0	0	35	33	6	0

TR-MX1 showed binding of β -LG and ovalbumin for pH 5-7, with some ovalbumin also being bound at pH 8. Lysozyme binding occurred at pH 8. No other binding was seen. Salt elution released β -LG and ovalbumin at pH 5-7 and lysozyme at pH 8.

Binding to TR-MX2 indicated weaker lysozyme binding behaviour than had been observed with the other mixed brush supports (figure 5.15; table 5.16). Binding of β -LG and ovalbumin is seen at pH 5 and 6, with some binding of ovalbumin also seen at pH 7 and 8.

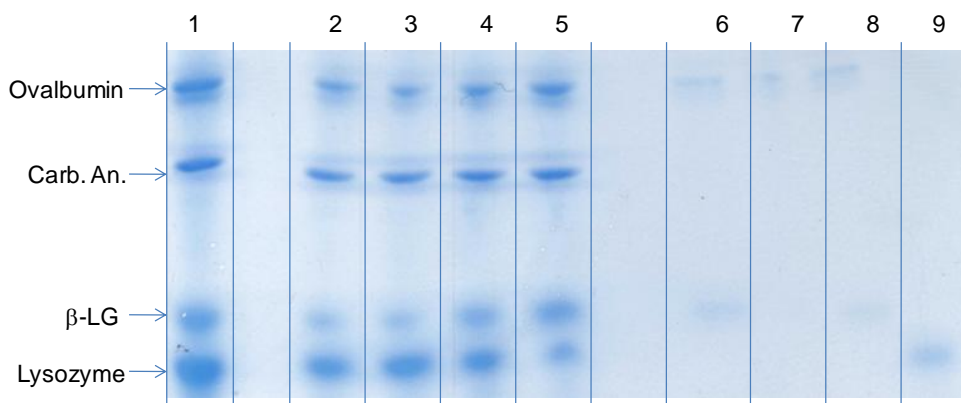


Figure 5.15. Binding of 4 protein solution on TR-MX2 with salt elution. Lane 1: Challenge; Lanes 2 to 5: Binding supernatants at pH 5-8; Lanes 6 to 9. Elution supernatants at pH 5-8.

Table 5.16. Binding study data for TR-MX2 with salt elution. Values show band intensity as a percentage of intensity seen in challenge band.

	Unbound @				Elution @			
	pH 5	pH 6	pH 7	pH 8	pH 5	pH 6	pH 7	pH 8
OVA	46	36	59	78	9	6	4	0
CA	89	93	88	86	0	0	0	0
βLG	42	45	85	104	19	3	7	0
LYS	99	107	81	43	0	0	0	35

The amount of P2VP grafted to the TR-MX2 surface (2.54 mmol P2VP per g M-PVA) is higher than the amount of PMAA present (1.50 mmol PMAA per g m-PVA). This may explain the appearance of anion binding behaviour on the TR-MX2 surface.

Binding at pH 5 followed by a shift to pH 6-8 produced elution of β-LG and ovalbumin at pH 8 (figure 5.16; table 5.17). The amount eluted with this pH shift was similar to

the amount released during salt elution. Binding at pH 8 followed by a shift to pH 5-7 gave elution of lysozyme for all three pH values.

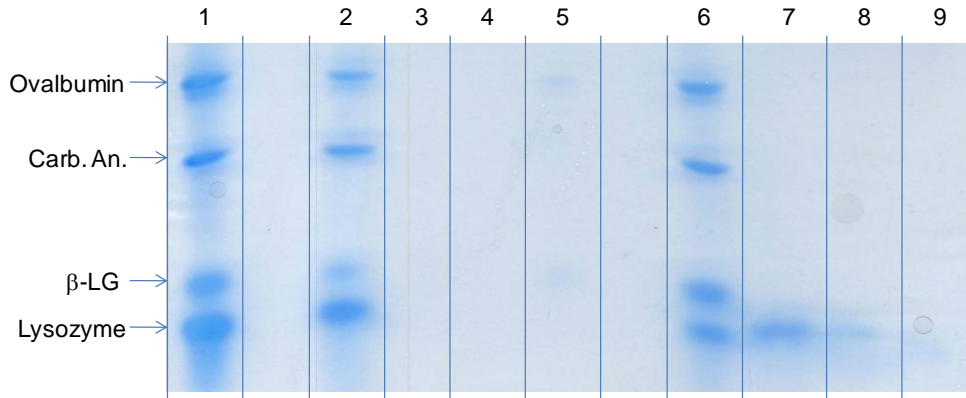


Figure 5.16. Binding of 4 protein solution on TR-MX2 with pH elution. Lane 1: Challenge; Lanes 2 to 5: Binding at pH 5 (lane 2), elution at pH 6-8 (lanes 3 to 5); Lanes 6 to 9: Binding at pH 8 (lane 6), elution at pH 5-7 (lanes 7 to 9).

Table 5.17. Binding study data for TR-MX2 with pH elution. Values show band intensity as a percentage of intensity seen in challenge band.

	U pH 5	Elution @			U pH 8	Elution @		
		pH 6	pH 7	pH 8		pH 5	pH 6	pH 7
OVA	44	0	0	8	68	0	0	0
CA	90	0	0	0	85	0	0	0
βLG	52	0	0	13	107	0	0	0
LYS	99	0	0	0	40	35	15	9

The lack of anion binding behaviour in TR-MX1, when compared to the presence of anion binding in TR-MX2, appears to come from the lower proportion of P2VP and higher proportion of PMAA on the TR-MX1 surface. TR-MX1 contains 1.35 mmol P2VP and 1.81 mmol PMAA per g m-PVA. This indicates a prevalence of PMAA groups at the surface. TR-MX2, on the other hand, has a prevalence of P2VP with

2.54 mmol P2VP compared to 1.50 mmol PMAA per g M-PVA. This higher proportion of P2VP may allow TR-MX2 to participate in anion exchange behavior.

5.3.5 Binding studies on mixed brush products from ATRP method

AT-MX1 showed binding of ovalbumin and β -LG at lower pH values and binding of lysozyme at higher pH, indicating that AT-MX1 possesses switchable binding properties (figure 5.17; table 5.18).

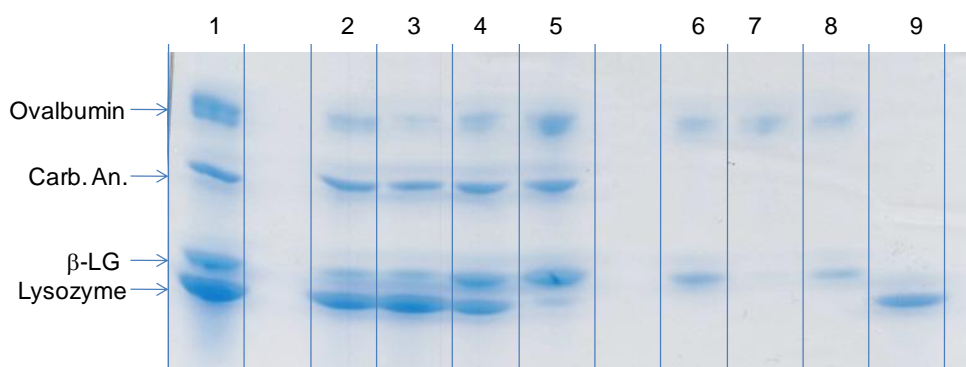


Fig 5.17. Binding of 4 protein solution on AT-MX1 with salt elution. Lane 1: Challenge; lanes 2 to 5: Binding supernatants at pH 5-8; lanes 6 to 9. Elution supernatants at pH 5-8.

Table 5.18. Binding study data for AT-MX1, with salt elution. Values show band intensity as a percentage of intensity seen in challenge band.

	Unbound @				Elution @			
	pH 5	pH 6	pH 7	pH 8	pH 5	pH 6	pH 7	pH 8
OVA	30	13	59	90	27	19	15	0
CA	92	85	94	110	0	0	0	0
β LG	52	41	91	98	4	0	2	0
LYS	95	72	17	0	0	0	0	46

Maximum ovalbumin and β -LG binding was seen at pH 6. Lysozyme binding was seen at pH 7-8 with some binding at pH 6. Salt eluted masses were considerably smaller than those expected from the binding values. This effect was larger than was seen for ACN grafted supports. pH elution from AT-MX1 showed some elution of ovalbumin and β -LG following binding at pH 5 and shift to pH 8 (figure 5.18; table 5.19). No elution was seen on shifting to pH 6 or 7. This is as expected, as the cationic binding properties expected at pH 8 are unsuitable for binding the anionic ovalbumin and β -LG groups. Binding at pH 8 followed by pH shift to pH 5-7 resulted in released of lysozyme at all three elution pH values, with the most protein eluted after shifting to pH 5. This result is also as expected.

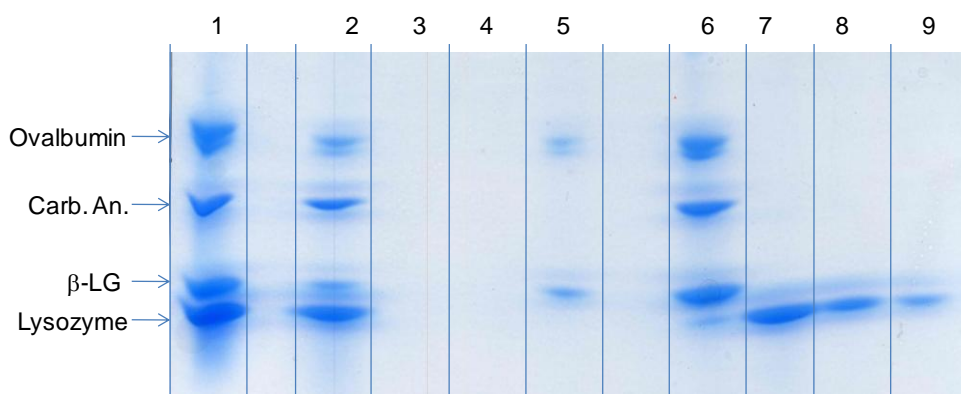


Figure 5.18. Binding of 4 protein solution on AT-MX1 with pH elution. Lane 1: Challenge; lanes 2 to 5: Binding at pH 5 (lane 2), elution at pH 6-8 (lanes 3 to 5); lanes 6 to 9: Binding at pH 8 (lane 6), elution at pH 5-7 (lanes 7 to 9).

Table 5.19. Binding study data for AT-MX1, with pH elution. Values show band intensity as a percentage of intensity seen in challenge band.

	U	Elution @			U	Elution @		
	pH 5	pH 6	pH 7	pH 8	pH 8	pH 5	pH 6	pH 7
OVA	55	0	0	9	99	0	0	0
CA	93	0	0	0	109	0	0	0
β LG	54	0	0	12	84	0	0	0
LYS	94	0	0	0	5	46	19	8

AT-MX1 showed binding of lysozyme at pH 7-8 with some binding at pH 6 (fig 5.19; table 5.20). Binding of ovalbumin and β -LG was not seen at any pH value. Salt elution showed release of lysozyme from supports bound at pH 6-8 and elution of small amount of carbonic anhydrase at pH 6-7.

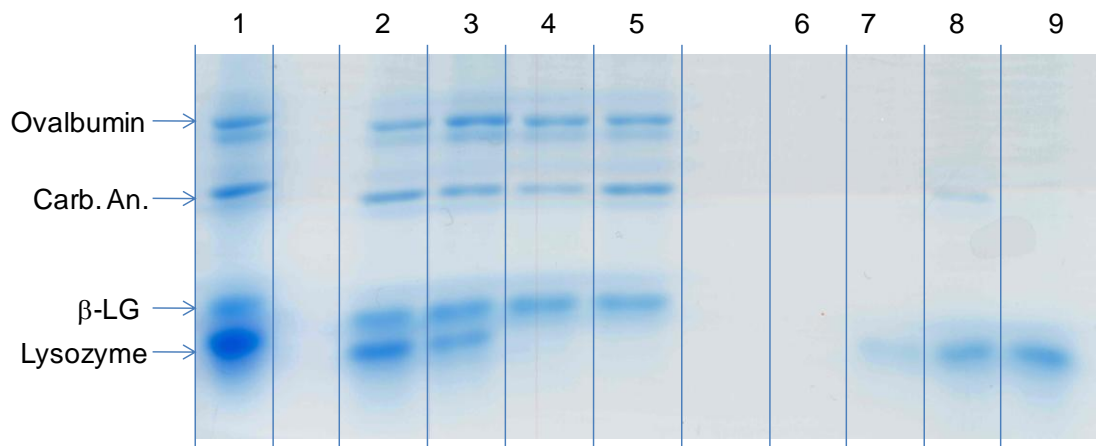


Figure 5.19. Binding of 4 protein solution on AT-MX2 with salt elution. Lane 1: Challenge; lanes 2 to 5: Binding supernatants at pH 5-8; lanes 6 to 9. Elution supernatants at pH 5-8.

Table 5.20. Binding study data for AT-MX2, with salt elution. Values show band intensity as a percentage of intensity seen in challenge band.

	Unbound @				Elution @			
	pH 5	pH 6	pH 7	pH 8	pH 5	pH 6	pH 7	pH 8
OVA	87	98	29	78	0	0	0	0
CA	111	113	54	107	0	0	8	0
β LG	105	95	87	82	0	0	0	0
LYS	103	67	0	0	0	30	41	64

Protein binding at pH 5 followed by shifting to pH 6-8 produced no elution (figure 5.20; table 5.21). Binding at pH 8 followed by shifting to pH 5-7 produced elution of lysozyme at pH 5-6, with more lysozyme eluted at pH 5. These results suggest that AT-MX2 is a cation exchanger at pH 6-8 and is neither a cation or anion exchanger at pH 5.

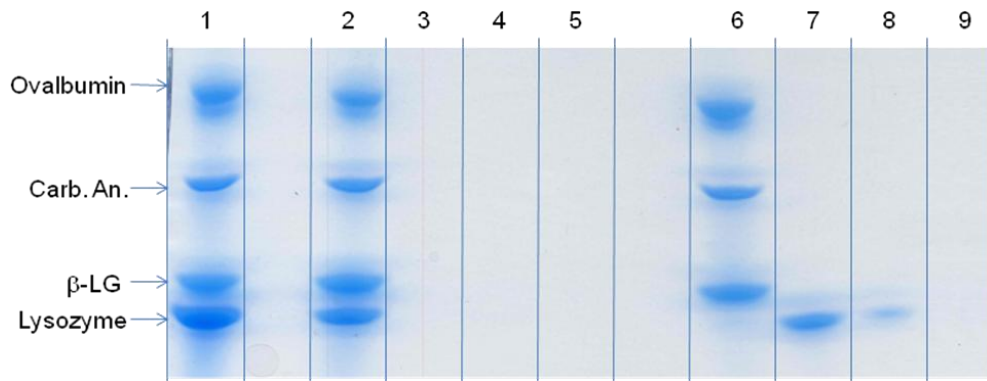


Figure 5.20. Binding of 4 protein solution on mixed AT-MX2 with pH elution. Lane 1: Challenge; lanes 2 to 5: Binding at pH 5 (lane 2), elution at pH 6-8 (lanes 3 to 5); lanes 6 to 9: Binding at pH 8 (lane 6), elution at pH 5-7 (lanes 7 to 9).

Table 5.21. Binding study data for AT-MX2, with pH elution. Values show band intensity as a percentage of intensity seen in challenge band.

	U	Elution @			U	Elution @		
	pH 5	pH 6	pH 7	pH 8	pH 8	pH 5	pH 6	pH 7
OVA	92	0	0	0	97	0	0	0
CA	102	0	0	0	98	0	0	0
β LG	94	0	0	0	100	0	0	0
LYS	91	0	0	0	6	31	13	0

The switchable binding behaviour displayed by AT-MX1 can be compared with the lack of anion binding behaviour seen in AT-MX2. This may be expected from the relative amounts of P2VP and PMAA on each support. AT-MX1 has 3.84 mmol of P2VP and 3.40 mmol PMAA grafted per g M-PVA, which gives a slight prevalence of P2VP on the surface. In contrast, AT-MX2 has 2.67 mmol P2VP and 4.03 mmol PMAA per g M-PVA. The higher proportion of PMAA on AT-MX2 predisposes it to cation binding behavior, whereas the more balanced proportion of P2VP and PMAA on the AT-MX1 surfaces appears to allow it to behave as either a cation or anion exchanger.

5.3.6 Summary of binding data for supports modified with Ce(IV), ATRP and tresyl grafted methods

The results described in this chapter indicate that synthetic procedures carried out during Chapter 2-4 have produced mixed polyelectrolyte grafted supports capable of switchable mixed charge brush behaviour. Although all mixed polyelectrolyte brushes used in this chapter possess a combination of basic and acidic proteins capable of anion and cation binding respectively some supports, namely TR-MX1 and AT-MX2, did not display significant anion binding behaviour (Table 5.22). It is

worth noting that these two supports have a low amount of P2VP grafted compared to PMAA, and it is P2VP which is responsible for anion binding behaviour in the supports. By comparison, support TR-MX2 has a low amount of PMAA grafted compared to P2VP but displays cation binding behaviour at pH 8. Under the conditions used, these results indicate a general bias towards cation binding behaviour for the P2VP/PMAA mixed brush system. Higher $2R_f/D$ values for the P2VP brush components also favour pH elution of bound anions. This is evidenced by the comparatively high mass of lysozyme eluted during pH elutions on mixed brushes. pH elutions of bound cations (ovalbumin and β -LG) were typically less effective. This may result from a weaker steric push from the PMAA brush components, which showed lower $2R_f/D$ values compared to P2VP components and are thus expected to show weaker brush behaviour.

Table 5.22. Summary of observed binding behaviours in M-PVA beads. Switchable charge behaviour is noted for those beads which possess both cation and anion binding modes.

Support	Anion binding	Cation binding	Switchable?
Unmodified M-PVA	No	No	No
TBMA grafted M-PVA	No	No	No
CE-AX	Yes	No	No
CE-CX	No	Yes	No
CE-MX1	Yes	Yes	Yes
CE-MX2	Yes	Yes	Yes
TR-MX1	No	Yes	No
TR-MX2	Yes	Yes	Yes
AT-MX1	Yes	Yes	Yes
AT-MX2	No	Yes	No

Ce(IV) grafted mixed brushes display a superior lysozyme binding ability, which may be expected due to the higher amounts of PMAA grafted on these supports (6.11 mmol PMAA per g M-PVA for CE-MX2). Although Ce(IV) grafted supports also have

comparatively large amounts of P2VP grafted, this does not lead to significantly improved ovalbumin or β -LG binding behaviour.

Mixed brushes grafted using ATRP and tresyl activation methods also display lysozyme binding behaviour, with ATRP grafted products binding more lysozyme than tresyl products at pH 6-8. This is as expected, as the ATRP products contain considerably more PMAA groups per g of M-PVA (3.40 mmol for AT-MX1 compared to 1.81 mmol for TR-MX1). The presence of a higher number of cation-binding groups in ATRP supports predictably leads to better cation binding behaviour. The higher binding capacities of Ce(IV) and ATRP grafted supports may also be due to the shorter chain lengths (see $n(\text{poly})/n(\text{init})$ values in table 5.2 and figure 5.21) of polymers grafted using these methods compared to those added during tresyl graft-to synthesis.

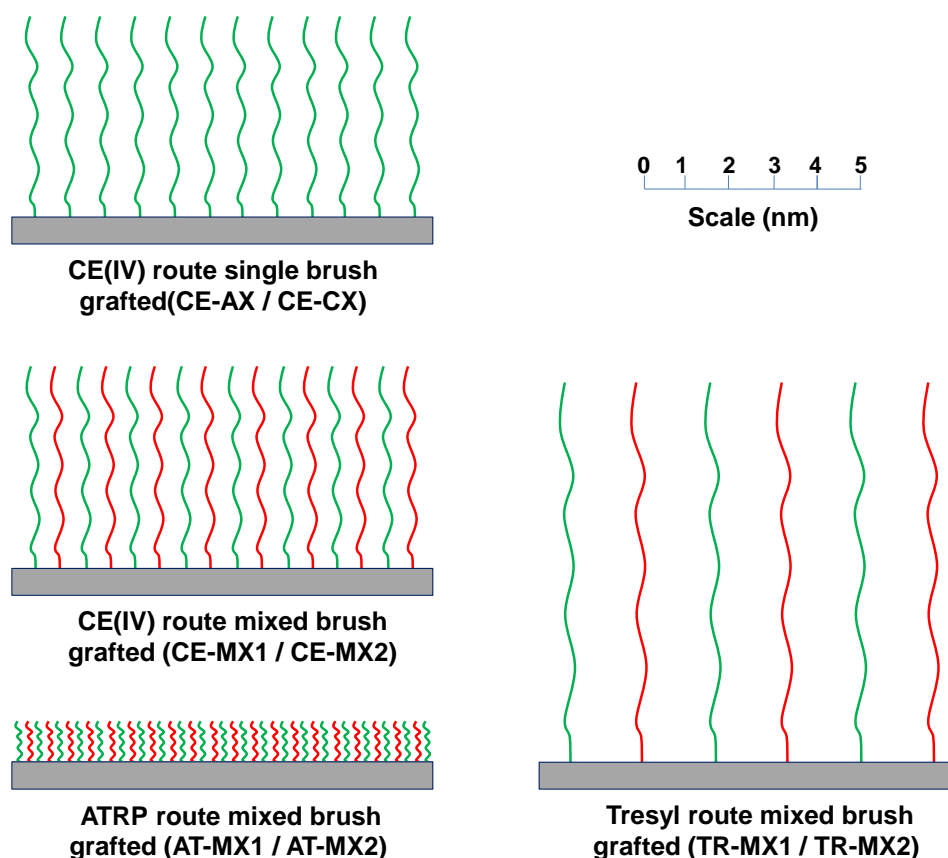


Figure 5.21. A single-scale representation of the relative brush densities and heights expected for supports used in chapter 5, based upon tabulated D and $n(\text{poly})/n(\text{init})$ values. The extended chain structure here is not accurate, but is used to clearly show chain lengths and intergraft distances.

The tresyl graft-to method produced graft polymers which are up to 50 times longer than those produced by the ATRP method. Intergraft spacing for tresyl route products is around 10 times higher than for ATRP route products. The longer, more widely spaced polymer brushes created by the tresyl method will have a lower maximum charge density than the denser brushes created using ATRP. According to Coulomb's law (see equation 1.14) the force experienced between charged diminishes as the distance between charges increases. Hence, proteins which sit at the ATRP brush surface are expected to experience a larger proportion of the brush's overall charge than proteins at the tresyl brush surface due to this difference in charge density and the associated distances between surface-bound proteins and charged units within the brush.

Comparison of pH elution abilities between brushes indicates that pH elution is more effective in Ce(IV) route products. Comparison between tresyl and ATRP route products shows little difference in pH elution results, in terms of mass of protein eluted. Considering that binding is more effective in ATRP products, with more protein bound, this suggests that the tresyl route products have superior pH elution properties. This superior elution ability may stem from the much longer chain lengths (see $n(\text{poly})/n(\text{init})$ values in table 5.2) of tresyl products), leading to more a pronounced 'switch' in brush height/composition/surface-charge when the pH is altered, resulting in more effective protein elution.

In relation to the effects of brush expansion as it relates to pH elution it should also be noted that although ellipsometric studies of P2VP/PAA mixed brushes have shown significant changes in the heights of brush components on switching between extreme pH values, at pH values closer to neutral the brush arrangements are more complicated. Hinrichs et al. (2009) identified a variety of distinct structures for P2VP/PAA mixed brushes (figure 5.22), the behavior of which are expected to be similar to that of the P2VP/PMAA mixed brush system used in this study. In the P2VP/PAA system it was found that at pH 2 an ionized, extended P2VP phase existed alongside collapsed PAA chains. At pH 10 the reverse was true, with negatively charged PAA extending from the surface above uncharged P2VP chains. At intermediate pH values these extensions were less pronounced and of most

interest. At pH 5 a 'mixed' phase was seen where the bottom part of the P2VP/PAA brush is rich in both P2VP and PAA, while the top part contains P2VP and water from the aqueous buffer. At pH 7 a similar 'mixed' phase structure is seen, with a P2VP/PAA phase at the bottom of the brush and PAA and water at the top. At pH 6 the brush exists as a uniform 'complex' phase of both P2VP and PAA and it is at this pH that the brush has its lowest net charge.

Between pH 5 and 7 the brush height remains largely unchanged (in Hinrich et al. 2009 the brush height at pH 5-7 is identified as 11 nm, compared to 23 nm at pH 2 and pH 10). In terms of creating a physical 'push' during the elution stage this lack of height change may limit elution efficiency, although a change in brush height does occur for the two individual polymer species between pH 5 and 7. The same relationship between brush structure and pH may be expected for the P2VP/PMAA system, albeit with slightly different pH values for the structures described.

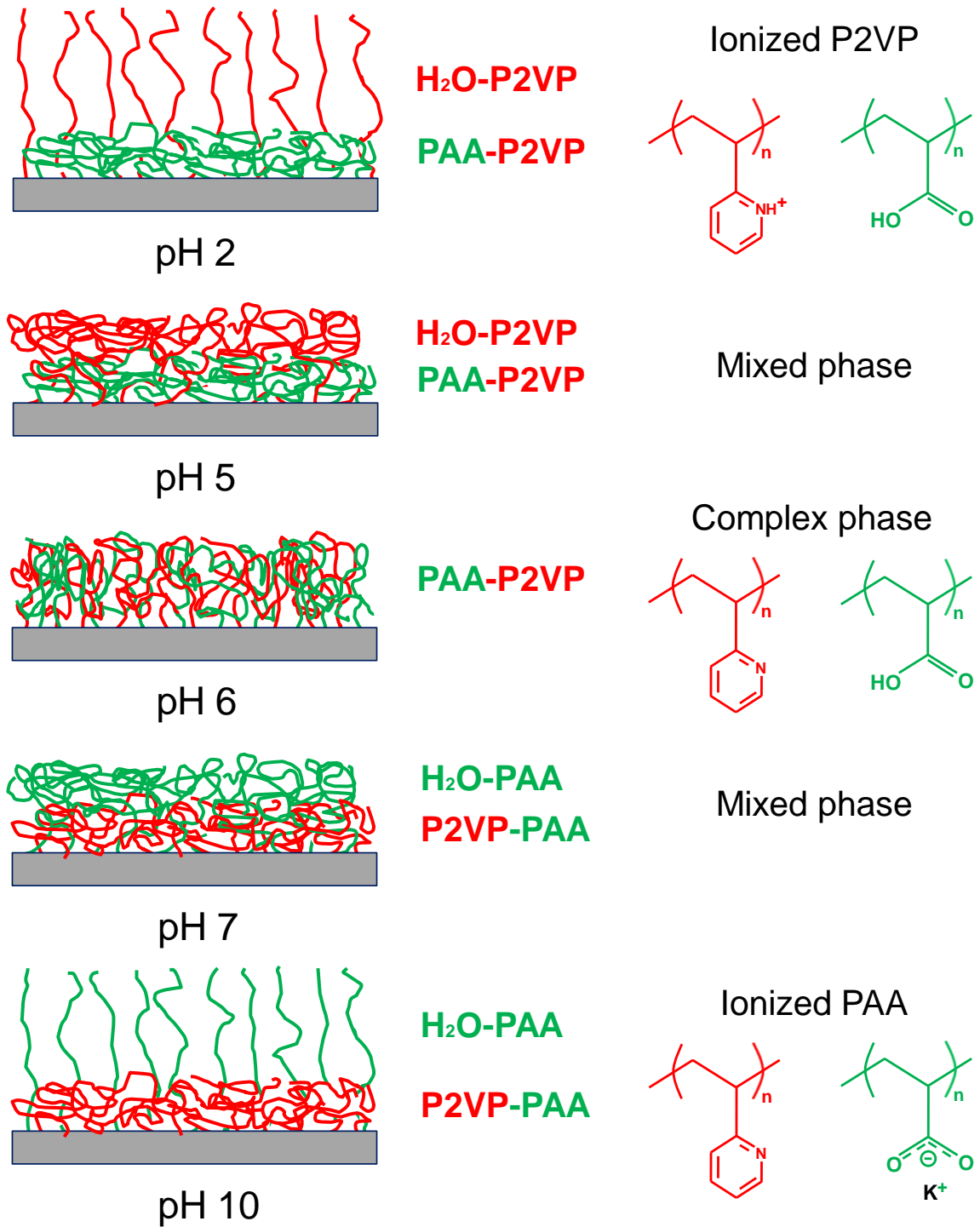


Figure 5.22. Structures of P2VP/PAA brush, including ‘Mixed’ phases at pH 5 and 7 and ‘complex’ phase at pH 6 (after Hinrichs et al. 2009).

5.4 Conclusions

Ce(IV), tresyl and ATRP (Chapters 2-4) led grafting of P2VP and PMAA onto M-PVA supports are all suitable for producing products capable of binding proteins by charge interactions. PMAA grafted M-PVA and P2VP grafted M-PVA show greater cationic and anionic binding properties respectively than supports grafted with mixed polymer brushes, but the presence of two polymer species at the M-PVA surface leads to switchable charge properties. These switchable properties were evidenced by binding studies which show acidic proteins binding to the support at lower pH values and basic proteins binding to the same support at higher pH values. The results indicate that the support switches between anion and cation binding behavior as the pH is altered. pH elution studies support this switchable charge model, and also give some support to the idea of polymer chains pushing proteins from the surface as they extend.

6 Conclusions and future work

The growth of chargeable polymer species from the surface of M-PVA (polyvinyl alcohol-magnetite composite) particles via Ce(IV) or ATRP led polymerization and the ability of amine terminated polymers to graft onto the surfaces of sulfonyl ester or alkyl bromide activated M-PVA particles were demonstrated in this study.

These techniques were successfully applied in the synthesis of homopolymer and heteropolymer/mixed polyelectrolyte brush layers on M-PVA supports. The ability of mixed polyelectrolyte surfaces to switch between cation and anion binding modes was comprehensively demonstrated in bind-elute experiments with models mixtures of acidic, neutral and basic proteins. The switchable behavior of the mixed polyelectrolyte brush surfaces allowed elution based on change in pH. The charge effects behind pH elution were possibly enhanced by physical brush expansion behaviour of the mixed polyelectrolyte surface, whose dimensions lay within those needed for brush behaviour.

The findings of this project may be furthered by comparative studies of ion exchange capacities and binding behaviour for single brush vs. mixed brush grafted supports and the economic relevance of producing mixed brush modified supports for large scale work. This includes application of the grafting techniques to other support types, especially chromatography supports.

Study of the properties of supports modified with single brush surfaces vs. those modified with mixed brush surfaces can indicate the value of the extra cost involved in a second grafting stage. In the case of "graft to" techniques, the grafting of a second polymer typically requires a large excess of polymer, making this stage considerably more costly than the first graft. For "graft from" techniques a second graft stage does not require such an excess of grafting reagent to achieve a balance mixed brush grafting, so in terms of processing cost the second graft stage may be similar to the first. In both cases additional graft stages adds extra cost to the support manufacturing process.

These extra costs may be weighed against the improvement seen in processing ability when using a mixed brush modified support for protein separations. Although mixed brush supports may present certain advantages vis a vis pH based elution, these advantages might be offset by a potential loss in achievable protein binding capacities. For example, a mixed brush PMAA/P2VP grafted support operating as a cation exchanger at pH 8 may be expected to have a lowered cation binding capacity due to presence of P2VP alongside the cation-exchanging PMAA chains. Some of this effect may be due to the presence of positively charged P2VP sideunits, which weaken the overall negative charge desired at a cation binding surface. In terms of binding capacity, the more important issue may be that grafting of P2VP alongside PMAA requires the sacrifice of surface sites which could instead be used to graft more PMAA. In the context of cation exchange behaviour grafting less PMAA would be expected to result in lower binding capacity. The use of mixed brushes thus can be predicted to impose certain limitations on the binding capacity of supports compared to the analogous binding on single brush modified supports. Clearly further studies on binding capacity and specificity of mixed brush vs. single species ion exchangers is required.

In order to compare the extra expense and capacity limitations expected for mixed brush supports with the benefits of using these supports, further research into comparative binding properties would be necessary. Other studies which would give useful information about the economics of single and mixed brush products are repeated bind and elute studies, with measurement of the binding/elution properties of beads following successive bind and elute steps. The magnetic susceptibility of supports following grafting and binding/elution can also be measured. By combining bind/elute and magnetic data for supports the lifetime of these supports, and hence their value, can be predicted. Additionally, the value of enhanced pH elutions seen in mixed brushes may be tested by further comparison with other elution methods (e.g. temperature elutions) and different combinations of proteins in the binding mixture.

In terms of translating the finding of this study to industry, another area of interest would be the modification of chromatography beads using the grafting techniques described. Chromatography beads are typically porous in structure, with a primary

concern being difficulty with elution and fouling due to weak fluid movement within the pore network. The grafting of polyelectrolyte brushes on chromatography support surfaces may be used as an aid in elution/cleaning processes. One avenue of research could be the use of single brush basic or acidic polymers within cation or exchange matrices respectively, using physical expansion properties of the polymer brush at low or high pH to force trapped species out of the support.

Of the specific grafting techniques employed in this work, the Ce(IV) graft from initiation described in Chapter 2 appears most suitable for future modifications of supports for protein recovery as it has produced the highest grafting yields. These translate to improved binding capacities (see Chapter 5) and it would also be expected that Ce(IV) grafting is the cheapest grafting method of those studied, requiring only one reaction step before quenching/washing and utilizing comparatively cheap materials for the grafting reactions.

7. Appendix

7.1 Testing hydrolysis of PTBMA chains

7.1.1 Background

Poly(*tert*-Butyl methacrylate) (PTBMA) is a protected form of poly(methacrylic acid) (PMAA). Reactions between the acidic MAA/PMAA groups and 2-vinyl pyridine groups are predicted during grafting reactions. In order to avoid these acid-base reactions syntheses were devised which allowed the grafting of PTBMA and poly(2-vinyl pyridine) (P2VP) brushes followed by acid hydrolysis or saponification (Clayden et al., 2001) of grafted PTBMA to produce a PMAA brush (figure 7.1).

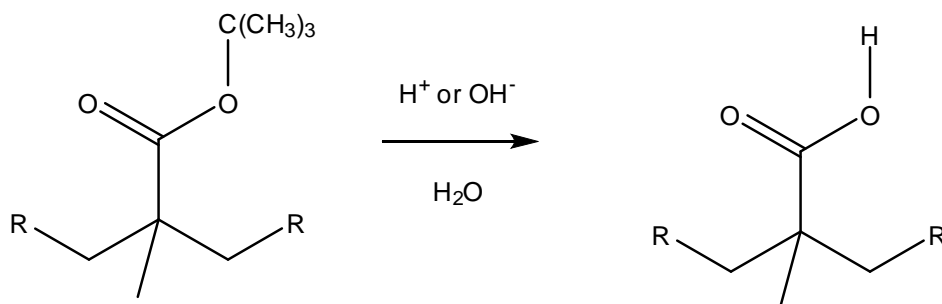


Figure 7.1 Hydrolysis/saponification of *t*-butyl ester side group to give carboxylic acid.

Conversion of *t*-butyl ester side-groups has been previously demonstrated for free polymers (Melenevskaya, 1993) and polymer brush layers (Houbenov, 2003) but had not been shown for polymers grafted onto small particles. Experimentation to identify and demonstrate the conversion of *t*-butyl groups to carboxylic acid groups was necessary.

7.1.2 Method

A series of hydrolysis/saponification reactions were performed and analysed using FTIR to find the best conditions for removal of ester sidegroups. PTBMA grafted supports (5 mg) were suspended in hydrolysis/saponification solution and mixed with heating (1 ml, 1 h, 60°C). The mixtures were then allowed to cool to RT and the supernatant was removed. Supports were washed with water (1 ml, x3), dried and

analysed using FTIR. Conversion was observed by disappearance of peaks associated with the t-butyl group.

7.1.3 Results

Hydrolysis reactions were attempted using p-toluenesulfonic acid (Houbenov et al., 2003; Bruening et al., 1997) and trifluoroacetic acid as catalysts. Saponification was attempted using sodium hydroxide (Clayden et al., 2001). A range of concentration conditions were used, with milder hydrolysis conditions being preferable for the integrity of the support.

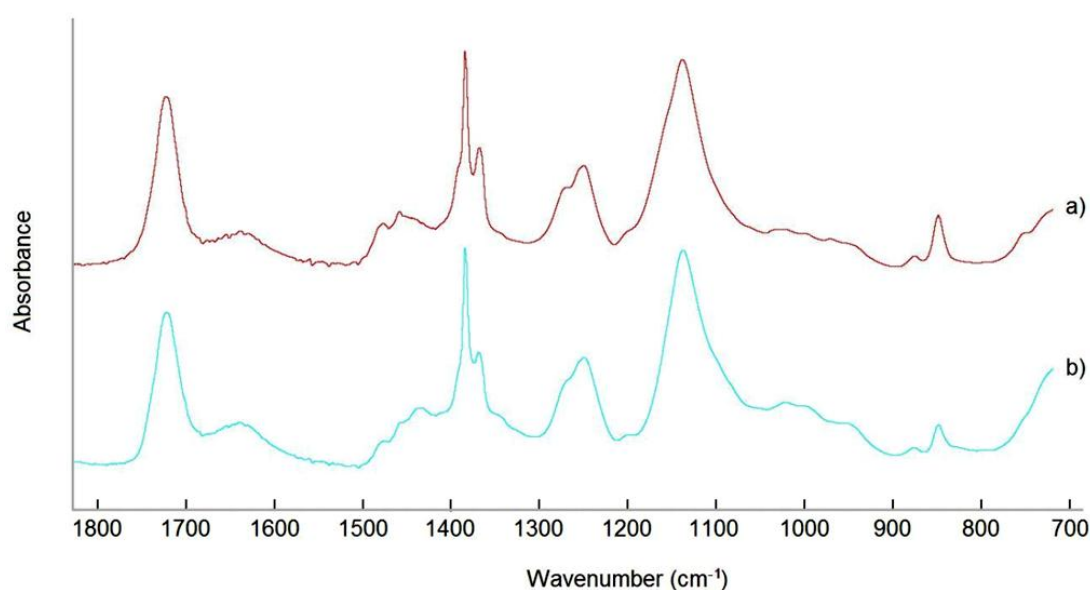


Figure 7.2. a) PTBMA grafted M-PVA; b) PTBMA grafted M-PVA following hydrolysis with 1 M p-tol in DMSO

Following a “graft from” synthesis with Ce(IV) activation, PTBMA grafted m-PVA (5 mg) was reacted with a solution of p-tol in DMSO (1 M, 1 ml, 60°C, 24 h). No new FTIR peaks were seen following reaction with the acid, indicating that hydrolysis of the ester group had not occurred (figure 7.2). The same result was seen in reactions 2-8 (table 7.1), performed with the same mass of support and same volume of solution but with varied concentrations of acid/base. Reaction with 50/50 TFA/water solution, however, led to loss of the characteristic t-butyl ester peaks alongside retention of some CH₃ and carbonyl peaks. This result would be expected for a successful hydrolysis reaction (figure 7.3).

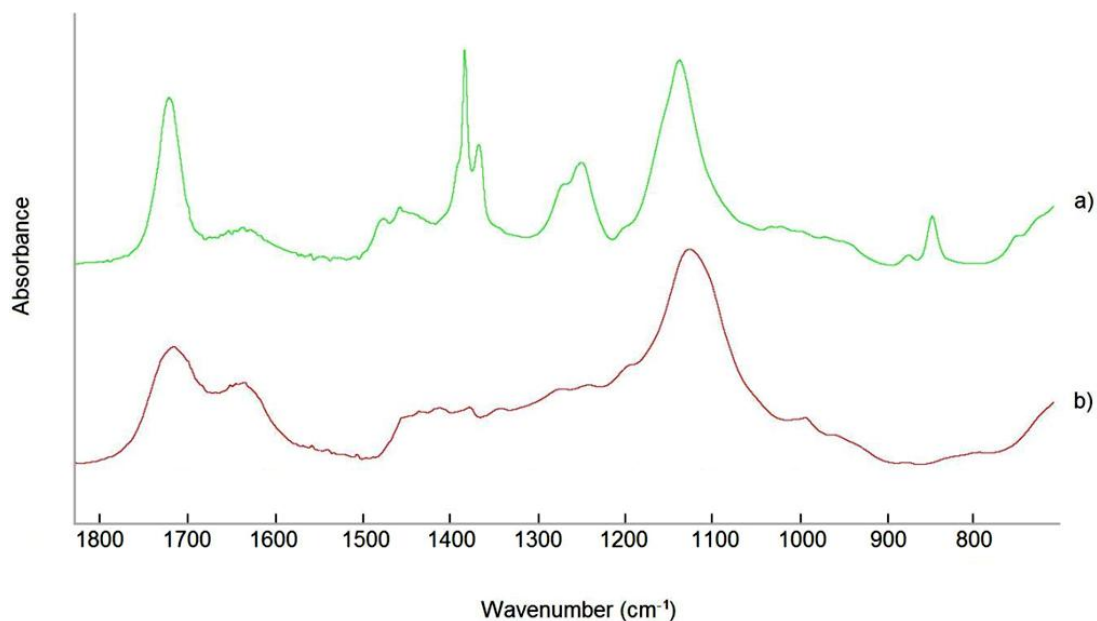


Figure 7.3. a) PTBMA grafted M-PVA; b) PTBMA grafted M-PVA following hydrolysis with 50% TFA_(aq).

Loss of peaks at 1390, 1370, 1250 and 850 cm^{-1} are observed following reaction with TFA. These wavenumbers correspond to methyl groups, primarily found on the t-butyl ester group which is lost during hydrolysis.

The carbonyl peak at 1720 cm^{-1} remains after hydrolysis but has become smaller and broader, reflecting a change from the localised ester C=O of t-butyl ester to the more delocalised carboxylic acid C=O of the methanoic acid side-group. Similarly, the original C-O peak at 1140 cm^{-1} is also seen to broaden and lose height for the same reasons. The success of this hydrolysis method is also evident during Chapter 5, with cationic binding behaviour absent in the PTBMA grafted support prior to hydrolysis but present following hydrolysis. This indicates the successful production of PMAA.

Table 7.1. Results for hydrolysis of Ce(IV) grafted M-PVA with acid or base catalysis.

Hydrolysis Number	Catalyst	Solvent	Catalyst conc.	Loss of t-butyl peaks
1	p-tol	DMSO	1M	No
2	TFA	DMSO	1M	No
3	p-tol	90% DMSO 10% water	1M	No
4	TFA	90% DMSO 10% water	1M	No
5	NaOH	Water	1M	No
6	p-tol	Water	1M	No
7	TFA	Water	1M	No
9	TFA	Water	50/50 (v/v)	Yes

7.1.4 Conclusion

Of the conditions tested, only 50/50 (v/v) TFA solution in water produced hydrolysed grafted polymers. Hydrolysis reaction catalysis does not involve the whole TFA or p-toluenesulfonic acid molecule, using only the dissociated protons/hydronium ion components. As catalysis only involves these small molecules, the low conversion under these conditions is unlikely to be due to steric hinderance by adjacent polymer chains. The more likely cause is steric and electronic effects of the methyl group which is attached to the polymer backbone. This methyl group hinders nucleophilic attack at the carbonyl carbon both sterically and by inductive effects, lowering the reactivity of this carbon to nucleophiles.

7.2 Calibration charts of monomers in DMSO (Ce(IV) reaction quantification)

7.2.1 Method:

Liquid samples for FTIR analysis and quantification were taken directly after reaction and compared to a solution containing the same proportions of monomer, nitric acid and DMSO as the initial reaction solution. Spectra were scanned with background substitution for DMSO + nitric acid without monomer, resulting in final spectra showing the absorbance of monomer under these solvent conditions. It was found that the presence of experimental concentrations of ACN had no immediate effect on monomer absorbance values, so ACN was omitted from quantification/calibration samples for simplicity. Quantification was performed by multiplying the difference in supernatant absorbance, ΔA , for a chosen wavenumber range by the gradient, M , obtained from a calibration plot of monomer volume vs. A . (equation 7.1; table 7.2; figures 7.4 -7.6)

$$\Delta V(\text{monomer}) = \frac{\Delta A(\text{monomer})}{M}$$

Equation 7.1.

Table 7.2. Calibration gradients ($\text{cm}^{-1} \cdot \text{mg}^{-1}$) chosen for quantification of monomers in 2 ml DMSO + 150 μl nitric acid.

Monomer	Wavenumber range (cm^{-1})	Gradient (M)
TBMA	1188-1121	3.56×10^{-3}
2VP	1484-1444	8.45×10^{-4}

This value for the volume of monomer consumed during reaction, ΔV , was then used to calculate the number of polymer units grafted per g of M-PVA during reaction. The assumption that number of graft sites was equal to the number of Ce(IV) initiators used allowed calculation of both the intergraft spacing and, following from ΔV , the average polymer chain length.

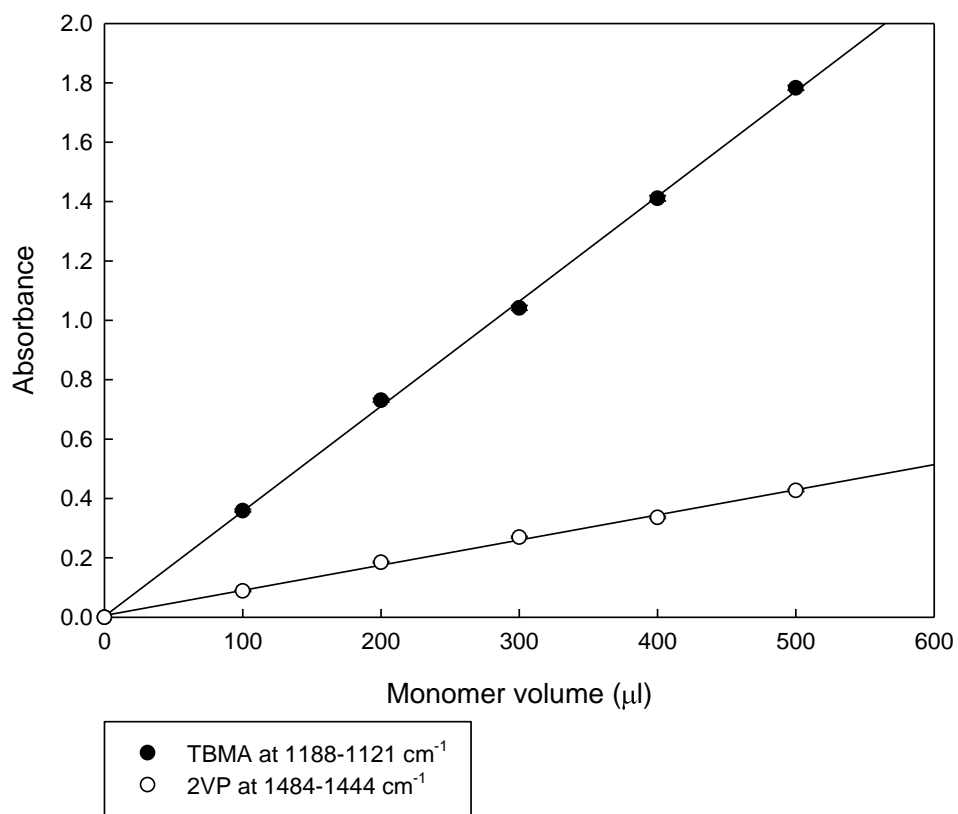


Figure 7.4. FTIR calibration graph for monomers in DMSO (2 ml) + nitric acid (150 ml, 2 M)

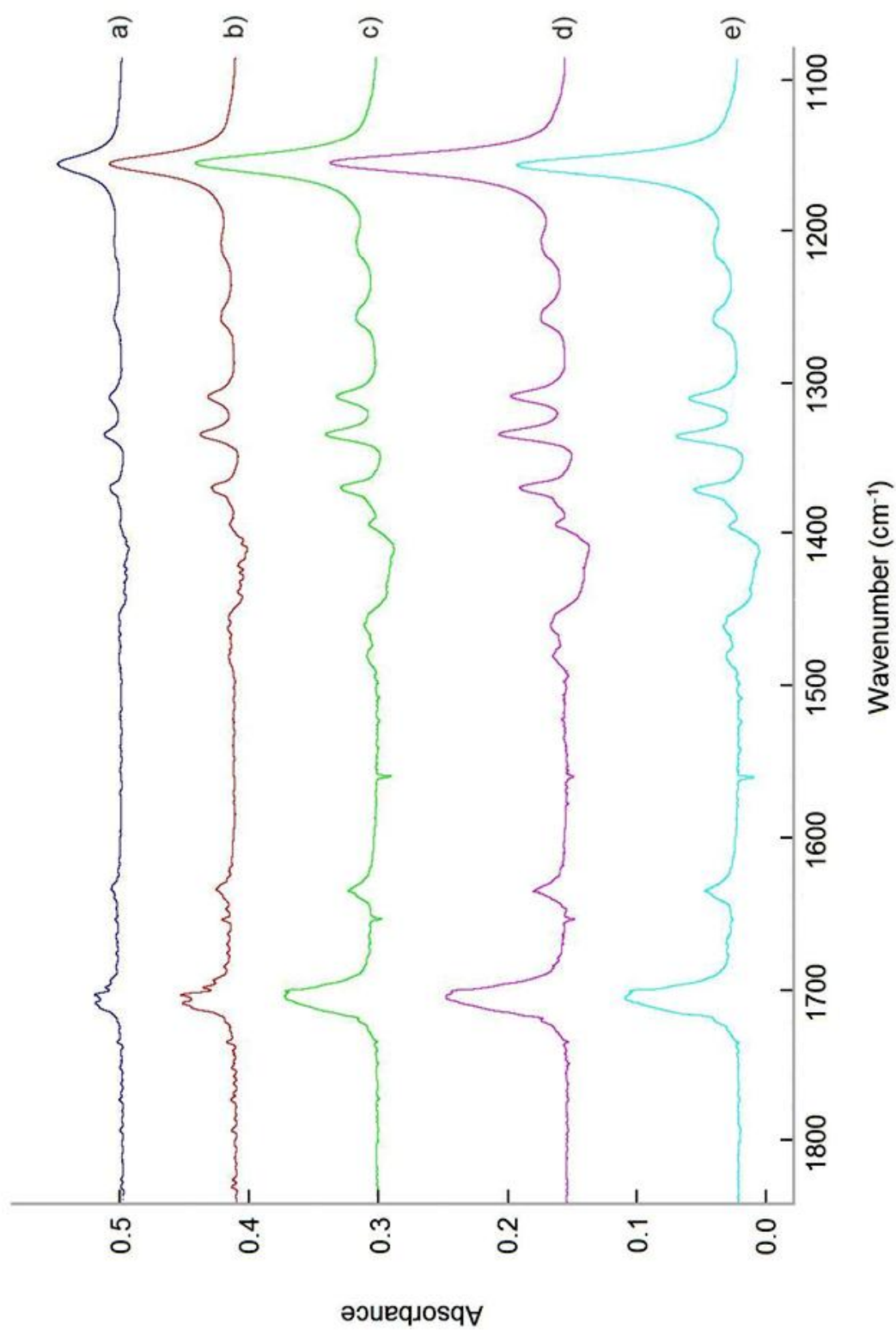


Figure 7.5. FTIR spectra of DMSO (2 ml) + nitric acid (150 ml, 2 M) containing TBMA monomer: a) 100 μ l; b) 200 μ l; c) 300 μ l; d) 400 μ l; e) 500 μ l.

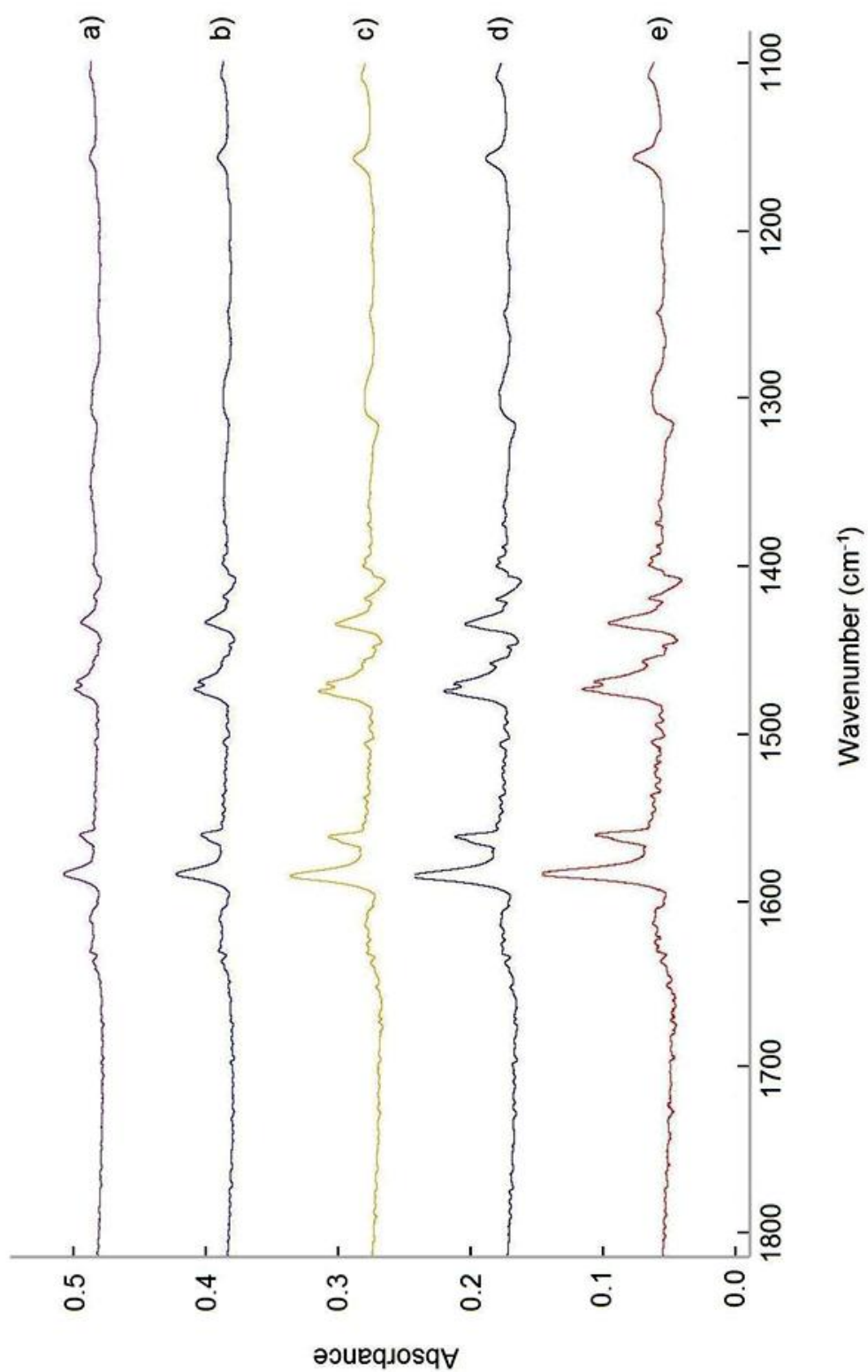


Figure 7.6. FTIR spectra of DMSO (2 ml) + nitric acid (150 ml, 2 M) containing 2VP monomer: a) 100 μ l; b) 200 μ l; c) 300 μ l; d) 400 μ l; e) 500 μ l.

7.3 Calibration charts of monomers from water into 1-butanol (ATRP)

7.3.1 Method:

Liquid samples for FTIR analysis and quantification were prepared by mixing the entire supernatant with 1-butanol (6 ml) and NaOH solution (10 M, 1 ml) for 60 s after ATRP reaction and then allowing the mixture to separate for 0.5 h. The organic phase was then analysed with FTIR, using the organic phase from a two phase mixture containing 1-butanol (6 ml), NaOH (10 M, 1 ml) and water (5 ml).

$\Delta A(\text{monomer})$ values for the supernatant following ATRP reaction were found by comparing a liquid sample of the final supernatant with a liquid sample containing the same reagent quantities as the starting supernatant. Calibration samples were prepared by mixing monomer with 1-butanol (6 ml), NaOH solution (10 M, 1 ml) and water (5 ml) for 60 s, then leaving to settle for 0.5 h and analysing the organic phase with FTIR (figures 7.7-7.9; table 7.3). ΔA values and calibration gradients were then used to calculate monomer consumption, mass of graft polymer per g of M-PVA and average polymer chain lengths as with Ce(IV) grafted products (see appendix 7.2).

Table 7.3. Calibration gradients ($\text{cm}^{-1} \cdot \text{mg}^{-1}$) chosen for quantification of monomers in 1-butanol.

Monomer	Wavenumber range (cm^{-1})	Gradient
TBMA	1377-1357	1.48×10^{-1}
2VP	1600-1575	4.17×10^{-1}

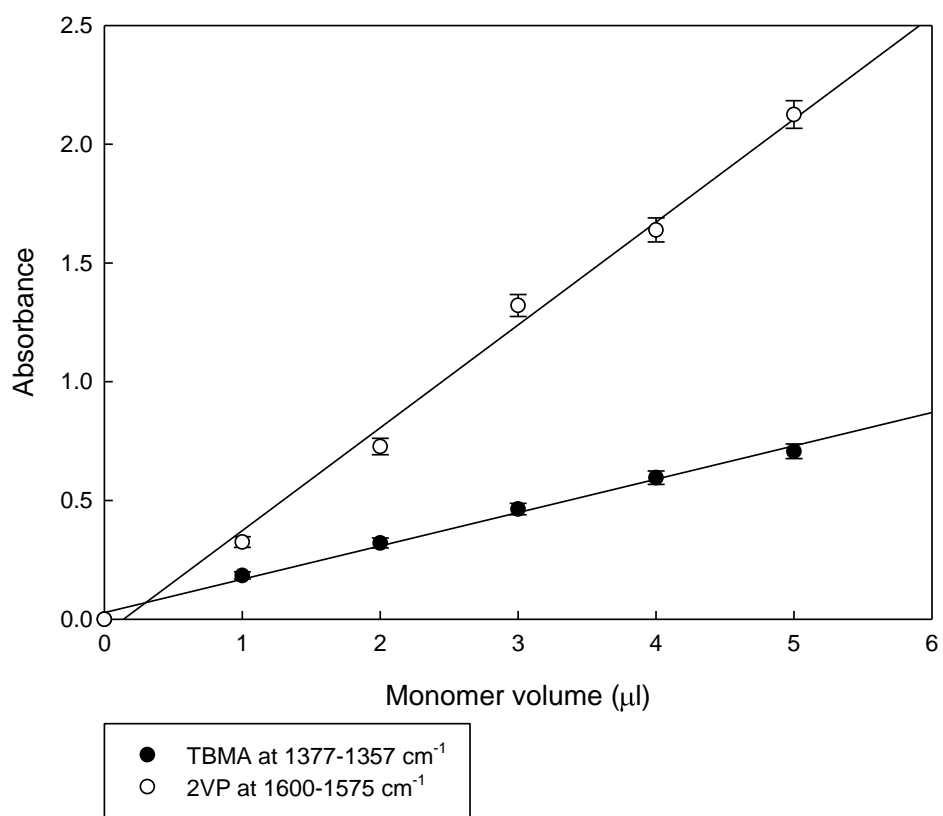


Figure 7.7. FTIR calibration graph for monomers in 1-butanol (6 ml)

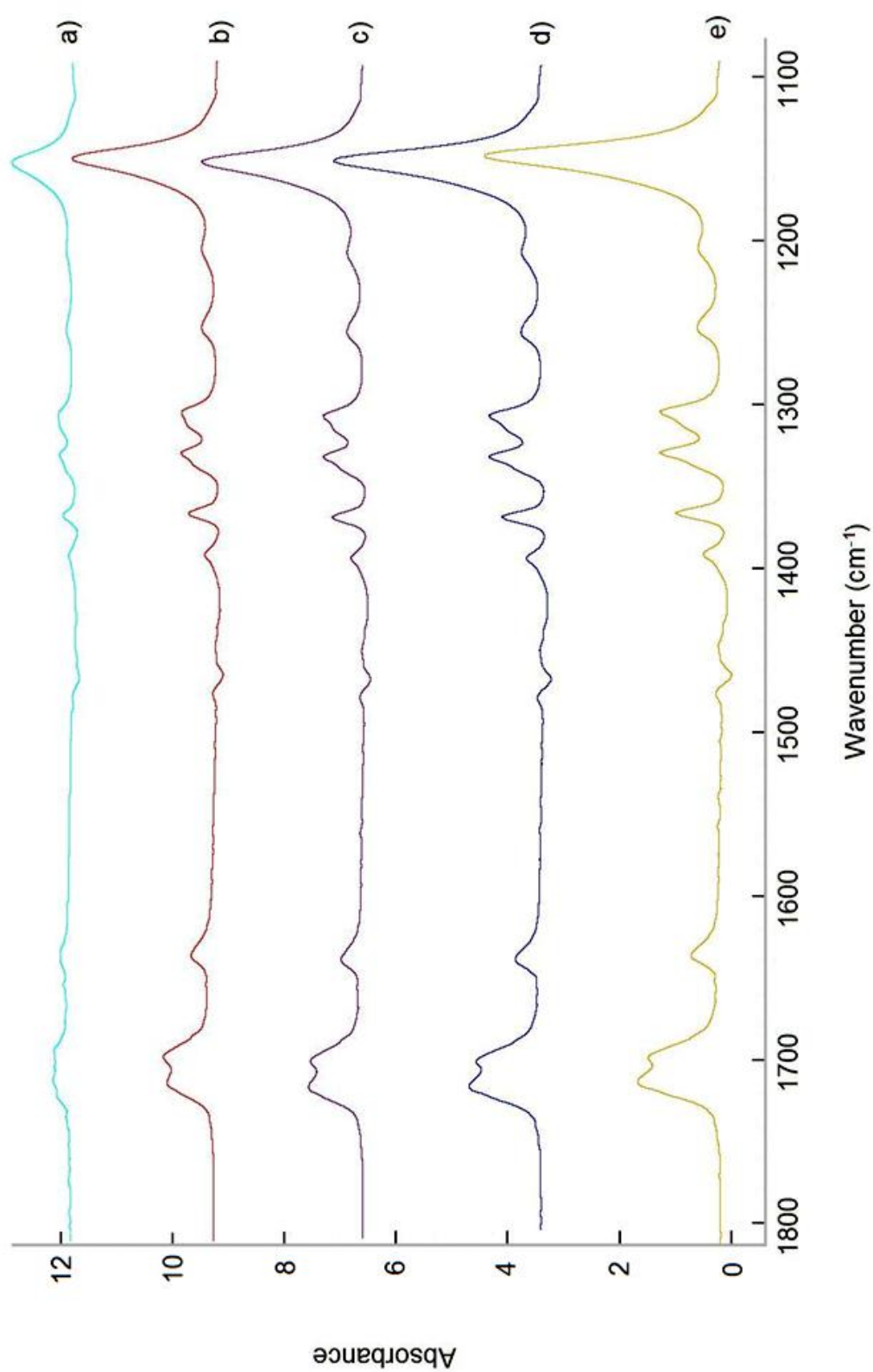


Figure 7.8. FTIR spectra of 1-butanol (6 ml) containing TBMA monomer: a) 1 ml; b) 2 ml; c) 3 ml; d) 4 ml; e) 5 ml

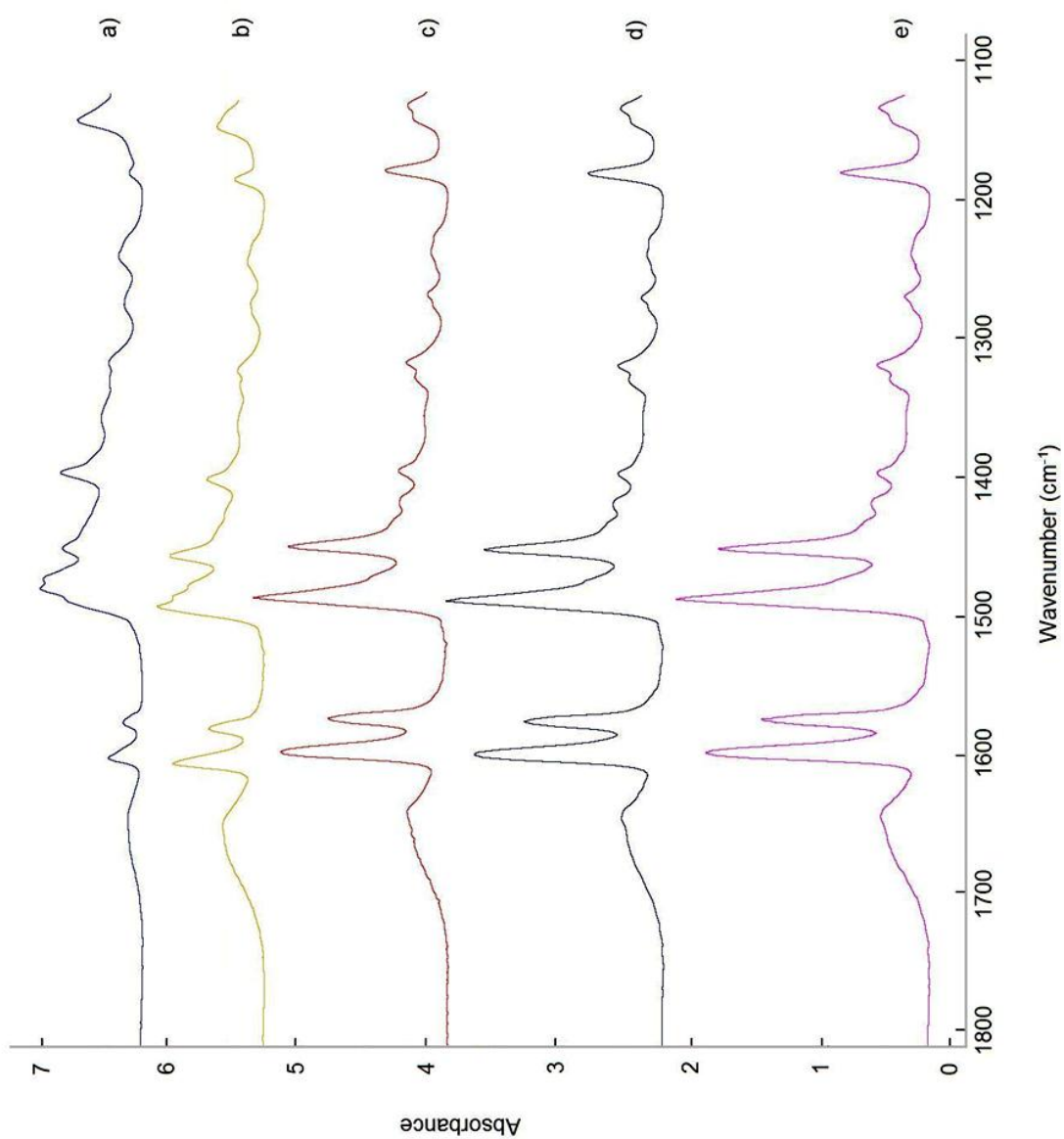


Figure 7.9. FTIR spectra of 1-butanol (6 ml) containing 2VP monomer: a) 1 ml; b) 2 ml; c) 3 ml; d) 4 ml; e) 5 ml

7.4 Calibration charts of 'graft to' polymers from acetone into 1-butanol

7.4.1 Method:

Liquid samples for FTIR analysis and quantification were taken directly after reaction and acetone was removed by evaporation (70 °c, 3 h). The unevaporated polymer was then mixed with 1-butanol (1ml, 600 s) and this solution was analysed using FTIR. Peak absorbances were compared to liquid samples prepared from the unreacted graft-to starting reagent (figures 7.10-7.12; table 7.4). Calibration data from samples of polymer in 1-butanol was then combined with ΔA values for the graft-to reaction supernatants to find polymer consumption and mass of polymer grafted per g M-PVA. This data was combined with polymer molecular weight data to calculate intergraft spacing values for the grafted polymers.

Table 7.4. Calibration gradients ($\text{cm}^{-1} \cdot \text{mg}^{-1}$) chosen for quantification of monomers in 1-butanol.

Monomer	Wavenumber range (cm^{-1})	Gradient
TBMA	1740-1680	3.97×10^{-3}
2VP	1610-1580	1.27×10^{-3}

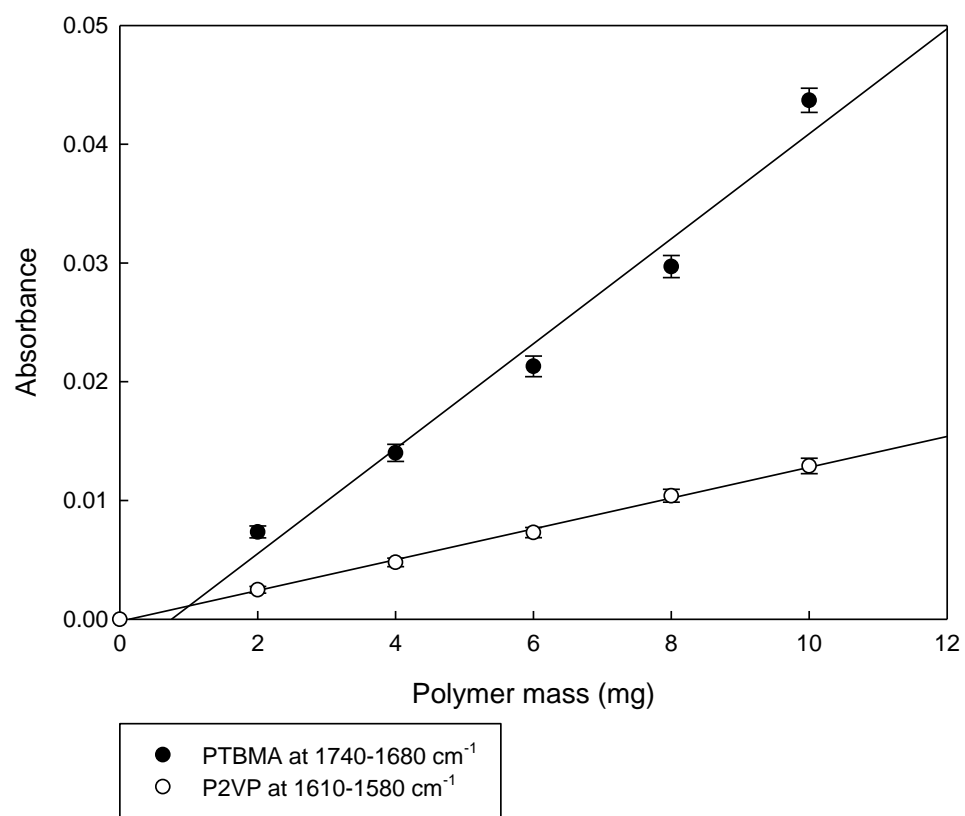


Figure 7.10. FTIR calibration graph for polymers in 1-butanol (1 ml)

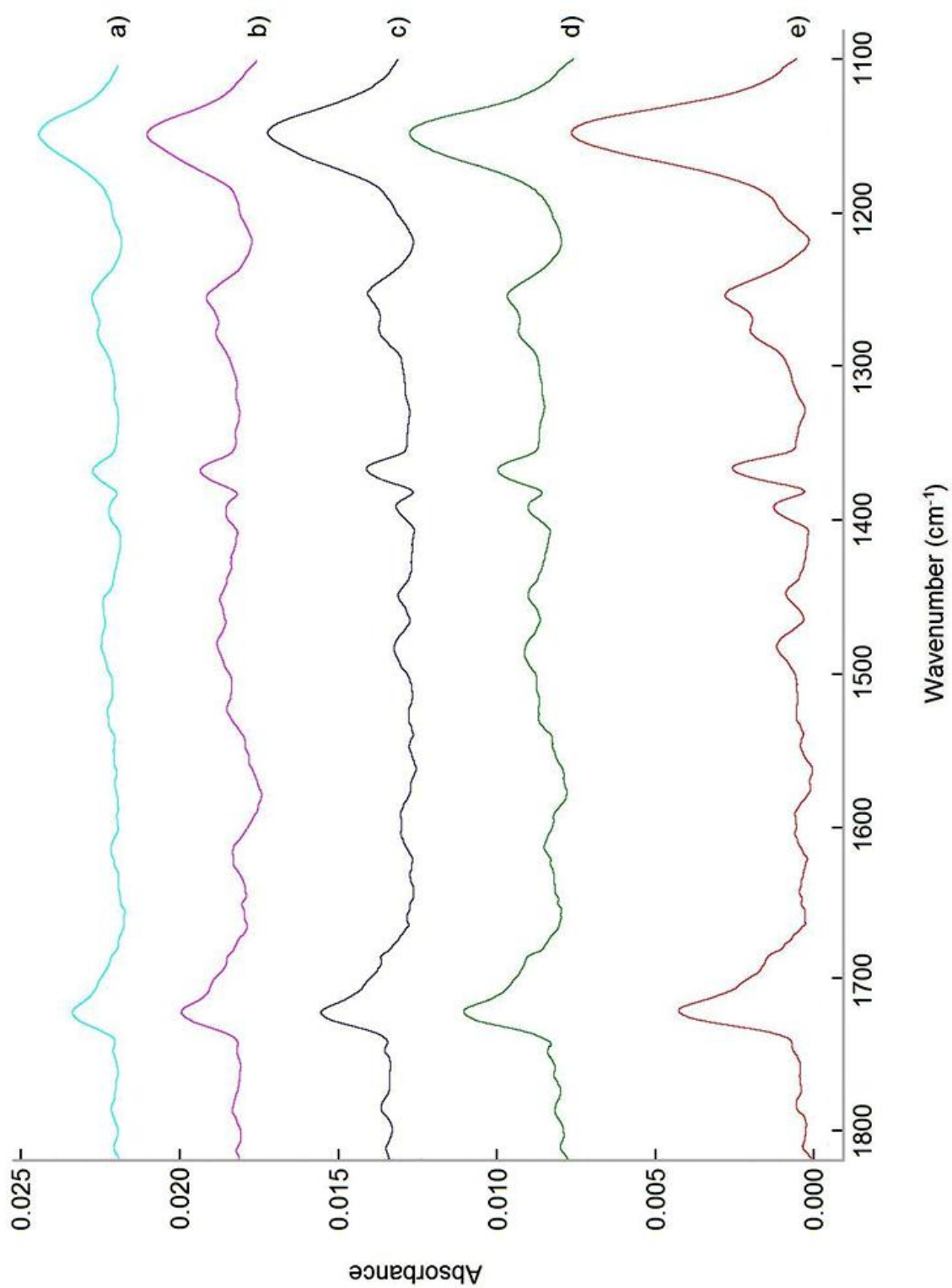


Figure 7.11. FTIR spectra of 1-butanol phase (1 ml) containing PTBMA. a) 2 mg; b) 4 mg; c) 6 mg; d) 8 mg; e) 10 mg.

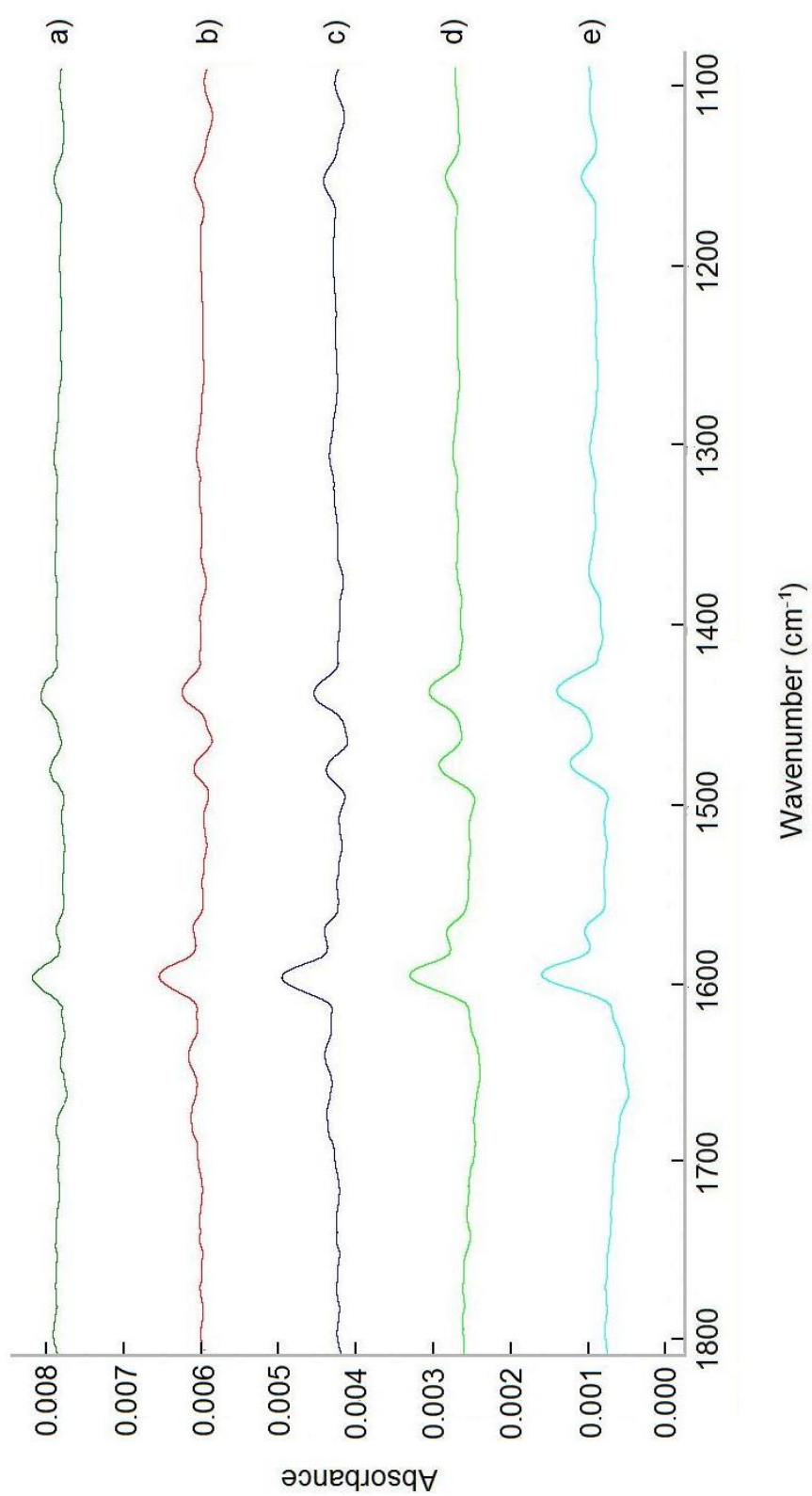


Figure 7.12. FTIR spectra of 1-butanol phase (1 ml) containing P2VP. a) 2 mg; b) 4 mg; c) 6 mg; d) 8 mg; e) 10 mg.

7.5 Comparison of bromine decay in DMSO to bromine decay in water – acidity of bromine in DMSO

7.5.1 Background

Br₂ and DMSO undergo an equilibrium reaction with one another (Aida et al., 1976). This reaction forms a α -bromo-sulfoxide and bromic acid (figure 7.13).

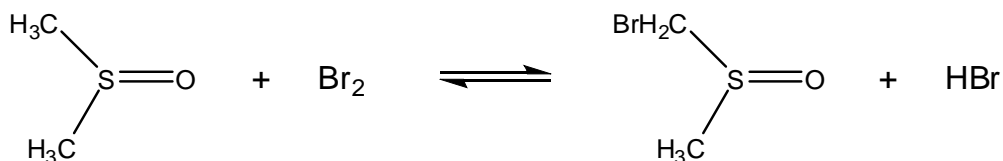


Figure 7.13. Reaction between DMSO and Br₂, with production of bromic acid.

Production of bromic acid leads to acidification of the solution, with the extent of acidification dependent upon the concentration of Br₂ and DMSO. For partial bromination of AGE sites in DMSO, consumption of Br₂ during this reaction may pose a problem for quantitative creation of dibrominated sites. The extent of Br₂ consumption prior to reaction with the surface allyl group may have a significant effect on the success and control of partial bromination reactions. For this reason bromic acid production and Br₂ absorbance decay were monitored for solutions of Br₂ in DMSO.

7.5.2 Method

Distilled DMSO (20 ml) was placed in a 50 ml conical flask and its pH measured. An aliquot of Br₂ (5 μ l) was added to the DMSO with mixing (60 s) and the solution pH was re-measured. This process was repeated until a total of 80 μ l Br₂ had been added.

7.5.3 Results

As Br₂ is added to DMSO, the acidity of the solution increases (figure 7.14). This indicates the production of bromic acid through reaction between DMSO and Br₂, as expected from the literature.

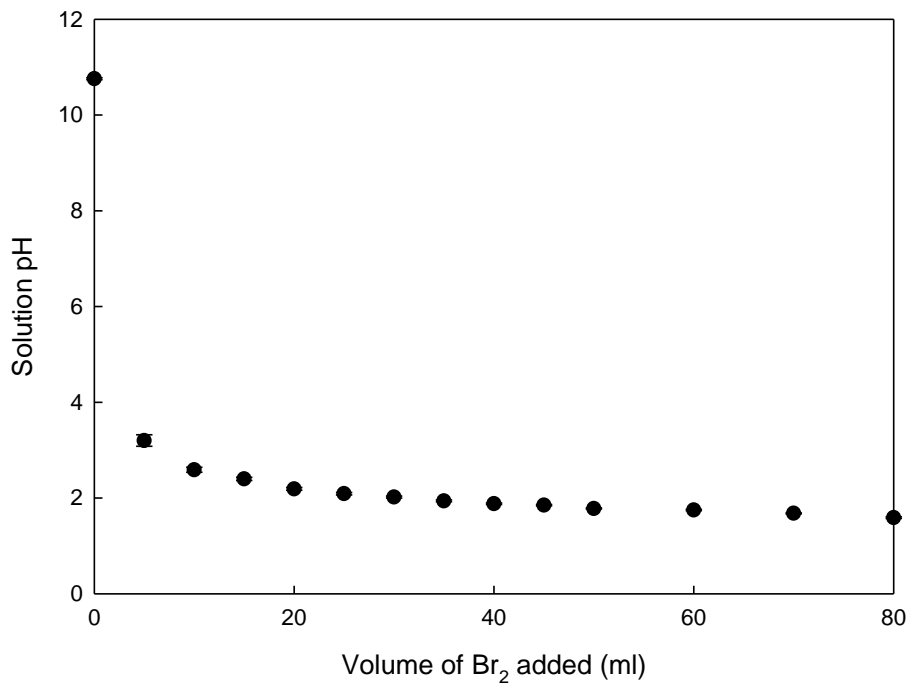


Figure 7.14. pH change of DMSO solution following addition of bromine.

The formula $[H^+] = 10^{(-pH)}$ gives the concentration of protons in the Br₂/DMSO solution at each stage (figure 7.15). This calculation does not take into account the extra volume provided by bromine.

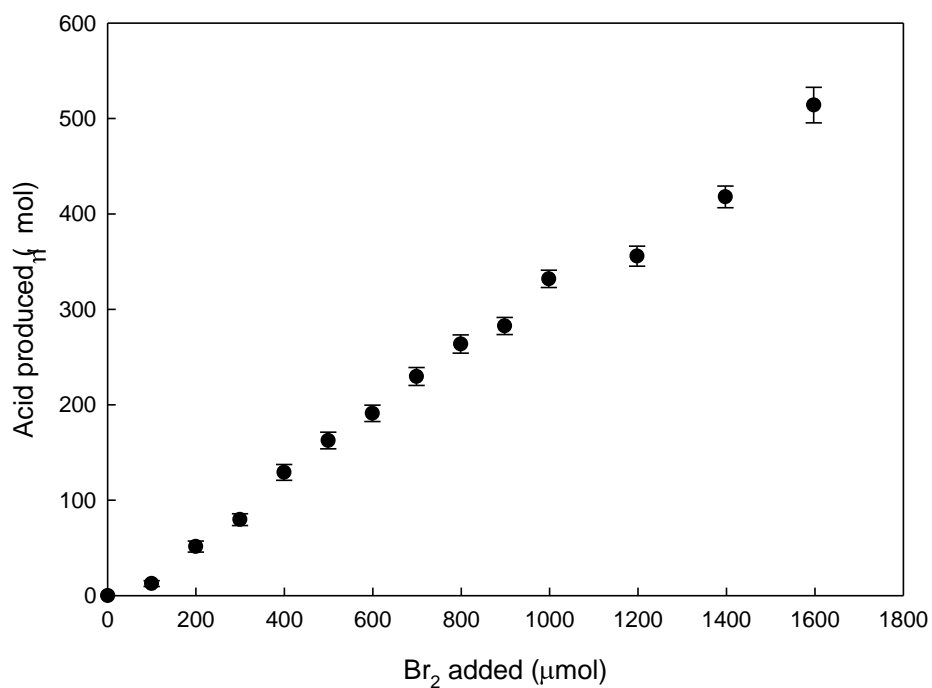


Figure 7.15. Acid production as Br₂ is added to DMSO solution.

[H⁺] and Br₂ addition show a clear linear relationship. The molar ratio Br₂ added:H⁺ released is approximately 5:1, indicating that most bromine is not converted into bromic acid within the timescale of this experiment.

7.6 Comparison of bromine decay in DMSO to bromine decay in water – A_{410} of bromine in DMSO

7.6.1 Background

Br_2 has a characteristic absorbance at 410 nm. Progression of the Br_2/DMSO reaction over time was followed by measuring A_{410} decay, allowing analysis of the effect of mixing time on the partial bromination solution.

7.6.2 Method

Br_2 (2 μl) was pipetted into water (10 ml) and mixed (15 s). Timing started once mixing of Br_2 began. An aliquot (1 ml) of the Br_2/DMSO solution was then transferred to a cuvette and its absorbance measured at 410 nm at 30 seconds intervals, over a period of 600 seconds. The cuvette was covered with a plastic film to minimise evaporation of bromine to the surroundings.

7.6.3 Results

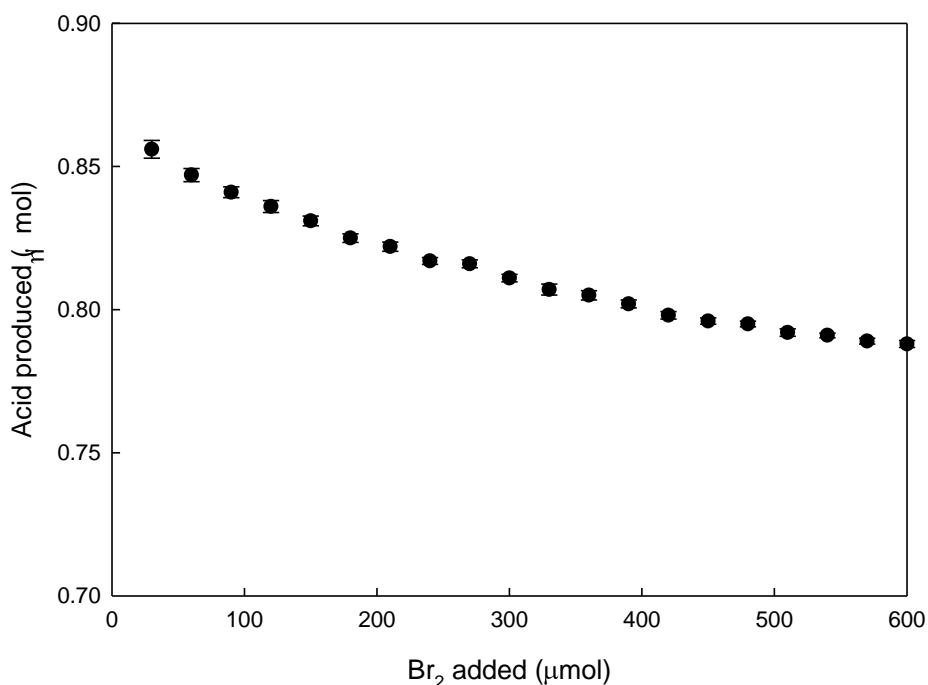


Figure 7.16. Decay of characteristic Br_2 absorbance in bromine-DMSO solution.

Some variation in A_{410} is seen during the experiment (figure 7.16). Preparation of the Br_2/DMSO solution and addition to M-PVA during partial bromination is typically performed within a timescale of 120 s. Figure 7.13 indicates that Br_2 loss during 120 s equates to

$$\frac{(0.86-0.83)\times 100}{0.86} = 3.5 \%$$

Equation 7.2.

3.5% of total bromine added under these conditions. As DMSO is in excess, the rate of this reaction is expected to be first-order with respect to Br_2 in a DMSO solvent. This means that the figure of 3.5 % total bromine consumed during 120 s can be expected for all of the dilute solutions of Br_2 in DMSO used for partial bromination. As the partial bromination reaction leads to consumption of Br_2 it is expected that the rate of Br_2 reaction with DMSO slows following mixing with M-PVA. It is also likely, following Le Chatelier's principle, that following removal of Br_2 from solution by the partial bromination reaction bromic acid and α -bromo-sulfoxide will react together to produce more Br_2 . Hence the expected loss of Br_2 for use in partial brominations is no more the 3.5 % by reaction with DMSO, and probably much less due to the reverse reaction of bromic acid and α -bromo-sulfoxide to produce Br_2 .

7.7 Comparison of bromine decay in DMSO to bromine decay in water – acidity of bromine in water

7.7.1 Background

Reaction between water and bromine in an aqueous bromine solution produces hydrobromous and bromic acids, leading to a decreased Br_2 concentration and increased acidity (figure 7.14).

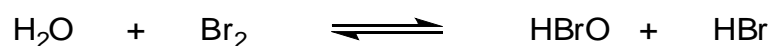


Figure 7.14. Reaction between water and bromine producing bromic and hydrobromous acids

7.7.2 Method

Distilled water (20 ml) was placed in a 50 ml conical flask and its pH measured. An aliquot of Br_2 (5 μl) was added to the DMSO with mixing (60 s) and the solution pH was re-measured. This process was repeated until a total of 80 μl Br_2 had been added.

7.7.3 Results

As Br_2 is added to water, the pH of the solution decreases due to production of bromic/hydrobromous acids (figure 7.17)

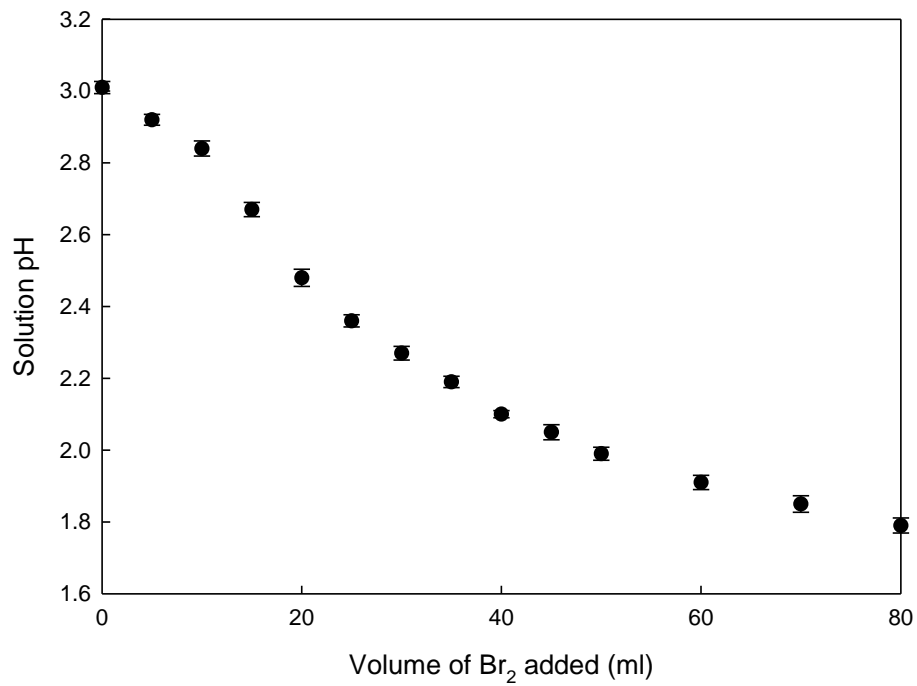


Figure 7.17. pH change of aqueous solution following addition of bromine.

The formula $[H^+] = 10^{(-pH)}$ gives the concentration of protons in the Br₂/water solution at each stage. This calculation does not take into account the extra volume provided by bromine.

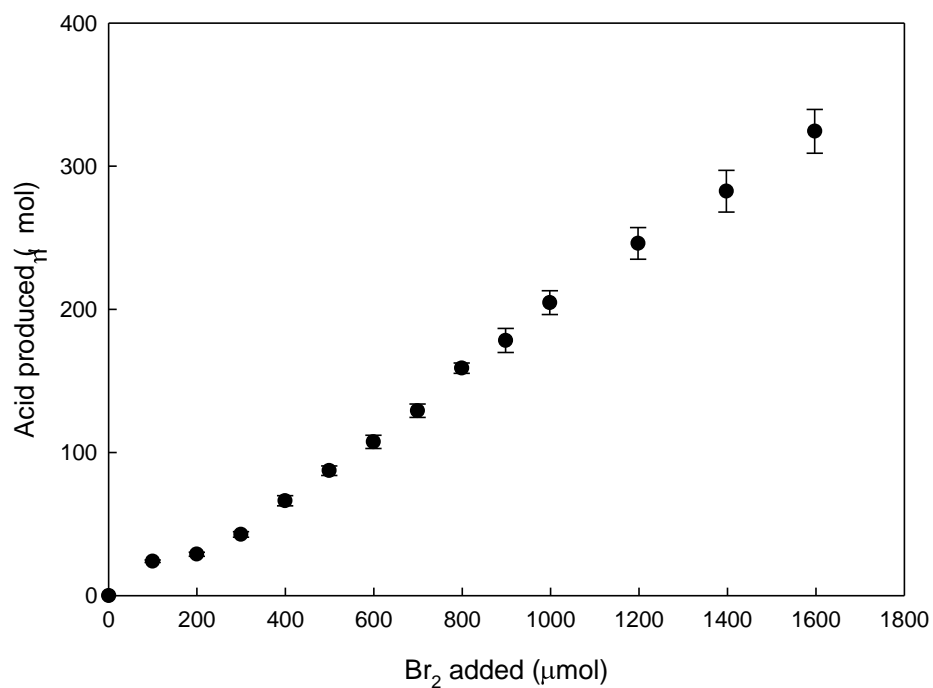


Figure 7.18. Acid production as Br₂ is added to aqueous solution.

[H⁺] and Br₂ addition show a clear linear relationship (figure 7.18). The molar ratio Br₂ added:H⁺ released is approximately 5:1, indicating that 10% of Br₂ added is converted into bromic/bromous acid during the timescale of this experiment (approx. 0.5 h).

7.8 Comparison of bromine decay in DMSO to bromine decay in water – A_{410} of bromine in water

7.8.1 Background

As with DMSO/ Br_2 reaction, the disappearance of Br_2 can be followed with spectrophotometry by monitoring the decrease in the characteristic absorbance by Br_2 at 410 nm.

7.8.2 Method

Br_2 (2 μl) was pipetted into water (10 ml) and mixed (15 s). Timing started once mixing of Br_2 began. An aliquot (1 ml) of the Br_2 /water solution was then transferred to a cuvette and its absorbance measured at 410 nm at 30 seconds intervals over a period of 600 seconds. The cuvette was covered with a plastic film to minimise evaporation of bromine to the surroundings.

7.8.3 Results

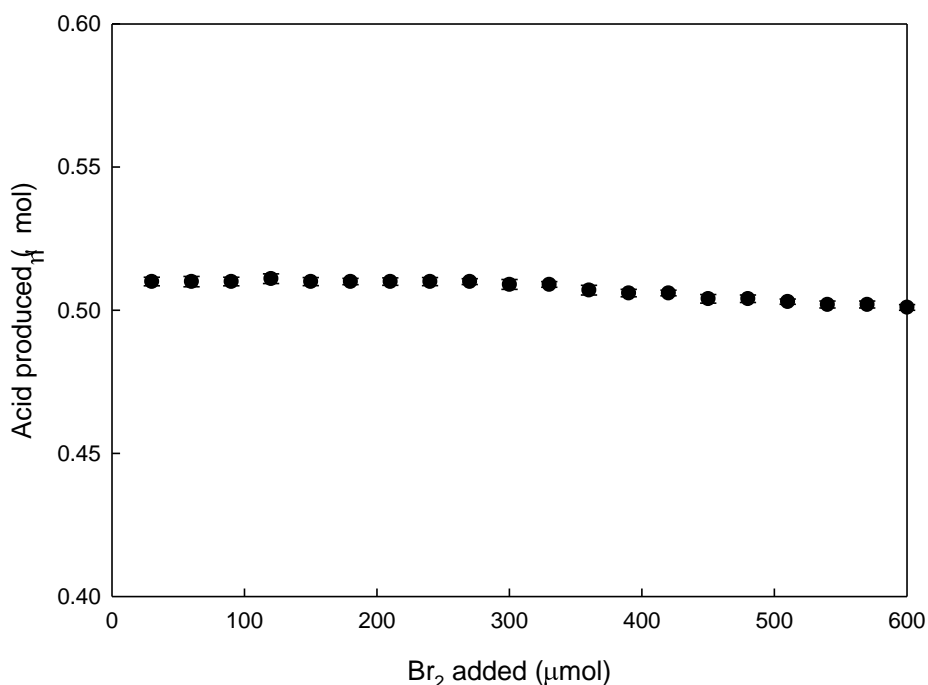


Figure 7.19. Decay of characteristic Br_2 absorbance in bromine-water solution.

Very little variation in A_{410} is seen during the experiment, with the total loss of initial Br_2 being calculated as (equation 7.3)

$$\frac{(0.51-0.50) \times 100}{0.86} = 1.0 \%$$

Equation 7.3.

As with the DMSO/Br_2 solution, the effective loss of available Br_2 for partial bromination is probably less due to reverse reaction production of Br_2 . So for partial halohydrin formation reactions it is expected that over 99 % of the initial Br_2 added is available for electrophilic addition.

7.9 Calculation of average R_f for mixed brushes

7.9.1 Background

Estimations of the overlap between brushes grafted at the M-PVA surface and their extent of their subsequent brush behaviour can be performed by calculating the relationship between Flory Radius, R_f , and intergraft spacing, D . When the condition $2R_f/D > 1$ is met extended brush behaviour is expected, with higher values of $2R_f/D$ indicating significant brush behaviour. Average Flory Radius for a set of grafted polymers can be calculated using equation 7.4 where 0.6 is a standard value for the Flory Exponent (Katao and Wadati, 2007), L is the length of the average chain in monomer units and A_m is the monomer size.

$$R_f \approx A_m L^{0.6}$$

Equation 7.4.

For a mixed brush a complication arises due to the presence of more than one monomer species, leading to more than one A_m value. In order to calculate an average R_f value, and hence an average $2R_f/D$ value for the entire mixed brush, it is necessary to find R_f with respect to the average A_m value. In this case A_m is not simply the average of the monomer sizes for all species present, but is the average monomer size when the proportion of each monomer species in the brush layer is taken into account.

7.9.2 Method

Three techniques for obtaining an average R_f were used, based upon

- i) Averaging R_f in relation to the number of monomer units of each species present in the grafted polymer layer.
- ii) Taking overall R_f as a number average of the R_f values calculated for each grafted polymer species, with R_f being averaged according to the number of polymer chains of each species present.
- iii) Calculating overall R_f as a 'weighted' average of the R_f values calculated for each polymer species and the number of chains of each

species present, with the average weighted towards chains with higher R_f values.

Method i) was based upon equation 7.5

$$R_f(av) = \frac{R_f(P2VP) \cdot n(P2VP) + R_f(PMAA) \cdot n(PMAA)}{n(P2VP) + n(PMAA)}$$

Equation 7.5

Where $R_f(P2VP)$ and $R_f(PMAA)$ are the Flory radii of P2VP and PMAA chains respectively while $n(P2VP)$ and $n(PMAA)$ are the number of monomer units of each species grafted.

Method ii) used equation 7.6

$$R_f(av) = \frac{R_f(P2VP) \cdot N(P2VP) + R_f(PMAA) \cdot N(PMAA)}{N(P2VP) + N(PMAA)}$$

Equation 7.6

Where $N(P2VP)$ and $N(PMAA)$ are the number of chains of each species grafted, estimated from the number of initiator groups used in 'graft from' methods and the mass of polymer grafted in 'graft to' methods.

And method iii) used equation 7.7

$$R_f(av) = \frac{R_f(P2VP)^2 \cdot N(P2VP) + R_f(PMAA)^2 \cdot N(PMAA)}{R_f(P2VP) \cdot N(P2VP) + R_f(PMAA) \cdot N(PMAA)}$$

Equation 7.7

Equations 7.6 and 7.7 were based upon number weight and molecular weight averaging methods as used in describing polymer molecular weights.

7.9.2 Results

Average R_f values were calculated for all supports for which quantification information was available. The two most interesting sets of results are shown here. Table 7.5 describes the supports used in binding studies (Chapter 5), while table 7.6 shows values for supports synthesised using a combination of ATRP and graft to at

brominated sites (Chapter 4). These results demonstrate that $2R_f/D$ values are reasonably consistent for all averaging techniques when R_f and D values for the two grafted species are similar. However, when R_f and D values for the two species differ, the three averaging techniques can produce vastly different results.

In the case of technique i) averaging with respect to number of monomers present can result in unrealistically high values of $2R_f/D$ for the mixed brush (e.g. an average mixed brush $2R_f/D$ value of 49.2 when the component brushes have values of 3.8 and 11.2 respectively). In the case of Table 7.6 this is due to the average R_f value being heavily influenced by the long GT chain length while the D value is more representative of the small ATRP intergraft spacings.

For technique ii) Table 7.6 once again shows unrealistic $2R_f/D$ values, with supports 3 and 4 showing average $2R_f/D$ values that are lower than one of their components. These values cannot be correct as mixed brushes are certain to involve more steric crowding, and hence higher $2R_f/D$ values, than the grafted component species.

Due to the unrealistic results obtained from averaging with methods i) and ii) the technique chosen for R_f averaging was iii), which produced much more realistic R_f values for the mixed brush ATRP/GT products.

Table 7.5. Data for polyelectrolyte grafted supports (see Chapter 5, Table 4.2). R_f values obtained using method i) averaging according to number of monomer units; ii) averaging according to number of polymer chains with equal weighting; iii) averaging according to number of polymer chains, weighted towards those with higher R_f .

Name	P2VP (mol/g)	P2VP R_f (nm)	P2VP D (nm)	P2VP 2 R_f /D	PMAA (mol/g)	PMAA R_f (nm)	PMAA D (nm)	PMA 2 R_f /D	Method i)			Method ii)			Method iii)		
									MIX R_f (nm)	MIX D (nm)	MIX 2 R_f /D	MIX R_f (nm)	MIX D (nm)	MIX 2 R_f /D	MIX R_f (nm)	MIX D (nm)	MIX 2 R_f /D
CE-MX1	4.88	5.48	0.82	13.4	4.56	2.59	0.82	6.3	4.08	0.58	14.1	4.03	0.58	14.0	4.55	0.58	15.7
CE-MX2	3.34	4.36	0.82	15.1	6.11	3.09	0.82	7.6	3.54	0.58	12.2	3.73	0.58	12.9	3.84	0.58	13.3
TR-MX1	1.35	13.04	3.20	8.1	1.81	5.29	2.36	4.5	8.60	1.90	9.1	8.01	1.90	8.4	9.72	1.90	10.2
TR-MX2	2.44	13.04	2.38	11.2	1.50	5.29	3.26	4.1	10.88	1.92	11.3	10.35	1.92	10.8	11.66	1.92	12.1
AT-MX1	3.84	1.25	0.26	9.5	3.40	0.57	0.26	4.3	0.94	0.19	10.0	0.91	0.19	9.8	1.04	0.19	11.2
AT-MX2	2.67	1.29	0.26	9.8	4.03	0.50	0.26	3.8	0.98	0.19	10.4	0.89	0.19	9.6	1.07	0.19	11.5

Table 7.6. Grafting yield following graft-to and ATRP reactions between amine terminated polymer and 50% brominated M-PVA (see Chapter 4). R_f values from method i) averaging by number of monomer units; ii) average from number of polymer chains with equal weighting for R_f values; iii) averaging according to number of polymer chains, weighted towards those with higher R_f .

Support	Stage	Method	Polymer grafted	Method i)			Method ii)			Method iii)		
				D (nm)	R_f (nm)	$2R_f/D$	D (nm)	R_f (nm)	$2R_f/D$	D (nm)	R_f (nm)	$2R_f/D$
1	Step 1	ATRP	P2VP	0.26	1.06	8.0	0.26	1.06	8.0	0.26	1.06	8.0
1	Step 2	Graft-to	PMAA	2.27	5.29	4.7	2.27	5.29	4.7	2.27	5.29	4.7
1	Finished		[(P2VP) $_x$ + (PMAA) $_y$]	0.26	2.72	20.7	0.26	1.11	8.5	0.26	1.33	10.1
2	Step 1	ATRP	PMAA	0.26	0.50	3.8	0.26	0.50	3.8	0.26	0.50	3.8
2	Step 2	Graft-to	P2VP	2.33	13.04	11.2	2.33	13.04	11.2	2.33	13.04	11.2
2	Finished		[(P2VP) $_x$ + (PMAA) $_y$]	0.26	6.46	49.2	0.26	0.66	5.0	0.26	3.64	27.8
3	Step 1	Graft-to	P2VP	2.60	13.04	10.0	2.60	13.04	10.0	2.60	13.04	10.0
3	Step 2	ATRP	PMAA	0.26	0.48	3.6	0.26	0.48	3.6	0.26	0.48	3.6
3	Finished		[(P2VP) $_x$ + (PMAA) $_y$]	0.26	5.97	45.5	0.26	4.6	4.6	0.26	3.23	24.6
4	Step 1	Graft-to	PMAA	2.67	5.29	4.0	2.67	5.29	4.0	2.67	5.29	4.0
4	Step 2	ATRP	P2VP	0.26	1.11	8.4	0.26	1.11	8.4	0.26	1.11	8.4
4	Finished		[(P2VP) $_x$ + (PMAA) $_y$]	0.26	2.37	18.0	0.26	1.15	8.7	0.26	1.29	9.8

7.10 Effect of bead curvature on intergraft distances

7.10.1 Theory

The effect of bead curvature on intergraft spacing can be modelled by a circle (figure 7.20).

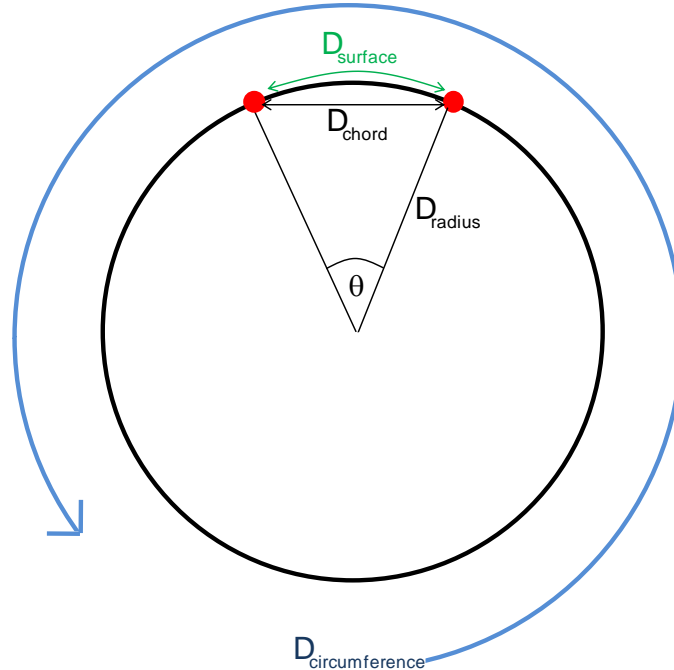


Figure 7.20. Intergraft distances in an M-PVA bead modelled as circle.

Where the distance between between graft sites along the particle surface, d_{radius} (as used in chapters 2-5) can be compared to the distance between graft sites as described by the minimum chord length between sites, d_{chord} . From figure 7.18 the surface and chordal intergraft distances can be related to the circumference ($d_{\text{circumference}}$) radius (d_{radius}) and angle between the two graft points (θ , radians) by equations 7.8-7.10.

$$D_{\text{chord}} = 2 \cdot D_{\text{radius}} \cdot \sin\left(\frac{\theta}{2}\right)$$

$$D_{\text{circumference}} = 2 \cdot \pi \cdot D_{\text{radius}}$$

$$\frac{D_{\text{surface}}}{D_{\text{circumference}}} = \frac{\theta}{2 \cdot \pi}$$

Equations 7.8-7.10

By combining these equations 7.8-7.10 it can be seen that

$$D_{\text{chord}} = 2 \cdot D_{\text{radius}} \cdot \sin\left(\frac{D_{\text{surface}}}{2 \cdot D_{\text{radius}}}\right)$$

Equation 7.11

For the M-PVA beads used in this project $r = 1000 \text{ nm}$ which means that equation 7.11 can be simplified to give equation 7.12.

$$D_{\text{chord}} = 2000 \cdot \sin\left(\frac{D_{\text{surface}}}{2000}\right)$$

Equation 7.12.

From this the relationship between D_{surface} and D_{chord} can easily be calculated for the grafted M-PVA beads.

7.10.2 Results

Re-calculation of the intergraft distances for the supports used in chapter 5 gives the values seen in table 7.7. For the intergraft spacings seen during this study, chordal (D_{chord}) and surface (D_{surface}) distances are effectively the same. This results from the much larger value of D_{radius} , leading to very little curvature of the surface between adjacent graft points. A significant difference between D_{chord} and D_{surface} will only be expected when the scale of intergraft distances is closer to that of D_{radius} .

Table 7.7. Calculation/comparison of surface and chordal distances for the supports used in chapter 5. Note that surface and chordal values are the same for the distances used here.

			Surface distance (D_{surface})			Chordal distance (D_{chord})					Surface distance (D_{surface})		Chordal distance (D_{chord})	
Name	Method	Graft order	P2VP R_f (nm)	P2VP D (nm)	P2VP $2R_f/D$	P2VP D (nm)	P2VP $2R_f/D$	PMAA R_f (nm)	PMAA D (nm)	PMAA $2R_f/D$	P2VP D (nm)	P2VP $2R_f/D$	P2VP D (nm)	P2VP $2R_f/D$
CE-AX	Ce(IV) (Ch. 2)	P2VP only	5.48	0.82	13.4	0.82	13.4	-	-	-				
CE-CX	Ce(IV) (Ch. 2)	PMAA only	-	-	-	-	-	3.09	0.82	7.6	0.82	7.6		
CE-MX1	Ce(IV) (Ch. 2)	1.P2VP 2.PMAA	5.48	0.82	13.4	0.82	13.4	2.59	0.82	6.3	0.82	6.3		
CE-MX2	Ce(IV) (Ch. 2)	1.PMAA 2.P2VP	4.36	0.82	15.1	0.82	15.1	3.09	0.82	7.6	0.82	7.6		
TR-MX1	Tresyl (Ch. 3)	1.P2VP 2.PMAA	13.04	3.20	8.1	3.20	8.1	5.29	2.36	4.5	2.36	4.5		
TR-MX2	Tresyl (Ch. 3)	1.PMAA 2.P2VP	13.04	2.38	11.2	2.38	11.2	5.29	3.26	4.1	3.26	4.1		
AT-MX1	ATRP (Ch. 4)	1.P2VP 2.PMAA	1.10	0.26	9.1	0.26	9.1	0.59	0.26	4.0	0.26	4.0		
AT-MX2	ATRP (Ch. 4)	1.PMAA 2.P2VP	1.29	0.26	9.8	0.26	9.8	0.50	0.26	3.8	0.26	3.8		

8 References

Advincula, R.C.; Brittain, W.J.; Caster, K.C.; Ruhe, J. (2004)

Polymer Brushes, 35-50

Wiley-VCH

(Asenjo and Leser, 1996)

Asenjo JA & Leser EW (1996) Downstream processing of natural products, Wiley, 123-138.

Akgol, S; Denizli, A. (2004)

Novel metal-chelate affinity sorbents for reversible use in catalase adsorption.

J Mol Catal B – Enzym. 28, 7–14.

Aida, T.; Akasaka, T.; Furukawa, N.; Oae, S. (1976)

Catalytic reduction of sulfoxide by bromine-hydrogen bromide system

Bulletin of the Chemical Society of Japan, 49 (4) 1117-1121

Al-Maawali, S.; Bemis, J.E.; Akhremitchev, B.B.; Leecharoen, R.; Janesko, B.G.;

Walker, G.C. (2001)

Study of the Polydispersity of Grafted Poly(dimethylsiloxane) Surfaces Using Single-Molecule Atomic Force Microscopy

J. Phys. Chem., 105, 3965-3971

Alexander, S. (1977)

Adsorption of chain molecules with a polar head a scaling description

J. Physique, 38, 983-987

Andrews, A.T. (1986)

Electrophoresis: Theory, techniques, and biochemical and clinical applications
2nd edition. P 3-4.

Clarendon Press

Anne, A.; Moiroux, J. (1999)

Quantitative characterization of the flexibility of poly(ethylene glycol) chains
attached to a glassy carbon electrode.

Macromolecules, 32, 5829-5835

Bajaj, P.; Sen, K.; Bahrami, S.H. (1996)

Solution polymerization of acrylonitrile with vinyl acids in dimethylformamide

J. Appl. Poly. Sci. 59 (10) 1539 – 1550

Balamurugan, S.; Mendez, S.; Balamurugan, S.S.; O'Brien, M.J.; Lopez, G.P.
(2003)

Thermal response of pol(N-isopropylacrlamide) brush probed by surface plasmon
resonance

Langmuir 19 (7) 2545-2549

Ballauff, M.; Borisov, O. (2006)

Polyelectrolyte brushes

Current opinion in colloid and interface science 11 (6) 316-323

Banerjee S.K.; Moskowitz B.M. (1985):

Ferrimagnetic properties of magnetite

In "Magnetite Biomineralization and Magnetoreception in Organisms."

New York: Plenum Press, 17-38.

Barnfield-Frej A-K.; Hjorth, R.; Hammarstroem, A. (1994)

Pilot scale recovery of recombinant annexin V from unclarified *E. coli*

homogenate using expanded bed adsorption. Biotechnol. Bioeng. 44: 922–929

Bartucci, R.; Pantusa, M.; Marsh, D.; Sportelli, L. (2002)

Interaction of human serum albumin with membranes containing polymer-grafted lipids: spin-label ESR studies in the mushroom and brush regimes

Biochimica et Biophysica Acta (BBA) – Biomembranes, 1564 (1) 237-242

Bayramoglu, G.; Gulsum, E.; Becirli, N. (2007)

Preparation of ion-exchange beads based on poly(methacrylic acid) brush grafted chitosan beads: Isolation of lysozyme from egg white in batch system

Colloids and surfaces. A, Physicochemical and engineering aspects, 310, (1-3), 68-77

Bean, C.P.; Livingston, J.D. (1959)

Superparamagnetism

J. Appl. Phys. 30, S120

Beers, K.L.; Gaynor, S.G.; Matyjaszewski, K.; Sheiko, S.S.; Moller, M. (1998)

The Synthesis of Densely Grafted Copolymers by Atom Transfer Radical Polymerization

Macromolecules, 31, 9413-9415

Belder, G.F.; Brinke, G. T.; Hasziioannou, G. (1997)

Influence of Anchor Block Size on the Thickness of Adsorbed Block Copolymer Layers Langmuir, 13, 4102-4105

Bershtein V.A.; Ryzhov V.A. (1994)

Far infrared spectroscopy of polymers

Advances In Polymer Science, 114, 43-121

Biesheuvel, P.M. and Stuart, M.A.C.(2006),

Cylindrical cell model for the electrostatic free energy of polyelectrolyte complexes.

Langmuir 20 (11) 4764-70.

Blanco, M.; Villarroya, I. (2002)

NIR spectroscopy: a rapid-response analytical tool

Trends in Analytical Chemistry, 21 (4) 240-250

Boerner, H.G.; Duran, D.; Matyjaszewski, K.; da Silva, M; Sheiko, S.S. (2002)

Synthesis of molecular brushes with gradient in grafting density by atom transfer polymerization

Macromolecules, 35, 3387-3394

Bonnerjea, J.; Oh, S.; Hoare, M.; Dunhill, P. (1986)

Protein purification: The right step at the right time

Biotechnology 4, 954-958

Boyes, S.G.; Brittain, W.J.; Weng, X.; Cheng, S.Z.D.; (2002)

Synthesis, Characterization, and Properties of ABA Type Triblock Copolymer Brushes of Styrene and Methyl Acrylate Prepared by Atom Transfer Radical Polymerization

Macromolecules, 35, 4960-4967

Braunecker, A.; Matyjaszewski, K. (2006)

Recent mechanistic developments in atom transfer radical polymerization

Journal of molecular catalysis A: chemical 254, 155-164

Bruening, M.L.; Zhou, Y.; Aguilar, G.; Agee, R.; Bergbreiter, D.E.; Crooks, R.M. (1997)

Synthesis and characterization of surface-grafted, hyperbranched polymer films containing fluorescent, hydrophobic, ion-binding, biocompatible, and electroactive groups

Langmuir, 13, 770-778

Chen J. ; Gardella, J. A. (1998)

Solvent effect on the surface composition of poly(dimethylsiloxane)-copolystyrene/polystyrene blends

Appl. Spectrosc. 52, 361-366

Cheng, G.; Boker, A.; Zhang, M.; Krausch, G.; Mueller, A.H.E. (2001)

Amphiphilic cylindrical core-shell brushes via a "grafting From" process using ATRP

Macromolecules, 34, 6883-6888

Chicz, R.M. and Regnier, F.E. (1988)

Surface-mediated retention effects of subtilisin type site-specific variants in cation exchange chromatography

J. Chromator. 443, 193-203

Clayden, J.; Greeves, N.; Warren, S.; Wothers, P. (2001)

Organic Chemistry

Oxford University Press

Crossland, R. K., Wells, W. E. Shiner, Jr., V. J. (1971).

Sulfonate leaving groups, structure and reactivity: 2,2,2-trifluoroethanesulfonate.

J. Am. Chem. SOC. 93, 4217-4219

Demiroglou, A., Bandel-Schlesselmann, C. and Jennissen, H. P. (1994).

A novel reaction sequence for the coupling of nucleophiles to agarose with 2,2,2-trifluoroethane-sulfonyl chloride.

Angew. Chem. Int. Ed. Engl. 33, 120-123.

DeGennes, P.G. (1976)

Scaling theory of polymer adsorption

J. Physique, 37, 1445

DePalma, A. 1995

Biomagnetic separations touted for their scalability and efficiency.

Genetic Eng. News, July: 6.

Draper, J.; Luzinov, I. (2004)

Mixed polymer brushes by sequential polymer additions: anchoring layer effect

Lanmuir, 20, 4064-4075

Ejaz, .M; Yamamoto, S.; Ohno, K.; Tsujii, Y.; Fukuda, T.; (1998)

Controlled graft polymerization of methyl methacrylate on silicon substrate by the combined use of the Langmuir–Blodgett and Atom Transfer Radical

Polymerization techniques

Macromolecules, 31, 5934-5936

Elmore, W.C. (1938)

The Magnetization of Ferromagnetic Colloids

Phys. Rev. 54, 1092 - 1095

Ewing, J.A.; Klaassen, H.G. (1893)

Magnetic Qualities of Iron

Proceedings of the Royal Society of London, 54, 75-77

Feng, W.; Brash, J.; Zhu, S. (2004)

Atom-transfer radical grafting polymerization of 2-methacryloyloxyethyl phosphorylcholine from silicon wafer surfaces

Journal of Polymer Science A: Polymer Chemistry, 42, 2931-2942

Feng, W.; Zhu, S.; Ishihara, K.; Brash, J. (2005)

Adsorption of fibrinogen and lysozyme on silicon grafted with poly(2-methacryloyloxyethyl phosphorylcholine) via surface-initiated Atom Transfer Radical Polymerization

Langmuir, 21, 5980-5987

Finch, C. A.

Polyvinyl Alcohol

Wiley: New York, 1973.

Fish M.F. and Lilly M.D. (1984)

The interactions between fermentation and protein recovery.

Bio/Technology, July: 623-627

Fischer, H. (1999)

The persistent radical effect in controlled radical polymerizations

Journal of polymer science part A: Polymer chemistry 37 (13) 1885-1901

Fritz, G.; Schadler, V.; Willenbacher, N.; Wagner, N.J. (2002)

Electrosteric stabilization of colloidal dispersions

Langmuir, 18, 6381-6390

Gerber, R. and Birss, R.R. (1983)

High gradient magnetic separation

John Wiley and Sons Ltd., Chichester

Girish V.; Vijayalakshmi A. (2004)

Affordable Image Analysis using NIH Image/ImageJ

Indian Journal of Cancer, 41 (1) 47

Govender, T.; Touraj Ehtezazi, T.; Stolnik, S.; Illum, L.; Davis, S.S. (1999)

Complex formation between the anionic polymer (PAA) and a cationic drug (procaine HC1): characterization by microcalorimetric studies

Pharmaceutical research 16 (7) 1125-1131

Grest, G.S. (1999)

Normal and Shear Forces Between Polymer Brushes

Polymers in confined environments 138, 149-184

Guan, Y. P.; Ma, Z. Y.; Liu, X. Q.; and Liu, H. Z. (2005)

Synthesis of magnetic chelator for high-capacity immobilized metal affinity

adsorption of protein by cerium initiated grafted polymerisation

Langmuir 21 (15) 6987-6994.

Guerrini, M.M.; Charleux, B.; Vairon, J-P. (2000)

Functionalized latexes as substrates for atom transfer radical polymerization

Macromol. Rapid Commun., 21, 669-674

Gunther, C.G. (1909)

Electro-magnetic Ore Separation.

McGraw-Hill Publishing Co., New York

Gupta, M. N. and Mattiasson, B. (1994)

Novel technologies in downstream processing.

Chem. Ind. 17, 673-675.

Gupta K. C.; Sahoo S. (2001)

Grafting of acrylonitrile and methyl methacrylate from their binary mixtures on cellulose using ceric ions,

J. Appl. Polym. Sci. , 79: 767–778.

Haddad, P.R.; Jackson, P.E. (2000)

Ion chromatography; principles and applications,

Elsevier, Amsterdam.

- Habicht, J.; Schmidt, M.; Ruehe, J.; Johannsmann, D. (1999)
Swelling of thick polymer brushes investigated with ellipsometry
Langmuir, 15, 2460-2465
- Halling, P.J. and Dunnill, P. (1979)
Improved nonporous magnetic supports for immobilised enzymes.
Biotechnol. Bioeng. 21: 396-416
- Halling, P.J. and Dunnill, P. (1980)
Magnetic supports for immobilized enzymes and bioaffinity adsorbents
Enzyme Microb. Technol. 2 : 2-10.
- Halperin, A.; Tirrell, M.; Lodge, T.P. (1992)
Tethered chains in polymer microstructures
Adv. Polym. Sci. 100, 31
- Hansson, M.; Stahl, S.; Hjorth, R.; Uhlen, M. ; Moks, T. (1994).
Single-step recovery of a secreted recombinant protein by expanded bed
adsorption.
Biotechnology, 12, 285-288.
- Hausera, P.S.; Ryan, R.O (2007)
“Expressed protein ligation using an N-terminal cysteine containing fragment
generated in vivo from a pelB fusion protein.”
Protein Expression and Purification, 54 (2) 227-233
- Heeboll-Nielsen, A.; Justesen, S.; Thomas, O.R.T.. (2001)
Product recovery for crude bioprocess liquors by high gradient magnetic fishing.
10th European Congress on Biotechnology: Madrid, Spain. 2001.

Heebøll-Nielsen A.; Justesen, S.F.L.; Thomas, O.R.T. (2004)
Fractionation of whey proteins with high-capacity superparamagnetic ion-exchangers.

Journal of biotechnology, 113 (1-3) 247-62.

Hermanson, G.T.; Mallia, A.K.; Smith, P.K. (1992)

Immobilized Affinity Ligand Techniques

Academic Press Inc, London.

Hester, J.F.; Olugebefola, S.C.; Mayes, A.M. (2002)

Preparation of pH-responsive polymer membranes by self-organization

Journal of membrane science 208 (1-2) 375-388

Hinrichs, K.; Aulich, D.; Ionov, L.; Esser, N.; Eichhorn, K-J.; Motornov, M.; Stamm, M.; Minko, S. (2009)

Chemical and Structural Changes in a pH-Responsive Mixed Polyelectrolyte Brush Studied by Infrared Ellipsometry

Langmuir 2009, 25(18), 10987–10991

Houbenov, N.; Minko, S.; Stamm, M. (2003)

Mixed polyelectrolyte brush from oppositely charged polymers for switching of surface charge and composition in aqueous environment

Macromolecules, 36 (16), 5897–5901

Hritcu, D., Muller, W.; Brooks D. E. (1999)

Poly(styrene) latex carrying Cerium(IV)-initiated terminally attached cleavable chains: Analysis of grafted chains and model of the surface layer,

Macromolecules, 32: 565-573.

Hubbuch, J.J.; Matthiesen, D.B.; Hogley, T.J.; Thomas, O.R.T. (2001)
High gradient magnetic separation versus expanded bed adsorption: a first
principle comparison
Bioseparation, 10, 99-112

Hubbuch, J.J.; Thomas, O.R.T. (2002)
High-Gradient Magnetic Affinity Separation of Trypsin from Porcine Pancreatin
Biotechnology and Bioengineering, 79 (3), 301-313

Huggins, C.; Tapley, D.F.; Jensen, E.V. (1950)
Mercaptan-Induced Coagulation of Proteins
Biochemistry, 36 (69), 5-699

Imanishi, Y.; Nagaoka, S.; Higashimura, T. (1973)
Polymerization of DL-phenylalanine N-carboxyanhydride by multifunctional
pyridine derivatives
Polymer Journal, 4 (6) 644-650

Ionov, L.; Sidorenko, A.; Stamm, M.; Minko, S.; Zdyrko, B.; Klep, V.; Luzinov, I.
(2004)
Gradient mixed brushes: "grafting to" approach
Macromolecules, 37, 7421-7423

Ionov L.; Houbenov, N.; Sidorenko, A.; Stamm, M.; Luzinov, I.; Minko, S (2004)
Inverse and Reversible Switching Gradient Surfaces from Mixed Polyelectrolyte
Brushes
Langmuir 20: 9916-19.

Ionov, L.; Sidorenko, A.; Eichhorn, K-J.; Stamm, M.; Minko, S.; Hinrichs, K.
(2005)
Stimuli-responsive mixed grafted polymer films with gradually changing
properties: direct determination of chemical composition
Langmuir 21, 8711-8716

Ivanova, V.; Hristov, J.; Dobrev, E.; Al-Hassan, Z.; Penchev, I. (1996)
Performance of a magnetically stabilized bed reactor with immobilized yeast cells
Applied Biochemistry and Biotechnology
59 (2) 187-198

Iwakura, Y.; Imai, Y. (1966)
Characterization of the poly(vinyl alcohol)-methyl methacrylate graft copolymers
prepared by the ceric ion method
Makromol. Chem., 98, 1.

Iwata, H.; Hirata, I.; Ikada, Y. (1997)
Atomic force microscopic images of solvated polymer brushes
Langmuir, 13, 3063-3066

Janson, J.C.; Ryden, L. (1998)
Protein Purification, 2nd ed., p 147-197.

Jeyaprakash, J.D.; Samuel, S.; Dhamodharan, R.; R  he, J. (2002)
Polymer Brushes via ATRP: Role of Activator and Deactivator in the Surface-
Initiated ATRP of Styrene on Planar Substrates,
Macromolecular Rapid Communications, 23 (4), 277 – 281

Johnck, M.; Muller, L.; Neyer A.; Hofstraat J.W. (2000)
Copolymers of halogenated acrylates and methacrylates for the application in
optical telecommunication: optical properties, thermal analysis and determination
of unsaturation by quantitative FT-Raman and FT-IR spectroscopy, *Eur. Polym. J.*
36 (2000) 1251–1264.

Jones, R.A.I.; Richards, R.W (1999)
Polymers at interfaces
Cambridge University Press, Cambridge

Jordan, R.; Ulman, A.; Kang, J.F.; Rafailovich, M.H.; Sokolov, J. (1999)
Surface-initiated anionic polymerization of styrene by means of self-assembled monolayers

J. Am. Chem. Soc., 121, 1016-1022

Justesen, S.F.L.; Nielsen, A.H.; Thomas, O.R.T. (2001)

High gradient magnetic fishing for the isolation of high-value proteins from sweet whey.

Danish Biotechnology Conference VII: Vejle, Denmark.

Julthongpiput, D.; Lin, Y.H.; Teng, J.; Zubarev, E.R.; Tsukruk, V.V. (2003)

Y-Shaped polymer brushes: nanoscale switchable surfaces

Langmuir, 19, 7832-7836

Katoa, H.; Wadati, M. (2007)

Density function analysis of single polymer chain

Chaos, Solutions and fractals

32 (4) 1250-1257

Kawaguchi, M.; Kawarabayashi, M.; Nagata, N.; Kato, T.; Yoshioka, A.;

Takahashi, A. (1988)

Adsorption of polybutadienes with polar group terminations on the solid surface.

1. Infrared study at the silica surface

Macromolecules, 21, 1059-1062

Kawai, T.; Saito, K.; Lee, W. (2003)

Protein binding to polymer brush, based on ion-exchange, hydrophobic and affinity interactions

Journal of chromatography, 790 (1-2) 131-142

Kim, J-B.; Bruening, M.L.; Baker, G.L. (2000)

Surface-initiated atom transfer radical polymerization on gold at ambient temperature

J. Am. Chem. Soc., 122, 7616-7617

Kittel, C. (1946)

Theory of the Structure of Ferromagnetic Domains in Films and Small Particles
Phys. Rev. 70, 965 - 971

Klein, J.; Kamiyama, Y.; Yoshizawa, H.; Israelachvili, J.N.; Fredrickson, G.H.; Pincus, P.; Fetters, L.J. (1993)

Lubrication forces between surfaces bearing polymer brushes

Macromolecules, 26, 5552-5560

Klein, J.; Kumacheva, E.; Mahalu, D.; Perahia, D.; Fetters, L.J. (1994)

Reduction of frictional forces between surfaces bearing polymer brushes

Nature, 370, 634-636

Kodera, D. (1905)

La separation electromagnetique et electrostatique des mineraux,
L'Eclairage Electrique, Paris

Kong, X.; Kawai, T.; Abe, J.; Iyoda, T. (2001)

Amphiphilic polymer brushes grown from the silicon surface by atom transfer radical polymerization

Macromolecules, 21, 1837-1844

Kurosawaa, S.; Aizawaa, H.; Taliba, Z. A.; Atthoffa, B.; Hilborne, J. (2004).

Synthesis of tethered-polymer brush by atom transfer radical polymerization from a plasma-polymerized-film-coated quartz crystal microbalance and its application for immunosensors,

Biosensors and Bioelectronics 20, 1165–1176

Kopaciewicz, W.; Rounds, M.A.; Fausnaugh, J.; Regnier, F.E. (1983)
Retention model for high performance ion-exchange chromatography
J. Chromatogr. 266, 3-21

Ladisch, M.R. (2001)
Bioseparations engineering: principles, practice and economics
Wiley interscience, John Wiley & Sons, Inc.

Laemmli, U.K. (1970)
Cleavage of structural proteins during the assembly of the head of bacteriophage
T4. Nature 227 (259): 680-785.

Lagos, A.; Yazdani-Pedram, M.; Reyes, J (1992)
Ceric ion-initiated grafting of poly(methyl acrylate) onto chitin
J M S—Pure Apply Chem A29, 1007-1015

Lane, F.C. (1963)
The economic meaning of the invention of the compass
The American Historical Review, 68 (3) 605

Langguth, F.; Halle, A.S. (1903)
Handbuch der Elelztrochemie Elektromagnetischse Aufbereitung
Willhelm Knapp

Leduc, M.R.; Hawker, C.J.; Dao, J.; Frechet, J.M.J. (1996)
Dendritic ilnitiators for “living” radical polymerizations: A versatile approach to the
synthesis of dendritic-linear block copolymers
J. Am. Chem. Soc., 118, 11111-11118

Lee, Y.; Rho, J.; Jung, B. (2003)

Preparation of magnetic ion-exchange resins by the suspension polymerization of styrene with magnetite

Journal of Applied Polymer Science, 89 (8) 2058 - 2067

Le Saux, A.; Ng, M.L.; Koh, J.Y.; Low, H.P.; Leong, E.L.; Ho, B.; Ding, J.L. (2008)

The Macromolecular Assembly of Pathogen-Recognition Receptors is Impelled by Serine Proteases, via Their Complement Control Protein Modules

Journal of Molecular Biology, 377 (3) 902-913

Levicky, R.; Koneripalli, N.; Tirrell, M.; Satija, S.K. (1998)

Concentration Profiles in Densely Tethered Polymer Brushes

Macromolecules, 31, 3731-3734

Liao, M.H.; Chen, D.H. (2002)

Fast and efficient adsorption/desorption of protein by a novel magnetic nano-adsorbent.

Biotechnol Lett. 24:1913–1917.

Mansky, P.; Liu, Y.; Huang, E.; Russell, T.P.; Hawker, C. (1997)

Controlling polymer-surface interactions with random copolymer brushes

Science, 275, 1458-1460

Matyjaszewski, K.; Xia, J. (2001)

Atom transfer radical polymerization

Chem. Rev. 101 (9) 2921-2990

Matyjaszewski, K.; Spanswick, J. (2005)

Controlled/living radical polymerization

Materials Today 8, 26-33

Ma, Z.Y.; Guan, Y.P.; Liu, X.Q.; Liu, H.Z. (2005)
Preparation and characterization of micron-sized non-porous magnetic polymer microspheres with immobilized metal affinity ligands by modified suspension polymerization
Journal of Applied Polymer Science, 96 (6) 2174 - 2180

McCreath, G. E., H. A. Chase, R. O. Owen, and C. R.. Lowe (1995)
Expanded bed affinity chromatography of dehydrogenase from bakers' yeast using dye-ligand per- fluoropolymer support.
Biotechnol. Bioeng. 48: 341-354

Melenevskaya, E.Y.; Zgonnik, V.N.; Leonteva, E.G.; Keвер, E.E.; Terenteva, I.V.; Shibaev, L.; (1993)
Synthesis and hydrolysis of styrene-tert-butyl methacrylate diblock copolymers with narrow molecular mass distribution
Polymer Science, 35, 445-448

Mendelsohn, R.; Brauner, J.W.; Gericke, A. (1995)
External infrared reflection absorption spectrometry of monolayer films at the air-water interface
Annu. Rev. Phys. Chem., 46, 305-334

Milner, S.T.; Witten, T.A.; Cates, M.E. (1988)
Theory of the grafted polymer brush
Macromolecules, 21 (8) 2610-2619

Milner, S.T. (1991)
Polymer Brushes
Science, 251 (4996) 905-914

Minko, S.; Muller, M.; Usov, D.; Scholl, A.; Froeck, C.; Stamm, M. (2002)
Lateral versus perpendicular segregation in mixed polymer brushes
Phys. Rev. Lett. 88, 035502

Minko, S.; Tokarev, I. ; Stamm, M. (2006),
Mixed Polymer Brushes by Sequential Polymer Addition: Anchoring Layer Effect.
Langmuir 20,4064-75.

Mino, G.; Kaizerman, S. (1958)
A new method for the preparation of graft polymers. Polymerization initiated by
ceric ion redox systems.
J. Polym. Sci. 31 (122); 242–243

Mino, G; Kaizermann, S; Rasmussen, E. (1959)
The oxidation of polyvinyl alcohol by ceric ion
J. Polym. Sci. 39, 523-529

Moritz, R.L.; Simpson, R.J. (2005)
Liquid based free-flow electrophoresis-reversed-phase HPLC: a proteomic tool.
Nature Methods (2): 863-873.

Mosbach, K. and Nilsson, K. (1981).
Immobilization of enzymes and affinity ligands to various hydroxyl group carrying
supports using highly reactive sulfonyl chlorides.
Biochem.Biophys. Res. Commun. 102, 449-457.

Müller, W. (1990)
New ion exchangers for the chromatography of biopolymers,
Journal of Chromatography A, 510, 133-140.

Munro, P.A.; Dunnill, P.; Lilly, M.D. (1977)

Nonporous magnetic materials as enzyme supports: studies with immobilized chymotrypsin

Biotechnol. Bioeng. 19. 101-124.

Nagasaw, M.; Murase, T.; Kondo, K. (1965)

Potentiometric titration of stereoregular polyelectrolytes

J. Phys. Chem., 1965, 69 (11) 4005-4012

Narita, H.; Okamoto, S.; Machida, S. (1969)

The polymerization mechanism of methyl methacrylate initiated with ceric ion

Makromol. Chem. 125, 15-23

Nixon, L.; Koval, C.A.; Noble, R.D.; Slaff, G.S. (1992)

Preparation and characterization of novel magnetite-coated ion-exchange particles.

Chem Mater. 4, 117–121

Odabas, M; Uzun, L; Denizli, A (2004)

Porous magnetic chelator support for albumin adsorption by immobilized metal affinity separation

Journal of Applied Polymer Science 93 (5) 2501 - 2510

Odian, G. and Kho, J.H.T., 1970.

Ceric-ion initiated graft polymerisation onto poly(vinyl)alcohol.

J. Macromol. Sci. Chem. A4, 317–330

Oesterling, R. E. (1961)

Process for fluoroalkyl sulfides

U. S. Patent 3,006,964

Ogiwara, Y.; Uchiyama, M. (1969)

Relationship between reduction of ceric ion with poly (vinyl alcohol) and graft copolymerization

J. Polym. Sci., Polym. Chem. Ed., 7, 1479-1488

O'Shannessy K, Scoble J & Scopes RK (1996)

A simple and economical procedure for purification of muscle lactate dehydrogenase by batch dye-ligand adsorption.

Bioseparation 6, 77-80

Painter, P.C; Rimmer, S. M. ; Snyder, R. W.; Davis A. (1981)

A fourier transform infrared study of mineral matter in coal: The application of a least squares curve-fitting program

Applied Spectroscopy, 35, 102-106

Patten, T.E.; Xia, J.; Abernathy, T.; Matyjaszewski, K. (1996)

Polymers with very low polydispersities from atom transfer radical polymerization

Science 272, 866-868

Pitfield, I. D. (1992)

Perfluorocarbon chromatographic supports,

PhD thesis, University of Cambridge, United Kingdom.

Robinson, P. J.; Dunnill, P.; Lilly, M. D. (1973)

The Properties of Magnetic Supports in Relation to Immobilized Enzyme Reactors,

Biotechnol. Bioeng., 15, 603-606.

Reddy, G.V.; Chandraganthi, R.; Vasanthi, K.; Sriram, R. (1995)

Vinyl Polymerization Initiated by Ceric Ion–Ethyl Cellosolve Redox System in Aqueous nitric acid

J M S—Pure Apply Chem A32, 1997.

Ryan, A.J.; Crook, C.J.; Howse, J.R.; Topham, R.; Geoghegan, M.; Martin, S.J.; Parnell, A.J.; Ruiz-Prez, L.; Jones, A.L. (2005)

Mechanical actuation by responsive polyelectrolyte brushes and triblock gels
Journal of Macromolecular Science B, 44 (6) 1103-1121

Safarikova, M.; Roy, I.; Gupta, M. N.; Safarik, I. (2003)

Magnetic alginate microparticles for purification of α -amylases
Journal of Biotechnology, 105 (3) 255-260

Sato, B.; Sako, Y.; Yamashina, S.; Ohnishi, S.-I. (1986)

A novel method for isolating specific endocytic vesicles using very fine ferrite particles coated with biological ligands and the high-gradient magnetic separation technique
100 (6) 1481-1492

Savina, I.N.; Galaev, I.Y.; Mattiasson, B. (2006)

Ion-exchange macroporous hydrophilic gel monolith with grafted polymer brushes
Journal of molecular recognition, 19 (4) 313-321

Schilli, C.; Lanzendrfer, M.G.; Miller, A.H.E. (2002)

Benzyl and cumyl dithiocarbamates as chain transfer agents in the RAFT Polymerization of N-isopropylacrylamide. In situ FT-NIR and MALDI-TOF MS investigation,
Macromolecules, 35 (18) 6819-6827

Seo, Y-S; Kim, K.S.; Galambos, A.; Lammertink, R.G.H.; Vancso, G.J.; Sokolov, J.; Rafailovich, M. (2004)

Nanowire and Mesh Conformations of Diblock Copolymer Blends at the Air/Water Interface
Nano Letters, 4 (3) 483-486

- Shusharina, N. P. and Linse, P. (2006)
Oppositely charged polyelectrolytes grafted onto planar surface: Mean-field lattice theory.
European Physical Journal 6 (2) 147-55.
- Sidorenko A.; Minko S. ;Schenk-Meuser K. ;Duschner H. ;Stamm M. (1999)
Switching of polymer brushes.
Langmuir 15.(24) 8349-55.
- Singh, N.; Husson, S.M.; Zdyrko, B.; Luzinov, I. (2005)
Surface modification of microporous PVDF membranes by ATRP
Journal of membrane science 262 (1-2) 81-90
- Singleton, D.A.; Nowlan, D.T.; Jahed, N.; Matyjaszewski, K. (2003)
Isotope effects and the mechanism of atom transfer radical polymerization
Macromolecules, 36, 8609-8616
- Simon, M.D.; Geim, A.K. (2000)
Diamagnetic levitation: Flying frogs and floating magnets
J. Appl. Phys. 87, 6200
- Siu, S.C.; Baldascini, H.; David C. Hearle, Mike Hoare, M.; Titchener-Hooker, N.J. (2006)
Effect of fouling on the capacity and breakthrough characteristics of a packed bed ion exchange chromatography column
Bioprocess and Biosystems Engineering, 28 (6) 405-414
- Slutsker, L.; Hoesly, F.C.; Miller, L.; Williams, L.P.; Watson, J.C.; Fleming, D.W.(1990).
Eosinophilia-myalgia syndrome associated with exposure to tryptophan from a single manufacturer. JAMA 264 (2) 213–7.

Solomons, T.W.G.; Fryhle, C.B. (2007)

Organic Chemistry

John Wiley and Sons, Inc.

Spalding, B.J. (1991),

Downstream processing: Key to slashing production costs 100 fold.

Bio/Technology 9, 229-233.

Story, R.F.; Goff, L.T. (1989)

Ceric ion initiation of vinylidene chloride from poly(vinyl alcohol)

Macromolecules 22, 1058

Su, Y.L.; Wang, J. ;Liu, H.Z. (2002)

FTIR Spectroscopic Study on Effects of Temperature and Polymer Composition on the Structural Properties of PEO-PPO-PEO Block Copolymer Micelles

Langmuir, 18 (14) 5370-5374

Svoboda, J. (1987)

Magnetic methods for th treatment of minerals

Elsevier Science Publishing Co., Amsterdam.

Thommes J. (1997),

Fluidized bed adsorption as a primary recovery step in protein purification.

Adv. Biochem. Eng. Biotechnol. 58, 185-230.

Tipson, R.S. (1944)

On esters of p-toluenesulfonic acid

J. Org. Chem., 9, 235

Tong, XD; Xue, B; Sun, Y. (2001)

A novel magnetic affinity support for protein adsorption and purification.

Biotechnol Progr. **17**,134–139.

Tong, X.D; Sun, Y (2009)

Agar-based magnetic affinity support for protein adsorption

Biotechnology Progress **17** (4) 738 - 743

Y. Tran and P. Auroy (2001)

Synthesis poly(styrene sulfonate) brushes

J. Am. Chem. Soc., **123** (16) 3644–3654

Truce, W.E. and Norell, J.R. (1963)

Thietane dioxide derivatives via the interaction of sulfonyl chlorides with ketene diethylacetal

J. Am. Chem. Soc., **85** (20) 3231-3236

Tsubokawa, N.; Fujiki, K.; Sone, Y. (1988)

Graft polymerization of vinyl monomers onto carbon black by use of the redox system consisting of Ceric ions and carbon black carrying alcoholic hydroxyl groups

J Macromol Sci—Chem A25, 1159-1171

Tugulu, S.; Arnold, A.; Sielaff, I.; Johnsson, K.; Klok, H.A. (2005)

Protein-functionalized polymer brushes

Biomacromolecules, **6**, 1602-1607

Uhlmann, P.; Houbenov, N.; Stamm, M.; Minko, S. (2005)

Surface functionalization by smart binary polymer brushes to tune physico-chemical characteristics at biointerfaces

E-Polymers (European Polymer Federation), 075

Uhlmann, P.; Houbenov, N.; Brenner, N.; Grundke, K.; Burkett, S.; Stamm, M. (2007)

In-situ investigation of the adsorption of globular model proteins on stimulo-responsive binary polyelectrolyte brushes
Langmuir, 23, 57-64

Unsworth, D.; Tun, Z.; Sheardown, H.; Brash, J.L. (2005)

Chemisorption of thiolated poly(ethylene oxide) to gold surface chain densities measured by ellipsometry and neutron reflectometry
Journal of colloid and interface science, 281, 112-121

Urbain, O.M. & Steman, W.R., (1941),

Process for treating liquids
US Patent 2232294.

Vera-Pacheco, M.; Vazquez-Torres, H.; Canche-Escamilla, J. (1993)

Preparation and characterization of hydrogels obtained by grafting of acrylonitrile onto cassava starch by ceric ion initiation.
J. Appl. Polym. Sci. **47**, 53–59

Wang, J-S.; Matyjaszewski, K. (1995)

Controlled/"living" radical polymerization. Atom transfer radical polymerization in the presence of transition-metal complexes
J. Am. Chem. Soc., 117 (20), 5614-5615

Wang, X.; Xiao, X.; Wang, X.; Zhou, J.; Li, L.; Xu, J.; Guo, B (2008)

Revisibly switchable double-responsive block copolymer brushes
Macromolecular rapid communications 28 (7) 828-833

Weber K.; Osborn M (August 1969).

"The reliability of molecular weight determinations by dodecyl sulfate-polyacrylamide gel electrophoresis."

J Biol Chem. 244 (16): 4406-4412

West, A. (1988)

Basic Solid State Chemistry, 2nd ed.

Wiley, New York

Wheelwright, S.M. (1989)

The design of downstream processes
for large-scale protein purification

Journal of Biotechnology, 11, 89-102

Wurtman R.J.; Hefti, F.; Melamed, E. (1980).

Precursor control of neurotransmitter synthesis

Pharmacol. Rev. 32 (4) 315–35.

Xu Z, Cornilsen B.C.; Popko D.C.; Pennington W.D.; Wood J.R.; Hwang J-Y
(2001)

Quantitative Mineral Analysis by FTIR Spectroscopy

The Internet Journal of Vibrational Spectroscopy (Wiley and Sons) 5 (4)

Xue, B; Sun, Y. (2001)

Protein adsorption equilibria and kinetics to a poly(vinyl alcohol)-based magnetic
affinity support.

J Chromatogr A. 921, 109–119.

Yamamoto, S.; Tsujii, Y.; Fukuda, T. (2002)

Atomic force microscopic study of stretching a single polymer chain in a polymer
brush

Macromolecules, 333, 5995-5998

Zhang, M.; Liu, L.; Zhao, H.; Yang, Y.; Fu, G.; He, B. (2006)

Double-responsive polymer brushes on the surface of colloid particles

Journal of colloid and interface science 301, 85-91

Zhang, Z.; O'Sullivan, D.A.; Lyddiatt, A. (1999)

Magnetically stabilised fluidised bed adsorption: practical benefit of uncoupling bed expansion from fluid velocities in the purification of a recombinant protein from *Escherichia coli*

J. Chem. Technol. Biotechnol. 74 (3) 270-274

Zhao, B.; Brittain, W.J. (2000)

Polymer brushes: surface-immobilized macromolecules

Progress in Polymer Science 25, 677-710